

Air Force Institute of Technology

AFIT Scholar

Theses and Dissertations

Student Graduate Works

9-2006

A General Framework for Analyzing, Characterizing, and Implementing Spectrally Modulated, Spectrally Encoded Signals

Marcus L. Roberts

Follow this and additional works at: <https://scholar.afit.edu/etd>



Part of the [Systems and Communications Commons](#)

Recommended Citation

Roberts, Marcus L., "A General Framework for Analyzing, Characterizing, and Implementing Spectrally Modulated, Spectrally Encoded Signals" (2006). *Theses and Dissertations*. 3336.
<https://scholar.afit.edu/etd/3336>

This Dissertation is brought to you for free and open access by the Student Graduate Works at AFIT Scholar. It has been accepted for inclusion in Theses and Dissertations by an authorized administrator of AFIT Scholar. For more information, please contact richard.mansfield@afit.edu.



A GENERAL FRAMEWORK FOR ANALYZING, CHARACTERIZING,
AND IMPLEMENTING SPECTRALLY MODULATED,
SPECTRALLY ENCODED SIGNALS

DISSERTATION

Marcus L. Roberts, Major, USAF

AFIT/DS/ENG/06-06

DEPARTMENT OF THE AIR FORCE
AIR UNIVERSITY

AIR FORCE INSTITUTE OF TECHNOLOGY

Wright-Patterson Air Force Base, Ohio

APPROVED FOR PUBLIC RELEASE; DISTRIBUTION UNLIMITED.

The views expressed in this dissertation are those of the author and do not reflect the official policy or position of the United States Air Force, Department of Defense, or the United States Government.

A GENERAL FRAMEWORK FOR ANALYZING, CHARACTERIZING,
AND IMPLEMENTING SPECTRALLY MODULATED,
SPECTRALLY ENCODED SIGNALS

DISSERTATION

Presented to the Faculty
Graduate School of Engineering and Management
Air Force Institute of Technology
Air University
Air Education and Training Command
In Partial Fulfillment of the Requirements for the
Degree of Doctor of Philosophy

Marcus L. Roberts, B.S.E.E., M.S.E.E.
Major, USAF

September 2006

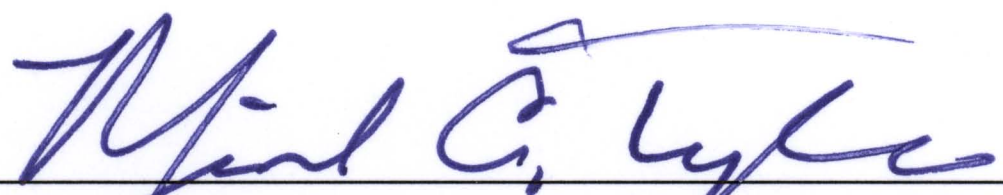
APPROVED FOR PUBLIC RELEASE; DISTRIBUTION UNLIMITED.

A GENERAL FRAMEWORK FOR ANALYZING, CHARACTERIZING,
AND IMPLEMENTING SPECTRALLY MODULATED,
SPECTRALLY ENCODED SIGNALS

Marcus L. Roberts, B.S.E.E., M.S.E.E.

Major, USAF

Approved:

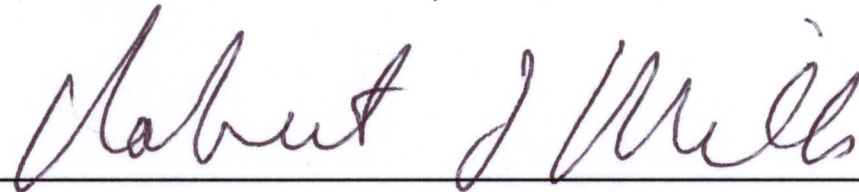

Dr. Michael A. Temple (Chairman)

11 Aug 06
date



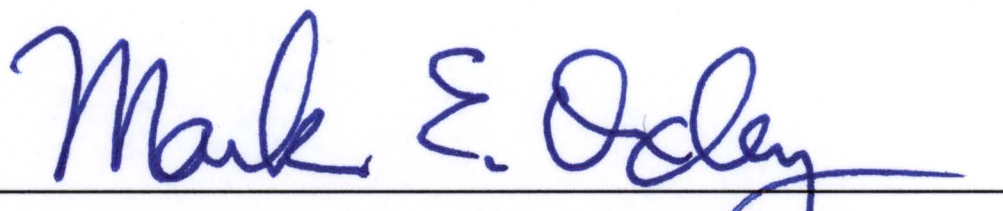
Dr. Alan W. Johnson (Dean's
Representative)

11 Aug 06
date

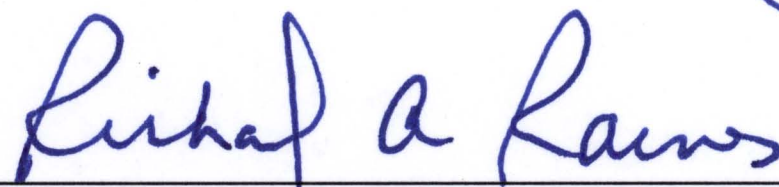


Dr. Robert F. Mills (Member)

11 Aug 2006
date


Dr. Mark E. Oxley (Member)

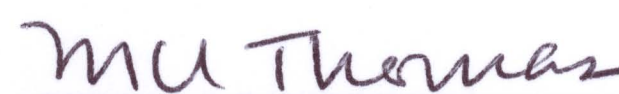
11 Aug 2006
date



Dr. Richard A. Raines (Member)

11 Aug 06
date

Accepted:



M. U. Thomas

Dean, Graduate School of Engineering and Management

22 Aug 06

Date

Abstract

Once a novelty enjoyed by few, wireless communication has quickly become a necessity for many in today's rapidly-paced mobile world. Future fourth generation (4G) communication systems may represent a revolutionary step as they aim to fuse cellular (voice) and internet (data) capabilities into a single operating environment. The 4G goal is to efficiently provide universal, ubiquitous, high-speed access for civilian and military communicators alike. One potential key to 4G implementation is software defined radio (SDR) technology, which enables adaptive signal generation. This adaptivity inherently provides waveform diversity which may ultimately be controlled through cognitive radio (CR) principles, i.e., by actively monitoring channel conditions, traffic loads, spectrum availability, etc., while tailoring waveform features to improve overall efficiency. The synergistic union of SDR control via CR principles is referred to herein as CR-based SDR. Although research is rapidly progressing in SDR hardware and software venues, current SDR research lacks the theoretical foundation and analytic framework to fuse these developments together to permit efficient implementation.

The research documented herein addresses this deficiency by providing a general analytic framework for analyzing, characterizing, and implementing spectrally modulated, spectrally encoded (SMSE) signals within a CR-based SDR architecture. Researchers agree that orthogonal frequency division multiplexing (OFDM) will be the bedrock modulation and multiplexing technique for 4G systems given it provides unique advantages for communicating in dense, fading environments. In this work, OFDM-based signals are collectively classified as SMSE given that data modulation and encoding (for multiple access, interference suppression, etc.) are both applied in the spectral domain. The proposed analytic framework, as developed around six key

waveform design variables, provides the desired analytic commonality and unification for a myriad of SMSE signals.

Applicability of the analytic framework is demonstrated using specific waveform design variable instantiations with the SMSE framework to generate analytic expressions for candidate 4G signals. The resultant SMSE expressions are compared with published results and consistency established for all signals considered. Next, framework adaptivity is demonstrated for seven distinct OFDM-based SMSE signals, with modeling and simulation results provided to demonstrate and reinforce framework utility. It is also shown that expected communication performance is maintained within various SMSE coexistence scenarios, i.e., scenarios containing multipath fading, multiple access interference (MAI), and partial band interference (PBI). Simulated bit error performance for various signals constructed within the unifying SMSE framework are shown to correlate well with theoretical predictions.

Acknowledgements

First and foremost, I humbly offer thanks and praise to the giver of all life, my Creator and Savior Jesus Christ. Through success, I see a direct reflection of Your blessings upon my life; through adversity, I recognize another opportunity for You to mold my character. To my beautiful wife, I thank you for your continual encouragement and support. Your sacrifice is beyond measure, and I never cease to be amazed by your thoughtfulness. To my children, I am honored to be your father. Your notes, smiles, and hugs help me maintain proper alignment of my priorities. Thank you for your patience as Daddy finished this research. To my parents, thank you for living a Godly example of excellence in every walk of life.

Thank you to my advisor, Dr. Mike Temple, for your positive outlook, technical guidance, and creative outside-of-the-box thinking. It has been a true joy to study under your wings the past three years. Thanks for encouraging me to pursue excellence (and for the catchy idioms). To my committee members, Dr. Mills, Dr. Oxley, and Dr. Raines, thank you for your valuable feedback and timely assistance. To my AFRL sponsors, Mr. Minges and Mr. Stephens, thank you for supporting this research. To Mr. Chakravarthy and Maj Nunez, thank you for your candid discussions and excellent advice. Finally, to my AFIT PhD brethren: we fought the fight, we finished the race, we kept the faith. I will recall our study sessions, PT workouts, and witty banter with delight, and I would gladly work with all of you again in the future.

Marcus L. Roberts

Table of Contents

	Page
Abstract	iv
Acknowledgements	vi
List of Figures	xi
List of Tables	xv
List of Symbols	xvi
List of Abbreviations	xix
 I. Introduction	 1
1.1 Research Motivation	2
1.1.1 General Overview	2
1.1.2 Technical Motivation	4
1.2 Research Contributions	7
1.2.1 Unification Desired	7
1.2.2 Framework Established	8
1.2.3 Applicability Demonstrated	9
1.2.4 Coexistence Maintained	9
1.3 Research Assumptions	9
1.4 Materials and Equipment	11
1.5 Dissertation Organization	11
 II. Background: The Path to Future Communications	 13
2.1 First Generation Systems (1G)	14
2.2 Second Generation Systems (2G)	17
2.2.1 TDMA Systems	19
2.2.2 CDMA Systems	22
2.3 Toward 3G Systems	25
2.3.1 TDMA Systems	26
2.3.2 CDMA Systems	30
2.4 Third Generation Systems (3G)	30
2.4.1 CDMA Systems: Wideband CDMA (W-CDMA)	34
2.4.2 CDMA Systems: CDMA2000	38
2.4.3 TDMA Systems	44
2.4.4 Hybrid Systems	45

	Page
2.4.5	FDMA Systems 46
2.4.6	3G Deployment Summary 47
2.5	Fourth Generation Systems (4G) 49
2.5.1	Current Status of Wireless Networks 49
2.5.2	What is 4G? 52
2.5.3	4G Enabling Technologies 54
2.6	Beyond 4G: Cognitive-Based SDR Implementation Using OFDM 66
2.7	Background Summary 68
III.	Analytic SMSE Framework Development 70
3.1	Unifying UWB Framework 71
3.2	Unifying SMSE Framework 72
3.3	SMSE Framework: Variables 73
3.4	SMSE Framework: Transmitter 75
3.5	Fading Channel 81
3.5.1	Key Parameters 82
3.5.2	Practical Description 84
3.5.3	Mathematical Representation 89
3.6	SMSE Framework: Receiver 93
3.7	SMSE Framework: MIMO Extension 98
3.7.1	Generalized MIMO Channel Model 98
3.7.2	Composite MIMO-SMSE Model 100
3.8	Summary of SMSE Analytical Framework 103
IV.	SMSE Framework Applications 104
4.1	Orthogonal Frequency Division Multiplexing (OFDM) Signals 104
4.2	Coded OFDM (COFDM) Signals 106
4.3	Multi-Carrier Code Division Multiple Access (MC-CDMA) Signals 107
4.4	Transform Domain Communication System (TDCS) Signals 110
4.5	Carrier Interferometry (CI) Signals 113
4.6	Summary of SMSE Framework Applications 116
V.	SMSE Framework Demonstration 118
5.1	Methodology 119
5.1.1	Transmitter Model 119
5.1.2	Channel Models 120
5.1.3	Receiver Model 122

	Page
5.1.4 Communication Performance	125
5.2 Baseline Results	130
5.2.1 OFDM Baseline	131
5.2.2 MC-CDMA Baseline	131
5.2.3 TDCS Baseline	133
5.2.4 SMSE ⁺ Baseline	133
5.2.5 Summary of Baseline Results	134
5.3 Fading Channel Demonstration	135
5.3.1 OFDM in a Fading Channel	135
5.3.2 MC-CDMA in a Fading Channel	135
5.3.3 TDCS in a Fading Channel	136
5.3.4 SMSE ⁺ in a Fading Channel	138
5.3.5 Summary of Fading Channel Demonstrations . .	139
5.4 Interference Suppression Demonstration	141
5.4.1 OFDM with Interference	141
5.4.2 SMSE ⁺ with Interference	142
5.5 Multiple Access Demonstration	146
VI. Conclusion	154
6.1 Research Contributions	154
6.2 Future Research	157
Appendix A. Ultra Wideband Signaling Theory, Framework, and Results	160
A.1 UWB Theory	160
A.1.1 Fundamental UWB Waveform	160
A.1.2 UWB Modulation Techniques	163
A.1.3 UWB Multiple Access Techniques	163
A.2 UWB Unified Framework	169
A.2.1 Transmitter Model	170
A.2.2 Rake Receiver Model	171
A.3 UWB TH-BPPM in a Fading Channel	173
A.3.1 Multipath Channel Model	174
A.3.2 Communication Performance: AWGN Channel .	175
A.3.3 Communication Performance: Fading Channel .	180
A.3.4 Summary of TH-BPPM Fading Channel Results	183
A.4 Spectral Coexistence Scenarios: In-Band Power Analysis	184
A.4.1 Energy Spectral Density (ESD) of Fundamental UWB Waveform	185
A.4.2 Power Spectral Density (PSD) of TH-PPM Signals	186
A.4.3 Power Spectral Density (PSD) of DS-UWB Signals	188

	Page
A.4.4 Analytical In-Band Power Expressions	191
A.4.5 In-Band Power Analysis Results	192
A.4.6 Summary of In-Band Power Analysis	194
A.5 Spectral Coexistence Scenarios: Bit Error Rate (BER) Analysis	195
A.5.1 Narrowband WLAN Signal	195
A.5.2 Interference-to-Signal (I/S) Ratio	196
A.5.3 UWB Coexistence with Narrowband WLAN in Multiple Access Environment	199
A.5.4 Summary of Bit Error Rate Analysis	202
Bibliography	204
Vita	222

List of Figures

Figure		Page
1.1.	Global Information Grid (GIG) and Full Spectrum Dominance	3
1.2.	4G Revolution: CR-Based SDR Communication System	6
1.3.	Research Contribution: A Unifying SMSE Framework	8
2.1.	General Convolutional Encoder	17
2.2.	Illustration of Various Multiple Access Schemes	18
2.3.	GSM TDMA/FDMA Frame Structure	20
2.4.	Block Diagram of IS-95 Forward Link Transmitter	24
2.5.	Evolution of Cellular Systems from 2G through 2.5G to 3G . .	25
2.6.	Data Modulation Constellations	29
2.7.	3G Standards as Defined within IMT-2000	32
2.8.	Concatenated Code Structures	33
2.9.	Block Diagram of 1×EV-DO Forward Link Transmitter	42
2.10.	Block Diagram of 1×EV-DV F-PDCH	44
2.11.	TD-SCDMA Channel Structure	47
2.12.	Voice Capacity Evolution for Common Cellular Systems	48
2.13.	Data Throughput Evolution for Common Cellular Systems . .	49
2.14.	Migration of Cellular and Wireless Networks Towards 4G . . .	53
2.15.	Illustration of MIMO System	55
2.16.	Multiple Access Illustration using VSF-OFCDM	59
2.17.	Illustration of OFDM and MC-CDMA ($F = 1$) Subcarriers . .	60
2.18.	UWB Waveform: Time Domain and ESD Representations . .	61
2.19.	Time Hopping UWB Waveform Illustration	63
2.20.	Direct Sequence UWB Waveform Illustration	63
2.21.	Representative Block Diagram of an OFDM-Based System . .	68
3.1.	Discrete Frequency Component Representation	75

Figure		Page
3.2.	Fading Channel Manifestations	86
3.3.	Fading Channel Designations in Time and Frequency	87
3.4.	Examples of Slowly-Fading Channels	88
3.5.	Examples of Fast Fading Channels	89
3.6.	Rayleigh Flat Fading Channel Model	90
3.7.	Tapped Delay Line Model of a Frequency Selective Channel	91
3.8.	MIMO Array Cube to Illustrate Variable Dimensions	102
4.1.	Illustration of OFDM and MC-CDMA ($F = 1$) Subcarriers	108
5.1.	Noise Distribution of AWGN Channel Model	121
5.2.	Distribution of Magnitude and Phase for Interference Signal	122
5.3.	Block Diagram for Partial Band Interference Generation	123
5.4.	Autoregressive Model	123
5.5.	OFDM Received Symbols for 16-QAM Modulation	125
5.6.	Baseline OFDM: P_b vs E_b/N_o for AWGN Channel	132
5.7.	Baseline MC-CDMA: P_b vs E_b/N_o for AWGN Channel	132
5.8.	Baseline TDCS: P_b vs E_b/N_o for AWGN Channel	133
5.9.	Baseline SMSE ⁺ : P_b vs E_b/N_o for AWGN Channel	134
5.10.	OFDM: P_b vs E_b/N_o for Flat Fading Channel	136
5.11.	MC-CDMA: P_b vs E_b/N_o for Flat Fading Channel	137
5.12.	MC-CDMA: P_b vs E_b/N_o for Frequency Selective Fading Channel	137
5.13.	TDCS: P_b vs E_b/N_o for Flat Fading Channel	138
5.14.	TDCS: P_b vs E_b/N_o for Frequency Selective Fading Channel	139
5.15.	SMSE ⁺ : P_b vs E_b/N_o for Flat Fading Channel	140
5.16.	SMSE ⁺ : P_b vs E_b/N_o for Frequency Selective Fading Channel	140
5.17.	OFDM: P_b vs I/S for AWGN Channel with PBI Present	142
5.18.	OFDM: P_b vs I/S for Flat Fading Channel with PBI Present	143
5.19.	OFDM: P_b vs E_b/N_o for AWGN Channel with PBI Present	143
5.20.	OFDM: P_b vs E_b/N_o for Flat Fading Channel with PBI Present	144

Figure		Page
5.21.	SMSE ⁺ : P_b vs I/S for AWGN Channel with PBI Present . . .	145
5.22.	SMSE ⁺ : P_b vs I/S for Flat Fading Channel with PBI Present	145
5.23.	SMSE ⁺ : P_b vs I/S for Frequency Selective Fading Channel with PBI Present	146
5.24.	SMSE ⁺ : P_b vs E_b/N_o for AWGN Channel with PBI Present .	147
5.25.	SMSE ⁺ : P_b vs E_b/N_o for Flat Fading Channel with PBI Present	147
5.26.	SMSE ⁺ : P_b vs E_b/N_o for Frequency Selective Fading Channel with PBI Present	148
5.27.	MC-CDMA: P_b vs N_U for AWGN Channel	151
5.28.	MC-CDMA: P_b vs N_U for Flat Fading Channel	152
5.29.	MC-CDMA: P_b vs E_b/N_o for AWGN Channel with MAI Present	153
5.30.	MC-CDMA: P_b vs E_b/N_o for Flat Fading Channel with MAI Present	153
A.1.	Fundamental UWB Waveform and ESD	162
A.2.	ESD of UWB Waveform for Different Gaussian Monocycles . .	162
A.3.	ESD of UWB Waveform for Different Pulse Widths	163
A.4.	TH-PPM Waveform Illustration	165
A.5.	Illustration of 4-ary Biorthogonal UWB Waveforms	166
A.6.	DS-UWB Waveform Illustration	168
A.7.	Multi-channel Correlation Receiver for UWB	176
A.8.	Processing Gain Impact on TH-PPM and TH-BPPM	177
A.9.	Multiple Access Performance for Three UWB Techniques . . .	179
A.10.	Representative Impulse Responses from UWB Fading Channel	181
A.11.	TH-BPPM: Single User, Varied Multipath Channels	182
A.12.	TH-BPPM Asynchronous Network: MPI and MAI Effects . .	184
A.13.	TH-BPPM Synchronous Network: MPI and MAI Effects . . .	185
A.14.	TH-PPM Analytic and Simulated PSD	189
A.15.	DS-UWB Analytic and Simulated PSD	190
A.16.	TH-PPM and DS-UWB PSD Responses over U-NII Bands . .	193

Figure		Page
A.17.	In-band Interfering TH-PPM Signal Power for PSD in Fig. A.16	193
A.18.	In-band Interfering DS-UWB Signal Power for PSD in Fig. A.16	194
A.19.	WLAN Interference: 1 User, TH-PPM	197
A.20.	WLAN Interference: 1 User, DS-UWB	197
A.21.	WLAN Interference: 12 Users, TH-PPM	198
A.22.	WLAN Interference: 12 Users, DS-UWB	198
A.23.	TH-PPM Synchronous Network in Interference Environment .	200
A.24.	TH-PPM Asynchronous Network in Interference Environment	201
A.25.	DS-UWB Synchronous Network in Interference Environment .	201
A.26.	DS-UWB Asynchronous Network in Interference Environment	202

List of Tables

Table		Page
2.1.	Comparison of 2G Systems in the Cellular Band	23
2.2.	Comparison of Data Rates for GSM-Based Systems	27
2.3.	GPRS Data Rates	27
2.4.	EDGE vs GPRS	28
2.5.	Comparison of 2G and 3G Systems	31
2.6.	Comparison of DSCH and HS-DSCH	38
2.7.	UTRA FDD vs CDMA2000 1× vs TD-SCDMA	40
2.8.	Comparison of Wi-Fi Variants	50
2.9.	Comparison of WiMAX Variants	51
2.10.	Comparison of 3G, Wi-Fi, WiMAX, and Mobile-Fi	52
2.11.	Comparison of 3G and 4G Systems	54
4.1.	Design Variable Instantiations for SMSE Implementation of OFDM and COFDM Signals	107
4.2.	Design Variable Instantiations for SMSE Implementation of MC- CDMA and TDCS Signals	113
4.3.	Design Variable Instantiations for SMSE Implementation of Car- rier Interferometry Signals	116
5.1.	Characteristics of Demonstrated SMSE-Candidate Signals . . .	131
5.2.	Summary of Errors in Fig. 5.6 through Fig. 5.9	134
5.3.	Summary of Errors in Fig. 5.10 through Fig. 5.16	141

List of Symbols

Symbol		Page
K	Convolutional Code Constraint Length	19
M	Number of Communication Symbols in Constellation . . .	33
F	MC-CDMA Subcarrier Spacing Parameter	59
$\mathfrak{F}\{\cdot\}$	Fourier Transform	73
$\mathfrak{F}^{-1}\{\cdot\}$	Inverse Fourier Transform	73
k	Data Symbol Index	74
v	User Index	74
t	Continuous Time Index	74
f	Continuous Frequency Index	74
n	Discrete Time Index	74
m	Discrete Frequency Index	74
c	SMSE Variable: Code	74
d	SMSE Variable: Data	74
w	SMSE Variable: Window	74
o	SMSE Variable: Orthogonality	74
N_F	Number of Available Frequency Components	74
a	SMSE Variable: Frequency Assignment	74
P_a	Number of Assigned Frequency Components	74
u	SMSE Variable: Frequency Use	74
P_u	Number of Used Frequency Components	74
\mathbf{S}_k	Spectral Content of the k^{th} Symbol	75
\odot	Hadamard Product	75
\mathbf{A}_k	Product of Magnitudes Matrix	75
$\mathbf{\Theta}_k$	Sum of Phases Matrix	75
N_U	Number of Users	75

Symbol		Page
\mathbf{F}	Frequency Component Identification Matrix	75
T_{sym}	Symbol Duration	76
Δf	Subcarrier Spacing	76
\bullet^r	Row-wise Inner (Dot) Product	79
N_{sym}	Number of Symbols	81
n_p	Path Loss Exponent	82
W	Signal Bandwidth	82
B_c	Coherence Bandwidth	82
σ_τ	Multipath RMS Delay Spread	82
B_d	Doppler Bandwidth	83
T_m	Multipath Spread	83
T_c	Coherence Time	84
λ	Signal Wavelength	84
b_R	Rayleigh Flat Fading Coefficient	90
N_{MP}	Number of Multipath Signals	90
\mathbf{H}	Matrix of Fading Coefficients	93
$\boldsymbol{\eta}$	Composite Noise and Interference Vector	94
\mathbf{H}_{rf}	Receiver RF Filter Transfer Function	94
\bullet^c	Column-wise Inner (Dot) Product	95
$\hat{\mathbf{z}}$	Single-Channel Test Statistic Vector	96
\hat{j}_k	Single-Channel Symbol Estimate	96
$\check{\mathbf{z}}$	Multi-Channel Test Statistic Vector	97
\check{j}_k	Multi-Channel Symbol Estimate	97
N_t	Number of Transmitters	99
N_r	Number of Receivers	99
P_I	Number of Frequency Components Occupied by PBI	122
T_{obs}	Observation Interval	123
$H(z)$	AR Filter Transfer Function	123

Symbol		Page
T_I	Adaptive Threshold for Interference Suppression	124
ω_I	Weighting Factor for Adaptive Threshold	124
e_b	Number of Bit Errors	125
n_b	Number of Transmitted Bits	125
P_b	Probability of Bit Error	125
μ	Cross-Correlation Coefficient	128
$\bar{\gamma}_c$	Average Received SNR per Channel	128
$\bar{\gamma}_b$	Average SNR per Bit	128
ξ	MAI Power Scaling Factor	149
N_{MAI}	MAI Power	149
N_c	Code Length	149
τ_m	Impulse Width Parameter	161
T_p	Pulse Width	161
f_c	Center Frequency	161
T_o	Symbol Repetition Interval	164
T_c	Spreading Code Chip Duration	164
N_{ss}	Number of Communication Symbol Repetitions	164
Δ	Relative PPM Offset	164
N_s	Number of Chip Intervals Within T_o	164
N_{rr}	Number of Rake Receiver “Fingers”	171
F_f	Filter Center Frequency	192

List of Abbreviations

Abbreviation		Page
1G	First Generation	1
2G	Second Generation	1
3G	Third Generation	1
4G	Fourth Generation	1
BPL	Broadband Power Line	2
QoS	Quality of Service	2
GIG	Global Information Grid	3
NCW	Network Centric Warfare	3
DARPA	Defense Advanced Research Projects Agency	3
XG	neXt Generation	3
TTNT	Tactical Targeting Network Technology	3
JTRS	Joint Tactical Radio System	4
SDR	Software Defined Radio	4
CR	Cognitive Radio	4
SMSE	Spectrally Modulated, Spectrally Encoded	7
FM	Frequency Modulation	13
FDMA	Frequency Division Multiple Access	13
IP	Internet Protocol	13
VoIP	Voice over IP	13
MTS	Mobile Telephone System	14
IMTS	Improved MTS	14
MS	Mobile Station	14
BS	Base Station	15
MCS-L1	Mobile Communication System L1	15
NTT	Nippon Telegraph and Telephone	15

Abbreviation		Page
AM	Amplitude Modulation	15
AMPS	Advanced Mobile Phone Service	16
FSK	Frequency Shift Keying	16
NMT	Nordic Mobile Telephone	16
TACS	Total Access Communication System	16
ETACS	Extended TACS	16
SNR	Signal-to-Noise Ratio	16
NAMPS	Narrowband AMPS	16
JTACS	Japanese TACS	16
NTACS	Narrowband TACS	16
VLSI	Very Large Scale Integration	17
DSP	Digital Signal Processor	17
ASICs	Application Specific Integrated Circuits	17
TDMA	Time Division Multiple Access	17
GMSK	Gaussian Minimum Shift Keying	18
PSK	Phase Shift Keying	18
QPSK	Quaternary Phase Shift Keying	18
CDMA	Code Division Multiple Access	18
FL	Forward Link	18
RL	Reverse Link	18
GSM	Groupe Spécial Mobile	19
CEPT	Conférence Européenne Postes des et Télécommunication .	19
GSM	Global System for Mobile communications	19
FDD	Frequency Division Duplexing	19
FH	Frequency Hopping	19
REL P	Residually Excited Linear Predictive	19
LTP	Long-Term Predictor	19
CRC	Cyclic Redundancy Check	19

Abbreviation		Page
DAMPS	Digital AMPS	20
USDC	U.S. Digital Cellular	20
VSELP	Vector Sum Excited Linear Predictive	21
DQPSK	Differential QPSK	21
ISI	InterSymbol Interference	21
PDC	Personal Digital Cellular	21
JDC	Japanese Digital Cellular	21
DS-SS	Direct Sequence-Spread Spectrum	22
PN	Pseudorandom Noise	22
QCELP	Qualcomm Code Excited Linear Predictive	23
BPSK	Binary Phase Shift Keying	24
OQPSK	Offset QPSK	25
IMT-2000	International Mobile Telecommunications-2000	25
HSCSD	High Speed Circuit Switched Data	26
GPRS	General Packet Radio Service	26
EDGE	Enhanced Data rates for GSM Evolution	27
EDGE	Enhanced Data rates for Global Evolution	27
GERAN	GSM/EDGE Radio Access Network	27
MCS	Modulation and Coding Scheme	28
IR	Incremental Redundancy	30
ITU-R	International Telecommun. Union - Radiocommunication .	30
FPLMTS	Future Public Land Mobile Telecommunications System .	30
MSS	Mobile Satellite Service	31
TDD	Time Division Duplexing	31
3GPP	Third Generation Partnership Project	31
UMTS	Universal Mobile Telecommunication System	31
RSC	Recursive Systematic Convolutional	32
QAM	Quadrature Amplitude Modulation	33

Abbreviation		Page
IMT-DS	IMT Direct Spread	34
UTRA	Universal Terrestrial Radio Access	34
W-CDMA	Wideband CDMA	35
BER	Bit Error Rate	35
FOMA	Freedom Of Mobile multimedia Access	35
AMR	Adaptive Multi-Rate	36
ACELP	Algebraic Code Excited Linear Prediction	36
FEC	Forward Error Correction	36
HSDPA	High Speed Downlink Packet Access	36
DSCH	Downlink Shared CHannel	36
F-PDCH	Forward Packet Data CHannel	36
AMR-WB	WideBand AMR	36
HS-DSCH	High Speed DSCH	37
VSF	Variable Spreading Factor	37
AMC	Adaptive Modulation Coding	37
HARQ	Hybrid Automatic Repeat Request	37
EUL	Enhanced Uplink	37
EU-DCH	Enhanced Uplink Dedicated Channel	37
HSUPA	High Speed Uplink Packet Access	38
IMT-MC	IMT Multi-Carrier	38
EV	EVolution	38
RTT	Radio Transmission Technology	38
DV	Data and Voice	38
DO	Data Optimized or Data Only	38
HRPD	High Rate Packet Data	39
STS	Space-Time Spreading	39
OTD	Orthogonal Transmit Diversity	39
SMV	Selectable Mode Vocoder	39

Abbreviation		Page
F-FCH	Forward Fundamental CHannel	40
F-SCH	Forward Supplemental CHannel	40
BSC	Base Station Controller	40
RLP	Radio Link Protocol	41
DRC	Data Rate Control	41
DSC	Data Sector Control	41
MAC	Medium Access Control	41
VMR-WB	Variable-Rate Multimode Wideband	43
IMT-SC	IMT Single Carrier	44
UWCC	Universal Wireless Communication Consortium	44
EGPRS	Enhanced GPRS over ANSI	45
ANSI	American National Standards Institute	45
WTDMA	Wideband TDMA	45
IMT-TC	IMT Time Code	45
TD-SCDMA	Time Division Synchronous CDMA	45
ETSI	European Telecommunications Standards Institute	45
CATT	China Academy for Telecommunications Technology	46
IMT-FT	IMT Frequency Time	46
DECT	Digital European Cordless Telephony	46
DECT	Digital Enhanced Cordless Telecommunications	46
AMR	Adaptive Multi-Rate	47
IEEE	Institute of Electrical and Electronics Engineers	49
WLAN	Wireless Local Area Network	50
Wi-Fi	Wireless Fidelity	50
PHY	PHYsical network layer	50
OFDM	Orthogonal Frequency Division Multiplexing	50
CCK	Complementary Code Keying	50
DPSK	Differential BPSK	50

Abbreviation		Page
PBCC	Packet Binary Convolutional Coding	50
WMAN	Wireless Metropolitan Area Network	51
WiMAX	Worldwide inter-operability for Microwave Access	51
Mobile-Fi	Mobile Fidelity	52
MBWA	Mobile Broadband Wireless Access	52
B3G	Beyond 3G	52
E3G	Enhanced 3G	52
NGN	Next Generation Network	52
PAN	Personal Area Network	53
MAN	Metropolitan Area Network	53
WAN	Wide Area Network	53
MIMO	Multiple Input Multiple Output	55
CMIMOR	Cooperative MIMO Relaying	55
VAA	Virtual Antenna Array	55
LDPC	Low Density Parity Check	56
PCCC	Parallel Concatenated Convolutional Coding	56
SCCC	Serial Concatenated Convolutional Coding	56
CPM	Continuous Phase Modulation	57
MHPM	Multi-Hop Phase Coded Modulation	57
MA	Multiple Access	58
OFCDM	Orthogonal Frequency / Code Division Multiplexing	58
OFDMA	Orthogonal Frequency Division Multiple Access	58
ICI	InterCarrier Interference	58
MC-CDMA	Multi-Carrier CDMA	59
UWB	Ultra WideBand	60
WPAN	Wireless PAN	60
TH-UWB	Time Hopping UWB	62
DS-UWB	Direct Sequence UWB	62

Abbreviation		Page
MB-OFDM	Multi-Band OFDM	62
CSM	Common Signaling Mode	64
SWR	SoftWare Radio	64
TX	Transmitted	67
RX	Received	67
FFT	Fast Fourier Transform	73
IFFT	Inverse FFT	73
SCA	Software Communication Architecture	73
IDFT	Inverse Discrete Fourier Transform	79
AWGN	Additive White Gaussian Noise	81
LOS	Line-Of-Sight	85
TDL	Tapped Delay Line	90
COFDM	Coded OFDM	106
TDCS	Transform Domain Communication System	110
CSK	Cyclic Shift Keying	110
BCSK	Binary CSK	111
CI	Carrier Interferometry	113
CI/OFDM	CI coding with OFDM	113
PO	Pseudo-Orthogonal	114
CIMA	CI Multiple Access	115
PBI	Partial Band Interference	118
MAI	Multiple Access Interference	118
AR	Auto-Regressive	123
C.I.	Confidence Interval	126
N-UII	National Unlicensed Information Infrastructure	161
PPM	Pulse Position Modulation	163
PAM	Pulse Amplitude Modulation	163
PRI	Pulse Repetition Interval	164

Abbreviation		Page
BPPM	Biorthogonal Pulse Position Modulation	165
PDP	Power Delay Profile	173
S-V	Saleh-Valenzuela	174
NLOS	Non-LOS	175
SOI	Signal of Interest	175
ML	Maximum Likelihood	175
MPI	MultiPath Interference	180
ESD	Energy Spectral Density	184
PSD	Power Spectral Density	184
NBI	NarrowBand Interference	196

A GENERAL FRAMEWORK FOR ANALYZING, CHARACTERIZING, AND IMPLEMENTING SPECTRALLY MODULATED, SPECTRALLY ENCODED SIGNALS

I. Introduction

Once a novelty enjoyed by few, wireless communication has quickly become a necessity for many in today's rapidly-paced mobile world. The growing need for information centrality is manifested in the current wireless infrastructure architecture and vision. Over the past two decades, cellular communication has progressed from transmitting analog voice, to digital voice, to high-speed digital data. Data networks have advanced from supporting wired data exchange, to wireless data exchange, to wireless multimedia exchange of both voice and data. Regardless of communication system specifics (physical layer, medium access control layer, transport layer, etc.), several trends are readily apparent, including a desire for higher data rates, better quality, improved mobility, and unified access.

Generally, communication systems are defined in terms of the “generation” in which specific technologies emerged in commercial applications. For example, first generation (1G) cellular systems began operation in 1979 and provided simple *analog* voice capability. In the early 1990s, *digital* voice capabilities emerged which marked the start of second generation (2G) systems. As early as 2001, third generation (3G) systems were being introduced and provided *high-speed* digital data capabilities. In each case, a new cellular “generation” was born when a major evolutionary step was made in emerging communication technologies.

Future fourth generation (4G) systems may very well represent a revolutionary (versus evolutionary) step in communications. The 4G system goals involve fusing information from different devices and different networks to efficiently provide nearly universal, ubiquitous, high-speed communication access. Marconi, the father of mod-

ern radio [191], would have marveled at the possibilities if he could have foreseen such developments back in 1897.

1.1 Research Motivation

1.1.1 General Overview. The 4G communication system attributes are envied by civilian and military communicators alike. The civilian motivation for such communication capabilities are readily apparent – provide users a “one-stop shop” for all their communication needs. Commercial vendors hope to offer high-speed multimedia communication, internet access, and unlimited connectivity within a single system. Ideally, this single system will connect all information sources: cellular, wireless networks (e.g., IEEE 802.11/802.16), broadband power line (BPL), Bluetooth, radio and television, Firewire (i.e., IEEE 1394), ultra wideband (i.e., IEEE 802.15.3), and satellite communications.

These ideas for 4G civil communications are perhaps reminiscent of *Popular Science* futuristic concepts, yet several applications such as wireless homes are becoming a reality [84, 153, 157, 182, 209]. Previous home network applications were data centric in nature (e.g., ethernet, IEEE 802.11, and HomePlug1.0) but are evolving and becoming more entertainment centric in nature [84]. This evolution demands more from communication systems – improved quality of service (QoS), higher throughput, better security, etc. Some emerging home network systems that will be appearing soon include ethernet with priority, ultra wideband (IEEE 802.15.3a), IEEE 802.11 enhancements (better QoS and higher data rates), wireless Firewire, and HomePlugA/V [84]. Additionally, “last mile” technologies into the home will impact 4G system capabilities by providing wired or wireless high-speed data rates. Some of the last-mile technologies under consideration include: fiber-to-the-home (FTTH), cable modem, digital subscriber line (DSL), and worldwide inter-operability microwave access (WiMAX) [34, 84].

Military applications could also be well served by the transparent communication boundaries, which are conducive to rapid and global information sharing. Joint

Vision 2020 emphasizes the significance of information sharing amongst U.S., Allied, and coalition forces [96, 150]. The proposed conduit for bringing this vision to life is the Global Information Grid (GIG), which is being developed to globally interconnect users for information sharing in hopes of enabling Network-Centric Warfare (NCW). The end goal of information sharing is enhanced situation awareness – providing a technological edge both on and off the battlefield.

The relationship between the GIG, NCW, and ultimately full spectrum dominance, is illustrated in Fig. 1.1 where each level is enabled by the foundation upon which it rests. For example, establishing a GIG enables NCW, which in turn enables information superiority. This pyramidal structure makes sense as the GIG focus is to enable information flow and the NCW focus is to enhance situational awareness in warfare. An army that achieves the former will likely achieve the latter.

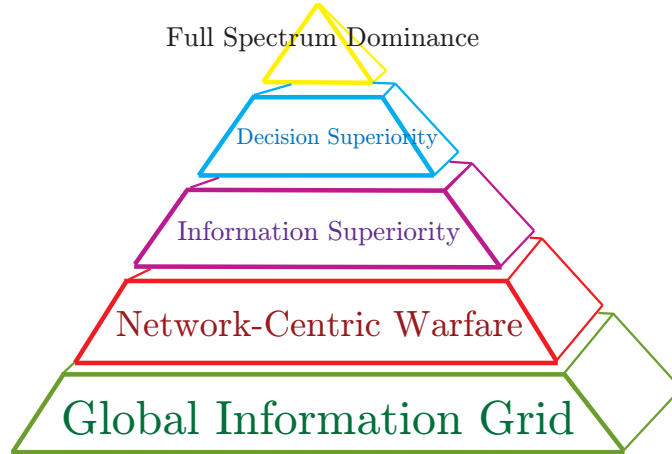


Figure 1.1: Global Information Grid (GIG) and Full Spectrum Dominance [150].

The Defense Advanced Research Projects Agency (DARPA) is funding several programs to support these efforts. The neXt Generation (XG) program is developing spectrum adaptation technologies and novel waveforms that can operate within a dynamically changing spectral environment. Another recent program called Tactical Targeting Network Technology (TTNT) focused on developing rapid data transfer technology for the purpose of getting information to end-users more quickly. Additionally, the U.S. Army has been spearheading the development of a Joint Tactical

Radio System (JTRS), a radio designed to support waveform flexibility and adaptivity. The JTRS program seeks to replace hardware radio components with software modules in what is now commonly called a software defined radio (SDR) architecture. The success of these programs will help enable 4G communication capability within both the military and civilian sectors [151, 152].

1.1.2 Technical Motivation. The simultaneous evolution of two major communication fields (cellular and wireless data networks) towards mobile, broadband capability has caused analysts to forecast a technological merger within future 4G systems [62, 88, 135, 217]. Not only will cellular and wireless LAN (WLAN) traffic merge, but Bluetooth, BPL, Firewire, radio and television, and satellite communications may also become more accessible from a single platform. This notional integrated concept is truly revolutionary and bringing it to fruition requires additional research in a number of key technology areas.

Numerous technologies have been identified as being “key” for enabling 4G capability, a few of which are described in Chapter II. To support higher data rates and enable signal coexistence (temporal and spectral), new multiple access schemes and smarter antenna concepts are being developed. To minimize signal perturbation errors, improved coding and multiple access schemes are being developed for integration with cognitive radio (CR) concepts. A detailed listing of potential 4G enabling technologies can be found in the Call for Papers for a recent communications conference [22]. The topics of interest include: multiple access schemes, radio transmission technologies, resource allocation issues, bandwidth on demand issues, variable rate modulation schemes, Turbo/LDPC coding, iterative decoding schemes, multi-user detection, channel modeling, convergence of 3G/WLAN/WPAN, software defined radio (SDR), multiple antenna techniques, and wireless application protocols.

According to the FCC, up to 95% of the available electromagnetic spectrum below 100 GHz goes unused at any time [132, 183]. Because bandwidth is a valuable commodity which is always in demand (and so much of it goes unused by both licensed

and unlicensed users), it is in the best interest of all parties (FCC and communication system designers) to develop smarter ways to cognitively use the available spectrum. In other words, systems should be designed to spectrally share, or spectrally coexist in, a given frequency band.

One way for radios to efficiently utilize spectrum, while decreasing spectral co-existence impacts, is to continuously monitor the changing channel conditions, traffic loads, interfering signals, and spectrum availability while generating waveforms that dynamically respond to these conditions. A radio which applies this technique is termed *cognitive*. Cognitive capability can be incorporated within SDR architectures that are striving to make more radio functions software-oriented and flexible, rather than hardware-oriented and inflexible. For discussion purposes, this research treats CR principles as a means for enhancing and advancing SDR functionality and capability. This synergistic union of concepts is referred to herein as *CR-based SDR*. That is, SDR capability provides the software controlled communication vehicle (core technology for air interface and waveform generation), the control and application of which is based on CR principles applied to spectral monitoring to achieve efficient spectrum use.

A top-level view for one possible 4G communication system using CR-based SDR principles is provided in Fig. 1.2. The transmitter and receiver blocks represent fully functional SDR architectures (wireless and/or mobile) which are driven by CR principles. Assuming the SDR architectures have some resemblance to current network stack layers, the upper layers are associated with the system brain and provide cognition. This “smart” section of the radio continuously monitors its surroundings and drives waveform adaptation to maximize system effectiveness. This process could involve direct communication with other radios which are perhaps part of a larger global “cognitive” network.

The cognitive transmit-receive cycle for the CR-based SDR is envisioned as follows. The brain chooses the means by which information is to be transmitted and

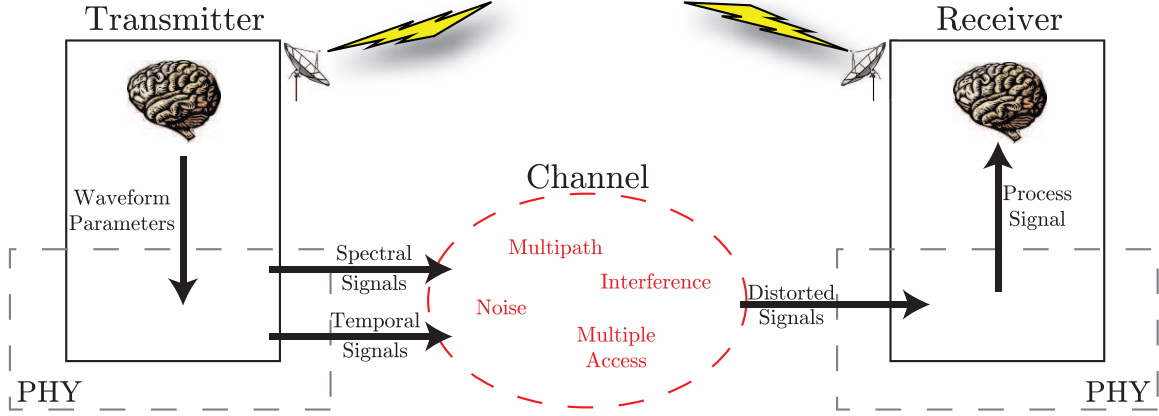


Figure 1.2: 4G revolution: A CR-based SDR communication system.

sends the appropriate waveform parameters to the physical (PHY) network layer. The PHY layer provides the air interface for waveform generation and transmission. The CR-based SDR may choose to transmit a temporally designed signal (e.g., ultra wide-band) or a spectrally designed signal (e.g., OFDM-based), both of which are leading candidates for future 4G waveform designs. In fact, multiple signals may be transmitted simultaneously if the radio further exploits spatial diversity (multiple antenna patterns and/or elements). In propagating through the channel, the transmitted signal experiences perturbations from a variety of sources: noise, signal reflections (multipath), other friendly signals (multiple access), and interference (intentional or incidental). Thus, the CR-based SDR receiver must be able to process the distorted signal(s) using methodology that mirrors the transmission process.

With proper selection of the PHY layer interface, the CR-based SDR architecture in Fig. 1.2 is one likely candidate for 4G communications (and beyond) because of its inherent flexibility and proclivity for implementing spectrally efficient signaling. One leading researcher has recently suggested that orthogonal frequency division multiplexing (OFDM) “commends itself” to CR applications by virtue of its flexibility and computational efficiency [82]. Furthermore, OFDM-based signals are designed in the spectral (frequency) domain and support high data rates, high spectral efficiency, and reduced multipath immunity [225]. These OFDM PHY layer attributes, coupled

with control and efficiency attributes of CR-based SDR architectures, provided the primary technical motivation and basis for the *spectrally modulated, spectrally encoded* (SMSE) framework developed herein.

1.2 Research Contributions

A general analytic framework has been recently proposed to accommodate the analysis, characterization, and implementation of *temporally* designed ultra wideband (UWB) signals [240]. The research presented herein uses this existing UWB framework as a springboard for developing a parallel analytic framework for representing *spectrally* designed signals [176, 177]. That is, a mathematical structure for SMSE signals is developed and characterized in support of ongoing hardware and software developments for 4G communications. For reasons highlighted in Section 1.1.2, emphasis is placed on CR-based SDR implementations using an OFDM PHY layer for data exchange.

Figure 1.3 graphically illustrates the primary research contribution: a unifying analytic framework for representing many spectrally designed signals. In this framework, a myriad of OFDM-based signals, as being proposed and developed for 4G communications, can be designed and implemented within a CR-based SDR architecture. Specific signal features are obtained through proper selection and instantiation of six key waveform design variables. Each paragraph below highlights a particular supporting element of the overall research contribution. Each of these elements has been independently assessed and their importance acknowledged through publication.

1.2.1 Unification Desired. The signals portrayed in the clouds in Fig. 1.3 are representative of what is being considered for 4G communications and is by no means an exhaustive listing of all possible SMSE signals. In fact, as wireless communications continue to evolve toward 4G and CR-based SDR implementations, other OFDM-based signaling techniques are likely to emerge. With each emerging technique, the pool of SMSE candidate signals expands accordingly. This expansion is

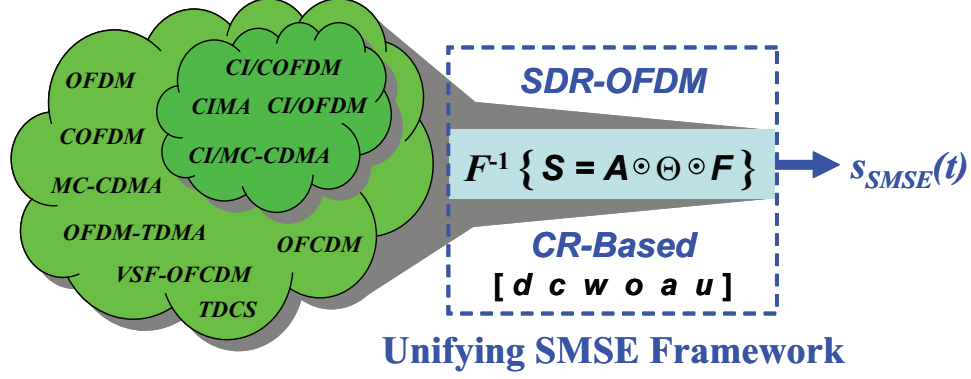


Figure 1.3: Research contribution: A unifying SMSE framework for OFDM-based signal implementation in a CR-based SDR architecture.

illustrated in Fig. 1.3 where the smaller inset cloud shows how the introduction of carrier interferometry (CI) expanded the potential signal set. As additional waveforms and techniques are introduced, the technical community becomes increasingly inundated with new acronyms and a misunderstanding of technical similarities and/or differences often occurs (ergo the cloud symbology used in Fig. 1.3). To better understand the significance of this issue, an extensive review of technical literature was conducted. This review exposed the evolutionary trail of 4G communication techniques and proved to be extremely valuable for the research, i.e., it provided the main research impetus by exposing a clear need for analytic commonality and operational unification of SMSE signals. The technical community substantiated this need and acknowledged its importance by publishing a survey based on the literature review [174]. Specific details on 4G system evolution and the path to future communications are provided in Chapter II.

1.2.2 Framework Established. Given the desire for analytic commonality and unification, a general analytic framework for SMSE signals was developed for CR-based SDR implementations [176]. In this case, six key waveform design variables are introduced to generate the desired OFDM-based SMSE waveforms. The actual variable instantiations for specific SMSE waveform implementations are controlled by the brain-empowered SDR. The analytic framework (spectral representation) is

a series of Hadamard vector products given by $\mathbf{S}_{SMSE} = \mathbf{A} \odot \mathbf{\Theta} \odot \mathbf{F}$, where the complex amplitude (\mathbf{A}), phase ($\mathbf{\Theta}$), and frequency (\mathbf{F}) factors are a function of the six waveform design variables (input data, coding, orthogonality, windowing, frequency component availability, and frequency component use). Specific framework details and its development are presented in Chapter III.

1.2.3 Applicability Demonstrated. Applicability is demonstrated using specific waveform design variable instantiations with the SMSE framework to generate analytic expressions for candidate 4G signals. The resultant SMSE expressions are then compared with published results and consistency determined. The utility and adaptivity of the framework is demonstrated for seven distinct SMSE signals using the variable instantiations provided in Chapter IV, and this application is presented in [176, 177].

1.2.4 Coexistence Maintained. In addition to analytic comparisons, modeling and simulation results are provided to reinforce framework utility. In this case, it is shown that expected communication performance is maintained within various SMSE coexistence scenarios, i.e., scenarios containing dense fading effects, partial band interference (PBI), and multiple access interference (MAI) [175]. Simulated bit error performance for various signals constructed with the unifying SMSE framework are shown to correlate well with theoretical predictions.

1.3 Research Assumptions

Definitions of mathematical symbols and terminology are provided throughout the document when the specific symbol or term is introduced. Results of all work presented should be interpreted within limits and constraints imposed by the assumptions which have been made. The following is a list of assumptions that have been made for the research.

- A cognitive “brain” exists in the upper network layer(s) of the radio architecture and is in constant communication with its surroundings and other users (e.g., a base station in a cellular network or a master node in an ad hoc network). The brain makes decisions on parameter selection and passes these parameters to the PHY layer of the radio for waveform generation and transmission. Hence, the research only addresses manipulation of the waveform design variables, not the selection or content of the variables.
- The specific location of the communication signals in the electromagnetic spectrum is irrelevant. Development and demonstration results are obtained at baseband, with results being readily extendable to an arbitrary spectral region.
- When working with discrete forms, sampling is performed to satisfy Nyquist criteria, i.e., the sampling frequency is greater than or equal to two times the highest frequency component being considered, $f_{\text{samp}} \geq 2f_{N_F}$.
- The transmitter and receiver platforms are relatively stable, i.e., the platforms are moving slowly enough such that channel conditions remain slowly-fading and the resultant Doppler shift is manageable.
- Demonstration results do not account for free-space path loss or large-scale fading loss. These are assumed known, and the fading demonstrations herein focus solely on small-scale fading loss from a multipath channel.
- The transmitter and receiver observe the same spectral environment or have an uninhibited ability to share knowledge of the electromagnetic environment. As a result, the transmitter and receiver use identical channel interference estimates during interference suppression demonstrations.
- The receiver perfectly estimates the phase shift on faded channel signals, which is a common assumption under slowly-fading channel conditions. Also, the receiver is able to estimate the channel fading coefficients for modeling wideband signals in fading channels.

- The receiver can perfectly synchronize to the communication symbol of interest using given header/pilot information.

1.4 Materials and Equipment

Simulations were run using **Matlab**[®] 7.0 on a desktop computer with a Pentium 4, 3.2 GHz processor and 4 GB of RAM *and* **Matlab**[®] 6.5 on a laptop computer with a Pentium 4, 1.7 GHz processor and 2 GB of RAM.

1.5 Dissertation Organization

This document is divided into six chapters and contains one appendix. Chapter II chronicles key developments using the evolutionary framework of cellular system deployment. These developments provide the technology background for wireless communications which will be used in subsequent chapters. Much of the information provided in Chapter II is taken from [174].

Chapter III provides the analytic framework for spectrally modulated, spectrally encoded (SMSE) signals. This framework allows for easy design *and* implementation of multiple candidate waveforms for 4G and CR-based SDR architectures. The SMSE framework is based on six key waveform design variables [176]. Analytic expressions are provided which encompass the complete transmitter-channel-receiver structure of an SMSE communication system.

The analytic framework of Chapter III is applied to seven distinct 4G-candidate waveforms in Chapter IV, with waveform design variable instantiation tables provided for each waveform. Using these instantiations, the SMSE framework provides analytic expressions matching those commonly found in literature [176,177].

Chapter V demonstrates the practical utility of the proposed SMSE framework via modeling and simulation. Baseline communication performance is provided for several waveforms from Chapter IV. Additional demonstrations are conducted which address the impact of multipath (to include block processing within a Rake receiver

structure), partial band interference, and multiple access interference. In each case, demonstration results are consistent with existing theoretical results, showing that the proposed framework is sufficient for accurately characterizing performance under these conditions.

Chapter VI provides some brief summary remarks and addresses the research impact on CR-based SDR implementation. Proposed ideas and topics for future research are provided as well.

Finally, Appendix A provides the signaling theory, analytic framework, and demonstration results from a parallel signal structure, i.e., one for ultra wideband signaling using temporal impulses. In light of the big picture offered in Fig. 1.2, Chapters III – VI address “spectral signal” design and Appendix A addresses “temporal signal” design.

II. Background: The Path to Future Communications

Early cellular networks used analog frequency modulation (FM) for voice communication and frequency division multiple access (FDMA) to accommodate multiple users. Despite their utility, these networks were often unstable and provided poor quality. Over the past 25 years, robust coding, modulation, and multiple access schemes have contributed greatly to improved, ubiquitous cellular service. Other portions of the cellular air interface have also evolved and greatly contributed to the present-day communication services, yet by primarily focusing on three aspects of the cellular air interface, one can more thoroughly understand wireless signaling issues in the existing and proposed cellular systems. Hence, this chapter chronicles the coding, modulation, and multiple access developments within the evolutionary framework of cellular communication systems from early first generation (1G) to future fourth generation (4G) systems.

In the 1980s, many people viewed cellular phones as luxury items. The bulky phones, engineering marvels to the common man, had just started supporting mobile voice telephony. The voice quality was poor and the access was sporadic in some markets, but customers appreciated the service. In the past 25 years, the cell phone has evolved from a mobile voice telephone to a mobile computer terminal. The newest, sleek phones support mobile customers by providing applications in communication, navigation, multimedia, entertainment, etc. Once perceived as luxury items, cell phones have become a necessity for many. A recent MIT survey listed cell phones as the most hated invention that Americans cannot live without, even more so than alarm clocks, televisions, razors, microwave ovens, computers, and answering machines [45].

Recently, it has become apparent that cellular technology is on a collision course with wireless network technology (i.e., networks based on IEEE 802 standards). Unlike cellular networks, which began by offering voice-only services and are now adding high-speed data services, wireless networks began by offering data-only services and are now adding voice over internet protocol (IP) (VoIP) services. Future wireless com-

munication will likely be very complex, with the next generation system combining cellular and wireless networks over an IP backbone [188, 217, 245].

This chapter chronicles the coding, modulation, and multiple access developments (changes and improvements) using the evolutionary framework of cellular communication system deployment. The evolutionary trail begins with an introduction of 1G cellular systems, passes through second generation (2G) and third generation (3G) systems, and ends with a forecast of enabling technologies for 4G systems. The generational/system contextual approach for presenting coding, modulation, and multiple access techniques permits a clearer understanding of the intertwining evolution of system *and* technology developments. Hence, this chapter is organized as follows. Sections 2.1 and 2.2 describe the pioneering 1G and 2G cellular systems, respectively. Migration from 2G into 3G systems is provided in Sections 2.3 and 2.4. Section 2.5 forecasts some enabling technologies for next generation 4G cellular systems, including a discussion of applicable coding, modulation, and multiple access technologies. Finally, Section 2.6 examines future communication beyond 4G, laying the background for the framework presented in Chapter III.

2.1 First Generation Systems (1G)

In 1946, the first public mobile telephone system (MTS) began operating in 25 American cities [30, 171, 219]. This system positioned a powerful transmitter on a tall building within a city and assigned mobile phones to a permanent single channel for sending and receiving via push-to-talk concepts. In the 1960s, the Improved MTS (IMTS) deployed and added dual channels for sending and receiving (i.e., full-duplexing) [30, 171, 219]. However, the system was impractical because of capacity constraints. In New York City, only 12 calls could be simultaneously supported over a 1,000 square mile area [171].

Demonstration of the cellular concept soon followed in 1968 at Bell Laboratories [30, 171]. The cellular concept featured two-way communication using a hexagonal, N -cell frequency reuse pattern with intracellular mobile stations (MS) controlled

by a base station (BS). Three components of the cellular concept bear further mention because they contribute greatly to increased capacity, the limiting factor in mobile telephony systems like IMTS: frequency reuse, sectorization, and handoff. By lowering the BS power in a given cell (i.e., reducing the cell size), the same frequency can be reused by another BS in a geographically remote cell. Furthermore, within a cell, directional antennas can be added to the BS to sector the cell (e.g., 60° or 120° sectors) and introduce greater capacity. Finally, handoff between base stations (hard or soft) dramatically increases the mobility afforded the customer, greatly expanding the user access area and also increasing capacity. For more information on other capacity-increasing measures and cellular concepts, the reader is directed to [171].

Numerous discoveries paved the way for modern cellular networks, but the true *enabler* of cellular communication was the invention of the microprocessor in 1971 [136]. This device was powerful enough to be embedded in a radio unit and provide the necessary processing power. Based on this development, 1G cellular systems, characterized by their analog nature, began operating within a decade following this invention.

The first commercial 1G cellular system was the Mobile Communication System L1 (MCS-L1), introduced in Japan in 1979 by Nippon Telegraph and Telephone (NTT) [30, 106, 171, 200]. MCS-L1 uses 600 frequency modulated (FM) full duplex 25 kHz channels in the 800 MHz band. In fact, all early 1G systems used FM and had channel bandwidths of 25 or 30 kHz despite the fact that two-way radios functioned with much less bandwidth using amplitude modulation (AM). The designers wanted voice quality comparable to wired telephones. Thus, they chose FM over AM because of its better noise immunity, despite the fact that FM systems require more bandwidth. Using frequency deviations of 6-12 kHz [159, 171] coupled with audio bandwidths of 3 kHz necessitated the use of 25 or 30 kHz channels. Designers also incorporated frequency partitioning to separate users, i.e., frequency division multiple access (FDMA). For MCS-L1, a 15 MHz spectral band was partitioned into 600 25 kHz channels.

The first commercial U.S. 1G cellular system arrived in 1983 when the Advanced Mobile Phone Service (AMPS) was introduced [171]. AMPS supports 832 FM full duplex 30 kHz channels in the 800 MHz band. AMPS also maintains a control channel at 10 kb/s, modulated using frequency shift keying (FSK) [159, 171]. To protect the FSK data on the control channel, a Manchester (or biphase) coding is applied along with a block code [171].

European 1G systems contain similar characteristics to the Japanese MCS-L1 and American AMPS systems [30, 159, 171]. Nordic Mobile Telephone (NMT) began operation in Scandinavia in 1981 and supports 1000 FM 25 kHz channels in the 900 MHz band. Total Access Communication System (TACS) and Extended TACS (ETACS) began operation in the United Kingdom in 1982 and 1985 and are very comparable to AMPS. Slightly smaller bandwidths yield slight decreases in signal-to-noise ratio (SNR) and coverage compared to AMPS. C-450 began operation in Germany in 1985 and supports 573 FM 10 kHz frequency-interleaved channels in the 450 MHz band. Radiocom 2000 began operation in France in 1985 and supports 560 FM 12.5 kHz frequency-interleaved channels in the 200 MHz band.

Despite frequency reuse benefits, capacity remained a key limitation of 1G systems. Ergo, in the late 1980s, new American and Japanese 1G systems reduced channel bandwidth in an attempt to improve capacity. In North America, narrowband AMPS (NAMPS) deployed which boosted the capacity three-fold by splitting each 30 kHz AMPS channel into three 10 kHz channels (frequency deviation decreased from 12 to 5 kHz) [138, 171]. In Japan, NTT deployed a high capacity system, which quadrupled capacity by reducing channel bandwidth from 25 to 6.25 kHz (using smaller channels and frequency interleaving) [159]. Japan also deployed the Japanese TACS (JTACS) and narrowband TACS (NTACS) systems, which are very similar to the NAMPS and NTT high-capacity systems.

2.2 Second Generation Systems (2G)

In the late 1980s, very large scale integration (VLSI) and signal processing technology matured, paving the way to the digital era. Just as the microprocessor was the enabler for 1G cellular, the digital signal processor (DSP) was the enabler for 2G cellular. Application specific integrated circuits (ASICs) led to reduced mobile phone sizes, and new signal processing features (with faster chips) contributed to soaring computing rates [17]. At the same time, 1G systems were reaching their capacity in city markets. Hence, as digital technology became more prevalent, analog 1G systems were progressively replaced by newer 2G cellular systems beginning in the early 1990s. 2G systems are characterized by their digital nature, offering better voice quality and rudimentary data services. 2G systems were designed for voice communication operation via circuit switching to guarantee link availability for telephone calls.

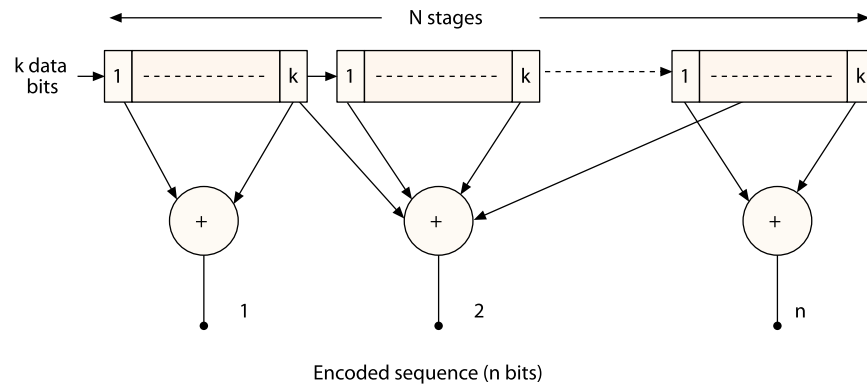


Figure 2.1: General convolutional encoder with rate $R = k/n$ (bits in over bits out) and constraint length $K = N$ (number of stages) [171].

Because 2G systems are inherently digital, they were the first cellular systems to employ block and/or convolutional coding (see Fig. 2.1) for error detection and correction on traffic channels. The introduction of such coding allowed for clearer voice transmissions and more reliable data transmission over fading channels. Furthermore, the digital nature of 2G systems naturally enabled the use of time and/or frequency division alternatives to separate users. Excluding the CDMAOne 2G system, time division multiple access (TDMA) was incorporated with FDMA in all 2G systems to separate users within designated frequency bands (see Fig. 2.2). The in-

troduction of TDMA subsequently spawned the use of additional digital modulations such as Gaussian minimum shift keying (GMSK) and quaternary phase shift keying (PSK) (QPSK). Code division multiple access (CDMA) was also considered an alternative for 2G implementation. However, only the Qualcomm-developed CDMAOne adopted it for multiple access implementation. Although researchers generally understood the advantages of CDMA at the time [98, 116], it was not broadly incorporated into other 2G systems for two primary reasons: 1) CDMA technology was not standardized until 1993 [171] which was about the same time that other 2G systems were deploying, and 2) TDMA-based architectures were somewhat more mature at the time, e.g., a digitally enhanced TDMA variant of AMPS, called DAMPS, was under development and the TDMA-based Groupe Spécial Mobile (GSM) system was chosen as a unifying European standard.

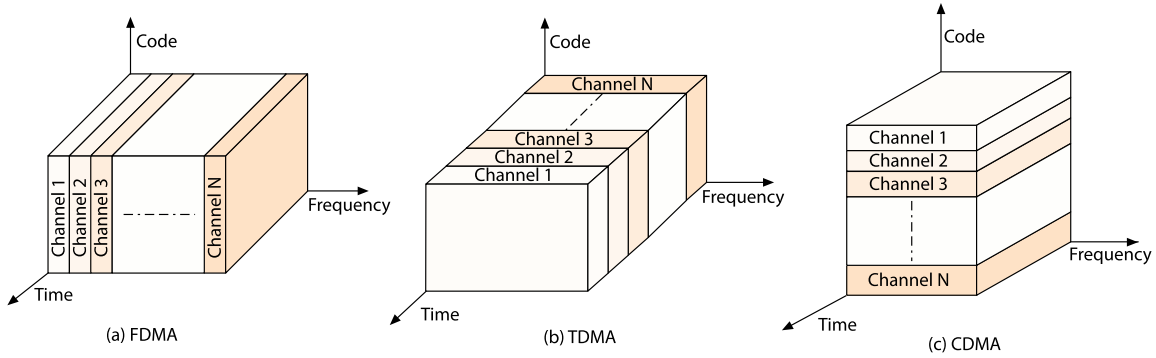


Figure 2.2: Illustration of various Multiple Access (MA) schemes: (a) Frequency Division (FDMA), (b) Time Division (TDMA), and (c) Code Division (CDMA) [171].

Four 2G systems, designed to operate in the 810 to 960 MHz cellular band, are described in greater detail in the following subsections. These systems are grouped by their multiple access technique, TDMA (see Sect. 2.2.1) and CDMA (see Sect. 2.2.2). For all subsequent references, the *base-to-mobile* transmission is called the downlink or *forward link* (FL), and the *mobile-to-base* transmission is called the uplink or *reverse link* (RL).

2.2.1 TDMA Systems.

2.2.1.1 *Groupe Spécial Mobile (GSM).* The Groupe Spécial Mobile (GSM) emerged from the Conférence Européenne Postes des et Télécommunication (CEPT) and was commercially introduced in 1991 [103]. Prior to this, different standards were used throughout the European continent. The emergence of GSM unified pan-European service and provided a single standard across the continent. In 1992, GSM was redesignated as the Global System for Mobile communications [171]. As of January 2004, GSM was the largest 2G system with over one billion GSM-compatible phones in use worldwide [213].

GSM uses both FDMA and TDMA to accommodate multiple users and frequency division duplexing (FDD) for FL/RL separation. In this case, FL transmissions occur in the 935-960 MHz band and RL transmissions occur in the 890-915 MHz band. In practice, the 25 MHz of available spectrum is divided into 124, 200 kHz channels with a 100 kHz guard band on the upper and lower ends of the spectrum [171]. Because the channels are large, GSM is sometimes referred to as broadband TDMA and some resolution of multiple signals is possible [159]. Each 200 kHz channel transmits information in 4.615 ms frames (216.7 frames/s) at an effective bit rate of 270.83 kb/s (eight slots/frame and 156.25 bits/slot) – see Fig. 3. GSM also supports slow frequency hopping (FH) at 217 hops per second, i.e., the system can hop to a new frequency after each TDMA frame [171]. FH, a spread spectrum technique in which the sequence of transmission frequencies is determined by a pseudorandom code, allows the system to potentially avoid areas of high interference at the cost of reduced maximum data rate.

A residually excited linear predictive (RELP) coder, enhanced by a long-term predictor (LTP), is used to code speech in GSM. The coder provides 260 bits per 20 ms block of speech. Error protection is applied to the most important 182 bits, including cyclic redundancy check (CRC) parity coding on the most important 50 bits followed by a rate 1/2 convolutional code of constraint length $K=5$. The 378

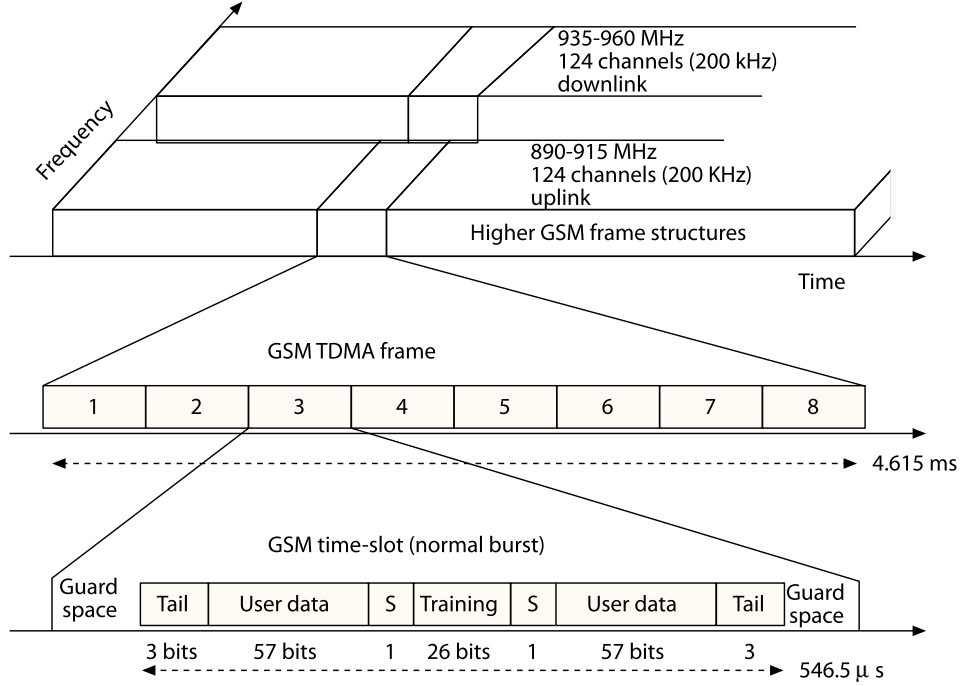


Figure 2.3: Global System for Mobile (GSM) communications TDMA/FDMA frame structure [190].

bits out of the error protection coder are concatenated with the 78 non-protected bits, forming a block of 456 bits per 20 ms speech frame for a gross data rate of 22.8 kb/s. Interleaving over eight time slots is subsequently used to minimize burst errors and channel fading effects. The modulation scheme, Gaussian minimum shift keying (GMSK), is a form of digital FM modulation that minimizes occupied bandwidth while increasing channel capacity. GMSK uses a pre-transmission Gaussian pulse shaping filter with binary digits transmitted at frequency offsets of ± 67.708 kHz ($1/4$ of the GSM carrier bit rate) about the carrier frequency [171].

2.2.1.2 Digital AMPS (DAMPS). Digital AMPS (DAMPS) is the 2G follow-on to the original 1G analog AMPS. The IS-54 standard was established in 1990 for a dual AMPS/DAMPS system. IS-54 Revision C, published in 1996, was synonymous with the IS-136 standard [30, 159]. Because it was widely deployed in the U.S., DAMPS is sometimes referred to as U.S. Digital Cellular (USDC) [171]. DAMPS provides six times the capacity of AMPS and was designed to share the same

base stations, frequencies, and frequency reuse plan as AMPS. This design allowed for a gradual upgrade from AMPS to DAMPS and provided simplified backwards compatibility. However, it also restricted DAMPS to narrowband TDMA operation with 30 kHz channels, much smaller than GSM. Hence, multiple signals cannot be resolved in a DAMPS system [159].

DAMPS uses both TDMA and FDMA with FDD for multiple access and FL/RL separation. Specifically, it divides the 25 MHz spectrum into 30 kHz channels, which are time divided into six slots to support three full-rate users or six half-rate users. IS-54 uses the same 10 kb/s FSK modulation as AMPS for FL and RL *control* channels. However, voice *traffic* channels use differentially encoded QPSK modulation at a channel rate of 48.6 kb/s. IS-136 upgraded the control channels so they also use 4-ary modulation versus FSK [171].

Each DAMPS frame is 40 ms (25 frames/sec) and contains 324 bits within each 6.67 ms slot for an effective bit rate of 48.6 kb/s. Speech is encoded using the vector sum excited linear predictive (VSELP) coder that yields a speech frame containing 159 bits every 20 ms for a bit rate of 7.95 kb/s. The 77 most important speech bits are error protected using a rate 1/2 convolutional code with constraint length $K = 6$. Additionally, the 12 most significant bits are further protected using a 7-bit CRC block code, yielding a gross bit rate after speech and channel coding of 13 kb/s. The resultant 260 coded speech bits are interleaved over two successive time slots to protect against burst errors and channel fading. DAMPS uses a spectrally-efficient, pulse-shaped, 4-phase modulation scheme, $\pi/4$ differential QPSK (DQPSK). Pulse shaping with a square-root raised cosine filter minimizes intersymbol interference (ISI) [171].

2.2.1.3 Personal Digital Cellular (PDC). Another large 2G system is Pacific Digital Cellular (PDC), also known as Japanese Digital Cellular (JDC) or Personal Digital Cellular [171]. PDC was developed in 1991 and began operation in Japan in 1993, replacing the NTT and JTACS analog systems. PDC uses TDMA with FDMA to accommodate multiple users. The deployment of PDC provided a

much needed capacity increase in the congested 1G Japanese cellular bands. As of December 2002, PDC had over 60 million subscribers but is slowly being phased out in favor of current 3G systems [48].

PDC operation is similar to the DAMPS system described above, with the primary differences being channel spacing and speech/channel coding. PDC uses 25 kHz channels (vice 30 kHz) and supports a channel data rate of 42 kb/s (vice 48 kb/s). Speech is encoded using a VSELP coder at 6.7 kb/s (unlike DAMPS VSELP speech coding at 7.95 kb/s). Channel coding protects the bits using a rate 9/17 convolutional code with constraint length $K = 5$. A combined 11.2 kb/s coding rate per user is provided by the joint speech and channel coding [171]. Perhaps the main contribution from PDC is that it introduced antenna diversity at the MS, which boosts system multiple access capability [50, 159, 226].

2.2.2 CDMA Systems.

2.2.2.1 CDMAOne. CDMAOne, or standard IS-95A, is the only 2G cellular system using “narrowband” CDMA technology (“wideband” CDMA is described later). IS-95A is another large 2G system and was widely deployed by 1996. The relatively late deployment of IS-95A, which occurred several years after other 2G systems, was primarily due to the TIA CDMA standard not being published until 1993 [171]. A comparison of CDMAOne and other 2G systems is shown in Table 2.1.

Unlike other 2G systems, IS-95A allows simultaneous transmissions in the same frequency band via CDMA (see Fig. 2.2). CDMA is a by-product of using direct sequence spread spectrum (DS-SS) techniques to spectrally spread the signal. DS-SS/CDMA signal discrimination is provided by assigning each user a unique pseudo-random noise (PN) code having low correlation with all other PN codes. Compared to the FH spread spectrum technique (as used in GSM), DS-SS allows for a higher maximum data rate (i.e., no time is wasted hopping to new frequencies), but the synchronization time is longer.

Table 2.1: Comparison of 2G systems in the cellular band [47, 171, 204, 219].

Parameter	GSM	PDC	DAMPS / USDC (IS-54 / IS-136)	CDMAOne (IS-95A)
Multiple Access	TDMA/FDMA	TDMA/FDMA	TDMA/FDMA	CDMA
Duplex Mode	FDD	FDD	FDD	FDD
Duplex Spacing	45 MHz	130 MHz	45 MHz	45 MHz
Freq (MHz)	890 – 915 (RL) 935 – 960 (FL)	810 – 830 (RL) 940 – 960 (FL)	824 – 849 (RL) 869 – 894 (FL)	824 – 849 (RL) 869 – 894 (FL)
# Carriers	124	800	832	10
# Ch/Carrier	8 (full-rate)	3 (full-rate)	3 (full-rate)	variable
# Ch/Cluster	$124 \times 8 = 992$	$800 \times 3 = 2400$	$832 \times 3 = 2496$	variable (≈ 1280)
Modulation	GMSK (BT = 0.3)	$\pi/4$ DQPSK	$\pi/4$ DQPSK	BPSK
Ch Bandwidth	200 kHz	25 kHz	30 kHz	1.25 MHz
Carrier Bit Rate	270.833 kb/s	42 kb/s	48.6 kb/s	1.288 Mb/s
Spectrum Eff	1.35 b/s/Hz	1.68 b/s/Hz	1.62 b/s/Hz	1.03 b/s/Hz
Speech Coding	RELTP-LTP: 13 kb/s	VSELP: 6.7 kb/s	VSELP: 7.95 kb/s	QCELP: 8 kb/s
Ch Coding	CRC with Conv, $R = 1/2, K = 5$	CRC with Conv	7 bit CRC with Conv, $R = 1/2, K = 6$	Conv, $R = 1/2, K = 9$ (FL) Conv, $R = 1/3$ (RL)
Frame Size	4.6 ms	40 ms	40 ms	20 ms
Interleaving	40 ms	2 slot	2 slot	Block, 20 ms
Pwr Control	Yes	Yes	Yes	Yes

IS-95A divides the 25 MHz of FL and RL spectrum into 1.25 MHz bands and uses FDD for separation. The basic data rate is 9.6 kb/s, but an extension exists which increases this to 14.4 kb/s [171]. Bits at that data rate are multiplied by the PN code with a chipping rate of 1.2288 Mchips/sec, yielding a processing gain of 128 (21 dB). Thus, the power of interfering signals is decreased by approximately 21 dB at the receiver when the PN code is reapplied to despread the signal. While DS-SS techniques also provide low probability of intercept and anti-jam benefits, IS-95A uses DS-SS primarily for its multiple access benefits [204].

On the IS-95A FL (see Fig. 2.4), speech signals are encoded with a Qualcomm code excited linear predictive (QCELP) coder and processed in 20 ms frames containing 192 bits for a bit rate of 9.6 kb/s. *All* bits are protected (unlike GSM and DAMPS) using a rate 1/2 convolutional code with constraint length $K = 9$, yielding a channel bit rate of 19.2 kb/s. Coded bits are interleaved using a 20 ms block interleaver, with 384 bits interleaved every 20 ms [171, 204].

Next, three separate codes are applied to the interleaved, coded bits for privacy, channelization, and BS identification as indicated in Fig. 2.4 [204]. The first code, a privacy code, is a long PN code implemented via a maximal-length, 42-stage shift

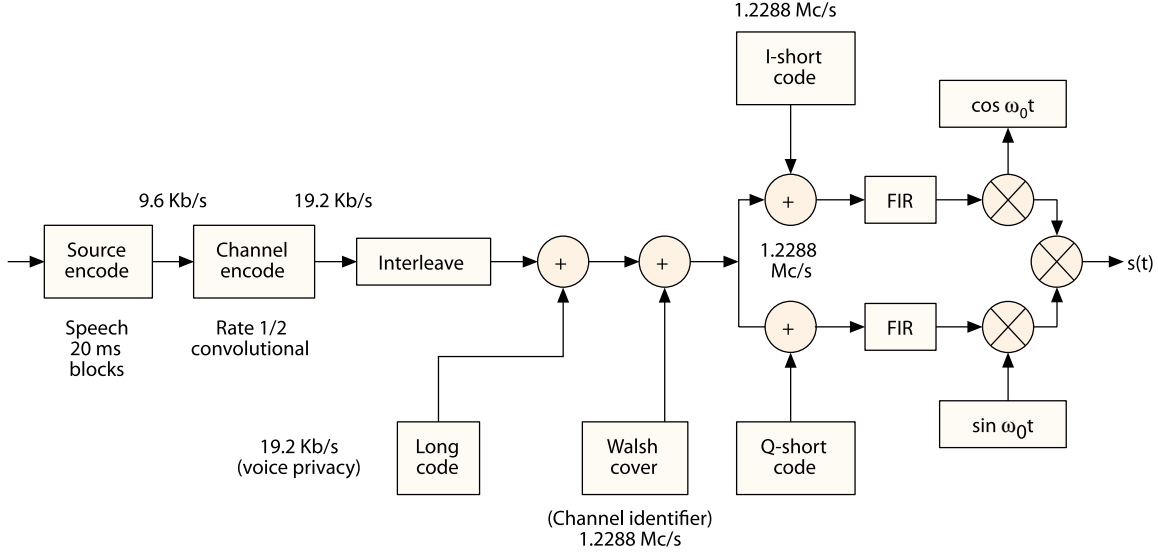


Figure 2.4: Block diagram of IS-95 forward link transmitter [204].

register, at 1.2288 Mchips/sec. Each MS is assigned a timing offset of this long code (it repeats every 41 days) for privacy (i.e., scrambling). This code is applied in decimated fashion, i.e., only every 64th bit of the code is actually used (this doesn't detract from the code's uniqueness) and the channel bit rate remains at 19.2 kb/s. The second code, a channelization (or user separation) code, uses 64 orthogonal sequences (Walsh codes, up to 61 of which can be used for traffic), and they are applied at the same chipping rate as the long privacy code. The third code, a short code used for BS identification, is produced by a 15-stage register and repeats every 26.67 ms. This code scrambles the signals, maintaining mutual randomness among users of different cells, via complex QPSK spreading. The spread signal is data modulated using binary phase shift keying (BPSK) [204].

The IS-95A RL contains several key differences from the FL [171,204]. First, it uses a rate 1/3 convolutional encoder which raises the data rate to 28.8 kb/s (from 19.2 kb/s on the FL). The added RL robustness is important since the BS receiver uses non-coherent detection and intracellular interference exists. Second, the RL does not use channelization coding; only privacy and short BS identification codes are needed. The long privacy code is not implemented in decimated fashion on the RL, so it provides for

privacy *and* user separation. Third, power control is required on the RL to mitigate near-far problems. Fourth, the RL spread signal is modulated using BPSK in offset QPSK (OQPSK) fashion for better spectral shaping and synchronization [171, 204]. Finally, Rake receivers are used on both the FL and RL to help combine multipath components such that the SNR increases. Mobiles and base stations use 3-finger and 4-finger Rake receivers, respectively [204].

2.3 Toward 3G Systems

Fundamentally, 2G networks use telephone-like circuit switching that is arguably optimal for voice communications (which require low latency) but is relatively inefficient for data communications which appear more burst-like in nature. This spectral inefficiency is the main reason why 2G systems are unable to transmit higher data rates. A desire for higher data rates (e.g., as required for multimedia applications) motivated the development of 3G systems, the characteristics of which are identified in the International Mobile Telecommunications-2000 (IMT-2000) standard. Requirements within IMT-2000 include: backward 2G compatibility, higher system capacity, multimedia support, and high-speed packet data service [198]. Systems should support data rates up to 2 Mb/s for stationary environments, 384 kb/s for pedestrian environments, and 144 kb/s for highly mobile environments.

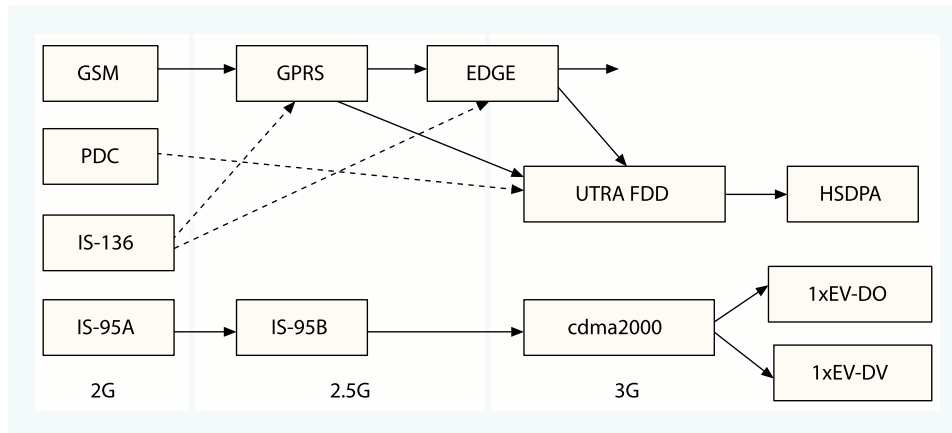


Figure 2.5: Evolution of cellular systems from 2G through 2.5G to 3G [251].

Intermediate systems were introduced beginning in the late 1990s to achieve medium data rates before activating 3G systems. As illustrated in the 2G to 3G evolution graphic in Fig. 2.5, these systems are designated “Towards 3G” (sometimes 2.5G) because they perform better than 2G, but they don’t yet meet the IMT-2000 3G standard. Four specific intermediate systems are described next grouped by access method, TDMA and CDMA.

2.3.1 TDMA Systems.

2.3.1.1 High Speed Circuit Switched Data (HSCSD). The first GSM upgrade was the High Speed Circuit Switched Data (HSCSD) system. HSCSD is a software-only upgrade that bundles time slots to get higher theoretical data rates of 115.2 kb/s (14.4 kb/s in 8 slots) [190]. Realistically, a MS is unable to request all eight time slots, so the advertised maximum throughput is 57.6 kb/s. Given system constraints, an expected data rate might be 28.8 kb/s [103].

Table 2.2 shows the theoretical maximum and realistic data rates achievable by various systems based upon the GSM core network. The theoretical maximum rates shown are typically based upon scenarios containing a stationary single user which occupies all available time slots while using the weakest coding scheme. In reality, limiting factors such as the number of users, handset capability/variability (manufacturer dependent), and channel fading can greatly reduce data rates [103]. However, the greatest practical limiting factor may be economics; a system cannot generally afford to assign all available time slots to a single user.

2.3.1.2 General Packet Radio Service (GPRS). The General Packet Radio Service (GPRS) is a GSM upgrade that emerged in 2001 and allows data to flow more easily via packet switching, making GPRS better suited than HSCSD to transmit higher data rates. Specifically, GPRS overlays a packet based interface with the existing circuit switched GSM network. Information is divided into packets before transmission and reassembled at the receiver.

Table 2.2: Comparison of data rates for GSM-based systems [103].

System	Theoretical Maximum	Realistic
GSM	> 40 kb/s	9.6 kb/s
HSCSD	115.2 kb/s	28.8 kb/s
GPRS	171.2 kb/s	40 kb/s
EDGE	384 kb/s	60-70 kb/s
UTRA FDD (UMTS)	2 Mb/s	100 kb/s

Table 2.3: GPRS data rates in kb/s [190].

Number of Slots	CS-1	CS-2	CS-3	CS-4
1 slot	9.1	13.4	15.6	21.4
2 slots	18.2	26.8	31.2	42.8
3 slots	27.2	40.2	46.8	64.2
4 slots	36.2	53.6	62.4	85.6
5 slots	42.3	67.0	78.0	107.0
6 slots	54.3	80.4	93.6	128.4
7 slots	63.4	93.8	109.2	149.8
8 slots	72.4	107.2	124.8	171.2

Theoretically, 171.2 kb/s data rates are attainable with GPRS (see Table 2.3) [190]. However, this rate is only achievable using the weakest coding scheme (CS) (best channel conditions) while occupying all eight time slots. Conversely, using the strongest coding scheme (poorest channel conditions) while occupying one slot generates a 9.1 kb/s data rate. Stationary users near the BS with a strong signal require less coding protection than mobiles with a weak signal. GPRS data rates are likely to be restricted with realistic rates ranging from 10 to 115 kb/s and average rates around 40 kb/s [103]. Finally, GPRS uses the same GMSK modulation as GSM.

2.3.1.3 Enhanced Data Rates for GSM Evolution (EDGE) . The

Enhanced Data rates for GSM Evolution (EDGE) system was designed to increase GSM/GPRS data rates. The “G” in EDGE was later redefined as Global, and EDGE continues to deploy worldwide [103]. The increased capability of EDGE results from using a modified air interface, called the GSM/EDGE radio access network (GERAN),

Table 2.4: EDGE vs GPRS: coding schemes, modulations, and data rates for one slot (kb/s) [43, 127].

System	Coding Scheme	Modulation	Data Rate
GPRS	CS1	GMSK	8.0
	CS2	GMSK	12.0
	CS3	GMSK	14.4
	CS4	GMSK	20.0
EDGE	MCS1	GMSK	8.4
	MCS2	GMSK	11.2
	MCS3	GMSK	14.8
	MCS4	GMSK	17.6
	MCS5	8-PSK	22.4
	MCS6	8-PSK	29.6
	MCS7	8-PSK	44.8
	MCS8	8-PSK	54.4
	MCS9	8-PSK	59.2

which provides nearly three times the capacity of GPRS using the same TDMA frame structure and 200 kHz bandwidth as GSM/GPRS.

EDGE can use GMSK or 8-ary phase shift keying (PSK) (see Fig. 2.6) modulation (in addition to GMSK) with each symbol representing three bits. By packing three bits into each communication symbol, more data is transferred in each time slot [103]. “As HSCSD makes it possible to use several time slots for each user, and GPRS introduces packet data services, EDGE allows transferring more data in each time slot” [103]. The cost of increased capacity is that the signal quality must be better. Thus, EDGE provides nine different modulation and coding schemes (MCS) with data rates varying from 8 to 60 kb/s for one slot (see Table 2.4). It is noted here that data rates reported in Table 2.3 and 2.4 for one GPRS slot are not identical. Upon reviewing the sources considered [43, 127, 190], it was determined that the inconsistencies are a result of the sources using different methods for calculating data rate. Accounting for the differences, the sources considered would report statistically identical results. As in GPRS, appropriate selection of the modulation and coding scheme is a function of estimated channel conditions, a process called *link adaptation*.

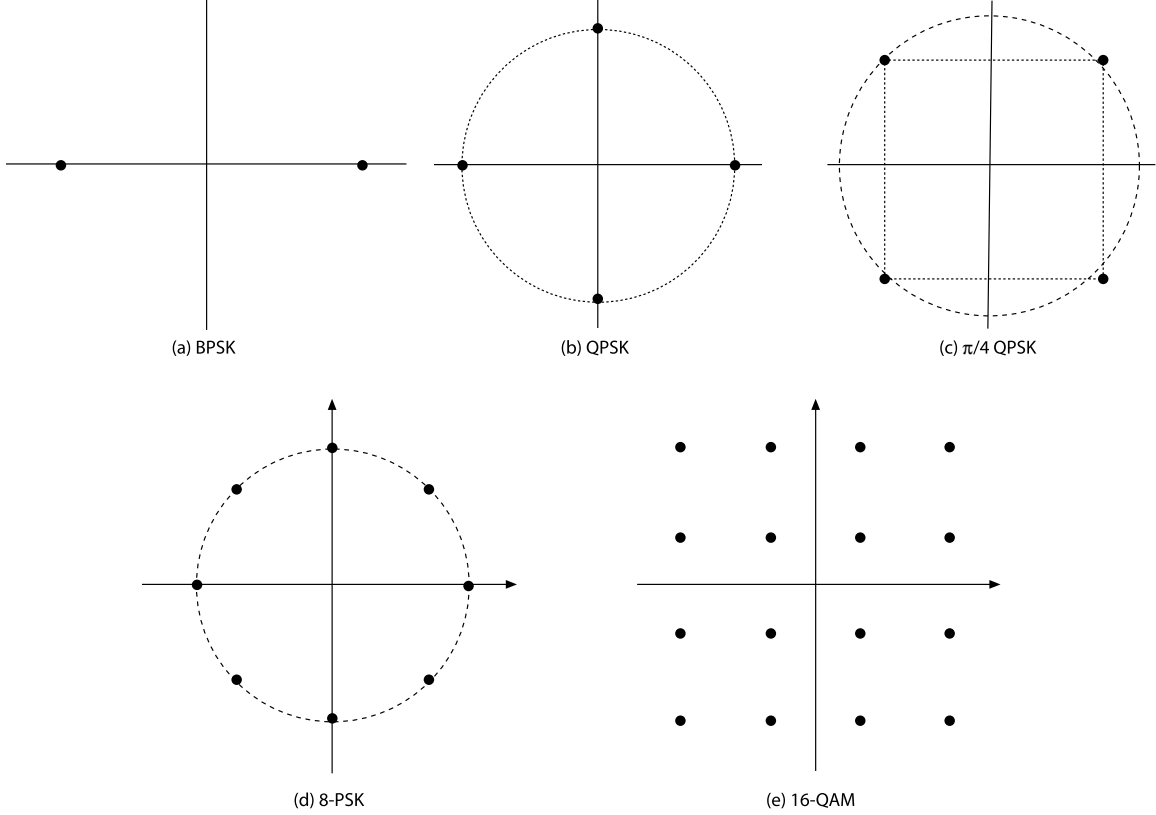


Figure 2.6: Data modulation constellations: a) Binary Phase Shift Keying (BPSK), b) Quaternary Phase Shift Keying (QPSK), c) $\pi/4$ QPSK, d) 8-ary Phase Shift Keying (8-PSK), and e) 16-ary Quadrature Amplitude Modulation (16-QAM) [171].

EDGE also adds an ability to retransmit a packet that is not decoded properly with a more robust MCS by a process called *resegmentation* (not available in GPRS). For example, if a user transmits three packets with a weak coding scheme (e.g., CS4) and the last packet is rejected, the GPRS system must continue to transmit the third packet with CS4. In EDGE, packets can be retransmitted using stronger coding schemes if necessary [43]. Resegmentation allows EDGE to be very aggressive in selecting an appropriate MCS. For example, an EDGE system can theoretically transmit all packets using MCS9 (the weakest coding scheme) to provide a high data rate and only use more robust coding for rejected packets. If no channel information is available, the system subsequently selects more robust coding schemes for rejected packets until the receiver gets all of the packets. This process of gradually transmit-

ting rejected packets with more robust coding (while the receiver combines accepted packets) is called *incremental redundancy* (IR).

Finally, EDGE features improved interleaving [43]. GSM/GPRS systems interleave a block of communication information over four bursts. If the GSM/GPRS systems are using their FH capability, the electromagnetic environment changes on a per-hop or per-burst basis. Consequently, one burst could very easily be sent over poor channel conditions and be lost. If one of the four bursts is not received, the GSM/GPRS transmitter must resend all four bursts. EDGE modifies this scheme such that the four bursts are divided into two halves. Therefore, if one burst is not received, only the first or second half of the block of information must be resent.

2.3.2 CDMA Systems.

2.3.2.1 IS-95B. The IS-95B standard was first published in 1995 (two years after IS-95A) and combines IS-95A, ANSI-JSTD-008 (an industry standard for CDMA in the PCS1900 band), and TSB-74 (an IS-95A variant that increases rates to 14.4 kb/s). Like GPRS, IS-95B provides higher data rates using packet switching. Specifically, IS-95B offers up to 115.2 kb/s packet-switched data in addition to voice services [204].

2.4 Third Generation Systems (3G)

The definition of a 3G system is contained within the IMT-2000 standard. Table 2.5 compares 2G and 3G systems for several key characteristics. The International Telecommunication Union - Radiocommunication (ITU-R) sector created the IMT-2000 standard with the original intent to unify all wireless systems (cellular, wireless local area networks (WLANs), satellite networks, and fixed wireless links) in the same frequency bands and on ATM-based protocols (under the FPLMTS acronym for Future Public Land Mobile Telecommunications Systems) [171]. The fixed and WLAN components were soon discarded from the IMT-2000 vision since fixed wire-

Table 2.5: Comparison of 2G and 3G systems.

Characteristics	2G	3G
Service	Voice, low-rate data	Multimedia
Data Rates	Up to 14.4 kb/s	Up to 2 Mb/s
Switching Method	Circuit switching	Packet routing

less operates better on higher frequencies, and WLANs can achieve higher data rates in unlicensed bands. Hence, the IMT-2000 standard only has cellular and satellite components. The satellite component, also called mobile satellite service (MSS), is designed to provide communication services when a user is outside the range of any land-based BS [42]. Further references herein to IMT-2000 refer to the cellular component of the standard.

In June 1996, the ITU-R invited proposals for cellular and satellite 3G concepts [198]. Although the original goal was to have a single worldwide cellular standard, down-selection to a single mode of operation for IMT-2000 proved difficult. In the summer of 1998, the ITU-R received 15 proposals for 3G system operation. In 2000, the final IMT-2000 recommendation ITU-R M.1457 featured five modes of operation: Direct Spread (IMT-DS), Multi-Carrier (IMT-MC), Time Code (IMT-TC), Single Carrier (IMT-SC), and Frequency Time (IMT-FT) [41, 198]. Of the five modes, three use CDMA (DS/MC/TC), three use TDMA (TC/SC/FT), one uses FDMA (FT), three use paired spectrum (DS/MC/SC), and two use unpaired spectrum (TC/FT) – see Fig. 2.7. Paired/unpaired spectrum implies that FDD or time division duplexing (TDD) is used for FL and RL separation, respectively.

The pursuit of 3G technologies and the process of down-selecting IMT-2000 candidate concepts spawned two major organizations (or partnerships) to manage the standards of the two main competing concepts: W-CDMA (IMT-DS) and CDMA2000 (IMT-MC) [17]. The Third Generation Partnership Project (3GPP) manages the Universal Mobile Telecommunication System (UMTS) specifications that apply W-CDMA concepts and build upon the GSM-MAP core network. The 3GPP2 organization manages the CDMA2000 specifications that build upon the ANSI/TIA/EIA-41

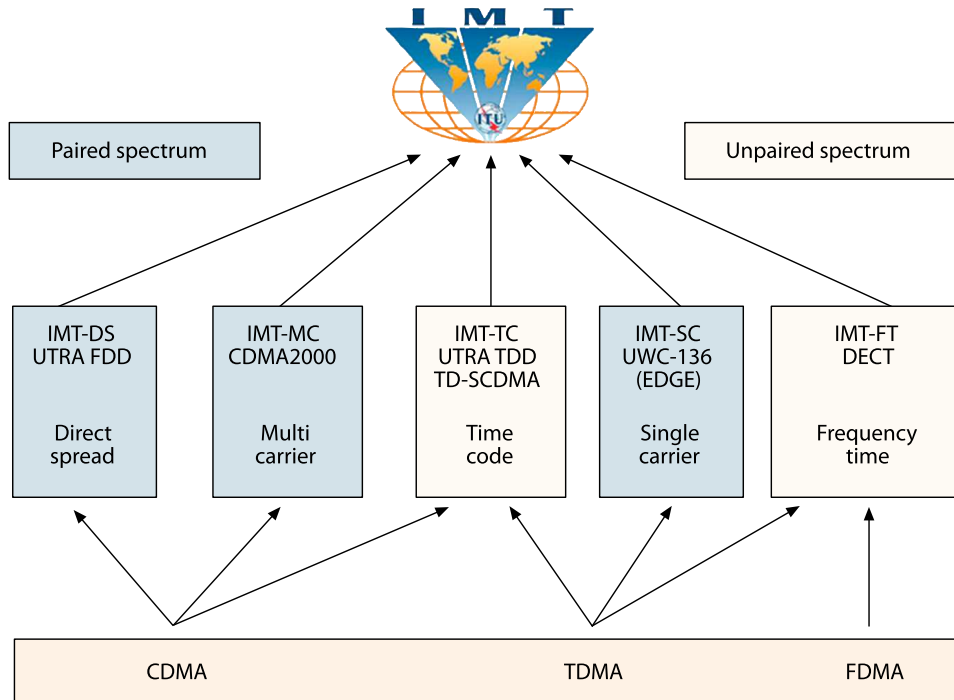


Figure 2.7: 3G standards as defined within IMT-2000 [91].

core network. These bodies unite regional standards organizations to submit unified proposals to the ITU and standardize system developments. In fact, 3GPP and 3GPP2 meet regularly to increase harmonization between the two main 3G concepts.

One of the biggest drivers for 3G development was the need for multimedia-level data rates. From a coding perspective, 3G systems require a coding capability that pushes performance closer to the Shannon limit than what was previously achieved with block and convolutional codes. Hence, many 3G systems quickly adopted Turbo coding [15, 16, 73], which significantly closed the gap on the Shannon limit (e.g., performance within 0.5 dB of the Shannon limit has been demonstrated at $P_b = 10^{-5}$). The Turbo coding research of Berrou and Glavieux [15, 16] was based on applying feedback techniques to coding in digital receivers [73]. Turbo codes are generated using a parallel organization of two recursive systematic convolutional (RSC) codes interconnected with an interleaver – see Fig. 2.8. While Turbo coding pushes performance limits toward channel capacity, it suffers from one important drawback; turbo coding exhibits excessive delay due to the interleaving and iterated decoding

processes. Therefore, like similar codes having very long codeword lengths, Turbo coding is not reliable for digital telephony, as well as, hard disk storage and optical transmission applications. However, Turbo coding can be used for data packet transmission and other applications where information transfer is not time-sensitive [73]. It is apparent that data applications give designers an option to use considerable time delay. This time delay is evident in error control techniques like Turbo coding, IR (see Sect. 2.3.1.3), and hybrid ARQ (see Sect. 2.4.2.2).

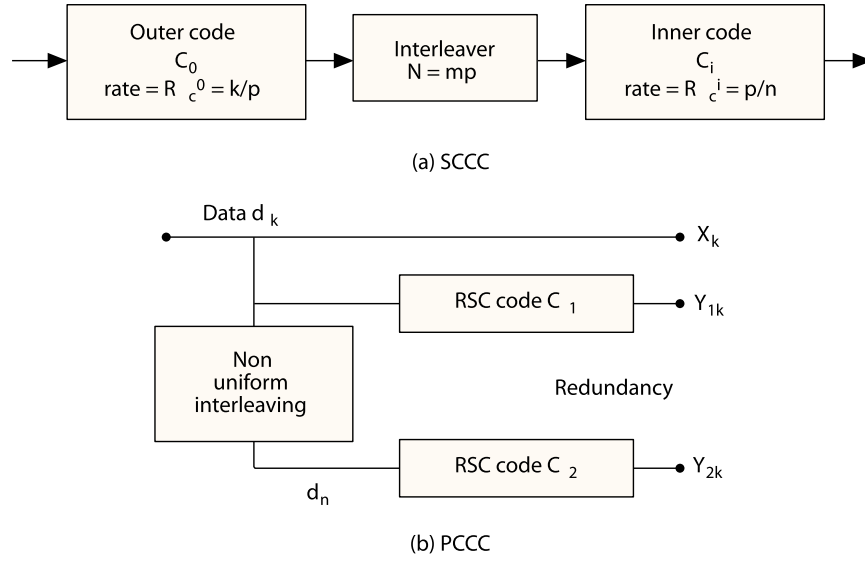


Figure 2.8: Concatenated code structures: a) general Serial Concatenated Convolutional Code (SCCC) with rate $R = k/n$ [40], and b) Parallel Concatenated Convolutional Code (PCCC), or Turbo code, using Recursive Systematic Convolutional (RSC) codes to achieve rate $R = 1/3$ [15].

From a modulation perspective, 3G systems require higher-order modulations to support higher required data rates. As a result, many 3G systems employ M -ary quadrature amplitude modulation (QAM) whereby both amplitude and phase are varied to generate communications symbols. The total number of symbols M is generally a power of 2 and varies from $M = 2$ to $M = 64$ – see Fig. 2.6. The M -QAM signal constellation is densely packed which allows for higher data rates. However, the increased density also creates a higher propensity for errors. While the use of Turbo coding with dense modulations can help offset some of the increased error, the use

of dense signal constellations is usually restricted to short range transmissions over relatively “clean” channels [204].

From a multiple access perspective, 3G systems are required to support a greater number of users while providing each user a higher available data rate. Therefore, most 3G systems adopt CDMA techniques, and more specifically, “Wideband” CDMA, to provide multiple access capability, given that CDMA offers keen advantages over TDMA/FDMA systems. For example, CDMA is more robust against multipath fading, provides greater coverage with fewer cell sites, enables better frequency reuse, and provides higher capacity [98, 116, 122, 141]. Yet, there are two relatively minor 3G modes of operation operating with TDMA, namely, IMT-SC and IMT-FT. While technical advantages of each multiple access scheme have been historically debated, and will likely be debated for generations to come, political and economic drivers (which are not the focus of this chapter) will continue to play a role in final technique selection.

A more detailed description of the five IMT modes is provided below and grouped by access method: W-CDMA (see Sect. 2.4.1), CDMA2000 (see Sect. 2.4.2), TDMA (see Sect. 2.4.3), Hybrids (see Sect. 2.4.4), and FDMA (see Sect. 2.4.5). A summary of current 3G deployment is also included in Sect. 2.4.6.

2.4.1 CDMA Systems: Wideband CDMA (W-CDMA). The first IMT-2000 mode of operation, designated IMT-DS for Direct Spread, relies on W-CDMA concepts for multiple access. IMT-DS is implemented via UTRA FDD, the 3G upgrade from the 2G GSM/GPRS system. Other sources imply that IMT-DS is generically implemented via UMTS. However, UMTS refers to the entire telecommunication system (wireless and wired portions) that deploys 3G services based on the GSM-MAP core network. The UMTS air interface is called the Universal Terrestrial Radio Access (UTRA), and since cellular communications travel along the air interface, it is more correct to identify this 3G mode of operation with UTRA (with FDD or TDD added to delineate between the different modes) rather than UMTS.

It is important to note that W-CDMA systems are *not* necessarily labeled as such based on occupied bandwidth relative to 2G systems [141]. Milstein opined that a W-CDMA system is one “wherein the spectral bandwidth of the underlying waveforms in the system typically exceeds the coherence bandwidth of the channel over which the waveforms are transmitted” [141], but firm criteria for distinguishing narrowband CDMA from W-CDMA could not be found, and indeed a standard definition for “Wideband CDMA” does not exist. However, Milstein adds that it appears “a spread bandwidth of about 10 MHz satisfies the intuitive requirement that the channel appear frequency selective to the transmitted waveform for a broad cross-section of scenarios” [141]. Thus, when conducting comparative analysis of W-CDMA systems, it is vital that one considers actual waveform characteristics (time and spectral) to ensure reliable results are obtained.

There are numerous advantages of using W-CDMA in multiple access applications, including higher data rates and greater robustness to multipath fading. For frequency selective fading (as often experienced in W-CDMA applications), the receiver can resolve and combine multipath components to improve SNR. In fact, through coherent recombination with perfect channel estimation, wideband spreading always performs better than narrowband spreading. Another W-CDMA advantage is that less power is needed to achieve a given level of performance as bandwidth increases, and if bit error rate (BER) is the criterion, wideband systems perform better than narrowband systems [141].

UTRA FDD was selected for UMTS public, wide-area service in 1998 and the IMT-DS standard was defined in 1999 [72]. The first commercial UTRA FDD system, Freedom Of mobile Multimedia Access (FOMA), deployed in 2001 [217]. The FL and RL of UTRA FDD operate in the 2110 to 2170 MHz and 1920 to 1980 MHz bands, respectively. Two 5.0 MHz sections within these bands are required to operate UTRA FDD, which can support approximately 200 voice channels [103]. UTRA FDD can support adaptive speech coding, Turbo channel coding, and QPSK modulation, which represent upgrades from the GSM/GPRS systems. For speech coding, UTRA FDD

uses an adaptive multi-rate (AMR) vocoder [155] based on algebraic code excited linear prediction (ACELP) techniques, which processes 160 bits per 20 ms speech frame. AMR selects one of eight different bit rates, from 4.75 to 12.2 kb/s, and can change this rate every frame based on channel conditions [194]. For forward error correction (FEC) coding, UTRA FDD uses either 1) rate 1/2 or rate 1/3 convolutional encoding with interleaving over periods of 10, 20, 40, or 80 ms, or 2) parallel turbo coding with rate 1/3 and block lengths of 320 to 564 bits [251].

UTRA FDD boosts the maximum data rate from 384 kb/s (EDGE) to 2.3 Mb/s (FL only, RL remains at 384 kb/s). This data rate is achieved using a low spreading factor (4) and an appropriate weaker coding scheme (5 parallel codes with rate 1/2 coding). More realistic data rates are on the order of 64 to 100 kb/s [103]. UTRA FDD increases voice capacity to 51 Erlangs/sector/5 MHz carrier [103]. (One Erlang represents a measure of traffic intensity handled by a completely occupied channel, e.g., 1 call-minute per minute, and is named after a Danish mathematician in the late 19th century who studied how large populations can be accommodated by a limited number of servers [171]). For comparison, the CDMA2000 1× system (described later) offers 26 Erlangs/sector/1.25 MHz carrier.

2.4.1.1 High Speed Downlink Packet Access (HSDPA). The High Speed Downlink Packet Access (HSDPA) concept is the first planned major upgrade to UTRA FDD. 3GPP is packaging HSDPA with Release 5 and began deploying it in the U.S. in late 2005 [133, 185]. Because it is an upgrade to the 3G UTRA FDD system, it is sometimes referred to as 3.5G. HSDPA is a continued evolution of the downlink shared channel (DSCH) in UTRA FDD (3GPP Release '99). The DSCH provides time-shared packet data among all UTRA FDD users at high data rates [130]. The new data link will be similar to the forward packet data channel (F-PDCH) of CDMA2000 1×EV-DV and will overlay on 3GPP Release '99 channels [104, 105]. Coincidentally, 3GPP Release 5 also incorporates a wideband AMR (AMR-WB) speech codec to support a wider audio bandwidth of 50 - 7000 Hz instead of the

standard audio bandwidth of 200 - 3400 Hz. The AMR-WB operates like AMR but supports nine bit rates ranging from 6.6 to 23.85 kb/s [155].

HSDPA creates a *high speed* DSCH (HS-DSCH) by replacing the variable spreading factor (VSF) and fast power control with adaptive modulation and coding (AMC), short packet size, multi-code operation, and fast hybrid automatic repeat request (HARQ). Using fast AMC versus fast power control boosts the power efficiency by eliminating power control overhead. Although the spreading factor is now fixed at 16, up to 15 codes may now be used concurrently, so a variety of data rates are still available. Increased link adaptation rate and AMC efficiency are also possible since the packet duration time decreases from 10 or 20 ms to a fixed duration of 2 ms. Thus, adaptation for channel conditions, data rates, and mobility is provided through selection of code rate, modulation scheme, number of multi-codes, and transmit power per code. The HS-DSCH channel will be coded by an improved version of the current UTRA FDD rate 1/3 Turbo coder, one that provides rate matching via puncturing and repetition. Additionally, HSDPA adds 16-ary QAM modulation to augment the current QPSK modulation [104, 105, 222, 237]. A comparison of the DSCH and HS-DSCH is shown in Table 2.6.

Twelve classes of data rates are available with HSDPA, ranging from 900 kb/s to 14.4 Mb/s. Whereas the theoretical maximum data rate is 14.4 Mb/s, a more practical limit is about 10 Mb/s. For example, a user with excellent channel conditions that is afforded 15 codes can achieve a theoretical data rate of 10.8 Mb/s using 16-QAM with rate 3/4 Turbo coding. Average simulated data rates of 2.5 Mb/s (with a fully capable MS) and 2 Mb/s (with a limited capability MS with 5/15 codes and no 16-QAM) have been reported [237].

2.4.1.2 Enhanced Uplink (EUL). Another planned major upgrade to UTRA FDD is the enhanced uplink (EUL) (also sometimes labeled as 3.5G). HSDPA provides higher data rates on the FL with 3GPP Release 5, so 3GPP Release 6 (expected in 2006) incorporates an enhanced uplink dedicated channel (EU-DCH)

Table 2.6: Comparison of DSCH and HS-DSCH [104,105].

Parameters	DSCH	HS-DSCH
Variable Spreading Factor (VSF)	Yes (4 to 256)	No
Power Control	Fast	None
Adaptive Modulation & Coding (AMC)	No	Yes
Fast L1 HARQ	No	Yes
Multi-Code Operation	Yes (4 to 256)	Yes, extended
Transmit Time Interval (TTI)	10 or 20 ms	2 ms

that provides higher data rates on the RL. This upgrade is also sometimes referred to as HSUPA for *high speed uplink packet access*.

Whereas HSDPA provides impressive peak data rates much greater than the simulated average data rates, EUL intends to optimize the *average* throughput. The baseline EUL design includes available transmission intervals of 2 or 10 ms, where a MS can only choose one interval per use. EUL will combine QPSK modulation, synchronous HARQ, and a retransmission upgrade (to include IR). EUL will provide data rates of 4.096 Mb/s and 819.2 kb/s using 2 ms and 10 ms transmission times, respectively [237].

2.4.2 CDMA Systems: CDMA2000. The next IMT-2000 mode of operation, designated IMT-MC for Multi-Carrier, also relies on CDMA concepts for multiple access. CDMA2000 is a 3G upgrade to the 2G IS-95 system [130]. CDMA2000 evolved from IS-95B and is also referred to as CDMA2000 1 \times , CDMA2000 1 \times EV, or CDMA2000 1 \times RTT, where “1 \times ” refers to the number of 1.25 MHz carriers, “EV” denotes an evolution towards 3G, and “RTT” stands for radio transmission technology.

In 2000, CDMA2000 split into two branches: IS-2000 which continued current development of voice and data communications, and IS-856 which focused solely on transmitting data more efficiently. IS-2000 became known as 1 \times EV-DV after Revision C (“DV” denotes Data and Voice), and published a new revision in March 2004, Revision D. The IS-856 branch became known as 1 \times EV-DO (“DO” denotes Data

Optimized or Data Only). $1\times$ EV-DO has also been referred to as high rate packet data (HRPD). Except where noted, all Section 2.4.2 material comes from [130].

2.4.2.1 $1\times$ Systems. CDMA2000 $1\times$ is considered the first 3G system built upon the ANSI-41 core network despite the fact that it does not provide 2 Mb/s data rates to stationary users. In this regard, it is similar to EDGE - see Section 2.4.3 - in that both systems contain all 3G characteristics except the 2 Mb/s data rate for stationary users. CDMA2000 $1\times$ systems use the same 1.25 MHz channel as IS-95 systems, and “ $1\times$ ” describes the number of channels used for transmitting on the FL.

There are numerous upgrades to the FL of CDMA2000 $1\times$ from IS-95. The first modification is that $1\times$ systems use QPSK versus BPSK data modulation which effectively doubles the number of Walsh codes that can be applied (from 64 to 128). Second, a new supplemental channel provides maximum data rates up to 153.6 kb/s (FL and RL), higher than the rates available with IS-95B. Next, the power control system provides quicker updates to better handle changing channel conditions. Also, the system is now capable of using Turbo codes for channel coding (high-rate data), the frame rate is variable (5, 20, 40, or 80 ms), and there is multi-frame interleaving [251]. Finally, the new system supports two optional transmit diversity schemes on the FL, including space-time spreading (STS) and orthogonal transmit diversity (OTD). The OTD option allows two orthogonal signals to be simultaneously broadcast from two antennas to the MS receiver [208]. The introduction of QPSK modulation, lower code rate ($1/4$ is now available), and quicker power control update nearly doubles the FL voice capacity to 26 Erlangs/sector/1.25 MHz carrier [237].

The main RL modification is that the BS receiver is now coherent and pilot channel assisted versus non-coherent (on IS-95B, only the FL was coherent), thus increasing the voice capacity on the RL [251]. Another upgrade (on the RL and FL) is the addition of a selectable mode vocoder (SMV) for speech coding. The SMV operates on 20 ms speech frames containing 160 bits and supports four different rates, the fastest being 8.5 kb/s [212]. Although CDMA2000 $1\times$ and UTRA FDD are more

Table 2.7: Key differences between UTRA FDD, CDMA2000 1 \times , and TD-SCDMA [122, 251].

Parameters	UTRA FDD	CDMA2000 1 \times	TD-SCDMA
Bandwidth	5 MHz	1.25 MHz	1.6 MHz
Multiple Access	CDMA	CDMA	TDMA/CDMA
Chip Rate	3.84 Mc/s	1.2288 Mc/s	1.28 Mc/s
Channel Code	Conv, Turbo	Conv, Turbo	Conv, Turbo
Spreading Code	OVSF	Walsh, PN Code	OVSF
Modulation Order (PSK)	FL: 4, RL: 2	FL: 4, RL: 2	4, 8 (optional)
Frame Duration	10 ms	10 ms	10 ms (2 frames)
Max Data Rate	2 Mb/s	2.4 Mb/s (EV-DO)	2 Mb/s
Power Control	1600 Hz	800 Hz	200 Hz
BS Synch	Asynch	Synch (GPS)	Synch

similar than their 2G predecessors IS-95A and GSM, important differences exist as shown in Table 2.7.

On the CDMA2000 1 \times FL, low-rate data is passed using the fundamental channel (F-FCH), which continually exists between all base and mobile stations. High-rate data (i.e., large packets) are transmitted via the supplemental channel (F-SCH), which is assigned to a specific MS for a 160 ms period. The base station controller (BSC), which constantly receives power control information from all BS under its control, controls the flow of packets on the FL and the assignment of the F-SCH.

This FL operation yields several important observations. First, control is too centralized (at the BSC), and individual base stations cannot rapidly respond to varying channel conditions. Second, the F-FCH is always present, resulting in unused spectrum when the F-SCH is assigned. Third, explicit channel assignments are sent to the mobile in advance (60 ms beforehand), and the F-SCH is assigned for a period of time (160 ms). Yet, channel path loss can vary within as little as 50 ms, so the channel can vary greatly throughout a large packet transmission. Finally, transmissions are power controlled throughout the process, resulting in excess power being transmitted.

2.4.2.2 1×EV-DO. In 2000, a branch emerged from the CDMA2000 1× standard called IS-856, now commonly termed 1×EV-DO. 1×EV-DO introduces a separate carrier just for data, providing data rates up to 3.1 Mb/s on the FL and 1.8 Mb/s on the RL.

A key enabler to higher data rates in 1×EV-DO is the HARQ protocol (also used in UTRA FDD). CDMA2000 1× uses the radio link protocol (RLP) at the link layer to decide when packets must be retransmitted. HARQ replicates RLP processes at the physical layer for 1×EV-DO. To use the HARQ protocol, each physical layer data packet is encoded into subpackets. The transmitter continues to send subpackets until notified otherwise. The identity of the subpackets is known at the receiver, and it combines subpackets for better decoding. Subpackets are accumulated at the receiver until the required SNR is met. The advantage of HARQ is that the transmitter only sends subpackets until the required minimum SNR is achieved, resulting in less wasted transmitted power and less interference to other users [108].

The 1×EV-DO FL operation is unlike the FL of CDMA2000 1×. Each MS relays its requested rate on the data rate control (DRC) channel and best sector ID on the data sector control (DSC) channel. The BS then selects the appropriate recipient and format for transmission. FL transmissions contain a preamble identifying the destination MS. Upon detecting its preamble, the MS combines and decodes the data and notifies the BS. The BS then decides whether it should send more subpackets.

To transmit to distant dynamic mobile stations, base stations use longer preambles (up to 1024 chips) with payload sizes of 128 to 1024 bits distributed over 16 slots using QPSK modulation. If the mobile is nearer the BS and/or more stationary, the preamble size is reduced (as low as 64 chips) with payload sizes up to 5,120 bits distributed over one slot using 16-QAM. Each 1.67 ms FL slot contains 2,048 chips of which 1,600 are for data and 448 are for medium access control (MAC) and pilot signals.

Another change is that the BS on the $1\times\text{EV-DO FL}$ (see Fig. 2.9) only transmits to one user at a time. In that respect, the FL is more TDMA-like (CDMA is only used for spreading), resulting in very short transmissions during which the propagation channel changes very little. In general, the TDM scheme allows the BS to transmit maximum power all the time to each single user. However, *multi-user* TDM packets may also be constructed and transmitted within a time slot, with each MS identifying its packets using specified MAC indices. The FL uses shorter interleaving times, and it eliminates power control. Since mobiles report the requested rate via the DRC, a power control loop is not needed. Because there is an established data link, there is no longer any reason to request an advance channel assignment (as with F-SCH), and the BS transmits one subpacket at a time.

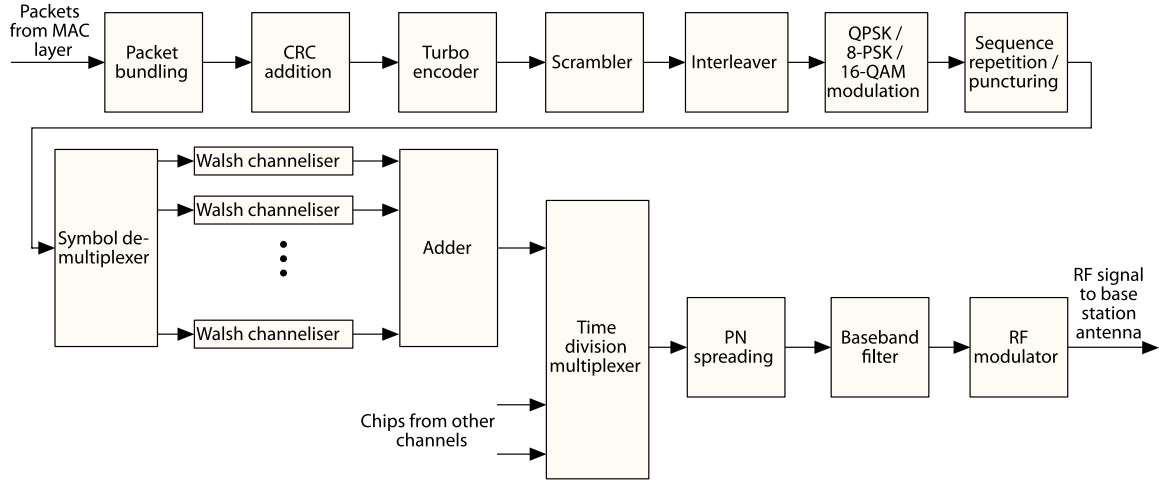


Figure 2.9: Block diagram of $1\times\text{EV-DO}$ forward link transmitter [3].

There are some key differences in $1\times\text{EV-DO RL}$ and FL operation. First, subpacket durations of 5 ms (RL) and 1.67 ms (FL) are used. The longer RL duration is needed because the MS power amplifier is smaller than the BS amplifier. Second, the FL only sends control information with the first subpacket. However, given low cost memory and available space, the BS buffers everything received from the MS and thus, all subpackets transmitted on the RL include control information. Third, BPSK (for low rates using one Walsh channel), QPSK (for medium rates using one or two Walsh channels), and 8-PSK (for high rates using two Walsh channels) modulations

are employed on the RL depending on required data rate. The FL employs QPSK, 8-PSK, and 16-QAM modulations. Twelve payload sizes offer data rates from 4.8 kb/s to 1.8 Mb/s, and all payload sizes may use up to four subpackets. Fourth, while the FL is migrating toward TDM like operation, the RL remains very dependent on CDM, using Walsh codes like IS-95A/B and CDMA2000 1 \times . Fifth, the RL remains power controlled (at 400 Hz) to address the near-far problem.

2.4.2.3 1 \times EV-DV. After CDMA2000 1 \times Revision C was published, the IS-2000 standard was renamed 1 \times EV-DV (and sometimes labeled as 3.5G). 1 \times EV-DV combines the data performance of 1 \times EV-DO (3.1 Mb/s on FL) with traditional voice services on a single new channel called the forward packet data channel (F-PDCH). F-PDCH is a high-rate channel that is rapidly time-shared among users and employs dynamic modulation and coding based on channel conditions. A major principle in the 1 \times EV-DV FL design is that modulation and coding are rapidly adapted for each subpacket, with adapted parameters based on available BS resources (e.g., number of Walsh codes and available power), the amount of data to transmit, and channel conditions - an application of cognitive radio principles. This adaptation allows for full use of spectrum resources. Revision D was published in 2004 and introduces a new high-speed packet data channel for RL data (1.8 Mb/s) and voice transfer [100].

The 1 \times EV-DV FL effectively pools all remaining Walsh codes and power into the F-PDCH channel – see Fig. 2.10. It integrates HARQ, short frames, rate adaptation, no advance signaling, and no power control on the F-PDCH. Meanwhile, all legacy channels from CDMA2000 1 \times can cohabit with the F-PDCH. Since each MS reports its interference level, the BS can decide what format to transmit. Finally, 1 \times EV-DV will incorporate a new variable-rate multimode wideband (VMR-WB) speech codec [4], similar to the AMR-WB speech codec in 3GPP Release 5, to replace the SMV codec used in 1 \times systems.

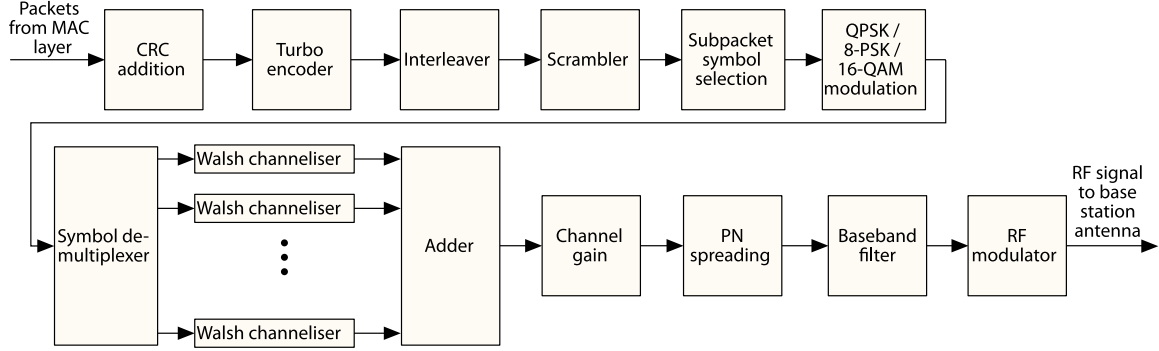


Figure 2.10: Block diagram of $1\times\text{EV-DV}$ forward link packet data channel (F-PDCH) [3].

The $1\times\text{EV-DV}$ RL is very similar to the $1\times\text{EV-DO}$ RL, but there are minor differences. First, the sub-packet duration is 10 ms (versus 5 ms) and there is a new CDM/TDM acknowledgement on the FL. Second, Walsh codes preserve orthogonality between RL channels of a mobile. Third, complex scrambling at the MS output differentiates the signal from different mobiles at the BS. Fourth, the selection of Walsh codes minimizes peak-to-average power allowing the MS to operate closer to its maximum transmit power. Finally, $1\times\text{EV-DV}$ adds an HARQ channel on the RL, and, unlike the FL HARQ, the RL HARQ is synchronous (i.e., the time interval between consecutive transmissions of the same subpacket is constant). This simplifies the subpacket reordering process at the BS [107].

2.4.3 TDMA Systems. Another IMT-2000 mode of operation, designated IMT-SC for Single Carrier, relies on TDMA concepts for multiple access. IMT-SC is implemented via UWC-136, a TDMA system co-monitored by 3GPP and the Universal Wireless Communication Consortium (UWCC). Since IMT-SC uses TDMA technology, EDGE is considered part of this 3G family because it is currently the most advanced TDMA system. The maximum data rate is 384 kb/s, but typical FL data rates are expected to be as high as 180 kb/s (50 to 70 kb/s average) and typical RL data rates are expected to be as high as 60 kb/s [103].

The 136HS Outdoor mode, also called EGPRS-136 for Enhanced GPRS over ANSI-136, is similar in operation to EDGE [156]. Packet radio techniques are used with adaptive modulation (GMSK and 8-PSK) to give EDGE and 136HS Outdoor all 3G characteristics except a 2 Mb/s indoor data rate. Using unsynchronized base stations, a GSM network can upgrade to EDGE using only 2.4 MHz of spectrum. If the BS are synchronized, this upgrade can be done with only 600 kHz of spectrum. Synchronization is a means of keeping base stations from transmitting while a designated beacon station is transmitting to its mobile stations.

The 136HS Indoor mode is also called Wideband TDMA (WTDMA) given it is a TDMA based concept using 1.6 MHz carriers with two different kinds of bursts [156]. High user data rates are handled using a 1/16 length burst of the 4.615 ms TDMA frame. Intermediate user data rates are handled using a 1/64 length burst of the 4.615 ms TDMA frame. Adaptive modulation is used with both kinds of bursts.

2.4.4 Hybrid Systems. Another IMT-2000 mode of operation, designated IMT-TC for Time Code, relies on a hybrid of CDMA and TDMA concepts for multiple access. IMT-TC is implemented via two distinct air interfaces, namely, UTRA TDD and time division synchronous CDMA (TD-SCDMA). 3GPP distinguishes the two interfaces based on their chip rates; UTRA TDD utilizes high chip rates and TD-SCDMA utilizes low chip rates. Each interface couples W-CDMA transmissions with a TDD link. The use of TDD instead of FDD offers several advantages for these systems, including 1) improved spectrum efficiency with asymmetric services, 2) only one frequency band is required for operation, and 3) diversity techniques are easily implemented since propagation characteristics are identical on the FL and RL [122].

In January 1998, the European Telecommunications Standards Institute (ETSI) chose two standards, UTRA FDD and UTRA TDD, for the UTRA interface in UMTS. The primary differences between UTRA FDD and UTRA TDD are the system goals and multiple access schemes. UTRA FDD aims to provide service in a wide area, global setting whereas UTRA TDD is designed for pico cells within smaller areas.

Hence, UTRA FDD is used for public mobile communications, and UTRA TDD is used for local indoor communication [103]. With regard to multiple access, UTRA TDD uses time division CDMA (TD-CDMA) with the forward and reverse links operating in the same frequency band but in different time slots. UTRA TDD uses the same 5.0 MHz channels as UTRA FDD but with smaller spreading ratios (1 to 16), the result of a CDMA code applied to spread the signal within its designated time slot [72]. UTRA TDD also employs the same UTRA FDD chip rate of 3.84 Mchips/sec.

The TD-SCDMA interface was originally proposed by the China Academy for Telecommunications Technology (CATT) in 1998. After being approved by the ITU in 2000, it joined 3GPP in March 2001 [122]. Along with UTRA FDD and CDMA2000, TD-SCDMA is considered one of the three main *de facto* 3G standards adopted in China (see Table 2.7). TD-SCDMA (see Fig. 2.11) uses three carriers and a low chip rate of 1.28 Mchips/sec with corresponding bandwidth of 1.6 MHz. Each TDMA sub-frame lasts 5 ms and is divided into 7 slots. TD-SCDMA incorporates QPSK and 8-PSK data modulations. While TD-SCDMA uses a TDMA backbone, its CDMA application differs from W-CDMA and CDMA2000. The number of codes per time slot is limited to 16 whereas W-CDMA and CDMA2000 permit many more codes. More information on TD-SCDMA implementation is provided in [122, 250].

2.4.5 FDMA Systems. The final IMT-2000 mode of operation, designated IMT-FT for Frequency Time, is implemented via DECT – see Fig. 2.7. DECT is technically a *cordless* telephony system, not a cellular system, but it is briefly introduced because of its inclusion in the IMT-2000 standard. Formerly known as Digital European Cordless Telephony, DECT is a TDMA/FDMA system that has evolved to include limited cellular capability and is now called Digital Enhanced Cordless Telecommunications. DECT operates over short ranges (50 m indoors to 300 m outdoors) in the 1880 – 1990 MHz band using 120 full TDD channels with 10 ms frames. Essentially, the spectrum is divided into 10 frequency bands (FDMA) with each band

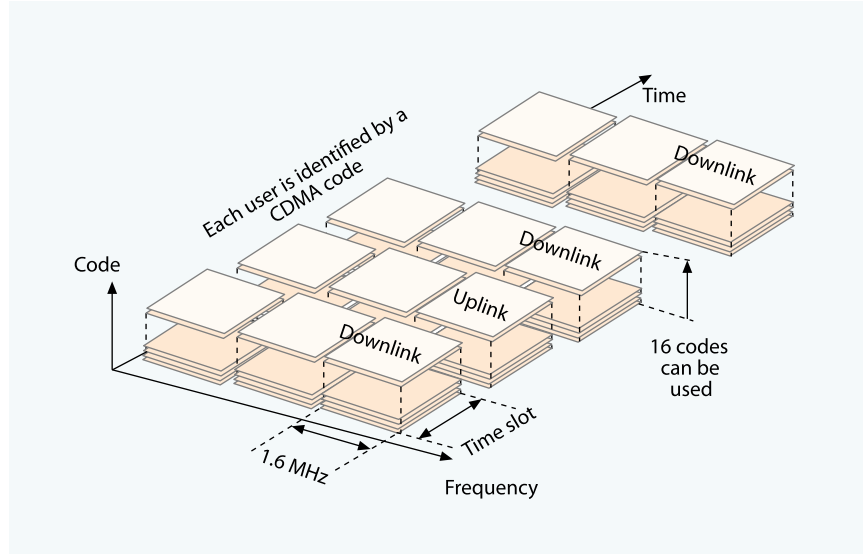


Figure 2.11: Time Division-Synchronous Code Division Multiple Access (TD-SCDMA) channel structure [122].

time-shared among 24 slots in each frame (TDMA). Each time slot contains 420 bits plus a $52 \mu\text{s}$ guard time, yielding a 0.4167 ms slot time. As with GSM, DECT uses GMSK modulation [190].

2.4.6 3G Deployment Summary. 3G systems began appearing in 2001, and their deployment is now finally in high-gear. As of June 2006, CDMA2000 1 \times has 223.9 million users, CDMA2000 1 \times EV-DO has 33.3 million users, and UTRA FDD has 66.6 million users [1].

Figures 2.12 and 2.13 show the evolution of voice capacity and data throughput over recent years as 3G systems came online. The voice capacity (for a 5.0 MHz bandwidth) ranges from about 50 to 170 Erlangs in 2005. Much of the improvement in Fig. 2.12 is attributable to adaptive multi-rate (AMR) technologies, improved diversity, and selectable mode vocoders (SMV) [211]. The maximum data throughput (for a 5.0 MHz bandwidth) ranges from about 1.4 Mb/s to 4.3 Mb/s in 2005. Much of the improvement indicated in Fig. 2.13 is attributable to dual antenna use, equalization, and the application of new coding schemes. For example, CDMA2000 1 \times EV-DO can provide an *average* aggregate throughput (for a 5.0 MHz bandwidth)

of about 4 Mb/s when using dual antennas and equalization improvements – see 2005 data in Fig. 2.13. Note that this exceeds the *maximum* 3.1 Mb/s data rate given in CDMA2000 1×EV-DO specifications, which apply to a 1.25 MHz bandwidth system using a single antenna [2].

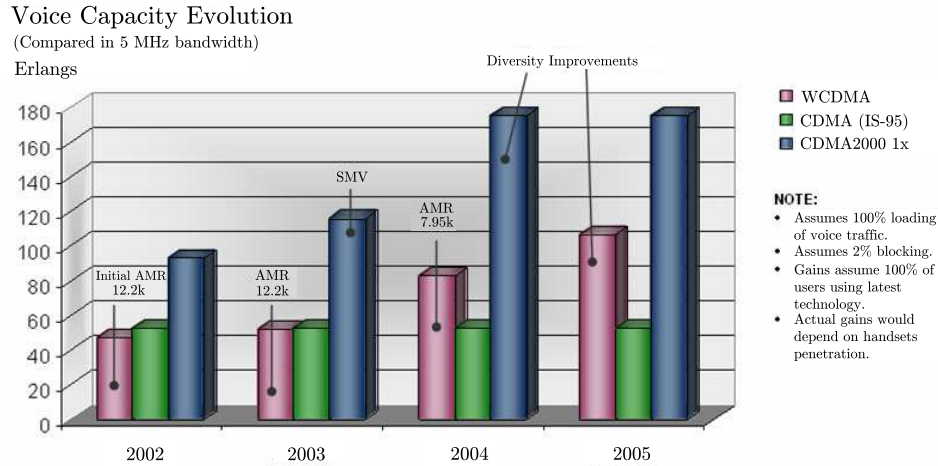


Figure 2.12: Voice capacity evolution: W-CDMA, IS-95, and CDMA2000 1× (5.0 MHz bandwidth) [237].

While all five modes of 3G operation are currently in use (not just conceptual ideas), the two predominantly used modes are UTRA FDD and CDMA2000, managed by 3GPP and 3GPP2, respectively. However, 3G modes are not user-selected; rather, they are determined by geographic regions and company architecture decisions. For example, users in North America, Europe, and China are more likely to use CDMA2000, UTRA FDD, and TD-SCDMA, respectively. Similarly, within the United States, Sprint and Verizon Wireless have chosen to adopt CDMA2000 technology and Cingular-AT&T Wireless has chosen to adopt UTRA FDD (using W-CDMA) technology [1]. Hence, subscribers within those networks will use those technologies by default. Other 3G systems, e.g., DECT and UTRA TDD, are used in special cases and situations as previously noted.

Evolution of Data Throughput
Average Aggregate Throughput
(Compared in 5 MHz bandwidth)

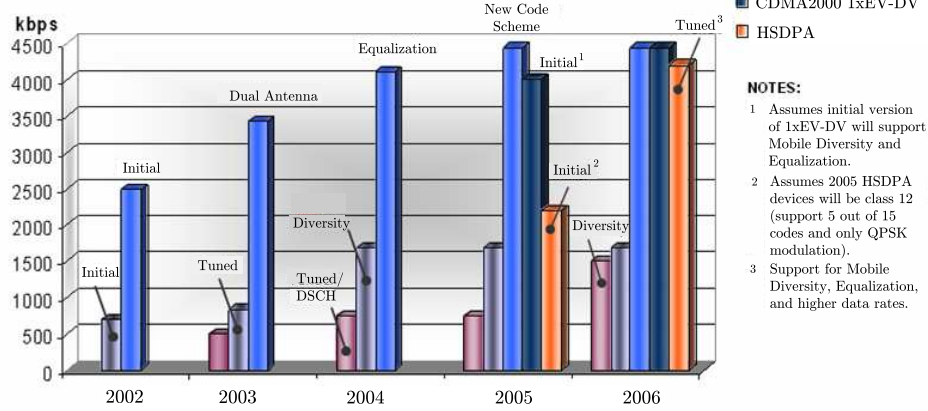


Figure 2.13: Data throughput evolution: average aggregate throughput for W-CDMA, CDMA2000 1x, CDMA2000 1xEV-DO, CDMA2000 1xEV-DV, and HSDPA (5.0 MHz bandwidth) [237].

2.5 Fourth Generation Systems (4G)

Recent research suggests that cellular and wireless networking technologies may merge in the next generation of cellular communication systems [22,188,217,245]. Cellular networks continue to provide higher data rates, and wireless networks continue to become more mobile and now offer VoIP services.

This section begins by providing a brief glimpse at the current status of coding, modulation, and multiple access technologies used in wireless networks. Even if the proposed cellular / wireless network merger is only partial and restrictive, the next generation of cellular systems may adopt some of these technologies. Hence, it is instructive to briefly examine the current status of wireless network technology. The capstone section describes 4G enabling technologies. The next generation of cellular systems will rely not only on technologies in existing 1G, 2G, 3G, and wireless network systems, but also on emerging research in key areas as identified in Sect. 2.5.3.

2.5.1 Current Status of Wireless Networks. A number of IEEE 802 wireless standards are redefining how consumers access wireless services. Offering larger “hot

Table 2.8: Comparison of Wi-Fi variants [109–111].

Traits	802.11a	802.11b	802.11g
Approval Date	July 1999	July 1999	June 2003
Spectrum	5 GHz Band	2.4 GHz Band	5 GHz Band
Max Data Rate	54 Mb/s	11 Mb/s	54 Mb/s
Modulation	OFDM	CCK,PBCC,DSSS	OFDM,PBCC,CCK,DSSS

spots” and higher data rates, these wireless networks have much in common with cellular systems. Some IEEE 802 standards include Wi-Fi, WiMAX, and Mobile-Fi.

802.11 is a wireless local area network (WLAN) standard developed in 1990 by the IEEE and is typically referred to as wireless fidelity, or simply Wi-Fi [61]. The 802.11 standard defines the medium access control (MAC) layer, and variants exist which describe the physical (PHY) layer, three of which are most predominant at this time: 802.11a, 802.11b, and 802.11g - see Table 2.8.

The 802.11a standard supports a maximum data rate of 54 Mb/s using orthogonal frequency division multiplexing (OFDM) in the 5 GHz band [109]. 802.11a uses 52 subcarriers (48 for data symbols, 4 for pilot symbols) that are modulated using BPSK, QPSK, 16-QAM, or 64-QAM. It protects the bits using a convolutional code with coding rates of $1/2$, $2/3$, and $3/4$ and constraint length $K = 7$.

The 802.11b standard supports a maximum data rate of 11 Mb/s using 8-chip complementary code keying (CCK) modulation in the 2.4 GHz band [110]. Four data rates are specified for the high rate PHY layer (all use DS-SS for spreading) based on modulation format: differential BPSK (DPSK), differential QPSK (DQPSK), or CCK. An 11-chip Barker sequence is the PN code sequence for the modulations of the two lower data rates. Eight chips are used for the complementary codes needed for CCK modulation at the two higher data rates.

The 802.11g standard is a high-speed extension of 802.11b, operating in the 2.4 GHz band and supporting a maximum data rate of 54 Mb/s [111]. This mode uses CCK, packet binary convolutional coding (PBCC), and/or OFDM modulation to support varying data rates from 1 to 54 Mb/s.

Table 2.9: Comparison of WiMAX variants [112–114, 221].

Traits	802.16	802.16a/d	802.16e
Approval Date	Dec 2001	Jan 2003 / Jun 2004	End of 2005
Spectrum	10 to 66 GHz	2 to 11 GHz	2 to 6 GHz
Max Data Rate	134 Mb/s (64-QAM, 28 MHz)	75 Mb/s (20 MHz)	15 Mb/s (5 MHz)
Modulation	QPSK,QAM	2/4-PSK,QAM,OFDM	same as 802.16d
Mobility	Fixed	Fixed, Portable	Mobility, Roaming

Other variants currently under development include 802.11i (enhanced security), 802.11e (QoS measures), 802.11f (interaccess point protocol), and 802.11n (multiple transmit and receive antennas with rates approaching 100 Mb/s) [61, 205].

The IEEE 802.16 is a wireless metropolitan area network (WMAN) standard commonly referred to as WiMAX for worldwide inter-operability for microwave access. The original 802.16 version defined the MAC layer protocol for the standard, and the PHY layer focused on the 10 to 66 GHz band [112]. Interest in lower frequencies (2 to 11 GHz) spurred the subsequent release of 802.16a, and upgrades are captured in 802.16d, also called 802.16-2004 [113, 114]. An extension to mobile applications is being pursued under 802.16e. The interested reader is referred to [66] for a thorough WiMAX overview. WiMAX has been recently tested in limited deployment [79].

Table 2.9 highlights major differences between these WiMAX variants. WiMAX is based on OFDM (with up to 2,048 subcarriers), supports higher-order modulations up to 64-QAM, and offers *raw* data rates up to 134 Mb/s (for 64-QAM and a channel size of 28 MHz) [66]. The channel bandwidth is restricted to 20 MHz or less and must be an integer multiple of 1.25 MHz, 1.5 MHz, or 1.75 MHz. Seven combinations of modulation and coding are provided to vary the output data rate. One major predictor of WiMAX system data rates is range from the “hot spot” antenna. At closer ranges, WiMAX can use M-ary QAM and support throughputs higher than 50 Mb/s. At longer ranges, lower order modulations must be used with lower-rate coding and the data throughput decreases. BPSK, QPSK, 16-QAM, and 64-QAM data modulations are supported, and a concatenated coding scheme is employed using

Table 2.10: Comparison of 3G, Wi-Fi, WiMAX, and Mobile-Fi.

Traits	3G	Wi-Fi	WiMAX	Mobile-Fi
Standard	W-CDMA, CDMA2000	IEEE 802.11g	IEEE 802.16a	IEEE 802.20 802.20
Max Data Rate	3 Mb/s	54 Mb/s	134 Mb/s	16 Mb/s
Coverage	Several km	100 m	40 km	Several km
Advantages	Range, mobility	Speed, cheap	Speed, range	Speed, mobility

an outer Reed-Solomon block code and an inner convolutional code with rates of $1/2$, $2/3$, or $3/4$ and constraint length $K = 7$ [66].

The IEEE 802.20 is a proposed WMAN standard sometimes referred to as Mobile-Fi (mobile fidelity) or MBWA (mobile broadband wireless access) [134]. The goal of Mobile-Fi is to provide WiMAX capabilities to wide-area, *mobile* users. Unlike 802.16e, which extends a fixed wireless broadband standard to support mobility, 802.20 is being specifically designed from the ground up to support mobility. Table 2.10 compares key wireless networks with 3G cellular services. Figure 2.14 shows a migration of WLAN, 3G, and fixed wireless broadband towards a future 4G system as envisioned by [197].

2.5.2 What is 4G? The next generation of cellular communications has inherited numerous labels including beyond 3G (B3G), enhanced 3G (E3G), next generation network (NGN), and 4G as used here. Currently, no formal standard or definition for 4G exists. While 3G systems focus primarily on supporting multimedia data rates and various classes of service, the focus of 4G systems is to seamlessly integrate existing wireless systems [88].

Despite disparities on timeline, throughput, and signaling, “the majority of vendors agree on 2 issues regardless of claims for throughput, bands, and timeline: the air link will be packet-switched and the protocol is IP” [81]. Keiji Tachikawa, the former president and CEO of NTT DoCoMo, Inc., who introduced the first 3G cellular system in Japan, thinks that 4G will be cellular-based and will incorporate

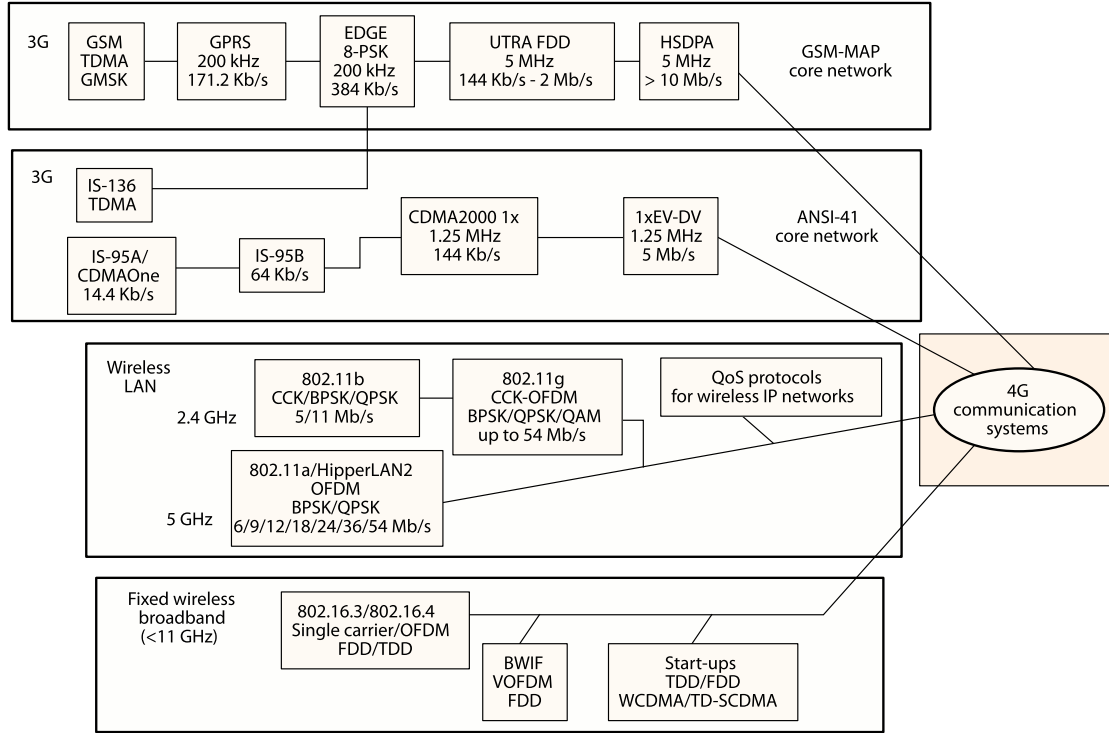


Figure 2.14: Migration of cellular and wireless networks towards a 4G system [197].

WLAN-type systems to achieve higher speeds in limited-mobility areas (e.g., hot spots, indoors, etc.) [217].

While higher data rates and ubiquitous access generally get most recognition as 4G-like traits, packet-switching and IP are perhaps the most agreed upon by researchers. Wireless networks already use packet-switching over an IP protocol and cellular networks are starting to use packet-switching for efficient data handling. It is no surprise that many believe the lifeblood of 4G involves the merger of cellular and wireless technologies, including the integration of technologies from personal area networks (PANs) (e.g., ultra wideband, Bluetooth), LANs (e.g., Wi-Fi), metropolitan area networks (MANs) (e.g., WiMAX), wide area networks (WANs) (e.g., cellular), and regional/global area networks (e.g., radio and television broadcasting, satellite communications). In essence, 4G aims to transition communication architectures from vertical stovepiped systems to horizontal integrated systems. While there cur-

Table 2.11: Comparison of 3G and 4G systems [126].

Traits	3G	4G
Key Req'ments	Voice (data is add-on)	Data and voice over IP
Architecture	Wide-area cell-based	WLAN, WMAN
Spectrum	1.8 to 2.5 GHz	2 to 8 GHz
Bandwidth	5 to 20 MHz	5 to 20 MHz (Max = 100)
Max Data Rate	2 Mb/s	20 Mb/s (or 100 Mb/s)
Multiple Access	W-CDMA, TDMA	MC-CDMA, OFDM
Coding	Conv, rates 1/2 & 1/3	Concatenated, LDPC
Switching	Circuit/Packet	Packet
Deployment	In progress	2010

rently appears to be no universal delimiter for 3G and 4G, there are some 4G traits which distinguish it from 3G as identified in Table 2.11.

Early 1G cellular systems became available in 1979 and remained in use until the early 1990s. Existing 2G digital systems are phasing out in favor of higher speed, packet-routed 3G systems. If history is an indicator, cellular generations spanning 10 to 12 years suggest that 4G systems may begin appearing in the 2010 to 2015 time frame [62, 126, 188].

2.5.3 4G Enabling Technologies. To meet the 4G requirements of Table 2.11, a number of technology areas and/or concepts must mature through development and refinement [22]. Hui and Yeung recently highlighted key challenges in migrating to 4G, noting that many challenges are not dependent upon one technology, but rather a combination of key technologies [88]. A brief look at several key 4G enabling technologies related to coding, modulation, and multiple access is provided below, including smart antenna concepts, advanced coding schemes, adaptive modulation, multiple access schemes, ultra wideband signaling, software defined radio, and security measures. These new technologies, used in conjunction with previous technologies of 1G, 2G, 3G, and wireless network systems, will provide a firm foundation for enabling 4G systems.

2.5.3.1 Smart Antenna Concepts. One key to 4G system realization is the incorporation of smart antenna concepts, including multiple-input, multiple-output (MIMO). MIMO, recently referred to as “the most important” wireless technology of the year (2004), is a key enabler to provide the high capacity and data rates required by 4G [205]. MIMO is a smart antenna system that incorporates multiple antennas at the input and/or output - see Fig. 2.15. Data transmitted at the same time using the same frequency is multiplexed spatially at the transmit end and combined at the receive end. MIMO provides high spectral efficiencies in rich scattering environments, since multiple data streams are transmitted over the same path simultaneously [7]. The spatial diversity and coding gain from using MIMO coupled with space-time coding has been shown to yield link budget gains of greater than 10 dB [197].

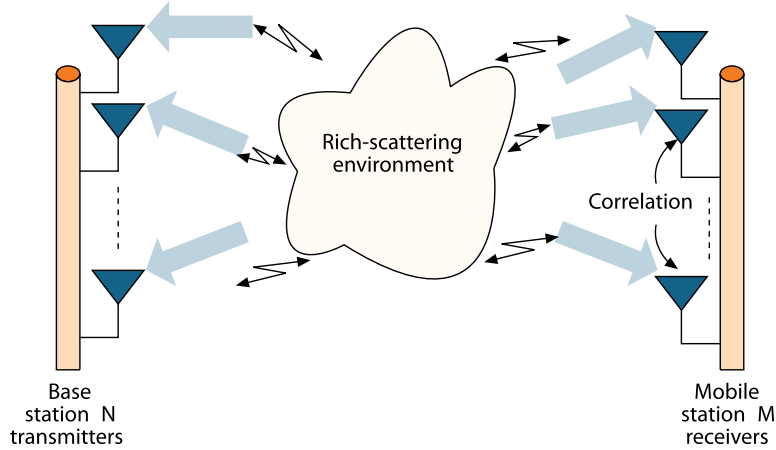


Figure 2.15: Illustration of Multiple-Input, Multiple-Output (MIMO) system using N base stations and M mobile receivers [158].

MIMO technology is an integral part of the planned 3GPP Release 7 [85] and the IEEE 802.11n WLAN variant, which claims to offer 100 Mb/s or higher data rates when deployed [206]. While MIMO shows great promise, it may be difficult to incorporate multiple antennas on mobile terminals that are shrinking every year. To address this concern, a new approach has been proposed called cooperative MIMO relaying (CMIMOR) or virtual antenna array (VAA) technology, which appears to be a valid approach to implementing a MIMO-type system in smaller mobile stations [210].

The VAA concept proposes using multiple mobile terminals as an antenna array to utilize MIMO concepts for a specified receiver.

2.5.3.2 Advanced Coding Schemes. Advanced coding schemes are another key 4G enabler and several have been proposed for future 4G communication systems including concatenated codes (parallel or serial – see Fig. 2.8) and low density parity check (LDPC) codes [73, 126, 131]. Coding performance is generally characterized relative to the Shannon limit which specifies the maximum theoretical channel capacity (bits/sec) of a communications channel for a given transmit power and BER [196]. The closer a given code’s performance comes to the Shannon limit, the better performance it provides. Both concatenated and LDPC coding have achieved performance which is very close to the Shannon limit [12–16, 59, 73, 131, 173].

Concatenated coding, first introduced in 1966, is fundamentally based on the union of two or more codes and an interleaving process [55]. The primary drawback of concatenated coding is increased computational complexity. As better algorithms become available and computational speed increases, more complex coding schemes can be developed and employed. One source suggests that 4G systems may use concatenated coding with Viterbi (convolutional) and Reed-Solomon coding [126], perhaps similar in nature to current IEEE 802.16 coding [114]. By combining codes, the system can transmit larger block sizes while reducing BER.

The most advanced coding scheme used in current 3G systems is Turbo coding [73], which is also referred to as parallel concatenated convolutional coding (PCCC) [13–16] – see Fig. 2.8. Additional research suggests that serial concatenated convolutional coding (SCCC) may outperform Turbo coding in certain scenarios [12].

LDPC coding was initially proposed by Gallager in 1962 [59]. At that time, LDPC codes were far too complex for technology to support and they were practically forgotten for nearly 30 years [73]. In the late 1990s, LDPC codes were re-introduced by MacKay when he showed that their performance was very good; in fact, the performance provided by Gallager’s LDPC codes “nearly surpasses” Turbo

coding while approaching the Shannon limit [131]. Additional research suggests that LDPC codes can “outperform” Turbo codes [73]. Regardless of whether or not LDPC code performance approaches or surpasses Turbo code performance, it is safe to say that their performance is “consistent” with Turbo coding which makes them a viable candidate for 4G systems. Two additional factors support the potential employment of LDPC coding in 4G systems. First, LDPC codes can be iteratively decoded which requires less computational complexity than what is required for SCCC and PCCC decoding [18, 73, 173]. Second, the patent on LDPC codes has expired which gives companies free use of this intellectual property [73].

2.5.3.3 Adaptive Modulation. Adaptive modulation techniques are key to 4G success in achieving higher data rates. Adaptive modulation involves varying transmit power, data rate, code type, and modulation format based on channel conditions [33]. Research has been done on reliable prediction of wireless channels for adaptive modulation [49]. Pairing an adaptive modulation scheme with accurate channel information *at the time of transmission* is the end goal. Better channel conditions permit higher order modulations (and a higher spectral efficiency) and poorer channel conditions dictate lower order modulations.

Several adaptive modulation techniques have been suggested for use with Turbo-coded MC-CDMA to achieve 4G data rates, including M-PSK, M-QAM, M-ary continuous phase modulation (CPM), M-ary multi-hop phase coded modulation (MHPM), and GMSK with a varying bit-duration-bandwidth product of the pre-modulation Gaussian filter [33]. Continuous phase modulations like GMSK, CPM, and MHPM provide better performance than PSK and QAM for a varying set of simultaneous users (performance here refers to BER versus number of users at a constant SNR). If the number of users is known to be less than 10, the QAM and PSK modes perform better. Overall, however, the M-MHPM modulation with a MC-CDMA system is reported to provide optimum adaptive modulation performance [33].

2.5.3.4 Multiple Access Schemes. The next 4G system enabler is the highly-debated area of multiple access (MA). Current 3G systems use W-CDMA or TDMA to accommodate multiple users. Future 4G systems are likely to employ improved MA schemes. Some proposed 4G MA schemes are described below, including: 1) OFDM coupled with TDMA (OFDM-TDMA), 2) a variable spreading factor (VSF)-orthogonal frequency/code division multiplexing technique (VSF-OFCDM), and 3) multi-carrier CDMA (MC-CDMA). An overview of potential 4G multiple access technologies is provided in [94].

As previously noted in Section 2.5.1, the next generation of wireless networks (WiMAX) uses orthogonal frequency division MA (OFDMA) [114]. Additionally, many researchers predict that 4G systems (merging wireless network and cellular technologies) will rely heavily on OFDM-based techniques [82, 117, 118, 217, 248, 250]. The pervasiveness of OFDM suggested by these predictions is apparent in the paragraphs below.

One MA alternative uses OFDM coupled with TDMA (OFDM-TDMA). OFDM is already used in Wi-Fi and WiMAX systems to provide high data rates [118]. OFDM is very robust and impervious to multipath fading effects, and when combined with TDMA, allows users to transmit OFDM-like signals in assigned time slots. OFDM supports M-QAM modulations for providing higher data rates. With OFDM, different users exploit different subcarriers for symbol transmission [243, 244]. Figure 2.17 illustrates the OFDM subcarrier structure. Bandwidth W is equally divided into N_F frequency bands ($N_F = 4$ illustrated) and N_F lower bit rate data streams are transmitted versus one high bit rate data stream. The N_F subcarriers are mutually orthogonal and spaced W/N_F apart. The insertion of a cyclic prefix at the front of each symbol acts as a guard space between successive symbols reducing potential ISI and intercarrier interference (ICI). Because of its construction, OFDM is generally considered more robust in the presence of fading and multipath than other MA schemes, resulting in better communication quality.

The VSF-OFCDM MA technique uses a VSF in conjunction with OFCDM – see Fig. 2.16. VSF-OFCDM adapts the OFCDM frequency and temporal domain’s spreading factor based on channel conditions, delay spreads, and Doppler frequencies. In a multi-cell environment, the spreading factor is larger than one (i.e., the signal is spread) to reduce intercellular interference. In isolated cells (e.g., indoor areas or hot spots), the spreading factor is set to one in OFDM mode to attain maximum throughput. This concept has been shown to achieve proposed 4G data rates [217].

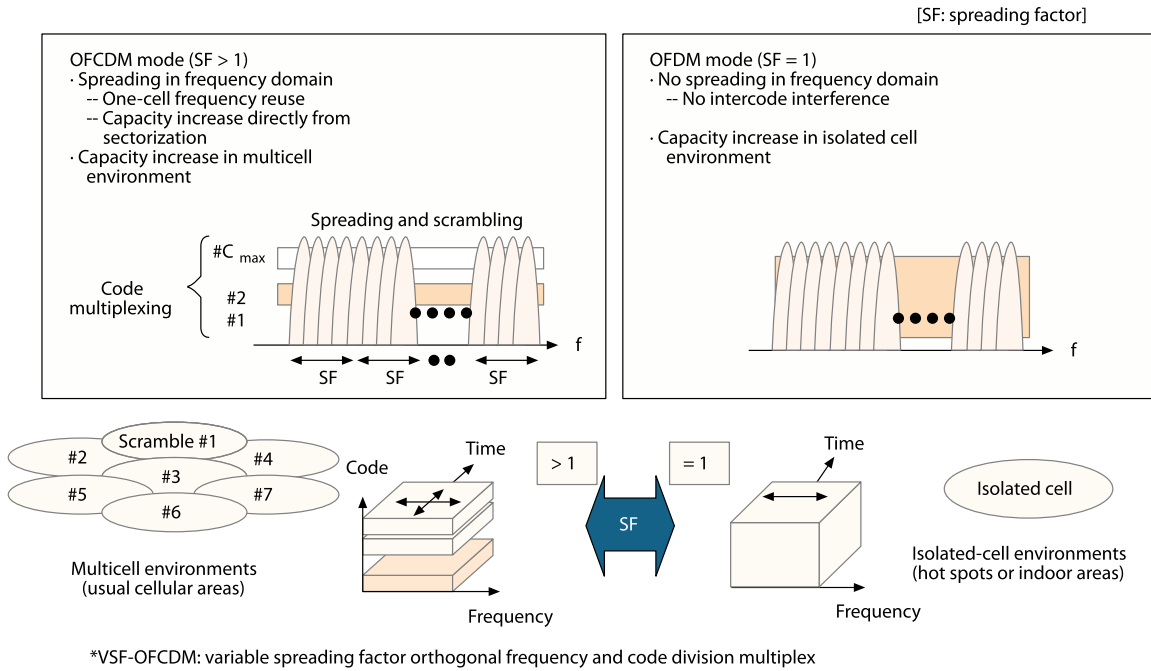


Figure 2.16: Multiple access illustration using a Variable Spreading Factor, Orthogonal Frequency and Code Division Multiplexing (VSF-OFCDM) technique [217].

Multi-carrier CDMA (MC-CDMA) is a third proposed 4G MA scheme [118]. In MC-CDMA, users are multiplexed using orthogonal coding and each user can be allocated several codes with data spread in time or frequency. MC-CDMA typically employs QPSK data modulation. Unlike OFDM, MC-CDMA users *share* subcarriers and transmit identical data over multiple subcarriers [80, 243, 244]. Overall MC-CDMA structure and performance depends upon an F parameter which represents subcarrier spacing. For $F = 1$, as illustrated in Fig. 2.17, the MC-CDMA signal

structure is similar to OFDM yet each transmits data differently. OFDM transmits different symbols on different subcarriers with a goal of reducing transmission rate and increasing symbol duration (to combat multipath fading effects), but MC-CDMA allows different users to share various combinations of subcarriers [243]. Each MC-CDMA user can use all subcarriers or a subset thereof to transmit symbols. Further differences between MC-CDMA and OFDM are described in [28, 80, 225].

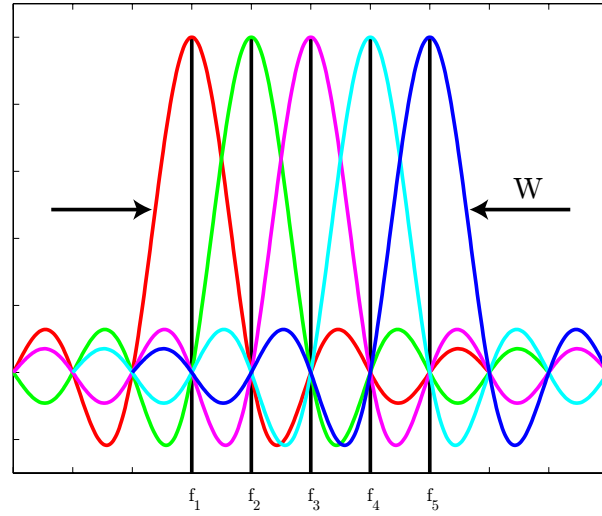


Figure 2.17: Illustration of OFDM and MC-CDMA ($F = 1$) subcarriers. The illustration is for 5 mutually orthogonal subcarriers spaced $W/5$ apart where W is the bandwidth.

2.5.3.5 Ultra Wideband (UWB). Ultra wideband (UWB) is also destined to be a key enabler of 4G communications systems offering high indoor wireless channel and wireless PAN (WPAN) data rates specified by IEEE 802.15.3a - over 110 Mb/s at 10.0 meters and over 480 Mb/s below 4.0 meters [44, 162, 183]. Despite the attraction of such data rates, some analysts assert that coexistence of multiple signals, systems, and networks may really be the beacon of future 4G communication systems [88, 117, 126, 135]. The technical requirements for IEEE 802.15.3a specify the need for UWB devices to coexist with other IEEE 802, cellular, Bluetooth, personal communication services (PCS), global positioning system (GPS), 2.4 GHz, and 5.0

GHz devices [44]. UWB is an interesting 4G enabler because unlike all other signals mentioned herein, this signaling scheme utilizes time hopping with ultra-short pulses.

Per FCC rulings [52, 195], a signal is defined as UWB if its bandwidth is greater than or equal to 500 MHz or if it has a fractional bandwidth greater than 20%; fractional bandwidth is the 10.0 dB bandwidth divided by the center frequency. The original FCC ruling [52] expanded UWB system operation into the 3.1 to 10.6 GHz spectrum. A more recent FCC ruling [195] increased peak power limits for three distinct frequency bands: 5.925 to 7.25 GHz, 16.2 to 17.2 GHz, and 23.12 to 29.0 GHz. A representative Gaussian-based UWB waveform and corresponding energy spectral density plot are provided in Fig. 2.18. Power limitations are imposed to permit spectral coexistence without inducing negative interference effects. Although these rulings impose very restrictive power spectral masks on UWB system operation, they have generated renewed interest in impulse signaling research not only for 4G communications but also applications such as radar, navigation, and imaging.

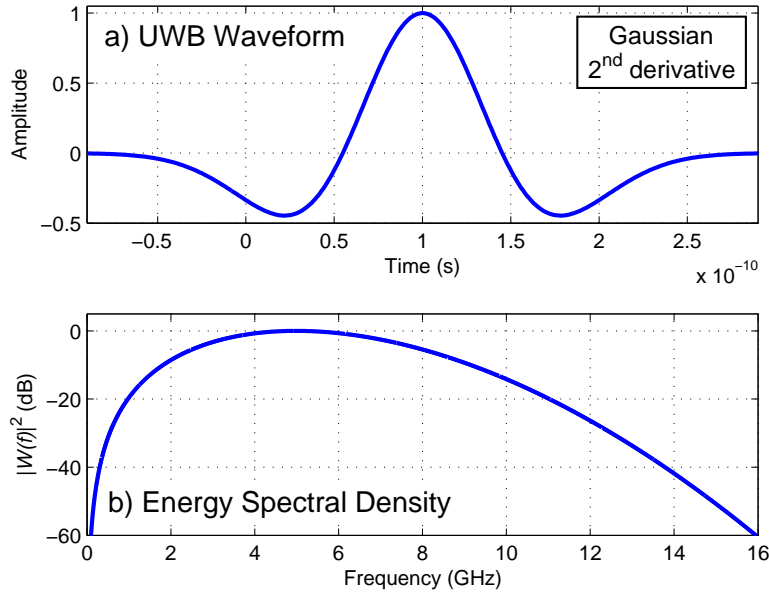


Figure 2.18: Ultra Wideband (UWB) waveform: a) Gaussian-based time domain response having a half-power pulse width response of approximately 0.40 ns, and b) Corresponding Energy Spectral Density (ESD) having a -10 dB bandwidth approximately spanning 2.0 to 9.0 GHz.

A detailed discussion of UWB application to high-speed wireless connectivity can be found in [183]. The ultra-short pulse duration of UWB signals inherently provides multipath immunity and minimizes ISI. Therefore, UWB is an attractive technology for mobile communications, providing high data rates while minimizing BER [126]. As currently developed, UWB is being targeted for short range applications and will likely be an important cog in 4G systems at the WPAN level.

Since UWB signals are generated by transmitting ultra-short duration pulses in the temporal domain, UWB communications inherently use different coding, modulation, and MA schemes. A survey of recent literature reveals two primary methods for achieving UWB MA capability, namely time hopping UWB (TH-UWB) and direct sequence UWB (DS-UWB) – see Fig. 2.19 and Fig. 2.20 [24, 54, 183, 207]. Hybrid techniques combining features of both TH-UWB and DS-UWB have also been proposed [83, 87, 186]. Pseudorandom time and phase coding (e.g., Gold codes [24]) are commonly employed with TH-UWB or DS-UWB techniques, respectively, to enable multiple user capability while minimizing collateral interference and permitting coexistence within existing licensed and unlicensed spectral regions. Such coding is not employed to spectrally “spread” the signal as with conventional DS-SS systems, but rather, coding is employed to permit multiple user signals to temporally and spectrally coexist. Such coexistence is possible because of the low transmit signal power, applied coding scheme, and noise-like properties of UWB signals. Data is conveyed by modulating a train of pulses and varying the amplitude, position, or phase of the individual pulses [24, 183, 207].

The IEEE adopted standard 802.15.3 for the UWB MAC layer and much has been reported on UWB PHY layer developments. Definition of the 802.15.3a PHY layer was underway by the IEEE 802.15 High Rate Alternative PHY Task Group (TG3a) for WPAN over the past few years [89]. Two competing technologies were vying for the PHY standard: direct sequence UWB (DS-UWB) and multi-band OFDM (MB-OFDM). In DS-UWB, multiple pulses are transmitted per bit in a given duration. The pulse sequence relates to a short (i.e., periodically repeated in each bit

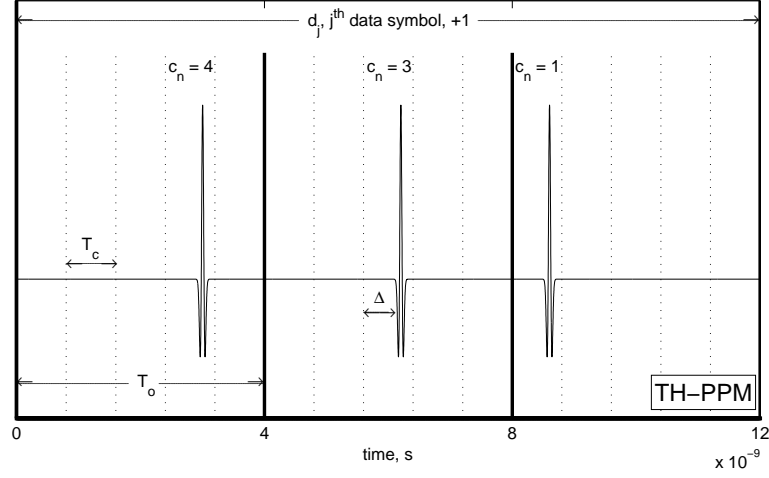


Figure 2.19: Time Hopping UWB (TH-UWB) waveform illustration. Assuming all time slots are available for use and only these intervals are used to transmit the j^{th} data symbol, $N_s = 5$ slots are available during each pulse repetition interval, T_o , and the spreading gain for symbol j is $N_{ss} = 3$. The j^{th} data symbol impacts the pulse position within chip interval T_c , and the n^{th} element of the chip offset sequence impacts the pulse position within T_o .

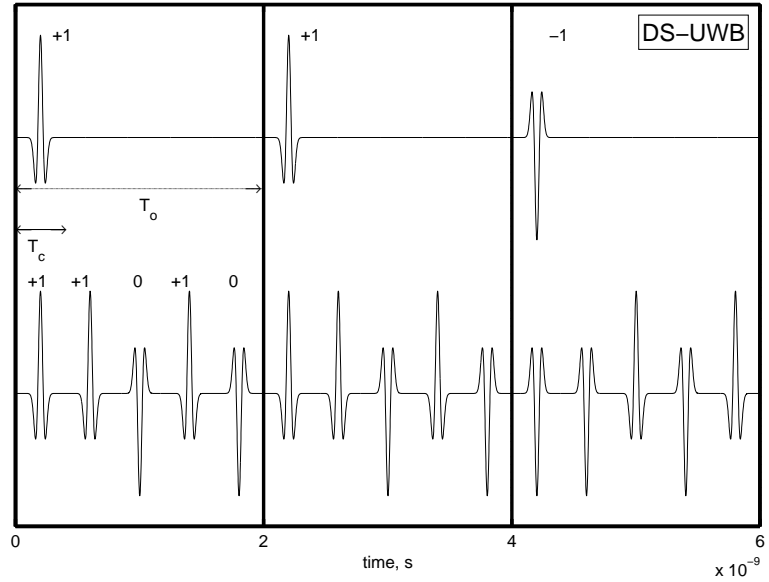


Figure 2.20: Direct Sequence UWB (DS-UWB) waveform illustration for a spreading gain, $N_{ss} = 5$. The j^{th} data symbol and the n^{th} element of the chip phase sequence directly impact the pulse phase within each T_c chip interval.

interval) binary PN code sequence for a user (analogous to CDMA) [183]. MB-OFDM takes an OFDM scheme and multiplexes it with other bands. Another proposal, Common Signaling Mode (CSM), would allow MB-OFDM and DS-UWB systems to coexist [223]. In the end, TG3a was unable to resolve the deadlock between the two camps and the group was disbanded in January 2006 [75]. The WiMedia Forum and the UWB Forum will continue to develop and promote MB-OFDM and DS-UWB, respectively, in a marketplace duel reminiscent of the VHS-Beta war in the 1980s. In fact, one company recently left the UWB Forum and is in the process of forming a Cable-Free Forum, which would result in three industry groups vying for the high-speed, short-range communication market [74].

2.5.3.6 Software Defined Radios. Software defined radio (SDR) techniques could prove vital for enabling 4G system operation and implementation. SDR and software radio (SWR) ideas are paving the way for cognitive radios, i.e., radios which adapt their signal characteristics (temporal, spectral, spatial, etc.) based on channel conditions, traffic loads, interfering signals, and spectrum availability [21, 39, 82, 142, 143].

The envisioned 4G coding, modulation, and multiple access techniques require adaptive waveforms, relying on the inherent flexibility afforded by SDR. As radios progress from analog to digital, more radio features can migrate to software. The benefit of incorporating modulation and/or coding functionality into software modules versus hardware is obvious. As standards, frequencies, and waveforms change, the radio can be easily upgraded by simply changing the software module. The obvious flexibility of this technology makes it a key enabler for 4G services which, on the surface, require flexibility at the waveform level. One such SDR design for communications is available from [70]. The Department of Defense (DoD) is also providing considerable funding to develop SDR and cognitive radio concepts. This funding includes efforts like the Joint Tactical Radio System (JTRS) program headed by the U.S. Army [95, 150] and various programs under the direction of the Defense Ad-

vanced Research Projects Agency (DARPA) such as the Tactical Targeting Network Technology (TTNT) program [151].

SDR also allows user terminals to operate in a multi-mode fashion, adapting themselves to various network wireless interfaces [88]. The goal is to allow a single user terminal to operate in many kinds of wireless networks, overcoming power, cost, size, and compatibility limitations. Some hardware issues to be addressed include determining how to use multiple antennas for one device, developing faster analog-to-digital converters, and developing faster parallel DSP chip sets.

2.5.3.7 Security Measures. Security is not so much an enabling technology as it is something that must be accounted for before users will adopt and use 4G devices. The area of communication security/privacy is sufficiently complex and broad (in and of itself) to warrant an evolutionary chapter of its own. However, a brief synopsis of some security challenges and research areas is provided for completeness.

As discussed in previous sections, 4G will be based on IP network architectures, and 4G networks will therefore need to deal with the same security issues found in traditional wired networks (such as denial-of-service attacks against the networking infrastructure). While there has been extensive research in wireline security technologies over the last 5-10 years, adapting these technologies to the mobile wireless environment will be difficult for a variety of reasons, most notably limitations in battery power, CPU processing power, and data storage in the handsets [163, 227]. Further, these challenges cannot be solved independently, due to the interrelationships involved. For example, coding, modulation, and multiple access selections can impact security at the physical layer. Mobility of the 4G devices presents physical security challenges as well, since control and configuration of the devices will be outside the purview of a dedicated network security administrator. Access control mechanisms, such as wireless public key infrastructure and biometrics, will be required to minimize the impact of loss, theft, or spoofing of 4G handsets [140].

Another interesting challenge is providing seamless, secure end-to-end communications to the mobile user in a heterogeneous network infrastructure. The problem is closely related to providing end-to-end quality of service tailored to the user's needs [57, 227], and as users traverse various networks (WLAN, UMTS, etc.), the security mechanisms must be seamlessly integrated and invisible to the user. Existing security schemes in 2G/3G systems are inadequate for 4G applications, because future requirements will include increased flexibility, reconfigurability, and scalability [6]. While reconfigurability (using SDR technology) is viewed as a huge benefit of 4G, the ability to change the performance of any layer of a network device via new software downloads presents security implications that have yet to be fully understood [163].

2.6 Beyond 4G: Cognitive-Based SDR Implementation Using OFDM

As noted in Section 2.5.2, 4G remains an undefined standard at this time. Perhaps the proposed merger of cellular and WLAN capabilities will be the key outcome of the push toward 4G implementation. Future efforts aimed at unifying technological platforms and devices may fall under a larger umbrella termed *cognitive radio* (CR). CR development is currently in the conceptual phase but may be considered an SDR implementation aid, i.e., the SDR becomes more intelligent and aware of its operating environment through CR principles such that adaptivity to sensed changes occurs in near real-time. For discussion purposes, this work treats CR principles as a means for enhancing and advancing SDR capability and refers to this synergistic union of concepts as *CR-based SDR*. That is, SDR capability provides the software controlled communication vehicle (core technology for air interface and waveform generation), the control and application of which is based on CR principles applied to spectral monitoring to achieve efficient spectrum use. In this sense, 4G enabling technologies can also be viewed as CR enabling technologies and the SDR discussion in Section 2.5.3.6 applies to CR-based SDR as well.

Haykin [82] provides some key concepts that he believes will catapult CR-based SDR systems into existence, systems which he refers to as “brain-empowered communications.” In addition to the 4G enabling technologies described previously, current protocol and regulations that dictate electromagnetic spectral partitioning must become more adaptive and responsive to changing environments, traffic loads, and networks. Only through more efficient use of the spectral bands can spectral and temporal coexistence truly be incorporated into communication systems.

One way to more efficiently use available spectrum in wireless applications is to employ OFDM-based systems, i.e., systems which transfer data using a series of orthogonal subcarriers. In fact, OFDM is identified by Haykin as one of the key bedrocks for CR-based SDR implementation [82]. As noted in Section 2.5.3.4, OFDM-based architectures will likely replace CDMA as the modulation and multiplexing scheme of choice in future 4G systems and beyond. Figure 2.21 shows a representative block diagram for an OFDM-based system [225]. Understanding the fundamental OFDM concept depicted in this figure is key to understanding the primary research contribution, namely, a unified analytic framework representing the plethora of existing OFDM-based signals that are implementable with a SDR system (framework details are presented in Chapter III).

Excluding processes in Fig. 2.21 which account for 1) timing, control, synchronization, etc., (e.g., cyclic extensions, pilot signals, etc.) and 2) conventional performance improvements (e.g., forward error correction, interleaving, etc.), there are two core functions in an OFDM-based system which are of primary interest to this work. These functions include 1) data modulation and/or coding prior to an IFFT operation which generates the transmitted (TX) waveform and 2) an FFT operation followed by data demodulation and/or decoding for processing the received (RX) waveform. As a result of using these N_F -point IFFT/FFT transforms, the waveform subcarriers are inherently orthogonal as depicted previously in Fig. 2.17.

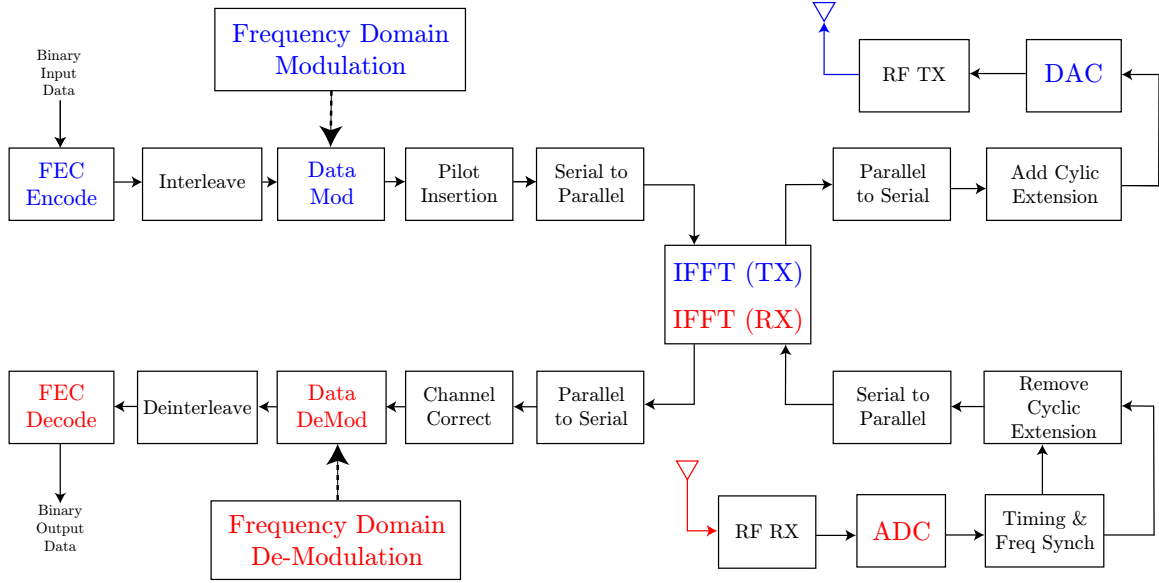


Figure 2.21: Representative block diagram of an OFDM-based system [225].

A plethora of existing signaling schemes (some previously described) use this core TX-RX process, including OFDM, coded OFDM (COFDM), MC-CDMA, VSF-OFCDM, carrier interferometry (CI) OFDM (CI/OFDM), CI/COFDM, CI/MC-CDMA, transform domain communication system (TDCS) variants, and others. These signals all share the property that the data modulation and various coding factors are applied in the spectral domain (before the IFFT), giving rise to the functionally descriptive term *spectrally modulated, spectrally encoded* (SMSE) as introduced here. The framework proposed in Chapter III is specifically designed for SMSE signals and allows for easy transferability to and implementation within a CR-based SDR architecture.

2.7 Background Summary

It is difficult to estimate when full migration to 4G systems will be completed. However, as coding, modulation, and multiple access techniques continue to mature, driven by customer demands for higher data rates, it is reasonable to believe that 4G

systems will emerge in the not too distant future. Early 1G analog cellular systems became available in 1979 and remained active into the early 1990s. Existing 2G digital cellular systems are phasing out in favor of higher speed, packet-routed 3G systems. Based on historical cellular migration, a cellular generation spans 10 to 12 years which suggests that 4G systems may begin appearing in the 2010 to 2015 time frame [62].

FEC coding has migrated from 2G block and convolutional codes to 3G Turbo coding with concatenated coding forecast for 4G systems. Modulation techniques have progressed from simple analog techniques of 1G systems to digital modulations, including the binary modulations of 2G systems, M-ary QAM of 3G systems, and adaptive M-ary techniques as forecast for 4G systems. Multiple access techniques have evolved from using one-dimensional time or frequency division (1G systems), to multi-dimensional time, frequency, and/or code division (spanning 2G and 3G systems).

The evolution toward 4G implementation has induced a surge in the development and exploitation of OFDM-based techniques, with a myriad of acronyms emerging to describe peculiarities associated with each. Given these techniques are fundamentally based on core OFDM principles, and that OFDM-based signals are envisioned as the bedrock of future cognitive-based SDR architectures, a unified analytic framework for spectrally modulated, spectrally encoded (SMSE) signals is proposed which 1) accurately represents existing OFDM-based signals and 2) makes these signals readily transferable to and implementable within an SDR architecture.

III. Analytic SMSE Framework Development

Recent research suggests that fourth generation (4G) communication systems may deploy within the next decade [62, 88, 126]. 4G communications, providing high data rates and ubiquitous, coexistent access over a packet-shared, IP backbone, will seamlessly integrate a myriad of wireless networks allowing nearly universal communication [5, 88, 126, 135]. The goal is to allow body and personal area (e.g., Bluetooth, ultra wideband), local area (e.g., WLAN), metropolitan area (e.g., WiMAX), wide area (e.g., cellular), and global area (e.g., SATCOM) networks to efficiently interface in real-time.

To expedite the development of 4G communication architectures, waveforms must be developed which can coexist within multiple access and multipath interference environments while operating efficiently among neighboring wideband and narrowband signals. As described in Section 2.5.3.6, software defined radio (SDR) is one key enabling technology for generating such waveforms and provides the conduit by which they can be efficiently fashioned and transmitted. Cognitive radio (CR) principles, which adapt the waveform to changing channel conditions, traffic loads, interfering signals, and available spectrum, guide SDR development and implementation [39, 82, 143].

Systems that provide waveform diversity via spectrally modulated, spectrally encoded (SMSE) techniques are prime candidates for future wireless communication architectures. As introduced here, signals are referred to as SMSE if both 1) data modulation (spectrally modulated) and 2) encoding (spectrally encoded) are applied as amplitude and/or phase variations on a discrete component-by-component basis in the frequency domain. In this context, “encoding” accounts for all waveform diversity excluding data modulation effects. This includes coding for multiple access, interference suppression, windowing, etc.

A unifying analytic framework for ultra wideband (UWB) signals has recently been proposed [238–240]. By allowing access to key design variables, this model supports the development, analysis, and implementation of the fundamental UWB wave-

forms most commonly considered at the physical (PHY) network layer. Specifically, the work in [238–240] provides unified models for a transmitter and Rake receiver while accounting for fading channel effects. The analytical SMSE framework presented in this chapter is founded upon the premise that analytical models similar to those developed for UWB would benefit SMSE waveform development and enhance CR-based SDR applications. The overarching goal is advancement towards a unifying SDR analytic framework that employs CR principles across all network layers for temporally designed (e.g., UWB) *and* spectrally designed (e.g., SMSE) signals.

Section 3.1 briefly introduces the unifying UWB framework. More details on UWB signaling, the unifying framework, and UWB coexistence scenarios are provided in Appendix A. Section 3.2 introduces the proposed SMSE framework and provides the impetus for this framework. Section 3.3 introduces key variables that provide generality and flexibility, while Sections 3.4 and 3.6 derive the transmitter and receiver models, respectively, accounting for fading channel effects described in Section 3.5. Section 3.7 extends the existing framework to a multiple-input, multiple-output (MIMO) scenario illustrating model adaptivity for spatial diversity. Finally, Section 3.8 summarizes key facets of the SMSE analytic framework presented in this chapter.

3.1 Unifying UWB Framework

Traditionally, UWB signals are temporally designed by appropriately selecting pulse shape and duration such that the transmitted pulse train consists of short-duration, low-power pulses having correspondingly wide bandwidth. The short pulse duration inherently provides multipath immunity and minimizes intersymbol interference (ISI), while the exceedingly large bandwidth suggests that such signals are inherently spread spectrum (although the extra bandwidth is obtained from the fundamental spectral characteristics of impulse signaling rather than the application of a spreading code). Section 2.5.3.5 describes two primary methods for UWB multiple access signaling: time hopping UWB (TH-UWB) and direct sequence UWB (DS-

UWB). Pseudorandom coding is commonly employed with TH-UWB and DS-UWB signaling to enable multiple user capability while minimizing collateral interference and permitting coexistence within existing licensed and unlicensed spectral regions. Such coexistence is possible because of the low transmit signal power, the applied coding scheme, and the noise-like properties of UWB signals.

Many UWB developments have been reported over the past decade. However, it was not until recently that an effort was made to construct a unifying analytic framework for UWB signals [238–240]. The work in [240] provides a unifying transmitter model for low duty-cycle UWB signals and a general Rake reception model for the same signals. That is, the framework and expressions therein provide for more general analysis, characterization, and implementation of UWB signals. Unique UWB signals are generated by appropriate selection of various waveform design parameters within the model, such as the spreading code, frame duration, chip duration, etc. The Rake receiver model demonstrates reception of this signal after transmission through a multipath fading channel. The entire process and framework lends itself to adaptive implementation within an SDR architecture.

This unifying UWB analytic framework motivates the development of a parallel, unifying analytic framework for spectrally designed signals that are emerging as prime candidates for CR-based SDR applications in 4G architectures and beyond. Detailed model variables and expressions for the existing UWB analytic framework are provided in Appendix A.

3.2 Unifying SMSE Framework

The proposed, unifying SMSE framework parallels the UWB development given by [240] for signals that are designed in the spectral domain. One motivation for spectrally designing signals is to improve spectral coexistence, i.e., decreasing performance degradation caused by multiple signals sharing a common spectrum. To date, several SMSE techniques have been proposed for future 4G systems [28, 29, 33, 94, 217, 250], including orthogonal frequency division multiplexing (OFDM), multi-carrier code di-

vision multiple access (MC-CDMA), other OFDM-based variants, carrier interferometry (CI) signaling, and the transform domain communication system (TDCS). Application of the SMSE framework to these signals is demonstrated in Chapter IV.

Figure 2.21 shows a block diagram of a representative OFDM-based system. According to [82], OFDM represents the bedrock modulation / multiplexing technique of future CR-based SDR communications. As noted in Section 2.6, the OFDM signal is completely designed in the frequency domain. The fast Fourier transform (FFT) and inverse FFT (IFFT) mechanisms ($\mathfrak{F}\{\cdot\}$ and $\mathfrak{F}^{-1}\{\cdot\}$, respectively) provide connectivity between the design and transmission domains (frequency and time in Figure 2.21, respectively). Although not investigated as part of this work, there is no practical reason why the proposed SMSE framework could not be applied using other transform mechanisms, e.g., a similar process could be followed and implemented in a time-frequency fashion using a wavelet transform.

Current SDR developments are focusing almost exclusively on software and hardware improvements. Software improvements include development of an architecture for SDR coding, performed under the auspices of the Software Communication Architecture (SCA) [166]. Hardware improvements include developing reconfigurable and adaptable radio components that are flexible enough to meet the demands of the SDR [76]. What these current SDR developments lack is the theory and analytic framework that fuses these developments together to permit subsequent implementation. The proposed framework aims to fill this void, providing a mathematical background for SMSE signal generation as envisioned in CR-based SDR applications.

3.3 *SMSE Framework: Variables*

The first consideration in developing a general, unifying framework is the number and type of waveform design variables required to ensure the desired level of diversity is achieved. A single user system is first considered with extension to a multi-user system following thereafter. For notational purposes, vectors (matrices) are represented by **bold** lower (upper) case letters. In general, the model specifies the

transmitted waveform design for the k^{th} data symbol of the v^{th} user. Time (frequency) indices for continuous and discrete expressions are t (f) and n (m), respectively.

The most readily apparent SMSE variables to include are the *code*, $\mathbf{c} = [c_1, c_2, \dots, c_{N_F}] = [c_i]_{i=1}^{N_F}$, $c_i \in \mathbb{C}$, and *data modulation*, $\mathbf{d} = [d_1, d_2, \dots, d_{N_F}] = [d_i]_{i=1}^{N_F}$, $d_i \in \mathbb{C}$, where both vectors have identical dimensions and \mathbb{C} denotes the complex numbers. Another important variable which provides for spectral shaping is the *window* function, $\mathbf{w} = [w_1, w_2, \dots, w_{N_F}] = [w_i]_{i=1}^{N_F}$, $w_i \in \mathbb{C}$. Another variable to consider is a phase-only *orthogonality* term, $\mathbf{o} = [o_1, o_2, \dots, o_{N_F}] = [o_i]_{i=1}^{N_F}$, $o_i \in \mathbb{C}$, $|o_i| = 1 \forall i$, that can be used to induce orthogonality amongst symbol streams and facilitate multiple access. These complex coding, data modulation, windowing, and orthogonality factors account for component-by-component amplitude and/or phase variations that are applied to frequency components.

Frequency component selection is a function of two variables. Given an N_F -point FFT process, N_F frequency components are initially available at the system level. This pool of frequencies is reduced by component selection to create a number of *assigned* and *used* frequencies, for which a clear distinction is made. For example, a system may choose to only assign a subset of the N_F frequencies to a user, where the *assignment* is accounted for by $\mathbf{a} = [a_1, a_2, \dots, a_{N_F}] = [a_i]_{i=1}^{N_F}$, $a_i \in \{0, 1\}$, where zeros indicate unassigned frequencies and there are $P_a \equiv \|\mathbf{a}\|^2 \leq N_F$ assigned frequencies, where $\|\bullet\|$ is the Euclidean norm. Such an assignment for \mathbf{a} could be controlled by a local base station (BS) or a cognitive master node operating within an ad hoc network. Within this reduced pool of frequencies, certain components may be locally unavailable due to excessive interference or system design. The *used* frequencies are identified through $\mathbf{u} = [u_1, u_2, \dots, u_{N_F}] = [u_i]_{i=1}^{N_F}$, $u_i \in \{0, 1\}$, where zeros indicate unused frequencies and there are $P_u \equiv \|\mathbf{u}\|^2 \leq P_a \leq N_F$ used frequencies. Thus for the v^{th} user, the used frequencies are those in which $a_i u_i = 1 \forall i$. Given that \mathbf{u} is less than \mathbf{a} , $\mathbf{u} \leq \mathbf{a}$, users can only transmit on assigned frequencies, where $\mathbf{u} \leq \mathbf{a}$ means $u_i \leq a_i$ for each $i = 1, 2, \dots, N_F$.

3.4 SMSE Framework: Transmitter

Accounting for all waveform design variables introduced in Section 3.3, the mathematical model representing the spectral content of the k^{th} SMSE transmitted symbol (\mathbf{S}_k) is given by [176]

$$\mathbf{S}_k = \mathbf{A}_k \odot \mathbf{\Theta}_k \odot \mathbf{F} \quad (3.1)$$

where \odot denotes the Hadamard product, an element-by-element array multiplication. Matrices \mathbf{A}_k and $\mathbf{\Theta}_k$ are of dimension $N_U \times N_F$ with each row corresponding to a distinct user (N_U total users) and each column corresponding to a distinct frequency component (N_F total frequencies). Likewise, matrix \mathbf{F} is of dimension $N_U \times N_F$ and is used to maintain frequency component identification. For example, $S_k(a, b)$ of $\mathbf{S}_{k, N_U \times N_F}$ contains the SMSE information for user a at frequency component b . For the *single* user case, $A_{1m} \in \mathbf{A} = [A_{11}, A_{12}, \dots, A_{1N_F}]_{1 \times N_F}$ is a product of magnitudes from spectral operations, $\Theta_{1m} \in \mathbf{\Theta} = [e^{j\theta_{11}}, e^{j\theta_{12}}, \dots, e^{j\theta_{1N_F}}]_{1 \times N_F}$ is a sum of phases from spectral operations, and $F_{1m} \in \mathbf{F} = [a_1 u_1, \dots, a_{N_F} u_{N_F}]_{1 \times N_F}$ is a frequency on-off indicator.

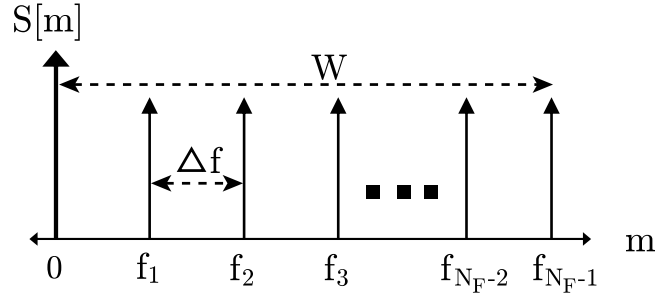


Figure 3.1: Discrete frequency components (N_F total) that are spectrally modulated and encoded prior to inverse transformation and transmission.

The development of (3.1) is provided next using the illustration in Fig. 3.1 as a starting perspective for the general model. A series of discrete frequency components are modified using the variables above to introduce waveform diversity. A continuous time-domain expression for the discrete frequency-domain signal represented in

Fig. 3.1 is found via an IFFT of $S[m]$ and a variable exchange to be

$$s_k(t) = \text{Re} \left\{ \mathfrak{F}^{-1} \left\{ r_m \delta(f - f_m) \right\} \right\}_{m=0}^{N_F-1} \quad (3.2)$$

where r_m is the weighting on the m^{th} spectral component, $t_i \leq t \leq t_i + T_{sym}$, $T_{sym} = N_F/W = N_F \Delta t = 1/\Delta f$, and Δf is the spacing between subcarrier frequency components. The choice of $\Delta f = 1/T_{sym}$ ensures mutual orthogonality between subcarriers over the symbol duration of interest, defined as [46]

$$\int_{t_i}^{t_i+T_{sym}} \psi_k(t) \psi_l^*(t) dt = \delta(k - l) \quad (3.3)$$

where $\psi(t)_k$ is a signal for the k^{th} subchannel. That is, the spectra of individual subchannels is zero at other subcarrier frequencies, eliminating interchannel interference [36, 220].

Using (3.2) and Fig. 3.1, an SMSE waveform expression can be developed by first applying the complex data modulation (**d**), coding (**c**), and windowing (**w**) design variables introduced in Section 3.3. The resultant baseband expression for the k^{th} data modulated symbol $\mathbf{s}_k[m]$ can be written as a sequence of N_F terms given by

$$\mathbf{s}_k[m]_{1 \times N_F} = \left[c_m d_{m,k} w_m e^{j(\theta_{d_{m,k}} + \theta_{c_m} + \theta_{w_m})} \right]_{m=0}^{N_F-1} \quad (3.4)$$

where m is the frequency component index and c_m , θ_{c_m} , $d_{m,k}$, $\theta_{d_{m,k}}$, w_m , and θ_{w_m} are the corresponding magnitudes and phases of the design variables. By design, the coding and windowing factors only vary with frequency index m while the data modulation factor obviously varies with symbol index k as well. The expression in (3.4) can be further modified to incorporate *orthogonality* (**o**) and account for frequency *assignment* (**a**) and *use* (**u**) via

$$\mathbf{s}_k[m]_{1 \times N_F} = \left[a_m u_m c_m d_{m,k} w_m e^{j(\theta_{d_{m,k}} + \theta_{c_m} + \theta_{w_m} + \theta_{o_{m,k}})} \right]_{m=0}^{N_F-1} \quad (3.5)$$

where the product $a_m u_m \in \{0, 1\}$ as indicated before and [232]

$$\theta_{o_m,k} = \left[a_m u_m \sum_{i=0}^{m-1} a_i u_i \right] (\Delta \theta_{o_k}) \quad (3.6)$$

where

$$\Delta \theta_{o_k} = \left(\frac{2\pi}{P_u} \right) \cdot k \quad (3.7)$$

and $P_u \leq N_F$ is the number of frequencies used (non-zero spectral component weights). The new phase term $\theta_{o_m,k}$ effectively places a linear phase progression across those frequency components that are used. This accommodates multiple access by ensuring orthogonality between users (or symbol streams), as controlled by cognitive assignment within \mathbf{a} . Substituting (3.7) into (3.6) yields

$$\theta_{o_m,k} = k \cdot \left(\frac{2\pi a_m u_m}{P_u} \right) \sum_{i=0}^{m-1} a_i u_i. \quad (3.8)$$

Since $\mathbf{u} \leq \mathbf{a}$, (3.8) can be simplified to

$$\theta_{o_m,k} = k \cdot \left(\frac{2\pi u_m}{P_u} \right) \sum_{i=0}^{m-1} u_i. \quad (3.9)$$

Two examples are introduced to illustrate how the $\theta_{o_m,k}$ term in (3.9) is used. For the first example, assume that $N_F = 5$ frequency components are assigned and all five are used, $i = 1, 2, \dots, 5$. In this case, m ranges from 0 to $N_F - 1 = 4$, $\mathbf{u} = [1 \ 1 \ 1 \ 1 \ 1]$, and

$$\begin{aligned} \theta_{o_m,k} &\in k \cdot \left[\frac{2\pi 1 \cdot 0}{5}, \frac{2\pi 1 \cdot 1}{5}, \dots, \frac{2\pi 1 \cdot 4}{5} \right] \\ &\in k \cdot \left[0, \frac{2\pi}{5}, \dots, \frac{8\pi}{5} \right]. \end{aligned}$$

For the second example, assume five frequency components are again assigned but the middle component is notched out such that only four frequency components are used. Hence, $\mathbf{u} = [1 \ 1 \ 0 \ 1 \ 1]$ and (3.9) yields

$$\begin{aligned}\theta_{o_{m,k}} &\in k \cdot \left[\frac{2\pi 1 \cdot 0}{4}, \frac{2\pi 1 \cdot 1}{4}, \frac{2\pi 0 \cdot 1}{4}, \frac{2\pi 1 \cdot 2}{4}, \frac{2\pi 1 \cdot 3}{4} \right] \\ &\in k \cdot \left[0, \frac{2\pi 1 \cdot 1}{4}, 0, \frac{2\pi 1 \cdot 2}{4}, \frac{2\pi 1 \cdot 3}{4} \right] \\ &\in k \cdot \left[0, \frac{\pi}{2}, 0, \pi, \frac{3\pi}{2} \right].\end{aligned}$$

All waveform design variables of Section 3.3 are now incorporated in (3.5) and the reference signal presented in Fig. 3.1 is properly *designed*, i.e., spectral data modulation and encoding factors are present. Considering the m^{th} term in (3.5) and combining magnitude, phase, and frequency terms as

$$\begin{aligned}A_{m,k} &= c_m d_{m,k} w_m \\ \Theta_{m,k} &= e^{j(\theta_{d_{m,k}} + \theta_{c_m} + \theta_{w_m} + \theta_{o_{m,k}})} \\ F_m &= u_m\end{aligned}\tag{3.10}$$

then (3.5) can be rewritten for the *multi-user* scenario as [176]

$$\mathbf{s}_k^{(v)}[m]_{1 \times N_F} = \left[A_{m,k}^{(v)} \Theta_{m,k}^{(v)} F_m^{(v)} \right]_{m=0}^{N_F-1}\tag{3.11}$$

where superscript (v) has been introduced to represent the v^{th} user. The expression in (3.11) is structurally and functionally consistent with (3.1) for a single user where frequency on-off indication is contained in \mathbf{F} . The analytic framework developed in (3.5) and (3.11) and modeled by (3.1) is simple to comprehend and apply yet broadly applicable and useful for representing most SMSE signals.

Now considering all N_U total users, the expression in (3.11) can be used to form a composite matrix for all users, given by

$$\mathbf{S}_k = \begin{bmatrix} \mathbf{s}_k^{(1)}[m] \\ \mathbf{s}_k^{(2)}[m] \\ \vdots \\ \mathbf{s}_k^{(N_U)}[m] \end{bmatrix} = \begin{bmatrix} \left[A_{m,k}^{(1)} \Theta_{m,k}^{(1)} F_m^{(1)} \right]_{m=0}^{N_F-1} \\ \left[A_{m,k}^{(2)} \Theta_{m,k}^{(2)} F_m^{(2)} \right]_{m=0}^{N_F-1} \\ \vdots \\ \left[A_{m,k}^{(N_U)} \Theta_{m,k}^{(N_U)} F_m^{(N_U)} \right]_{m=0}^{N_F-1} \end{bmatrix} \quad (3.12)$$

$$\mathbf{S}_k = \mathbf{A}_k \odot \Theta_k \odot \mathbf{F} \quad (3.13)$$

where \mathbf{S}_k is of dimension $N_U \times N_F$ and (3.13) matches the expression in (3.1).

The SMSE symbol generation process [225] for a given user first involves transforming (3.11) into the time domain using an inverse discrete Fourier transform (IDFT). The n^{th} component of an N_F -point IDFT operating on $Y[m]$ ($n = 0, 1, \dots, N_F - 1$) is given by [92]

$$y[n] = \frac{1}{N_F} \sum_{m=0}^{N_F-1} Y[m] e^{j \frac{2\pi n m}{N_F}}. \quad (3.14)$$

The SMSE time-domain symbols are generated by applying this IDFT operation to (3.11) and taking the real part, expressed as

$$s_k^{(v)}[n]_{1 \times 1} = \text{Re} \left\{ \frac{1}{N_F} \sum_{m=0}^{N_F-1} A_{m,k}^{(v)} \Theta_{m,k}^{(v)} \underbrace{F_m^{(v)} e^{j(2\pi f_m t_n)}}_{\bar{F}_m^{(v)}} \right\} \quad (3.15)$$

$$\mathbf{s}_k[n]_{N_U \times 1} = \text{Re} \left\{ \frac{1}{N_F} \mathbf{A}_k \odot \Theta_k \bullet^r \bar{\mathbf{F}} \right\} \quad (3.16)$$

where $f_m = m/(N_F \Delta t)$, $t_n = n \Delta t$ [228, 252], $\bar{F}_m^{(v)}$ incorporates IDFT sinusoidal factors and on-off frequency identification elements, \bullet^r is a row-wise inner (dot) product,

and \mathbf{s}_k is of dimension $N_U \times 1$. Equation (3.15) can be equivalently represented as

$$s_k^{(v)}[n]_{1 \times 1} = \frac{2}{N_F} \sum_{m=0}^{N_F-1} A_{m,k}^{(v)} F_m^{(v)} \cos \left(2\pi f_m t_n + \theta_{c_m}^{(v)} + \theta_{d_{m,k}}^{(v)} + \theta_{w_m}^{(v)} + \theta_{o_{m,k}}^{(v)} \right) \quad (3.17)$$

for $t_i \leq t_n \leq t_i + T_{sym}$, $T_{sym} = N_F \Delta t = 1/\Delta f$, and $f_m = m\Delta f$, where Δf is the frequency resolution shown in Fig. 3.1.

Now accounting for N_U total users, simultaneously and independently operating in a multi-channel system, (3.17) is expanded to yield

$$s_k[n]_{1 \times 1} = \frac{2}{N_F} \sum_{v=1}^{N_U} \sum_{m=0}^{N_F-1} A_{m,k}^{(v)} F_m^{(v)} \cos \left(2\pi f_m t_n + \theta_{c_m}^{(v)} + \theta_{d_{m,k}}^{(v)} + \theta_{w_m}^{(v)} + \theta_{o_{m,k}}^{(v)} \right). \quad (3.18)$$

This expression can be more succinctly written using (3.16) as

$$s_k[n]_{1 \times 1} = \text{Re} \left\{ \mathbf{1}_{1 \times N_U} \left(\frac{1}{N_F} \mathbf{A}_k \odot \Theta_k^r \bar{\mathbf{F}} \right) \right\} \quad (3.19)$$

where $\mathbf{1}_{1 \times N_U}$ is a $1 \times N_U$ vector of ones. Thus, the k^{th} SMSE symbol (vector) is completely described in the time-domain as

$$\mathbf{s}_k = \{s_k[0], s_k[1], \dots, s_k[N_F - 1]\} \quad (3.20)$$

which temporally represents one symbol interval, $t_i \leq t_n \leq t_i + T_{sym}$. Prior to transmission, this signal is generally concatenated with multiple, identically constructed, independent signals to create a data *frame*. A preamble containing synchronization and other header information may also be temporally prepended to identify this frame at the receiver. These temporal operations are merely concatenation; conceptually, the signal is constructed completely in the spectral domain. The composite transmitted signal (accounting for multiple users, preambles, and data frames) can be represented in the time domain as

$$\mathbf{s}_s = [\mathbf{s}_{pre} \ \mathbf{s}_1 \ \mathbf{s}_2 \ \dots \ \mathbf{s}_{N_{sym}}]_{1 \times [N_F N_{sym} + \text{preamble}]} \quad (3.21)$$

where \mathbf{s}_{pre} represents preamble information and there are N_{sym} temporally concatenated symbols per data frame.

Symbol concatenation can be mathematically introduced in the spectral domain by introducing an appropriate phase shift on each symbol to be concatenated. The SMSE framework is easily expanded to accommodate this factor. Consider the addition of another spectral phase term to represent time delays as phase shifts (basic Fourier relationship), i.e., $\theta_{t_k} = e^{-j2\pi f_m t_k}$ where t_k is the time delay for the concatenated k^{th} symbol. In this case, Equation (3.1) can be rewritten as

$$\mathbf{S}_k = \mathbf{A}_k \odot \mathbf{\Theta}_k \odot \mathbf{F} \odot \mathbf{\Theta}_{t_k} \quad (3.22)$$

where $\mathbf{\Theta}_{t_k} = \theta_{t_k} \times \mathbf{1}_{N_U \times N_F}$. Then, the transmitted signals shown in (3.18) and (3.19) are modified to be

$$\begin{aligned} s_k[n]_{1 \times 1} &= \frac{2}{N_F} \sum_{v=1}^{N_U} \sum_{m=0}^{N_F-1} A_{m,k}^{(v)} F_m^{(v)} \cos \left(2\pi f_m t_n + \theta_{c_m}^{(v)} + \theta_{d_{m,k}}^{(v)} + \theta_{w_m}^{(v)} + \theta_{o_{m,k}}^{(v)} - \theta_{t_k} \right) \\ &= \text{Re} \left\{ \mathbf{1}_{1 \times N_U} \left(\frac{1}{N_F} \mathbf{A}_k \odot \mathbf{\Theta}_k \bullet^r \bar{\mathbf{F}} \odot \mathbf{\Theta}_{t_k} \right) \right\}. \end{aligned} \quad (3.23)$$

3.5 Fading Channel

The channels supporting SMSE signals will inherently degrade transmitted signal quality. In realistic, dynamic environments (e.g., urban or office settings), severe multipath fading may be present, implying that an additive white Gaussian noise (AWGN) channel model does not sufficiently represent more realistic wireless communication channels (although it can provide a best-bound on performance). The subsections below introduce key fading channel parameters, three fading channel losses, different kinds of fading channels, and mathematical descriptions of the channels. Unless otherwise mentioned, all material in Section 3.5 is taken from [171, 204].

3.5.1 Key Parameters. Several key parameters are used to identify the type of fading channel. Generally, three kinds of losses are identified within the fading channel: free-space path loss, large-scale fading, and small-scale fading.

Free-space path loss is affected by a path loss exponent n_p , which varies based on frequency, antenna height, and the operating environment. For free-space propagation, $n_p = 2$ with smaller values occurring in some cases (e.g., urban streets with strong waveguide attributes) and larger values occurring in others (e.g., amidst terrain obstacles).

Large-scale fading is primarily characterized by a shadowing term, X_σ , which is a zero-mean Gaussian random variable with standard deviation σ . Small-scale fading is characterized by three terms in either the time or frequency domain. From a frequency domain perspective, three parameters characterize the small-scale fading environment.

- **Signal Bandwidth:** A range of frequencies over which the signal of interest spans. A general rule-of-thumb expression for communication *signal bandwidth* W is

$$W \approx \frac{1}{T_{sym}} \quad (3.24)$$

where T_{sym} is the transmitted symbol duration (period).

- **Coherence Bandwidth:** A range of frequencies over which all spectral components of the signal of interest are passed with equal gain (attenuation) and linear phase. A general rule-of-thumb expression for *coherence bandwidth* B_c is

$$B_c \approx \frac{1}{5\sigma_\tau} \quad (3.25)$$

where σ_τ is the *root-mean-square (rms) delay spread* of the multipath channel.

- **Doppler Bandwidth:** A range of frequencies that quantify the amount of spectral broadening that occurs in the signal of interest due to motion. This is

also referred to as Doppler spread, fading bandwidth, fading rate, and spectral broadening. One expression for *Doppler bandwidth* B_d is

$$B_d = \frac{v}{\lambda} \quad (3.26)$$

where v is relative velocity between the transmitter and receiver and λ is the signal of interest wavelength.

The dual time-frequency relationship allows for small-scale fading to be characterized by three related parameters from a time-domain perspective.

- **Symbol Period:** The time required to transmit one communication symbol. A general rule-of-thumb expression for *symbol period* is

$$T_{sym} \approx \frac{1}{W}. \quad (3.27)$$

- **Multipath Spread:** The time period (i.e., delay) during which the multipath components exceed a specified power relative to the strongest multipath component. Multipath spread T_m is generally a reciprocal of the coherence bandwidth

$$T_m \approx \frac{1}{B_c}. \quad (3.28)$$

However, this is not the best indicator of system performance during signal propagation because channels with identical T_m can possess widely different signal-intensity profiles. Hence, a more useful parameter is the *rms delay spread*, which is determined using the following rule-of-thumb

$$\sigma_\tau \approx \frac{1}{5B_c}. \quad (3.29)$$

- **Coherence Time:** The time period during which the channel remains steady, i.e., no temporal or spectral variations occur. A general rule-of-thumb expression

for coherence time T_c is

$$T_c = \sqrt{\frac{9}{16\pi B_d^2}} \approx \frac{0.423}{B_d}. \quad (3.30)$$

3.5.2 Practical Description. In a perfect operating environment, a communication system only experiences free-space path loss, i.e., no other signal degradation mechanisms exist within the channel. Signal path loss is generally represented as

$$L_s(d) = \left(\frac{4\pi d}{\lambda} \right)^{n_p} \quad (3.31)$$

where d is the transmitter-receiver distance, λ is the signal wavelength, and $n_p = 2$ is the path loss exponent in free-space. The incident received signal power (in decibels) is given by

$$P_r = EIRP(dB) - 10\log_{10} L_s(d) \quad (3.32)$$

where $EIRP = P_t \times G_t$, P_t is transmitter power into the antenna, and G_t is the transmit antenna gain in the direction of the receiver.

However, communication systems seldom operate in perfect environments and generally suffer the effects of multiple reflective paths (i.e., multipath). Reflected signals from multiple paths constructively and destructively interfere due to propagation mechanisms such as reflection, diffraction, and scattering. This interference causes fluctuations in signal amplitude, phase, and angle-of-arrival, creating a phenomenon called fading. Two types of fading effects characterize mobile, wireless communication: large-scale fading and small-scale fading.

Large-scale fading refers to the average signal path loss from motion over large areas. This phenomenon is marked by shadowing from prominent terrain features and is typically described via a mean path loss and a log-normally distributed variation. The mean path loss is proportional to the n_p^{th} power of the transmitter-receiver

distance d relative to a reference distance d_0 , and is expressed as [204]

$$\overline{L_p}(d) = L_s(d_0) + 10 n_p \log_{10} \left(\frac{d}{d_0} \right) \quad (3.33)$$

where $L_s(d_0)$ has units of dB, is given by (3.31), and d_0 usually equals 1 km for large cells, 100 m for microcells, and 1 m for indoor cells. Accounting for shadowing, the path loss is

$$L_p(d) = L_s(d_0) + 10 n_p \log_{10} \left(\frac{d}{d_0} \right) + X_\sigma \quad (3.34)$$

where X_σ is a zero-mean, Gaussian random variable with standard deviation σ . Process X_σ can take on values as high as 6 to 10 dB. Hence, large-scale fading can be statistically described and accounted for if the reference distance, path-loss exponent, and standard deviation of X_σ are known.

Small-scale fading refers to abrupt changes that can occur in the signal characteristics as a result of small changes (a couple of wavelengths) in the spatial positioning between a transmitter-receiver pair. The manifestation of small-scale fading is based upon two factors: signal time-spreading due to multipath and channel time-variance due to motion-induced Doppler. Figure 3.2 shows a breakdown of how fading effects can be viewed from time and frequency domain perspectives.

Small-scale fading is referred to as Rayleigh fading when there are many reflective paths (more than 30 to invoke the central limit theorem) and there is *no* line-of-sight (LOS) path. The amplitude envelope of the received signal is described using a Rayleigh probability density function (pdf) [171]

$$p(r) = \begin{cases} \frac{r}{\sigma^2} \exp \left(-\frac{r^2}{2\sigma^2} \right) & (0 \leq r \leq \infty) \\ 0 & (r < 0) \end{cases} \quad (3.35)$$

where σ^2 is the time-average received signal power before envelope detection. Meanwhile, a signal containing a dominant LOS path is characterized as a Ricean fading

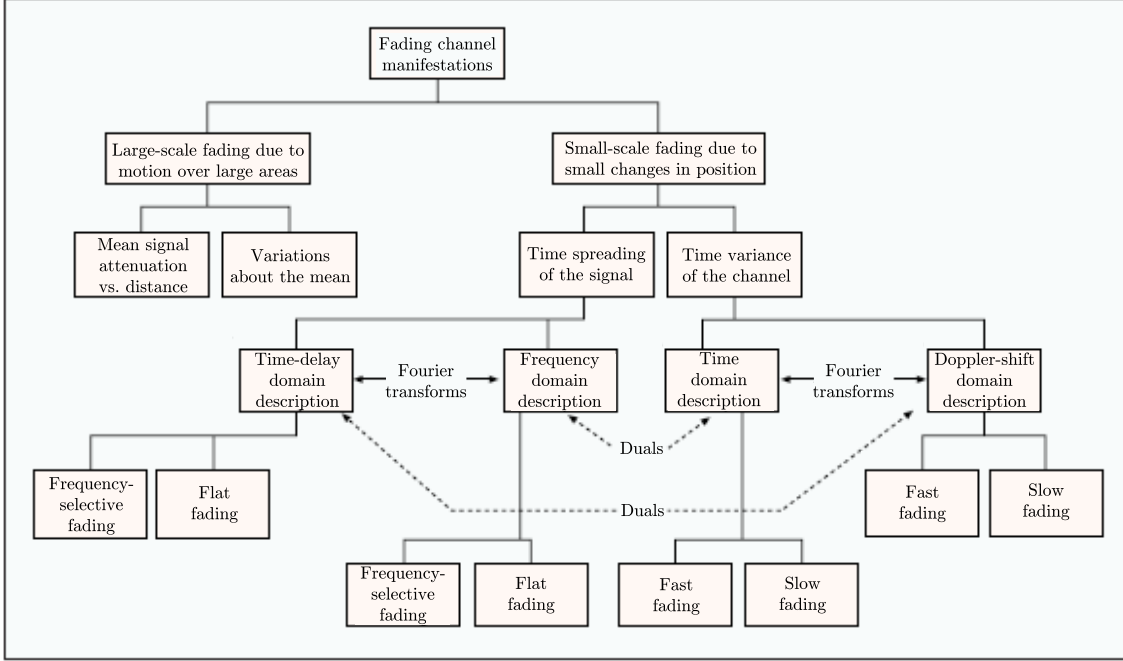


Figure 3.2: Fading channel manifestations: large-scale vs small-scale, slow vs fast, and flat vs frequency selective [204].

channel using the Ricean pdf [204]

$$p(r) = \begin{cases} \frac{r}{\sigma^2} \exp\left(-\frac{r^2 + A^2}{2\sigma^2}\right) I_0\left(\frac{Ar}{\sigma^2}\right) & (A \geq 0, r \geq 0) \\ 0 & (r < 0) \end{cases} \quad (3.36)$$

where σ^2 is again the time-average received signal power before envelope detection, A is the peak amplitude of the LOS signal, and $I_0(\bullet)$ is a modified Bessel function of the first kind and zero-order.

Thus, according to [204] a signal encounters three primary loss mechanisms in a channel: 1) mean path loss, which is a function of transmitter-receiver separation distance, 2) large-scale fading (normally 6 to 10 dB), which is a function of terrain obstacle shadowing, and 3) small-scale fading (normally 20 to 30 dB), which is a function of signal time-spreading or channel time-variant characteristics. A mobile wireless radio must be able to process a signal that is affected by all three mechanisms, with system error budgets accounting for expected losses.

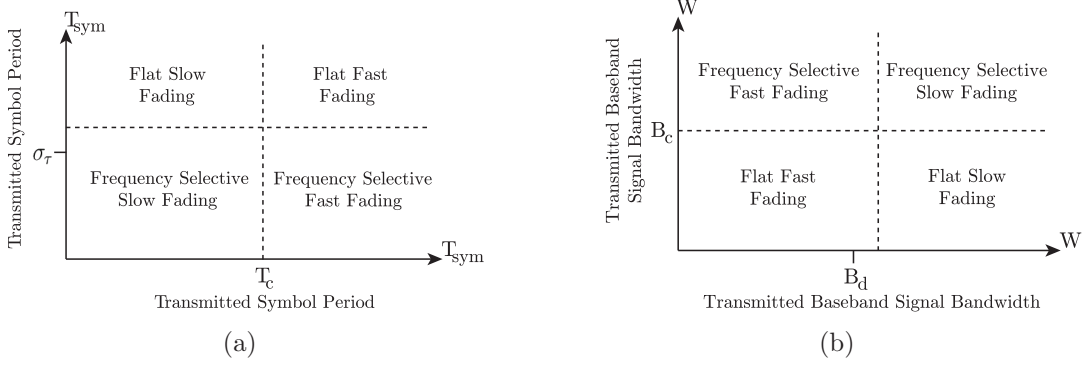


Figure 3.3: Fading channel characterization: (a) as a function of transmitted symbol period T_{sym} and (b) as a function of signal bandwidth W [171].

The different small-scale fading channels are broken down in Figure 3.3 based upon the parameters described in Section 3.5.1. *Frequency selective* implies that signal bandwidth is greater than coherence bandwidth ($W > B_c$) and symbol period is less than rms delay spread ($T_{sym} < \sigma_\tau$). Wideband channels generally contain frequency selective fading, and when a channel is frequency-selective, individual multipath components are resolvable. *Flat*, or non-frequency selective, implies that $W < B_c$ and $T_{sym} \gg \sigma_\tau$. Narrowband channels generally induce flat fading. *Slow fading* implies that $W \gg B_d$ (Doppler bandwidth) and $T_{sym} < T_c$ (coherence time). Transmissions from relatively stationary radios generally traverse slowly-fading channels. *Fast fading* implies that $W < B_d$ and $T_{sym} > T_c$. Transmissions from relatively high-speed radios undergo a large Doppler spread and generally traverse fast fading channels. Four examples are provided below which demonstrate different channel conditions.

3.5.2.1 Example #1: Flat, slowly-fading channel. Consider a scenario where an analyst downloads mission data to a GSM cell phone while riding in a vehicle through a suburban environment. The GSM phone (with $W = 200$ kHz channels) receives the download at 950 MHz while moving 100 km/hr. The Doppler spread is $B_d = 88$ Hz, so the channel is slowly-fading because $W \gg B_d$. A typical rms delay spread for a suburban environment is 400 ns, with a corresponding coherence bandwidth of $B_c = 500$ kHz. Thus, the channel is also flat because $W < B_c$.

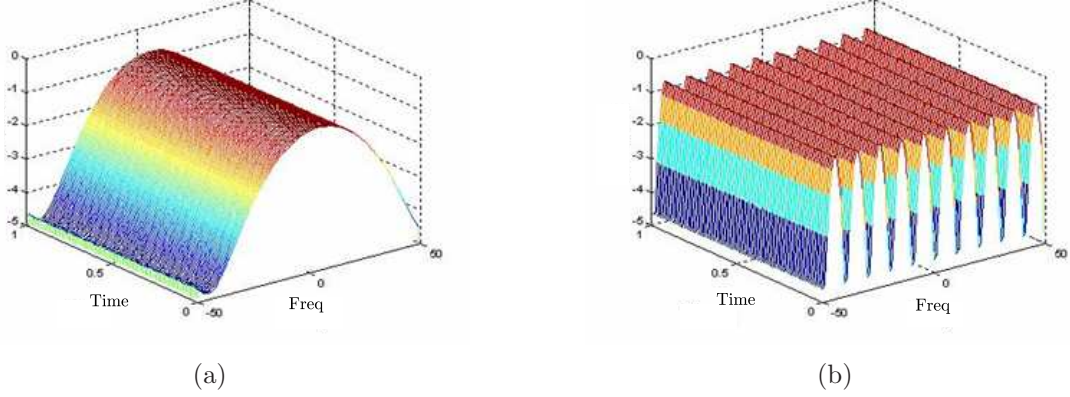


Figure 3.4: (a) Example #1: Flat, slowly-fading channel. (b) Example #2: Frequency selective, slowly-fading channel. [10]

3.5.2.2 Example #2: Frequency selective, slowly-fading channel. In this scenario, the analyst uses a new 3G wireless device with CDMA2000 1×EV-DO technology. The 1×EV-DO device downloads information at 875 MHz over a $W = 1.25$ MHz channel. The Doppler spread slightly drops to $B_d = 81$ Hz due to the slight change in operating frequency, but the channel remains slowly-faded because $W \gg B_d$. However, W is now larger than the coherence bandwidth, 1.25 MHz $>$ 500 kHz, so the channel is now frequency selective. Figure 3.4 illustrates the time-frequency relationship of slowly-fading channels.

3.5.2.3 Example #3: Flat, fast fading channel. In this scenario, the analyst uses a new covert wireless device for increased security. The analyst selects the lowest data rate available (256 b/s over a $W = 100$ Hz channel) to download the non-time-sensitive data. Also, this new device operates in a higher PCS band (1900 MHz) and the analyst is now traveling in a high-speed train at 200 km/hr. The Doppler spread is $B_d = 351$ Hz, so the channel is fast-fading since $W < B_d$. Obviously, since W is really small and the analyst is still in a suburban environment, the channel remains flat.

3.5.2.4 Example #4: Frequency selective, fast fading channel. Now the analyst is downloading information in the U-NII band at 5.4 GHz using a low-rate

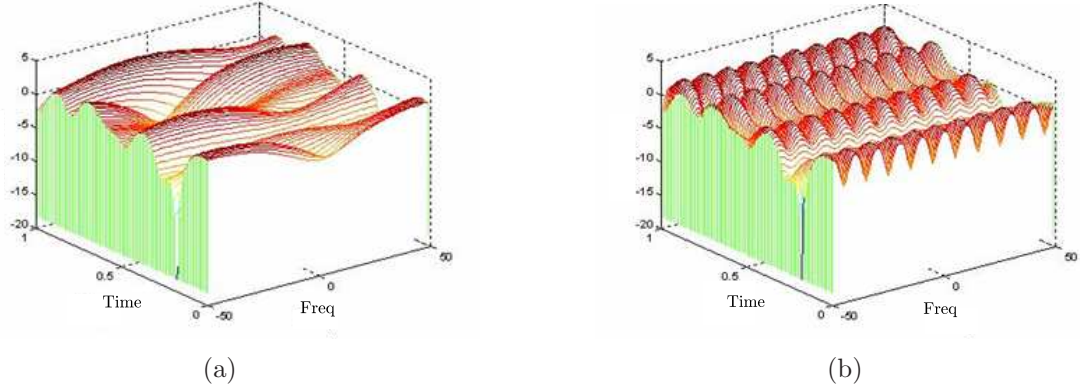


Figure 3.5: (a) Example #3: Flat, fast fading channel. (b) Example #4: Frequency selective, fast fading channel. [10]

$W = 4.8$ kHz channel, while traveling through a severe urban multipath environment, where the coherence bandwidth is $B_c = 4$ kHz. Also, the high-speed train is an experimental, near-supersonic version traveling at 300 m/s, or ~ 700 mph. The Doppler spread for the train speed and U-NII frequency range is $B_d = 5.36$ kHz. Because $W < B_d$, the channel is fast-fading, and because $W > B_c$, the channel is frequency selective. This type of fading channel is arguably the most uncommon in wireless communication applications because Doppler bandwidth is rarely higher than the coherence bandwidth. Figure 3.5 illustrates the time-frequency relationship of fast fading channels.

3.5.3 Mathematical Representation. For SMSE analytical development, three channels are considered with the simplest being AWGN. In AWGN channels, a complex random process is summed with the transmitted signal to form the received signal

$$r_k(t) = s_k(t) + n(t). \quad (3.37)$$

The noise process $n(t)$ is normally distributed in the real and imaginary channels and has a two-sided power spectral density of $N_o/2$ Watts/Hz.

The second channel considered is a Rayleigh flat, slowly-fading channel. In a Rayleigh flat fading channel, it is assumed there is only one signal path between the

transmitter and receiver (a valid assumption provided that the signal bandwidth is less than the coherence bandwidth) [165]. The signal along this path is weighted by a complex Rayleigh fading coefficient having a Rayleigh-distributed magnitude response and uniformly-distributed phase response. In this case, $r_k(t)$ is the sum of the weighted signal and AWGN noise process

$$r_k(t) = b_R s_k(t) + n(t) \quad (3.38)$$

where b_R is the Rayleigh fading coefficient. This expression assumes that the channel is “slow” enough such that the receiver can perfectly estimate the channel phase shift without error. Figure 3.6 shows a block diagram for incorporating this flat fading channel effect.

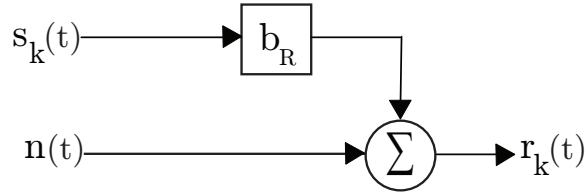


Figure 3.6: Rayleigh flat fading channel model.

The third channel considered is a Rayleigh frequency selective, slowly-fading channel which can be modeled using a tapped delay line (TDL) model – see Fig. 3.7. The channel impulse response from the TDL model can be represented as [60, 165]

$$h(t) = \sum_{l=0}^{N_{MP}} b_l(t) \delta[t - \tau_l(t)] \quad (3.39)$$

$$= \sum_{l=0}^{N_{MP}} \gamma_l(t) e^{j\theta_l(t)} \delta[t - \tau_l(t)] \quad (3.40)$$

where $0 \leq \tau \leq T_{sym}$, there are N_{MP} multipath signals, $b_l(t) = \gamma_l(t) e^{j\theta_l(t)}$, and $b_l(t)$, $\gamma_l(t)$, $\theta_l(t)$, and $\tau_l(t)$ are the time-varying complex coefficient, magnitude, phase, and delay of the l^{th} multipath signal, respectively. For the direct path signal ($l = 0$),

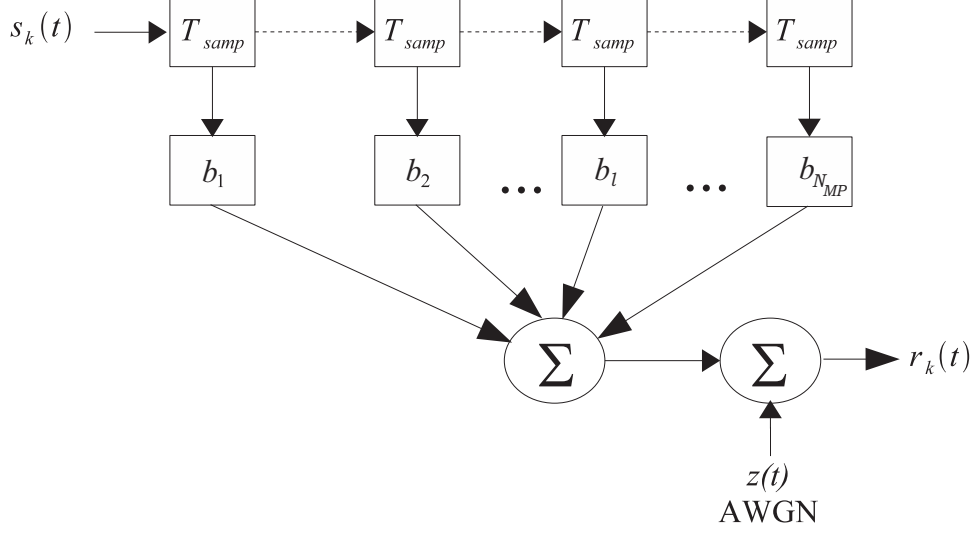


Figure 3.7: Tapped delay line model of a frequency selective, slowly-fading multi-path channel [60].

$b_l = \gamma_l = 1$ and $\theta_l = \tau_l = 0$. The corresponding channel transfer function is [60, 165]

$$H(f) = \int_{-\infty}^{\infty} h(t) e^{-j2\pi ft} dt \quad (3.41)$$

$$\begin{aligned} &= \int_{-\infty}^{\infty} \sum_{l=0}^{N_{MP}} \gamma_l(t) e^{j\theta_l(t)} \delta(t - \tau_l(t)) e^{-j2\pi ft} dt \\ &= \sum_{l=0}^{N_{MP}} \int_{-\infty}^{\infty} \gamma_l(t) e^{j\theta_l(t)} \delta(t - \tau_l(t)) e^{-j2\pi ft} dt \\ &= \sum_{l=0}^{N_{MP}} \gamma_l(\tau_l(t)) e^{j\theta_l(\tau_l(t))} e^{-j2\pi f\tau_l(t)} \\ &= \sum_{l=0}^{N_{MP}} b_l(\tau_l(t)) e^{-j2\pi f\tau_l(t)}. \end{aligned} \quad (3.42)$$

The fading channel statistics (i.e., for $b_l(\tau_l)$) can vary but it is common to use Rayleigh statistics (see (3.35) in Section 3.5.2) to represent general fading considerations when a LOS signal is not present (e.g., urban and/or office environments). Ergo, this development considers complex Rayleigh fading with distributions $\gamma_l(\tau_l) \sim \text{Rayleigh}(\sigma)$ and $\theta_l(\tau_l) \sim \text{U}[0, 2\pi)$ [60].

After sampling the multipath channel at the same rate as the signal, the discrete representation of the channel impulse response is [60]

$$h[n] = \sum_{l=0}^{N_{MP}} b_l \delta[n-l] \quad (3.43)$$

$$= \sum_{l=0}^{N_{MP}} \gamma_l e^{j\theta_l} \delta[n-l] \quad (3.44)$$

for $n \in \{0, 1, \dots, N_F - 1\}$.

The corresponding transfer function of the discrete expression in (3.43) describes the frequency content and is provided in (3.45). Note that (3.45) assumes that b_l is zero-padded to length N_F and that an N_F -point FFT is determined [60].

$$H[m] = \sum_{n=0}^{N_F-1} h[n] e^{-j2\pi nm/N_F} \quad (3.45)$$

$$= \sum_{n=0}^{N_F-1} \sum_{l=0}^{N_{MP}} b_l \delta[n-l] e^{-j2\pi nm/N_F} \quad (3.46)$$

$$= \sum_{l=0}^{N_{MP}} b_l e^{-j2\pi lm/N_F} \quad (3.47)$$

$$= B_m \equiv H_m e^{j\theta_m} \quad (3.48)$$

where $m \in \{0, 1, \dots, N_F - 1\}$, $H_m = |B_m|$, and $\theta_m = \arg(B_m)$.

A matrix of transfer functions can now be constructed such that each row contains a different transfer function for a different channel.

$$\mathbf{H}_{N_U \times N_F} = \begin{bmatrix} H^{(1)}[m] \\ H^{(2)}[m] \\ \vdots \\ H^{(N_U)}[m] \end{bmatrix} = \begin{bmatrix} \left[\sum_{l=0}^{N_{MP}} b_l^{(1)} e^{j2\pi lm/N_F} \right]_{m=0}^{N_F-1} \\ \left[\sum_{l=0}^{N_{MP}} b_l^{(2)} e^{j2\pi lm/N_F} \right]_{m=0}^{N_F-1} \\ \vdots \\ \left[\sum_{l=0}^{N_{MP}} b_l^{(N_U)} e^{j2\pi lm/N_F} \right]_{m=0}^{N_F-1} \end{bmatrix} \quad (3.49)$$

$$= \begin{bmatrix} \left[B_m^{(1)} \right]_{m=0}^{N_F-1} \\ \left[B_m^{(2)} \right]_{m=0}^{N_F-1} \\ \vdots \\ \left[B_m^{(N_U)} \right]_{m=0}^{N_F-1} \end{bmatrix} \\ = \mathbf{B} \equiv \mathbf{H}_{N_U \times N_F} \quad (3.50)$$

where the superscript is indexed by user since each user occupies a separate channel. In \mathbf{H} , a matrix of fading coefficients, N_U rows represent channels for different users and N_F columns represent discrete frequency values.

3.6 SMSE Framework: Receiver

The following comments pertaining to notation will ease the understanding of receiver expressions within this section. First, the expressions assume that analog-to-digital conversion has already occurred, and thus $[n]$ ($[m]$) denote the appropriate discrete time (frequency) indices. Second, **bold** lower (upper) case letters denote vectors (matrices) as before. Finally, as previously noted, subscripts s and k denote samples corresponding to a complete data frame and communication symbol, respectively.

The received signal is a modified version of the transmitted signal for which channel fading, noise, and interference has degraded the signal quality. Generally, the received signal, given the transmitted signal in (3.21), is

$$\mathbf{r}_s[n] = \mathbf{s}_s[n] * \mathbf{h}_s[n] + \boldsymbol{\eta}[n] \quad (3.51)$$

where $*$ denotes convolution, \mathbf{h}_s is the channel impulse response, and $\boldsymbol{\eta}$ is a composite noise and interference vector. Recall that \mathbf{s}_s is a data frame containing a preamble and concatenated symbols, where each symbol is summed over all users. Because each user's signal experiences a different channel realization (although the channel responses themselves might be identical), it is useful to begin the receiver signal development by examining the received signal in matrix form. That is, \mathbf{S}_s , a matrix data frame with N_U rows, is examined instead of \mathbf{s}_s , i.e., separate user-channel combinations are viewed in separate rows rather than summed in vector form. Thus, (3.51) can be represented as

$$\mathbf{R}_s[n] = \mathbf{S}_s[n] \overset{r}{*} \mathbf{H}_s[n] + \boldsymbol{\Upsilon}[n] \quad (3.52)$$

where $\overset{r}{*}$ denotes that the convolution is performed row-wise, \mathbf{R}_s , \mathbf{S}_s , and \mathbf{H}_s are of dimension $N_U \times [N_F N_{sym} + \text{preamble}]$, \mathbf{H}_s contains separate channel realizations for each user in each row, and $\boldsymbol{\Upsilon}$ is a matrix containing the interference seen by each user in each row (a matricized version of $\boldsymbol{\eta}$).

Assume, without loss of generality, that the receiver correctly chooses the k^{th} symbol after synchronization and pre-processes the header information using the preamble. Then, the receiver input expression is modified to be

$$\mathbf{R}_k[n]_{N_U \times N_F} = \mathbf{S}_k[n] \overset{r}{*} \mathbf{H}_k[n] + \boldsymbol{\Upsilon}_k[n] \quad (3.53)$$

where \mathbf{H}_k and $\boldsymbol{\Upsilon}_k$ represent the time samples of \mathbf{H}_s and $\boldsymbol{\Upsilon}$ corresponding to \mathbf{S}_k in \mathbf{S}_s .

Every practical receiver includes an RF filter at its front-end for noise reduction. This filtering process is represented by \mathbf{H}_{rf} , an $N_U \times N_F$ matrix in which each row is

a duplicate of the first row, and is readily incorporated into (3.53) as

$$\mathbf{R}_k[n]_{N_U \times N_F} = \left(\mathbf{S}_k[n] \overset{r}{*} \mathbf{H}_k[n] + \mathbf{\Upsilon}_k[n] \right) \overset{r}{*} \mathbf{H}_{rf}[n]. \quad (3.54)$$

The receiver next performs an FFT on \mathbf{R}_k to prepare for subsequent decoding and demodulation in the spectral domain (which matches the reverse SMSE process in the transmitter). Applying the fundamental Fourier property that correlation in the time domain (row-wise in this case) corresponds to a product in the frequency domain (Hadamard in this case) generates the following frequency domain expressions

$$\mathbf{R}_k[m]_{N_U \times N_F} = \left(\mathbf{S}_k[m] \odot \mathbf{H}_k[m] + \mathbf{\Upsilon}[m] \right) \odot \mathbf{H}_{rf}[m] \quad (3.55)$$

$$R_k^{(v)}[m]_{1 \times 1} = \left(S_k^{(v)}[m] H_k^{(v)}[m] + \Upsilon^{(v)}[m] \right) H_{rf}^{(v)}[m] \quad (3.56)$$

where the received spectral *coefficient* is determined by a multiplication and sum of the identified coefficients.

Thus far, the received signal expressions represent a matrix in which each user signal occupies a separate row. Practically, the true received signal expression is a vector because all time-coexistent signals are summed at the receiver input before RF filtering. Hence, the true received signal expression is

$$\mathbf{r}_k[m]_{1 \times N_F} = \sum_{N_U} \mathbf{R}_k[m] \quad (3.57)$$

$$= (\mathbf{1}_{1 \times N_U} (\mathbf{S}_k[m] \odot \mathbf{H}_k[m]) + \boldsymbol{\eta}[m]) \odot \mathbf{h}_{rf}[m] \quad (3.58)$$

$$= (\mathbf{S}_k[m] \overset{c}{\bullet} \mathbf{H}_k[m] + \boldsymbol{\eta}[m]) \odot \mathbf{h}_{rf}[m] \quad (3.59)$$

where $\boldsymbol{\eta}[m]$ and $\mathbf{h}_{rf}[m]$ are of dimension $1 \times N_F$. Again, $\mathbf{1}$ is a vector of ones (of the annotated length) and $\overset{c}{\bullet}$ represents a column-wise sum over all users (i.e., a column-wise inner product). The effects of the channel propagation on the received signal are apparent, i.e., multiplication of transmitted and fading coefficients in the frequency

domain as given by

$$\mathbf{S}_k[m] \odot \mathbf{H}_k[m]. \quad (3.60)$$

Substituting the expression for \mathbf{S}_k given in (3.1) and the expression for \mathbf{H}_k given in (3.50) into (3.60) yields

$$[\mathbf{A}_k \odot \mathbf{\Theta}_k \odot \mathbf{F}] \odot \mathbf{B}_k. \quad (3.61)$$

Given the Hadamard product is associative and commutative, this expression can be rearranged as

$$[\mathbf{A}_k \odot \mathbf{\Theta}_k \odot \mathbf{B}_k] \odot \mathbf{F}. \quad (3.62)$$

As done when developing (3.59), the column-wise sum over N_U rows can be represented by an inner product with \mathbf{F} instead of a matrix multiply with $\mathbf{1}_{1 \times N_U}$. Making this change and substituting (3.62) into (3.59) yields

$$\mathbf{r}_k[m]_{1 \times N_F} = \left[([\mathbf{A}_k \odot \mathbf{\Theta}_k \odot \mathbf{B}_k] \bullet^c [\mathbf{F}] + \boldsymbol{\eta}[m]) \odot \mathbf{h}_{rf}[m] \right]_{m=0}^{N_F-1}. \quad (3.63)$$

Thus, the m^{th} received spectral component depends upon the terms in (3.10), (3.50), frequency assignment vector \mathbf{u} , composite noise and interference vector $\boldsymbol{\eta}$, and RF filtering.

After the received signal is processed by an RF filter and transformed to the frequency domain, it is processed by the demodulator and symbol estimates are determined based upon test statistics. Two receiver architectures are considered, with each having inherently different test statistic expressions and methodology. First, a *single-channel receiver* is considered. In this case, the receiver can only exploit $L = 1$ order of diversity, regardless of the channel type and the size of N_{MP} . To demodulate the signal, the receiver removes all non-data weights from $\mathbf{r}_k[m]$ in (3.63) and averages over the number of frequencies over which the data is spread. The output of this process is a complex number in the frequency domain which is then compared to M possible constellation values to form a single-channel test statistic vector, $\hat{\mathbf{z}}$. The single-channel symbol estimate \hat{j}_k is chosen based on the element in $\hat{\mathbf{z}}$ which represents

the minimum distance between the received symbol and possible symbols. Notationally, assuming the transmitted signal contains a coding weight but no windowing or orthogonality weights, $\hat{\mathbf{z}}$ and \hat{j}_k can be represented as

$$\hat{\mathbf{z}}_{j,k} = \left| \mathbf{d}_j - \frac{1}{N_F} \mathbf{r}_k \mathbf{c}^H \right|, \quad j \in \{1, 2, \dots, M\} \quad (3.64)$$

$$\hat{j}_k = \arg \min_{j \in \{1, 2, \dots, M\}} \left[\hat{\mathbf{z}}_{j,k} \right] \quad (3.65)$$

where \mathbf{d}_j denotes the constellation data vector and the H superscript denotes a Hermitian matrix.

Next, a *multi-channel receiver*, commonly referred to as a Rake receiver, is considered. A Rake receiver exploits L -order diversity, where L is the number of tap weights and delays in the TDL model used to represent a frequency selective fading channel. (Generally, the TDL model can be truncated after $L = \lfloor W/B_c \rfloor + 1$ taps [165].) The Rake receiver assumes a maximum likelihood posture, such that all communications symbols have equal probability of being transmitted. In doing so, a correlation is performed between the received vector and M possible waveforms. However, within the SMSE framework, these operations are performed in the spectral domain based upon dual expressions transformed from temporal domain Rake receiver expressions in [165]. The multi-channel test statistic vector, $\hat{\mathbf{z}}$, is formed by spectrally multiplying the received waveform with the Hermitian of the M possible waveforms. In this case, as in [165], it is assumed the receiver can perfectly estimate the channel tap weights. (In practice, good tap weight estimates can be made if channel fading is “sufficiently slow,” or $T_c/T_{sym} \geq 100$ [165]). In conjunction with maximum likelihood receiver operation, the multi-channel symbol estimate \hat{j}_k is chosen based upon the

maximum test statistic in $\check{\mathbf{z}}$. Notationally, $\check{\mathbf{z}}$ and \check{j}_k can be represented as

$$\check{\mathbf{z}}_{j,k} = \int_0^{T_{sym}} r_k(t) \underbrace{\sum_{l=1}^L c_l(t) s_j^*(t - l/W)}_{\mathfrak{F}^{-1}\{\psi\}} dt, \quad j \in \{1, 2, \dots, M\} \quad (3.66)$$

$$\check{\mathbf{z}}_{j,k} = \mathbf{r}_k(\psi_j^H), \quad j \in \{1, 2, \dots, M\} \quad (3.67)$$

$$\check{j}_k = \arg \max_{j \in \{1, 2, \dots, M\}} \left[\check{\mathbf{z}}_{j,k} \right] \quad (3.68)$$

where ψ_j represents the j^{th} waveform.

3.7 SMSE Framework: MIMO Extension

As shown, the SMSE framework is an excellent candidate for 4G communication applications from a *spectral-time diversity* standpoint. What has not been considered in the SMSE framework under the adaptive SDR umbrella is the incorporation of *space-time diversity*. In this case, spatial diversity is added by incorporating multiple-input, multiple-output (MIMO) channel modeling into the SMSE framework. Given that MIMO spatial diversity is achieved using multiple antenna elements (at both transmitter and receiver locations), there is the inherent capability to consider *polarization diversity* as well given that antennas are polarization selective. Accounting for waveform electrical and physical propagation characteristics, the ultimate cognitive SDR solution may, in fact, emerge as providing a hybrid form of *time-spectral-space-polarization diversity*.

This section extends the general framework presented in Section 3.4 and Section 3.6 to incorporate MIMO capability. Before the MIMO architecture is represented within the SMSE framework, a brief overview of the MIMO channel model considered for this work is presented as found in [236].

3.7.1 Generalized MIMO Channel Model. The basic MIMO channel model of [236] is considered for initial integration with the SMSE framework. This particular

model was chosen for demonstration purposes to illustrate framework flexibility. There were no optimization criteria used in making this selection and several other MIMO channel models exist which could have been chosen as well.

As commonly done in channel modeling, the electromagnetic field (and thus the received antenna response) at a given point in free-space can be represented as the superposition of all impinging waves. Furthermore, the medium through which the waves propagate is modeled using a “black box” approach whereby the transmitted wave experiences changes in amplitude, phase, propagation direction, and time delay as it propagates through the media.

A *general* signal expression for an *input-channel-output system*, given a time-variant, frequency-selective MIMO channel with N_t transmitters and N_r receivers, is written as [236]

$$\mathbf{y}(t) = \int \mathbf{H}_{\mathbf{c}}(t, f) \mathbf{x}(f) \exp\{j2\pi ft\} df + \mathbf{n} \quad (3.69)$$

where $\mathbf{y}(t)_{N_r \times 1}$ represents the output signal vector, $\mathbf{x}(t)_{N_t \times 1}$ represents the input signal vector, $\mathbf{n}_{N_r \times 1}$ represents the noise vector, and $\mathbf{H}_{\mathbf{c}}_{N_r \times N_t}$ represents the continuous channel transfer function.

The discrete-time variant of the MIMO channel, necessarily wideband in that it accommodates multipath delays, is the channel transfer matrix \mathbf{H} , which depends on four variables: N_r , N_t , N_{MP} , and N_F . The MIMO channel model builds \mathbf{H} based on provided statistical properties for the channel. Further refinement of this general \mathbf{H} is contained in [236].

A specific expression for the received signal is given as [236]

$$\mathbf{r}(s) = \sum_{b=1}^{N_{base}} \sqrt{P_b \gamma_b} \sum_{l=1}^{N_{MP}} \mathbf{H}_{b,l}(s) \mathbf{x}_b(s - \tau_{b,l}) + \mathbf{n}(s) \quad (3.70)$$

where \mathbf{r} is a received vector at time s , P_b is the b^{th} station transmit power (N_{base} total stations), γ_b is the large-scale path gain from the b^{th} station, $\tau_{b,l}$ is the l^{th} multipath delay for the b^{th} station, \mathbf{x}_b is the transmitted signal vector from the b^{th}

base station at time s , and $\mathbf{H}_{b,l}$ is the continuous time channel transfer function at time s . Examination of (3.70) shows that \mathbf{H} can be represented as a two-dimensional matrix of dimension $N_r \times N_t$ at a specific moment in time s , where each matrix element is a sum over multiple paths (N_{MP}).

3.7.2 Composite MIMO-SMSE Model. From (3.70), it is apparent that the SMSE framework can be extended to incorporate a MIMO channel provided that the channel transfer function is of dimension $N_r \times N_t$. The composite output from the $s_k[n]$ expression given in (3.15) is a matrix of dimension $N_U \times N_F$, where N_U in the SMSE framework corresponds to N_t in MIMO applications (such as [236]) and N_F represents the number of discrete frequency components before the IFFT and the number of discrete time samples in (3.17) after the IFFT.

Considering the special case for a single receive antenna element, $N_r = 1$ and \mathbf{H} is an $N_U \times N_F$ matrix in which the v^{th} row represents the channel impulse response of the path between the v^{th} transmitter and the single receiver. Hence, \mathbf{H} can be written as

$$\mathbf{H}[n]_{N_U \times N_F} = \begin{bmatrix} \mathbf{h}_1[n] \\ \vdots \\ \mathbf{h}_v[n] \\ \vdots \\ \mathbf{h}_{N_U}[n] \end{bmatrix}. \quad (3.71)$$

Correspondingly, the signal at the receiver is a superposition of convolutions between the transmitted signals and their channel impulse responses:

$$\mathbf{r}^{(1)}[n] = \sum_{i=1}^{N_t} \mathbf{S}_k^{(i)}[n] * \mathbf{H}^{(i)}[n] \quad (3.72)$$

$$= \sum_{i=1}^{N_t} \mathfrak{F}^{-1} \left\{ \mathbf{S}_k^{(i)}[m] \mathbf{H}^{(i)}[m] \right\} \quad (3.73)$$

$$= \mathfrak{F}^{-1} \left\{ \sum_{i=1}^{N_t} \mathbf{S}_k^{(i)}[m] \mathbf{H}^{(i)}[m] \right\} \quad (3.74)$$

$$= \mathfrak{F}^{-1} \left\{ \mathbf{S}_k \bullet^r \mathbf{H} \right\} \quad (3.75)$$

where $\mathbf{S}_k^{(i)}$ and $\mathbf{H}^{(i)}$ in (3.72) represent the i^{th} row of \mathbf{S}_k in (3.1) and the i^{th} row of \mathbf{H} in (3.71), respectively, and \bullet^r denotes row-wise inner (dot) product over the spectral values.

The single receiver element $\mathbf{r}^{(1)}$ expression in (3.72) can be readily extended to account for multiple receiver elements ($N_r > 1$). If that extension is carried out, the channel transfer function becomes

$$\mathbf{H}[n] = \begin{bmatrix} h_{11}[n] & h_{12}[n] & \cdots & h_{1,N_t}[n] \\ h_{21}[n] & h_{22}[n] & \cdots & h_{2,N_t}[n] \\ \vdots & \vdots & \ddots & \vdots \\ h_{N_r,1}[n] & h_{N_r,2}[n] & \cdots & h_{N_r,N_t}[n] \end{bmatrix} \quad (3.76)$$

for each $n \in \{0, \dots, N_F - 1\}$, which is a two-dimensional $N_r \times N_t$ channel matrix *at a given time sample*, n , from the range of time samples $n \in \{0, \dots, N_F - 1\}$. The channel transfer function variation with time n is expressed along a third dimension, such that the array \mathbf{H}_{3D} of dimension $N_r \times N_t \times N_F$ represents the entire channel transfer function. A fourth dimension, multipath, is inherent in each h_{ij} element, which can be defined arbitrarily as a sum over N_{MP} paths (see (3.43)), where each path has a different fading coefficient and time delay.

The corresponding received signal using this MIMO channel is

$$\mathbf{R}[n] = \begin{bmatrix} r_{11}[n] & r_{12}[n] & \cdots & r_{1,N_t}[n] \\ r_{21}[n] & r_{22}[n] & \cdots & r_{2,N_t}[n] \\ \vdots & \vdots & \ddots & \vdots \\ r_{N_r,1}[n] & r_{N_r,2}[n] & \cdots & r_{N_r,N_t}[n] \end{bmatrix} \quad (3.77)$$

for $n \in \{0, \dots, N_F - 1\}$, where each matrix element $r_{ij}[n]$ represents the n^{th} sample from $n \in [0, \dots, N_F - 1]$ for a time-domain convolution between the corresponding channel impulse response in (3.76) and the transmitted signal. Again, the received signal variation with time n is expressed along the third dimension, such that the array \mathbf{R}_{3D} of dimension $N_r \times N_t \times N_F$ represents the entire received block signal.

Figure 3.8 graphically illustrates \mathbf{H}_{3D} and \mathbf{R}_{3D} construction to accommodate MIMO signals as described in [236]. When $N_r = 1$, the lightly-shaded front face of the array cube in Fig. 3.8 represents the \mathbf{H} and \mathbf{R} (non-summed) of (3.71) and (3.72), respectively, which was the case used for SMSE framework development. When $N_r > 1$ for MIMO applications, a third dimension is added. A transpose of the n^{th} slice of the array cube in Fig. 3.8 represents the content shown in (3.76) and (3.77).

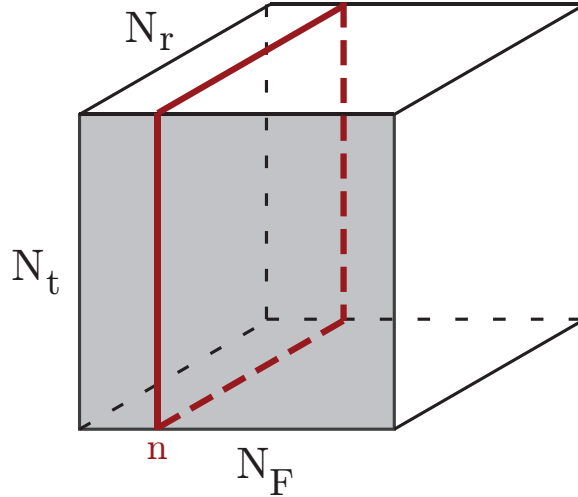


Figure 3.8: Array cube to illustrate the \mathbf{H}_{3D} and \mathbf{R}_{3D} dimensions in MIMO applications. Note: N_t is the number of transmitters, N_r is the number of receivers, and N_F is the number of discrete time samples.

3.8 Summary of SMSE Analytical Framework

A general analytic framework is proposed for SMSE signals. This work represents a significant step toward obtaining a single, unifying framework for developing, analyzing, and implementing SMSE techniques. The proposed framework parallels the development of a unifying UWB framework presented in [240] and is motivated by an OFDM-based architecture, hailed by [82] as an excellent candidate for future CR-based SDR applications. The framework as developed is adaptive and readily implementable through control of six key waveform design variables (vectors) that, upon definition by a cognitive brain within the radio or at a base station, can be used to appropriately design a number of SMSE-candidate waveforms. The specific application of the framework to select waveforms is demonstrated in Chapter IV.

Different channel models and receiver architectures are considered as well. Specifically, the effects of additive white Gaussian noise and Rayleigh slowly-fading (flat and frequency selective) channels are addressed. Additionally, single-channel and Rake receiver implementations are analyzed, with test statistic and symbol estimate expressions provided based on common receiver demodulation structures. Finally, the SMSE framework is extended to incorporate MIMO channel modeling capability. As shown, the SMSE framework can adequately incorporate MIMO capability by properly constructing the channel transfer function to account for multiple transmit and/or receive elements, multipath, and time/frequency samples/components. With the described structure, SMSE signals are readily implementable via adaptive SDR techniques.

IV. SMSE Framework Applications

The general analytic framework developed in Chapter III for spectrally modulated, spectrally encoded (SMSE) signals is applied to multiple SMSE signals in this chapter, illustrating model adaptability and applicability. Final expressions obtained by applying the SMSE framework to these signals match expressions commonly found in literature for such signals; indeed, a similar process can be implemented within a cognitive radio (CR)-based software defined radio (SDR) module in future wireless communication systems.

Discrete expressions are denoted using time and frequency indices, n and m , respectively. Lower (upper) case **bold** variables denote vectors (matrices). Throughout the chapter, tables are provided showing the instantiations of waveform design variables (**d**, **c**, **w**, **o**, **a**, and **u**) required to generate specific SMSE signals within a CR-based SDR architecture. For clarity, the waveform design variable definitions from Chapter III are reintroduced here.

$$\begin{aligned}
\text{Data : } \mathbf{d} &= [d_1, d_2, \dots, d_{N_F}], \quad d_m \in \mathbb{C} \\
\text{Code : } \mathbf{c} &= [c_1, c_2, \dots, c_{N_F}], \quad c_m \in \mathbb{C} \\
\text{Window : } \mathbf{w} &= [w_1, w_2, \dots, w_{N_F}], \quad w_m \in \mathbb{C} \\
\text{Orthogonality : } \mathbf{o} &= [o_1, o_2, \dots, o_{N_F}], \quad o_m \in \mathbb{C}, \quad |o_m| = 1 \\
\text{Freq Assignment : } \mathbf{a} &= [a_1, a_2, \dots, a_{N_F}], \quad a_m \in \{0, 1\} \\
\text{Freq Use : } \mathbf{u} &= [u_1, u_2, \dots, u_{N_F}], \quad u_m \in \{0, 1\}
\end{aligned} \tag{4.1}$$

4.1 Orthogonal Frequency Division Multiplexing (OFDM) Signals

The uncoded OFDM technique of [31, 32, 187] is considered first and only includes spectral data modulation with no encoding. This differs from coded OFDM (COFDM) [119, 252] which codes the transmitted data to help mitigate channel fading effects.

For uncoded OFDM, the analytic model is simplified by setting $a_m = u_m$, $|w_m| = 1$, and $\theta_{w_m} = 0$ for all m , i.e., all spectral components are used with no spectral windowing. Also, uncoded OFDM does not use the protective coding of COFDM and no additional orthogonality control is applied, thus $|c_m| = 1$ and $\theta_{c_m} = \theta_{o_m} = 0$ for all m . Substituting these conditions into (3.5) yields the N_F spectral components for the k^{th} uncoded OFDM communication symbol given by

$$\mathbf{s}_k[m] = \left[a_m d_{m,k} e^{j(\theta_{d_{m,k}})} \right]_{m=0}^{N_F-1} \quad (4.2)$$

where $d_{m,k} e^{j\theta_{d_{m,k}}}$ represents the complex spectral data modulation. Rewriting the data modulation in rectangular form as $d_{m,k} e^{j\theta_{d_{m,k}}} = (\alpha_{m,k} + j\beta_{m,k})$ and substituting into (4.2) yields

$$\mathbf{s}_k[m] = \begin{cases} [(\alpha_{m,k} + j\beta_{m,k})]_{m=0}^{N_F-1} & \text{for } a_m = 1 \\ 0 & \text{for } a_m = 0 \end{cases} \quad (4.3)$$

where $\alpha_{m,k}$ and $\beta_{m,k}$ vary according to the data modulation employed, e.g., $\alpha_{m,k}, \beta_{m,k} \in \{-1, +1\}$ for QPSK and $\alpha_{m,k}, \beta_{m,k} \in \{\pm 1, \pm 3\}$ for 16-QAM.

Performing an N_F -point IFFT operation on the spectral components of (4.3) and taking the real part yields the transmitted OFDM signal given by

$$s_k[n] = \frac{1}{N_F} \text{Re} \left\{ \sum_{m=0}^{N_F-1} (\alpha_{m,k} + j\beta_{m,k}) e^{j(2\pi f_m t_n)} \right\} \quad (4.4)$$

$$= \frac{2}{N_F} \sum_{m=0}^{N_F-1} d_{m,k} \cos(2\pi f_m t_n + \theta_{d_{m,k}}) \quad (4.5)$$

where, from Section 3.4, $f_m = m/(N_F \Delta t)$ and $t_n = n \Delta t$ for $n = 0, 1, \dots, N_F - 1$ [228, 252]. These final expressions are consistent with the OFDM representations offered in [46, 119, 125, 187], suggesting the general SMSE framework is applicable for modeling uncoded OFDM signals.

4.2 Coded OFDM (COFDM) Signals

Although there is some utility for considering the uncoded OFDM case, it is generally not implemented due to adverse channel fading effects. In practice, coding is applied to the OFDM signal to protect individual subcarriers from channel fading [46, 119, 252].

The analytic model for COFDM is simplified in the same manner as done for uncoded OFDM except that the coding design variables are no longer ignored. In Section 4.1, uncoded OFDM was simplified by setting $a_m = u_m$, $|w_m| = 1$, $\theta_{w_m} = 0$, and $\theta_{o_m} = 0$ for all m . For COFDM, instantiation of complex coding variable \mathbf{c} is required. In this case, the magnitude ($|c_m|$) and phase (θ_{c_m}) factors vary as a function of applied coding, e.g., trellis coded modulation [252], Reed-Solomon codes [99], Turbo codes [119], low-density parity check codes [58], etc. The COFDM instantiation is manifested by setting $|c_m| = 1$ and $\theta_{c_m} \in \{0, \pi\}$ for all m .

Substituting these conditions into (3.5) yields the N_F spectral components for the k^{th} COFDM communication symbol given by

$$\mathbf{s}_k[m] = \left[a_m d_{m,k} e^{j(\theta_{d_{m,k}} + \theta_{c_m})} \right]_{m=0}^{N_F-1} \quad (4.6)$$

where $d_{m,k} e^{j\theta_{d_{m,k}}}$ represents the complex spectral data modulation. Rewriting the data modulation in rectangular form as $d_{m,k} e^{j\theta_{d_{m,k}}} = (\alpha_{m,k} + j\beta_{m,k})$ and substituting into (4.6) yields

$$\mathbf{s}_k[m] = \begin{cases} [(\alpha_{m,k} + j\beta_{m,k}) e^{j(\theta_{c_m})}]_{m=0}^{N_F-1} & \text{for } a_m = 1 \\ 0 & \text{for } a_m = 0 \end{cases} \quad (4.7)$$

where $\alpha_{m,k}$ and $\beta_{m,k}$ vary according to the data modulation employed, e.g., $\alpha_{m,k}, \beta_{m,k} \in \{-1, +1\}$ for QPSK and $\alpha_{m,k}, \beta_{m,k} \in \{\pm 1, \pm 3\}$ for 16-QAM.

Performing an N_F -point IFFT operation on the spectral components of (4.7) and taking the real part yields the transmitted COFDM signal given by

Table 4.1: Design variable instantiations for SMSE implementation of OFDM and COFDM signals [176, 177].

Operation	OFDM	COFDM
Data Modulation	MPSK, MQAM relies on m, k	MPSK, MQAM relies on m, k
Coding	$\mathbf{c} = \mathbf{1}$ $\theta_{\mathbf{c}} = \mathbf{0}$	$\mathbf{c} = \mathbf{1}$ $\theta_{c_m} \in \{0, \pi\}$
Windowing	$\mathbf{w} = \mathbf{1}$ $\theta_{\mathbf{w}} = \mathbf{0}$	$\mathbf{w} = \mathbf{1}$ $\theta_{\mathbf{w}} = \mathbf{0}$
Orthogonality	$\theta_{\mathbf{o}} = \mathbf{0}$	$\theta_{\mathbf{o}} = \mathbf{0}$
Frequency Assignment	\mathbf{a}	\mathbf{a}
Frequencies Used	$\mathbf{u} = \mathbf{a}$	$\mathbf{u} = \mathbf{a}$

$$s_k[n] = \frac{1}{N_F} \text{Re} \left\{ \sum_{m=0}^{N_F-1} (\alpha_{m,k} + j\beta_{m,k}) e^{j(2\pi f_m t_n + \theta_{c_m})} \right\} \quad (4.8)$$

$$= \frac{2}{N_F} \sum_{m=0}^{N_F-1} d_{m,k} \cos(2\pi f_m t_n + \theta_{d_{m,k}} + \theta_{c_m}). \quad (4.9)$$

These expressions are consistent with descriptions offered by [119, 125, 252], suggesting the general SMSE framework can be readily extended from OFDM to COFDM signals. Table 4.1 summarizes the instantiation of waveform design variables required in (3.5) to achieve OFDM and COFDM signaling within a CR-based SDR architecture.

4.3 Multi-Carrier Code Division Multiple Access (MC-CDMA) Signals

The MC-CDMA technique considered here is based on original work in [244]. MC-CDMA differs from OFDM in several key ways. Unlike OFDM, MC-CDMA users *share* subcarriers with each user transmitting identical communication symbols (data) across multiple subcarriers [164, 225, 243, 244] (the data modulation is effectively *spread* across frequency).

MC-CDMA performance is dependent upon a parameter $F \in \mathbb{Z}^+$ (where \mathbb{Z}^+ denotes positive integers [9]), which dictates subcarrier spacing (MC-CDMA carrier spacing is $F \cdot \Delta f$ for Δf in Fig. 3.1). For the $F = 1$ case illustrated in Fig. 4.1, the MC-CDMA signal structure is similar to OFDM yet each system transmits data differently. OFDM systems use distinct, independent data modulation on separate subcarriers while MC-CDMA systems allow users to spread their data modulation across all subcarriers or a subset thereof [243]. Further differences between MC-CDMA and OFDM are noted in [225].

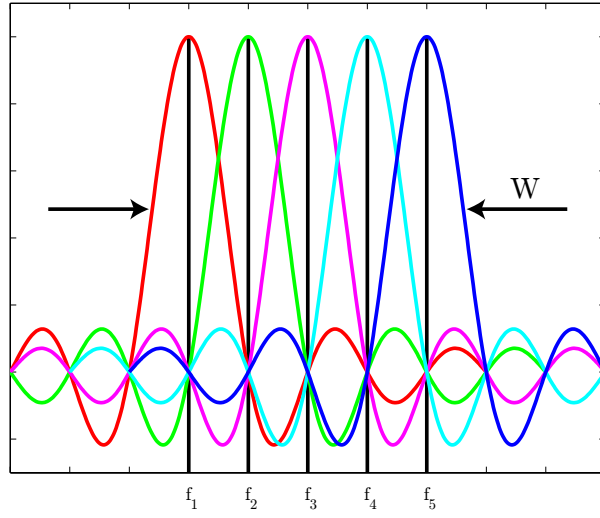


Figure 4.1: Illustration of OFDM and MC-CDMA ($F = 1$) Subcarriers.

The analytic model for MC-CDMA is simplified by setting $|w_m| = 1$ and $\theta_{w_m} = 0 \forall m$ (no windowing). Also, $\theta_{o_m} = 0 \forall m$ and there is no orthogonality control applied. Finally, the data variables only depend upon k because of the spectral spreading. Substituting these conditions into (3.5) yields the N_F spectral components for the k^{th} MC-CDMA communication symbol given by

$$\mathbf{s}_k[m] = \left[a_m u_m c_m d_k e^{j(\theta_{d_k} + \theta_{c_m})} \right]_{m=0}^{N_F-1}. \quad (4.10)$$

where the F parameter is accounted for in u_m and $\mathbf{u} \leq \mathbf{a}$.

Spectral data modulation spreading is accomplished using a random application of two phase values such that $|c_m| = 1$ and $\theta_{c_m} \in \{0, \pi\} \forall m$. Applying this to (4.10) yields

$$\mathbf{s}_k[m] = \begin{cases} \left[d_k e^{j(\theta_{d_k} + \theta_{c_m})} \right]_{m=0}^{N_F-1} & \text{for } u_m = 1 \\ 0 & \text{for } u_m = 0 \end{cases}. \quad (4.11)$$

An elegant comparison of OFDM, COFDM, and MC-CDMA can be drawn from [125]. For \mathbf{z} , an N_F -element column vector carrying a *frame* of user data, \mathbf{s} an N_F -element column vector of user signals, and \mathbf{C} an $N_F \times N_F$ code matrix, then $\mathbf{z} = \mathbf{C}\mathbf{s}$. For OFDM, $\mathbf{C}_{N_F \times N_F} = \mathbf{I}_{N_F}$, i.e., $\mathbf{z} = [z_0 = c_{11}s_0, z_1 = c_{22}s_1, \dots, z_{N_F-1} = c_{N_F N_F}s_{N_F-1}]^T$, where $c_{ii} = 1 \forall i$. For COFDM, $\mathbf{C}_{N_F \times N_F} = \mathbf{D}_{N_F}$, i.e., \mathbf{z} is defined the same way, but $c_{ii} \in \{1, -1\}$ defines elements in the diagonal matrix \mathbf{D}_{N_F} (entries are no longer unity as in \mathbf{I}_{N_F}). For MC-CDMA, the v^{th} column of \mathbf{C} is the spreading code of the data stream for the v^{th} user. In this case, $\mathbf{z} = [z_0 = c_{11}s_0 + c_{12}s_1 + \dots + c_{1N_F}s_{N_F-1}, \dots, z_{N_F-1} = c_{N_F1}s_0 + c_{N_F2}s_1 + \dots + c_{N_F N_F}s_{N_F-1}]^T$. The \mathbf{C} matrix in this comparison can be constructed by taking the \mathbf{c} vectors from each user signal, stacking them on top of each other, and transposing the resultant code matrix.

For complex data modulation, $d_k e^{j\theta_{d_k}} = (\alpha_k + j\beta_k)$ and (4.11) can be rewritten as

$$\mathbf{s}_k[m] = \begin{cases} [(\alpha_k + j\beta_k) e^{j\theta_{c_m}}]_{m=0}^{N_F-1} & \text{for } u_m = 1 \\ 0 & \text{for } u_m = 0 \end{cases} \quad (4.12)$$

where α_k and β_k depend on the modulation type being employed. After an IFFT operation on (4.12), the baseband transmitted MC-CDMA signal is given by

$$s_k[n] = \frac{1}{N_F} \text{Re} \left\{ \sum_{m=0}^{N_F-1} (\alpha_k + j\beta_k) e^{j(2\pi f_m t_n + \theta_{c_m})} \right\} \quad (4.13)$$

$$= \frac{2}{N_F} \sum_{m=0}^{N_F-1} d_k \cos(2\pi f_m t_n + \theta_{d_k} + \theta_{c_m}) \quad (4.14)$$

where $f_m = m(F/T_{sym})$ such that $f_m t_n = mnF/N_F$ for given subcarrier parameter m , subcarrier spacing F , time sample n , and N_F subcarriers. These expressions are consistent with the MC-CDMA representations offered in [164, 225, 243, 244], suggesting the general SMSE framework is suitable for modeling MC-CDMA signals.

4.4 Transform Domain Communication System (TDCS) Signals

The Transform Domain Communication System (TDCS) technique, as originally proposed in [8, 64] and subsequently examined in [154, 168, 179], is considered here with one minor modification. As reported in [28], the TDCS process applies data modulation in the time domain following an IFFT operation on a spectrally encoded waveform. Herein, TDCS data modulation is applied in the spectral domain before the IFFT. As originally developed, a TDCS adaptively tailors signal characteristics to avoid interference [28, 29]. Like MC-CDMA and unlike OFDM, the TDCS transmits the same data symbols across the usable frequency spectrum. Unlike MC-CDMA, TDCS adapts the signal structure (eliminates specific spectral components) in near real-time to avoid interference.

For basic TDCS implementation, the analytical model is simplified by setting $|w_m| = 1$ and $\theta_{w_m} = 0 \forall m$ (no windowing). Coding is applied as pseudorandom phase variations in $\theta_{c_m} \in [0, 2\pi)$ and $|c_m| = 1 \forall m$. Data variables only depend upon k because of spectral spreading. Orthogonality control may be introduced in TDCS if using cyclic shift keying (CSK) modulation [154]. However, the application of pseudorandom phase variations, as envisioned in [8, 64] for pseudo-orthogonality to accommodate multiple users, is suitable for demonstration and examined first; hence, $\theta_{o_m} = 0 \forall m$. Substituting these conditions into (3.5) yields the N_F spectral components for the k^{th} TDCS communication symbol given by

$$\mathbf{s}_k[m] = \left[a_m u_m d_k e^{j(\theta_{d_k} + \theta_{c_m})} \right]_{m=0}^{N_F-1}. \quad (4.15)$$

As indicated in (4.15), data modulation d_k is constant (spread) across all frequency components while random (pseudorandom) phases are applied to independent components. The $a_m u_m$ term depends not only on cognitive assignment, but also on the adaptive TDCS notching process which identifies specific frequency components as being “unusable” based on channel interference characterization. For these *notched* components, $u_m = 0$ and the resultant signal is given by

$$\mathbf{s}_k[m] = \begin{cases} \left[d_k e^{j(\theta_{d_k} + \theta_{c_m})} \right]_{m=0}^{N_F-1} & \text{for } u_m = 1 \\ 0 & \text{for } u_m = 0 \end{cases}. \quad (4.16)$$

Performing an N_F -point IFFT operation on the spectral components of (4.16) and taking the real part yields the transmitted TDCS signal given by

$$s_k[n] = \frac{1}{N_F} \text{Re} \left\{ \sum_{m=0}^{N_F-1} d_k e^{j(2\pi f_m t_n + \theta_{d_k} + \theta_{c_m})} \right\} \quad (4.17)$$

$$= \frac{2}{N_F} \sum_{m=0}^{N_F-1} d_k \cos \left(2\pi m \frac{n}{N_F} + \theta_{d_k} + \theta_{c_m} \right). \quad (4.18)$$

A common data modulation for implementing and demonstrating TDCS performance is CSK. Normally, CSK modulation is applied in the time domain via cyclic shifts of TDCS fundamental waveforms. However, it is possible to replicate the CSK process using spectral modulation. For binary CSK (BCSK) implementation, this is accomplished by zeroing out the Nyquist component and alternately adding $\theta_{d_{m,k}} \in \{0, \pi\}$ to the phase of every spectral component, where $\{0, \pi\}$ forms an *orthogonality set*. For 4-ary CSK implementation, the Nyquist component is zeroed out and elements from the orthogonality set, $\{0, \pi/2, \pi, 3\pi/2\}$, are iteratively added to the phase of every spectral component. In general, to implement M -ary CSK through spectral encoding, zero out the Nyquist frequency component and add

$$\theta_{d_{m,k}} = \text{mod}_{2\pi} \left(\frac{2\pi(m-1)}{M} \right) \quad (4.19)$$

to each subsequent spectral component, where there are M communication symbols. As an example, for 16-ary CSK add $\text{mod}_{2\pi} [2\pi(3 - 1)/16] = \pi/4$ to the third frequency component's phase, $\text{mod}_{2\pi} [2\pi(4 - 1)/16] = 3\pi/8$ to the fourth frequency component's phase, and so on.

To maintain orthogonality among TDCS users, *two* conditions must be maintained. *First*, the number of frequencies used (P_u) must be an integer multiple of M . For example, if using 4-ary CSK modulation then P_u must satisfy the condition: $\text{mod}(P_u = \|\mathbf{u}\|^2, 4) = 0$ (recall that the number of non-zero elements in u_m is the number of frequencies used). *Second*, the collection of phase values for components to be removed by \mathbf{u} , the total number of which is determined by notching and condition one, must form an orthogonality set. For example, consider a system using 4-ary CSK modulation with $N_F = 16$ and all frequencies assigned, i.e., $\mathbf{a} = \mathbf{1}$. Within this set of assigned frequencies, assume two frequencies must be notched by the TDCS system due to excess interference. From the first condition, four total frequencies must be notched so that $P_u = 12$, a multiple of four. Assuming the phase values on the two frequencies containing interference are 0 and $\pi/2$, then condition two dictates that one component having phase of π and one component having phase of $3\pi/2$ must be removed, given these are the two remaining elements of the $\{0, \pi/2, \pi, 3\pi/2\}$ orthogonality set.

The TDCS expressions in (4.16) through (4.18) match the TDCS discrete-time representation offered in [60, 154] and associated references, suggesting the general framework is suitable for modeling TDCS signals. Note that (4.16) resembles the MC-CDMA expression of (4.12). However, given the values of θ_{c_m} used in the TDCS process and that spectral notching/avoidance is employed, the actual signals generated with (4.16) and (4.12) are truly different. Table 4.2 summarizes the instantiation of waveform design variables required in (3.5) to achieve MC-CDMA and TDCS signaling within a CR-based SDR architecture.

Table 4.2: Design variable instantiations for SMSE implementation of MC-CDMA and TDCS signals [176].

Operation	MC-CDMA	TDCS
Data Modulation	MPSK, MQAM relies on k	MPSK, MQAM relies on k
Coding	$\mathbf{c} = \mathbf{1}$ $\theta_{c_m} \in \{0, \pi\}$	$\mathbf{c} = \mathbf{1}$ $\theta_{c_m} \in [0, 2\pi)$
Windowing	$\mathbf{w} = \mathbf{1}$ $\theta_w = 0$	$\mathbf{w} = \mathbf{1}$ $\theta_w = 0$
Orthogonality	$\theta_o = 0$	$\theta_o = 0$
Frequency Assignment	\mathbf{a}	\mathbf{a}
Frequencies Used	u_m depends on F -parameter	u_m depends on notching process

4.5 Carrier Interferometry (CI) Signals

Carrier interferometry (CI) considers the interaction and interference patterns of superposed carrier electromagnetic waves [148]. CI coding has recently been applied to OFDM-based systems to obtain desired bit error performance without decreasing bit rate [147, 148, 230–232] and to suppress narrowband interference [235]. For example, it has been shown that coupling CI coding with OFDM (CI/OFDM) can provide COFDM performance with the throughput of OFDM [232].

The motivation for coupling CI coding with OFDM is to improve OFDM performance without resorting to bandwidth expansion or suffering from reduced data rates [230]. Advantages of using CI coding instead of pseudorandom coding are described in [149, 232, 235]. As in OFDM, there are N_F possible equally-spaced, orthogonal subcarriers. However, in a CI/OFDM system, each data modulated symbol is simultaneously transmitted over *all* carriers. Orthogonality between the transmitted symbols is maintained via the inclusion of an additional phase term [230]. The inclusion of orthogonal phase coding and removal of pseudorandom coding are just two characteristics that distinguish CI/OFDM from MC-CDMA.

The analytic model is simplified in the same manner as OFDM and COFDM with the following changes. First, because the data modulation is spread over all

carriers, $d_{m,k} \in \mathbb{C}$ only varies with k , i.e., $d_{m,k} = d_k$. Second, the additional CI/OFDM phase term is accounted for by changing $\theta_{o_m} = 0 \forall m$, to $\theta_{o_{m,k}} = m\Delta\theta_k$, where $\Delta\theta_k = k(2\pi/P_u)$ [230]. Recall from Section 3.3 that $P_u \leq P_a \leq N_F$ is the number of used frequencies. Third, coding is incorporated through the orthogonal phase term and thus $|c_m| = 1$ and $\theta_{c_m} = 0 \forall m$. Substituting these conditions into (3.5) yields the N_F spectral components for the k^{th} CI/OFDM communication symbol given by

$$\mathbf{s}_k[m] = \left[u_m d_k e^{j(\theta_{d_k} + \theta_{o_{m,k}})} \right]_{m=0}^{N_F-1}. \quad (4.20)$$

Performing an N_F -point IFFT operation on the spectral components of (4.20) and taking the real part, yields the transmitted CI/OFDM signal given by

$$s_k[n] = \frac{1}{N_F} \text{Re} \left\{ \sum_{m=0}^{N_F-1} d_k e^{j(2\pi f_m t_n + \theta_{d_k} + \theta_{o_{m,k}})} \right\} \quad (4.21)$$

$$= \frac{2}{N_F} \sum_{m=0}^{N_F-1} d_k \cos \left(2\pi f_m t_n + \theta_{d_k} + \frac{2\pi m k}{P_u} \right). \quad (4.22)$$

Performance can be further improved by adding pseudorandom coding to the CI/OFDM system, i.e., CI/COFDM. In this case, \mathbf{c} is modified as in COFDM such that $c_m = 1$ and $\theta_{c_m} \in \{0, \pi\} \forall m$. Modifying (4.20) to account for this change and performing an IFFT operation yields

$$s_k[n] = \frac{1}{N_F} \text{Re} \left\{ \sum_{m=0}^{N_F-1} d_k e^{j(2\pi f_m t_n + \theta_{d_k} + \theta_{o_{m,k}} + \theta_{c_m})} \right\} \quad (4.23)$$

$$= \frac{2}{N_F} \sum_{m=0}^{N_F-1} d_k \cos \left(2\pi f_m t_n + \theta_{d_k} + \frac{2\pi m k}{P_u} + \theta_{c_m} \right). \quad (4.24)$$

By loosening the restriction on orthogonality, the authors in [232] improve system capacity, matching COFDM performance with OFDM throughput. Specifically, [232] introduces a pseudo-orthogonal (PO) CI/COFDM system by iteratively

adding a phase term $m\Delta\theta_{po,k}$ with

$$\Delta\theta_{po,k} = \begin{cases} 0 & \text{for } k = 1, 2, \dots, P_u \\ \frac{\pi}{P_u} & \text{for } k = P_u + 1, P_u + 2, \dots, 2P_u \end{cases} \quad (4.25)$$

where $2P_u$ symbols are simultaneously transmitted over P_u frequencies. Hence, for a PO-CI/COFDM system, the orthogonality phase term within (4.23) and (4.24) is modified and becomes

$$\theta_{o_{m,k}} = \frac{2\pi mk}{P_u} + m\Delta\theta_{po,k}. \quad (4.26)$$

Interestingly enough, the first P_u symbols ($\Delta\theta_{po,k} = 0$) that are transmitted are orthogonal to one another, the second P_u symbols ($\Delta\theta_{po,k} = \pi/P_u$) that are transmitted (simultaneously over the same P_u frequencies) are orthogonal to one another, but the two sets of P_u symbols are only pseudo-orthogonal to each other [232].

Finally, CI coding can also be coupled with MC-CDMA systems yielding CI/MC-CDMA, also referred to in the literature as CI multiple access (CIMA) [147–149, 220]. Unlike MC-CDMA, which uses a pseudorandom sequence to achieve multiple access, CIMA uses an orthogonality sequence to achieve multiple access. The key difference between implementing MC-CDMA and CI/MC-CDMA signals within the SMSE framework is the inclusion of the orthogonal phase term and the deletion of a pseudorandom spreading code in the CI/MC-CDMA implementation.

Adding the orthogonal phase term and deleting the spreading code from the MC-CDMA expression in [176] yields a transmitted CI/MC-CDMA signal of the form

$$s_k[n] = \frac{1}{N_F} \text{Re} \left\{ \sum_{m=0}^{N_F-1} (\alpha_k + j\beta_k) e^{j(2\pi f_m t_n + \theta_{o_{m,k}})} \right\} \quad (4.27)$$

$$= \frac{2}{N_F} \sum_{m=0}^{N_F-1} d_k \cos(2\pi f_m t_n + \theta_{o_{m,k}} + \theta_{d_k}) \quad (4.28)$$

where, as before, $f_m = m(F/T_{sym}) = m(F/N_F\Delta t)$ and $t_n = n\Delta t$.

Table 4.3: Design variable instantiations for SMSE implementation of three carrier interferometry (CI) signals [176].

Operation	CI/OFDM	CI/COFDM	CI/MC-CDMA
Data Modulation	MPSK, MQAM relies on k	MPSK, MQAM relies on k	MPSK, MQAM relies on k
Coding	$\mathbf{c} = \mathbf{1}$ $\theta_{\mathbf{c}} = \mathbf{0}$	$\mathbf{c} = \mathbf{1}$ $\theta_{c_m} \in \{0, \pi\}$	$\mathbf{c} = \mathbf{1}$ $\theta_{\mathbf{c}} = \mathbf{0}$
Windowing	$\mathbf{w} = \mathbf{1}$ $\theta_{\mathbf{w}} = \mathbf{0}$	$\mathbf{w} = \mathbf{1}$ $\theta_{\mathbf{w}} = \mathbf{0}$	$\mathbf{w} = \mathbf{1}$ $\theta_{\mathbf{w}} = \mathbf{0}$
Orthogonality	$\theta_{o_m} = \frac{2\pi mk}{P_u}$	$\theta_{o_m} = \frac{2\pi mk}{P_u}$	$\theta_{o_m} = \frac{2\pi mk}{P_u}$
Frequency Assignment	\mathbf{a}	\mathbf{a}	\mathbf{a}
Frequencies Used	$\mathbf{u} = \mathbf{a}$	$\mathbf{u} = \mathbf{a}$	u_m depends on F -parameter

The expressions in (4.21), (4.23), and (4.27), for CI/OFDM, CI/COFDM, and CI/MC-CDMA, respectively, are consistent with the discrete-time representations and descriptions offered in [147, 148, 230–232], suggesting the general SMSE framework is suitable for characterizing OFDM and MC-CDMA signals that incorporate CI techniques to introduce orthogonality between users. Table 4.3 summarizes the instantiation of waveform design variables required in (3.5) to achieve CI/OFDM, CI/COFDM, and CI/MC-CDMA signaling within a CR-based SDR architecture.

4.6 Summary of SMSE Framework Applications

The general analytic SMSE framework of Chapter III is applied to seven different signals which exist or are emerging as 4G communication candidates. The four existing signals considered include: OFDM, COFDM, MC-CDMA, and TDCS. Carrier interferometry (CI) signaling techniques are emerging as likely candidates for future wireless communications, especially when considering the diversity required for cognitive-based, software defined radio (SDR) technologies. The three CI-based techniques considered include: CI/OFDM, CI/COFDM, and CI/MC-CDMA. Introduced

here as SMSE variants, each of the seven signaling techniques is readily implementable by proper instantiation of SMSE waveform design variables (using the tables provided herein). For all waveforms considered, the SMSE analytic expressions resulting from the instantiations provided are shown to be consistent with published results.

V. SMSE Framework Demonstration

The practical utility of the general analytic framework proposed in Chapter III for spectrally modulated, spectrally encoded (SMSE) signals is reinforced via modeling and simulation demonstrations. Communication performance is characterized through probability of bit error P_b for a given transmit-channel-receive structure. Simulations are conducted using specific instantiations of the six SMSE waveform design variables to generate desired signals, thus simulating non-real-time behavior of what could be achieved using a cognitive radio(CR)-based, software defined radio (SDR) architecture.

A subset of orthogonal frequency division multiplexing (OFDM)-based signals is considered for these demonstrations, including: uncoded OFDM, multi-carrier code division multiple access (MC-CDMA), transform domain communication system (TDCS), and SMSE⁺. As introduced here, SMSE⁺ represents a composite signal structure that combines characteristics from the other three signals, i.e., spectral modulation and coding, spectral spreading, complex phase coding, and adaptive notching are employed. Each of the signals considered are constructed in accordance with the scenarios presented in the sections below.

Section 5.1 begins by describing the general modeling and simulation methodology, identifying key features of the transmitter, channel, and receiver models and providing theoretical P_b expressions. Section 5.2 follows by establishing baseline performance of the four signals in additive white Gaussian noise (AWGN) channels. The results are then extended to account for fading channel effects in Section 5.3. Interference suppression capability of SMSE signals is demonstrated in Section 5.4 using partial band interference (PBI) and multiple access interference (MAI) performance is characterized in a multi-user environment in Section 5.5.

The analytic versus simulated bit error performance results in Section 5.2 through Section 5.5 are not a contribution in and of themselves. Rather, the results are provided to substantiate the flexibility and applicability of the proposed SMSE framework for future CR-based SDR implementations; collectively, these results represent a key

research contribution. It is shown in Chapter IV that the unifying SMSE framework generates analytic signal expressions which match theoretical expressions found in published literature. Results in this chapter demonstrate that practical implementation of the unifying SMSE framework via software (using various instantiations of six key waveform design variables) has virtually no impact on performance when compared to systems employing dedicated hardware and having fixed capability.

5.1 Methodology

This section begins by describing the modeling and simulation methodology used to generate SMSE results. Theoretical P_b expressions are provided for each signal type considered and are used to establish confidence in the results.

5.1.1 Transmitter Model. As described in Chapter III, the transmitted signal is designed via proper instantiation of six waveform design variables, including: frequency assignment (**a**), frequency use (**u**), data (**d**), coding (**c**), windowing (**w**), and orthogonality (**o**). Specific variable instantiations are provided in Table 4.1 through Table 4.3 for several signals being considered for CR-based SDR implementation.

Frequency control is governed by cognitive assignment within **a** and adaptive use within **u**. Unless otherwise specified, the simulations assume that all N_F available frequency components are assigned. All simulations use $N_F = 256$ frequency components except for those identified in Section 5.5 for multiple access scenarios where $N_F = 32$ is used. Thus, **a** = **1** for all scenarios. Frequency use varies based on signal type (OFDM, MC-CDMA, etc.), and without loss of generality, **u** = **a** except for interference suppression characterization. For interference suppression scenarios, the transmitter may choose to suppress interference (equivalent to removing or not using specific frequency components) by adopting a process from [101]. Further details on spectral estimation and thresholding are provided in Section 5.1.3.

The used frequency components are Gray-code data modulated based on **d** using binary phase shift keying (BPSK), quaternary PSK (QPSK), 8-ary PSK, or

16-ary quadrature amplitude modulation (QAM). The code weight applied to each used frequency component from \mathbf{c} varies depending on signal type. Uncoded signal implementations effectively ignore coding by setting $\mathbf{c} = \mathbf{1}$ and $\boldsymbol{\theta}_{\mathbf{c}} = \mathbf{0}$, while coded signal implementations use either bi-phase coding with $\theta_{c_m} \in \{\pi, -\pi\}$ or poly-phase coding with $\theta_{c_m} \in [0, 2\pi), \forall m$. Window and orthogonality vectors permit further waveform diversity. For simplicity, the signals in the demonstration simulations do not require this diversity and thus $\mathbf{w} = \mathbf{1}$, $\boldsymbol{\theta}_{\mathbf{w}} = \mathbf{0}$, and $\boldsymbol{\theta}_{\mathbf{o}} = \mathbf{0}$.

Once the waveform design variables have been instantiated, the transmitted signal $s_k(t)$ is generated per the process detailed in Section 3.4 using an inverse fast Fourier transform (IFFT). This signal is then input to various channel models which are described next.

5.1.2 Channel Models. The SMSE signal $s_k(t)$ is propagated through three different channel models, including: AWGN, Rayleigh flat fading, and Rayleigh frequency selective fading. For some scenarios, additional interference from a partial band interferer or multiple users introduced as well. The composition of the noise model, fading channel models, and interference model are described in the following subsections.

5.1.2.1 AWGN Model. For the AWGN channel, complex noise $n(t)$, with Gaussian distribution in both the I (real) and Q (imaginary) components (see Fig. 5.1), is added to the transmitted signal to form the received signal $r_k(t)$. The resulting complex Gaussian noise has uniform phase.

5.1.2.2 Fading Channel Models. The first fading model considered is a *Rayleigh flat fading* channel which is commonly found in wireless, narrowband communication applications. In a Rayleigh flat fading channel, it is assumed there is only one signal path between the transmitter and receiver. This assumption remains valid provided that the signal bandwidth is less than the channel bandwidth [165].

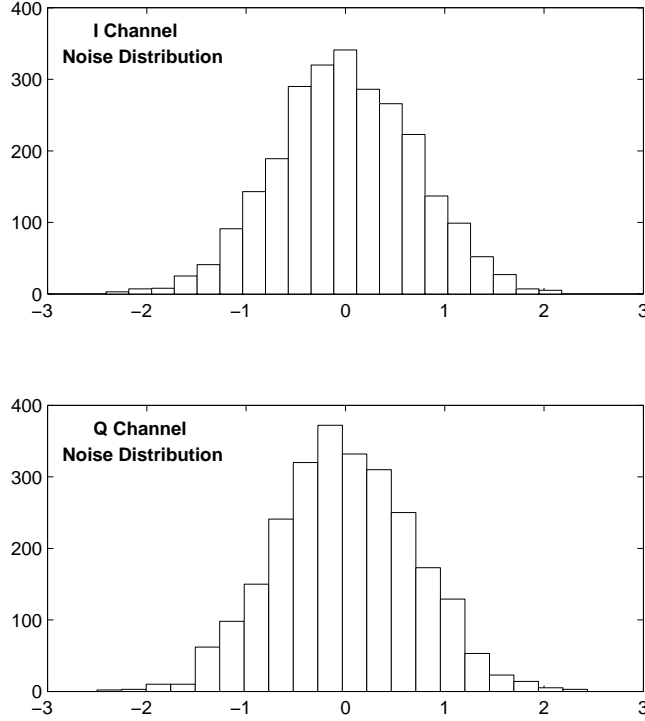


Figure 5.1: Representative noise distribution on I & Q components of AWGN channel model (2,560 realizations illustrated).

In this case, the signal is weighted by a complex Rayleigh fading coefficient having a Rayleigh-distributed magnitude and uniformly-distributed phase – see Fig. 3.6.

The second fading model considered is a *Rayleigh frequency selective fading* channel which is implemented using a tapped delay line (TDL) model as described in Section 3.5.3 and shown in Figure 3.7. For general application, and without loss of generality, the frequency selective channels used herein are modeled as having two multipath returns ($N_{MP} = 2$). Each of the multipath returns is weighted by a complex Rayleigh fading coefficient and the second return is delayed by one time sample relative to the first.

5.1.2.3 Interference Model. Occasionally, additional interference may exist in a channel which serves to further corrupt the signal. For interference charac-

terization in this research, partial band interference (PBI) is generated to represent a noise-like signal. This complex interference, having a Gaussian distribution in both the I and Q components, has a Rayleigh-distributed magnitude and a uniformly-distributed phase between $-\pi$ and π (see Fig. 5.2). In this case, the PBI occupies a specific portion of the spectrum dictated by P_I as designated in the model. For all results contained herein, the number of components represented in P_I are chosen to span 10% of the system frequency components. The resultant time-domain interference signal is added to the channel-weighted signal and noise at the receiver input. Figure 5.3 shows a block diagram of PBI signal generation process.

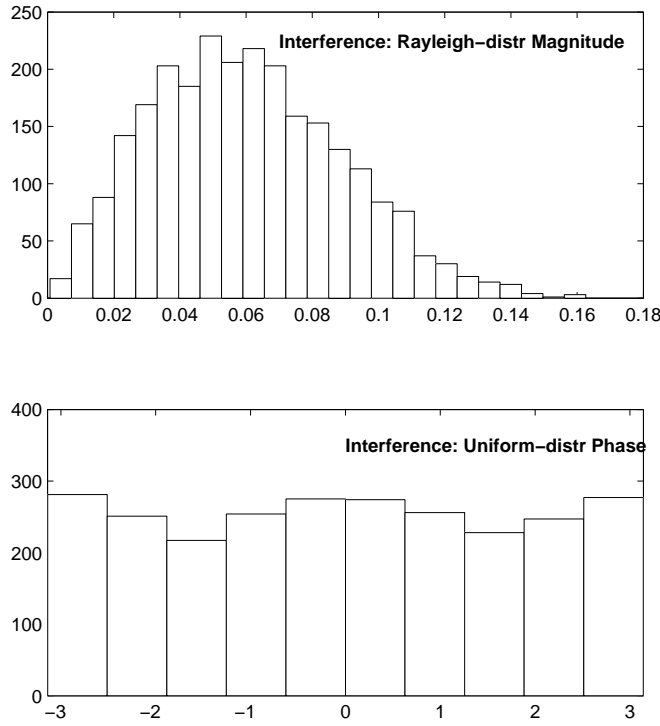


Figure 5.2: Magnitude and phase distributions for Partial Band Interference (PBI) signal (2,560 realizations illustrated).

5.1.3 Receiver Model. The spectral estimation, interference suppression, and coding processes follow the general methodology described in [101, 171]. The

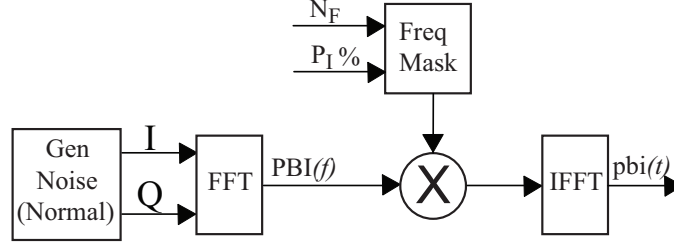


Figure 5.3: Block diagram for Partial Band Interference (PBI) generation.

spectral estimation process begins when the receiver performs an auto-regressive (AR) estimate over an observation interval T_{obs} . The AR estimation is used to obtain a smooth estimate of the local electromagnetic spectrum [180]. Conceptually, the AR model (see Fig. 5.4) is based on an all-pole filter which processes a “white noise” signal [168, 180]. The AR filter $H(z)$ is defined as [168]

$$H(z) = \frac{1}{A_z} = \frac{1}{1 + a_1^* z^{-1} + a_2^* z^{-2} + \dots + a_B^{-B}} \quad (5.1)$$

where the a_i coefficients satisfy the system of equations given by

$$\begin{bmatrix} R_y[0] & R_y[1] & \dots & R_y[B-1] \\ R_y[-1] & R_y[0] & \dots & R_y[B-2] \\ \vdots & \vdots & \ddots & \vdots \\ R_y[-B+1] & \vdots & \dots & R_y[0] \end{bmatrix} \begin{bmatrix} a_1 \\ a_2 \\ \vdots \\ a_B \end{bmatrix} = \begin{bmatrix} -R_y[-1] \\ -R_y[-2] \\ \vdots \\ -R_y[-B] \end{bmatrix} \quad (5.2)$$

and R_y is a Toeplitz autocorrelation matrix of order B . A 10^{th} order AR filter is used for spectral estimation in this research, which matches the AR filter order used in other research [168, 179, 215].

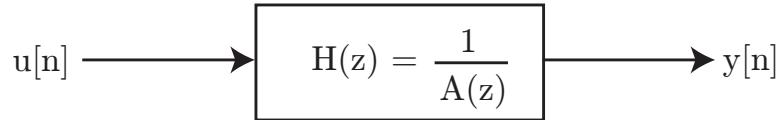


Figure 5.4: Auto-Regressive (AR) model [168].

Depending on adaptation capabilities, the CR-based SDR may choose to suppress interference by excising or removing frequencies containing excessive power. If adaptation is enabled, the SMSE transmitter applies an interference suppression technique that removes $P_I\%$ of the jammer power via adaptive thresholding and then modifies its frequency use vector \mathbf{u} to transmit zero energy in the identified spectral components. In this research, it is assumed that the transmitter and receiver view identical electromagnetic environments and hence, the receiver suppresses energy in identified spectral components that directly correlate to the spectral components the transmitter avoided using.

Previous research with SMSE-like signals applied a fixed threshold at a given percentage of the peak estimated value [168,179]. The research herein adopts an adaptive approach that is readily implementable within a CR-based SDR. The adaptive threshold (T_I) can be expressed as

$$T_I = \omega_I \sum_{m=1}^{N_F} |y[m]|^2 \quad (5.3)$$

where ω_I is a weighting factor which dictates the amount of interference power removed, $y[m] = \mathfrak{F}\{y[n]\}$, and $y[n]$ is the output from the AR spectral estimation model shown in Fig. 5.4.

Following spectral estimation and thresholding, the received signal is processed via a front-end RF filter and undergoes an FFT transform as explained in Section 3.6. The scenarios herein assume an ideal front-end RF filter, i.e., all energy over the N_F frequency components is passed and zero energy outside the N_F frequency components is passed. The resulting frequency domain signal is then decoded and demodulated to determine symbol estimates.

Two demodulation techniques are implemented in the results that follow. For scenarios including transmission over AWGN or Rayleigh flat fading channels, symbol estimation is determined based upon the minimum distance to local constellation values. For example, assume that the symbol spectral coefficient following the FFT is

represented by the solid dot shown in Fig. 5.5a. The Euclidean distance between this received coefficient and all constellation points (circles) is calculated and a symbol estimate is chosen based upon the minimum. Fig. 5.5b shows an example of 1,024 symbols being received under the same signaling conditions: OFDM with 16-QAM modulation at 10 dB E_b/N_o .

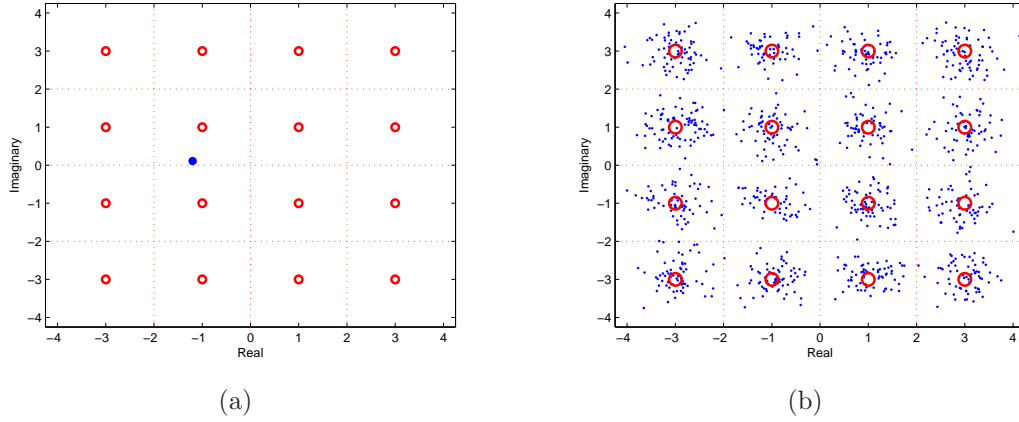


Figure 5.5: OFDM symbol estimation using 16-QAM modulation (circles represent constellation points). The two figures show (a) One received symbol (solid dot), and (b) 1,024 received symbols for $E_b/N_o = 10$ dB.

For scenarios involving Rayleigh frequency selective fading channels, a TDL model is used to represent the channel. Symbol estimation is then based upon the maximum correlation value obtained from correlating the received waveform with each of M possible waveforms. Assuming perfect channel estimation, the receiver has knowledge of the M possible waveforms and this process results in maximum likelihood estimation.

5.1.4 Communication Performance. Simulation results are compared to analytical results to validate SMSE communication performance. Simulated bit error probabilities are determined by counting the number of bit errors e_b and dividing by the total number of transmitted bits n_b , i.e., estimated $P_b = e_b/n_b$. Confidence levels are increased by counting more errors and/or transmitting more symbols in Monte

Carlo fashion. The confidence interval (C.I.) can be calculated via [23, 60, 93]

$$\begin{aligned} 100(1 - \alpha) \% \text{ C.I.} &= P_b \mp r \\ &= P_b \mp z_{(1-\alpha/2)} \cdot \sqrt{\frac{P_b \cdot (1 - P_b)}{n_b}} \quad \text{for } n_b \cdot P_b \geq 10 \end{aligned} \quad (5.4)$$

where α is the significance level and z_x is the x^{th} -quantile of a standard normal distribution. Substituting in $\alpha = 0.05$, $z = 1.96$, and $n_b = e_b/P_b$ yields [23, 37]

$$95\% \text{ C.I.} = P_b \mp 1.96 \cdot \sqrt{\frac{P_b^2 \cdot (1 - P_b)}{e_b}} \quad \text{for } n_b \cdot P_b \geq 10. \quad (5.5)$$

The simulation results in this chapter are based upon a minimum of 300 accumulated bit errors. That is, the Monte Carlo simulations run until a preset minimum of transmitted bits (usually 100,000) *and* a preset minimum number of errors (≥ 300) occurs. For $e_b = 300$ in (5.5), the resultant data is within $r/P_b = 11\%$ of the mean with 95% confidence. The resultant bit error curves are subsequently compared with theoretical results. This subsection provides expressions (by channel type) for the theoretical results shown in subsequent plots.

5.1.4.1 AWGN Channel. The theoretical bit error probability P_b for Gray-coded binary PSK (BPSK), M -ary PSK, and M -ary QAM modulations over AWGN channels with matched filter detection (or correlator implementation thereof) is given in (5.6), (5.7), and (5.8), respectively.

Communication performance for BPSK data modulation over an AWGN channel is given by [165]

$$P_{b,BPSK-AWGN} = Q\left(\sqrt{\frac{2E_b}{N_o}}\right) \quad (5.6)$$

where $Q(x) = 1/\sqrt{2\pi} \int_x^\infty \exp(-t^2/2) dt$, $x \geq 0$, E_b is the average bit energy, N_o is the noise power density, and E_b/N_o is sometimes referred to as the “signal-to-noise ratio per bit” [165].

Communication performance for MPSK data modulation over an AWGN channel is given by [165]

$$P_{b,MPSK-AWGN} = \frac{2}{k} Q \left(\sqrt{\frac{2kE_b}{N_o}} \sin \left(\frac{\pi}{M} \right) \right) \quad (5.7)$$

where $k = \log_2 M$ is the number of bits per symbol. When $M = 4$ (QPSK modulation), (5.7) reduces to (5.6). That is, Gray-coded QPSK is essentially the quadrature phase pairing of two BPSK signal sets and has equivalent P_b performance for a given E_b/N_o .

Communication performance for MQAM (rectangular constellation) over an AWGN channel is given by [165]

$$P_{b,MQAM-AWGN} = \frac{1}{k} \left(1 - \left[1 - 2 \left(1 - \frac{1}{\sqrt{M}} \right) Q \left(\sqrt{\frac{3k}{M-1} \frac{E_b}{N_o}} \right) \right]^2 \right) \quad (5.8)$$

where all variables have been previously defined.

5.1.4.2 Rayleigh Fading Channels. The theoretical bit error probability P_b for BPSK and MPSK modulations over Rayleigh frequency selective fading channels is given in (5.9) and (5.15), respectively. These expressions assume that N_{MP} independent multipath replicas are present. For $N_{MP} = 1$, (5.9) simplifies to (5.12) and (5.15) simplifies to (5.16). The P_b expression in (5.20) for 16-QAM modulation over Rayleigh fading channels applies the variable definitions in (5.21) and (5.22) for flat and frequency selective fading conditions, respectively.

Communication performance for BPSK data modulation over a Rayleigh frequency selective fading channel can be expressed as [165]

$$P_{b,BPSK-FreqSel} = \frac{1}{2} \left[1 - \mu \sum_{l=0}^{N_{MP}-1} \binom{2l}{l} \left(\frac{1-\mu^2}{4} \right)^l \right] \quad (5.9)$$

$$\mu = \sqrt{\frac{\bar{\gamma}_c}{1 + \bar{\gamma}_c}} \quad (5.10)$$

$$\bar{\gamma}_b = \bar{\gamma}_c \frac{N_{MP}}{k} \quad (5.11)$$

where μ is the “cross-correlation coefficient” under the assumption of perfect channel estimation, $\bar{\gamma}_c$ is the average received SNR per channel, and $\bar{\gamma}_b$ is the average SNR per bit. When $N_{MP} = 1$, (5.9) reduces to [165]

$$P_{b,BPSK-Flat} = \frac{1}{2} \left(1 - \sqrt{\frac{\bar{\gamma}_b}{1 + \bar{\gamma}_b}} \right). \quad (5.12)$$

When $\bar{\gamma}_c \gg 1$ and $\bar{\gamma}_b \gg 1$, (5.9) and (5.12) can be approximated by [165]

$$P_{b,BPSK-FreqSel} \approx \left(\frac{1}{4\bar{\gamma}_c} \right)^{N_{MP}} \binom{2N_{MP}-1}{N_{MP}} \quad (5.13)$$

$$P_{b,BPSK-Flat} \approx \frac{1}{4\bar{\gamma}_b}. \quad (5.14)$$

Communication performance for MPSK data modulation over a Rayleigh frequency selective fading channel can be generally expressed as [165]

$$P_{b,MPSK-FreqSel} = \frac{1}{k} \frac{(-1)^{N_{MP}-1} (1-\mu^2)^{N_{MP}}}{\pi (N_{MP}-1)!} \left(\frac{\partial^{N_{MP}-1}}{\partial b^{N_{MP}-1}} \left\{ \frac{1}{b-\mu^2} \left[\frac{\pi}{M} (M-1) - \frac{\mu \sin(\pi/M)}{\sqrt{b-\mu^2 \cos(\pi/M)}} \cot^{-1} \left(\frac{-\mu \cos(\pi/M)}{\sqrt{b-\mu^2 \cos(\pi/M)}} \right) \right] \right\} \right)_{b=1} \quad (5.15)$$

where μ was defined in (5.10).

An approximate expression is found for MPSK data modulation over Rayleigh flat fading channels by modifying (5.15), setting $N_{MP} = 1$ and assuming $\bar{\gamma}_b \gg 1$ [165]

$$P_{b,MPSK-Flat} \approx \frac{1}{k} \frac{M-1}{(M \log_2 M) [\sin^2(\pi/M)] 2\bar{\gamma}_b}. \quad (5.16)$$

For 4-ary PSK (QPSK) data modulation, the expression in (5.15) simplifies to [165]

$$P_{b,QPSK-FreqSel} = \frac{1}{2} \left[1 - \rho \sum_{l=0}^{N_{MP}-1} \binom{2l}{l} \left(\frac{1-\rho^2}{4} \right)^l \right] \quad (5.17)$$

$$P_{b,QPSK-Flat} = \frac{1}{2} (1 - \rho) \quad (5.18)$$

where

$$\rho = \frac{\mu}{\sqrt{2 - \mu^2}}. \quad (5.19)$$

Communication performance for 16-QAM data modulation (rectangular constellation) over a Rayleigh fading channel can be expressed as [214]

$$P_{b,MQAM-Fade} = \frac{1}{2} P_{b1} + P_{b3} \quad (5.20)$$

where

$$\begin{aligned} P_{b1-Flat} &= \frac{1}{2} \left[1 - \frac{1}{2} \sqrt{\frac{2E_b/N_o}{5 + 2E_b/N_o}} - \frac{1}{2} \sqrt{\frac{18E_b/N_o}{5 + 18E_b/N_o}} \right] \\ P_{b3-Flat} &= \frac{1}{2} \left[1 - \sqrt{\frac{2E_b/N_o}{5 + 2E_b/N_o}} - \frac{1}{2} \sqrt{\frac{18E_b/N_o}{5 + 18E_b/N_o}} + \right. \\ &\quad \left. \frac{1}{2} \sqrt{\frac{50E_b/N_o}{5 + 50E_b/N_o}} \right] \end{aligned} \quad (5.21)$$

for flat fading. For frequency selective fading, different P_{b1} and P_{b3} expressions are used as follows [214]

$$\begin{aligned}
P_{b1-FreqSel} &= \frac{1}{2} (P_1 + P_2) \\
P_{b3-FreqSel} &= \frac{1}{2} (2P_1 + P_2 - P_3) \\
P_{i,i \in \{1,2,3\}} &= \left(\left[\frac{1}{2} (1 - \mu_i) \right]^{2L} \right) \sum_{j=0}^{2L-1} \binom{2L-1+j}{j} \left[\frac{1}{2} (1 + \mu_i) \right]^j
\end{aligned} \tag{5.22}$$

where an L -order spatial diversity receiver is used, L represents the number of Rake receiver fingers [214], and

$$\begin{aligned}
\mu_1 &= \sqrt{\frac{E_b/N_o}{5L + E_b/N_o}} \\
\mu_2 &= \sqrt{\frac{9E_b/N_o}{5L + 9E_b/N_o}} \\
\mu_3 &= \sqrt{\frac{25E_b/N_o}{5L + 25E_b/N_o}}.
\end{aligned} \tag{5.23}$$

5.2 Baseline Results

The performance of four SMSE-candidate signals is demonstrated via modeling and simulation using the SMSE analytic framework. These results demonstrate expected communication performance for single-user systems over AWGN channels with no interference present, establishing a baseline for SMSE communication performance that matches theoretical results in the literature.

Table 5.1 presents the characteristics of SMSE-candidate signals used for demonstration. The TDCS signal modeled herein differs slightly from the published technique for TDCS signal creation [28]. The conventional TDCS modulation process involves application of the data modulation in the time domain following an IFFT of the spectral encoding process. The data modulation of interest for the results of this work is PSK, which can be effectively applied in the frequency domain. However,

Table 5.1: Characteristics of demonstrated SMSE-candidate signals.

Signal Type	Data Modulation	Coding	Spectral Spreading	Data Demod	Adaptive Notching
OFDM	BPSK, QPSK, 8-PSK, 16-QAM	None	No	Freq	No
MC-CDMA	BPSK, QPSK, 8-PSK	bi-phase $\theta_c \in \{0, \pi\}$	Yes	Freq	No
TDCS	BPSK, QPSK, 8-PSK	poly-phase $\theta_c \in [0, 2\pi)$	Yes	Time	Yes
SMSE ⁺	BPSK, QPSK, 8-PSK	poly-phase $\theta_c \in [0, 2\pi)$	Yes	Freq	Yes

demodulation of the TDCS signals is still done in the time domain in accordance with [28]. As introduced earlier, the SMSE⁺ signal uses a collection of attributes from the OFDM, MC-CDMA, and TDCS signals.

5.2.1 OFDM Baseline. Baseline OFDM performance is demonstrated using the SMSE framework. As shown in Fig. 5.6, the simulated performance closely matches the theoretical expressions for BPSK, QPSK, 8-PSK, and 16-QAM over AWGN channels. Collectively, the data exhibits a mean absolute error of 4.9×10^{-3} and standard deviation of 4.8×10^{-3} for E_b/N_o values from 0 to 9 dB.

5.2.2 MC-CDMA Baseline. Baseline MC-CDMA performance, using an m -sequence code with $\theta_{c_m} \in \{0, \pi\}$ in a single user scenario, is demonstrated using the SMSE framework. As shown in Fig. 5.7, the simulated performance closely matches the theoretical expressions for BPSK, QPSK, and 8-PSK over AWGN channels. Collectively, the data exhibits a mean absolute error of 4.2×10^{-3} and standard deviation of 3.8×10^{-3} for E_b/N_o values from 0 to 9 dB. These results are representative of the performance achieved when using either random or Walsh codes in a single-user scenario.

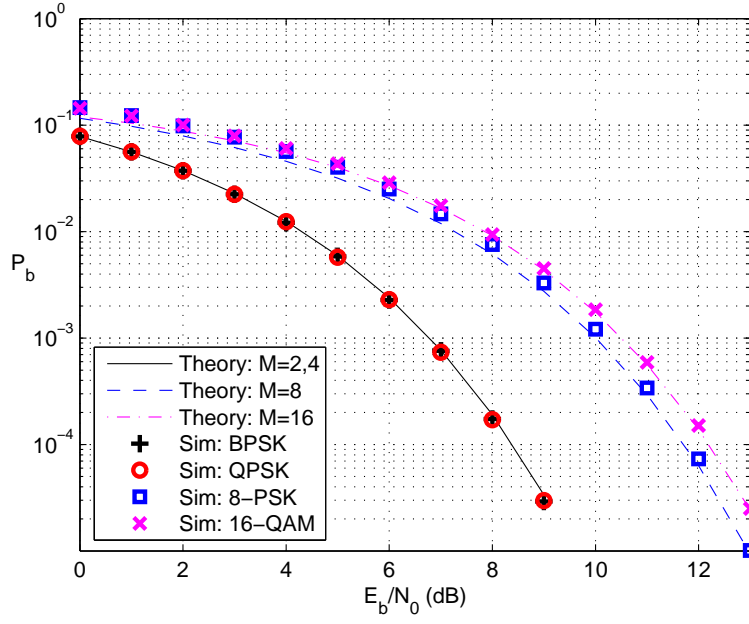


Figure 5.6: Baseline OFDM performance: P_b vs E_b/N_o in AWGN channel with *No Interference Present*. (Analytic results are taken from [165].)

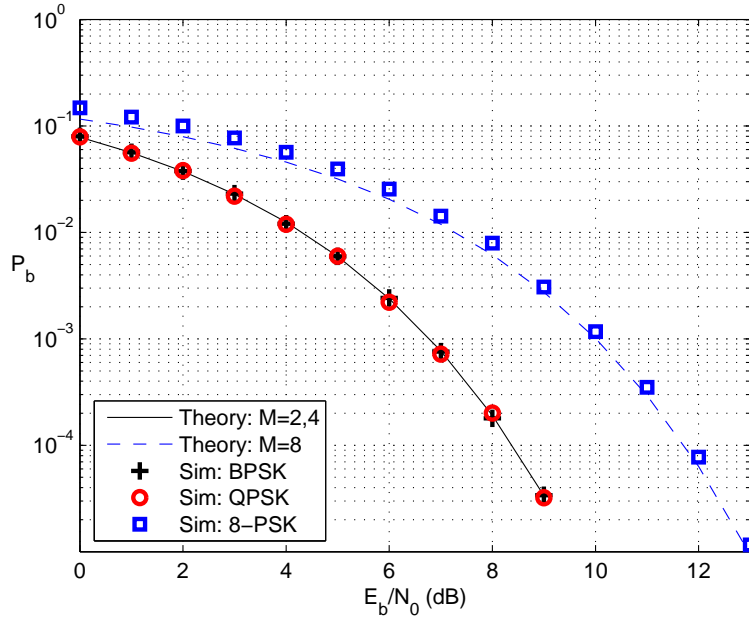


Figure 5.7: Baseline MC-CDMA performance: P_b vs E_b/N_o in AWGN channel with *No Interference Present*. (Analytic results are taken from [165].)

5.2.3 TDCS Baseline. Baseline TDCS performance, as modified to incorporate spectral data modulation, is demonstrated using the SMSE framework. As shown in Fig. 5.8, the simulated performance closely matches the theoretical expressions for BPSK, QPSK, and 8-PSK over AWGN channels. Collectively, the data exhibits a mean absolute error of 4.6×10^{-3} and standard deviation of 4.1×10^{-3} for E_b/N_o values from 0 to 9 dB.

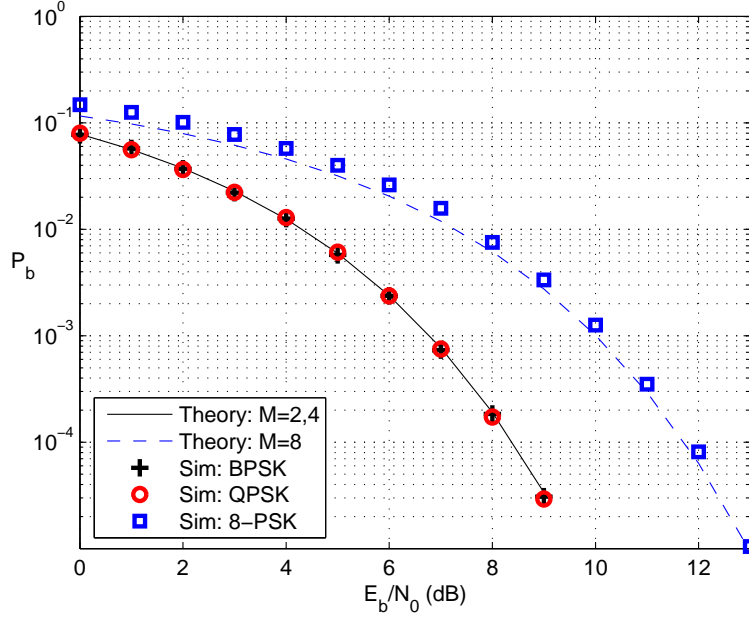


Figure 5.8: Baseline TDCS performance: P_b vs E_b/N_o in AWGN channel with N_o Interference Present. (Analytic results are taken from [165].)

5.2.4 SMSE⁺ Baseline. Baseline SMSE⁺ performance is demonstrated using the SMSE framework. The SMSE⁺ signal is a generic OFDM-based signal combining attributes from OFDM, MC-CDMA, and TDCS signals as detailed in Table 5.1. As shown in Fig. 5.9, the simulated performance closely matches the theoretical expressions for BPSK, QPSK, and 8-PSK over AWGN channels. Collectively, the data exhibits a mean absolute error of 4.7×10^{-3} and standard deviation of 4.0×10^{-3} for E_b/N_o values from 0 to 9 dB.

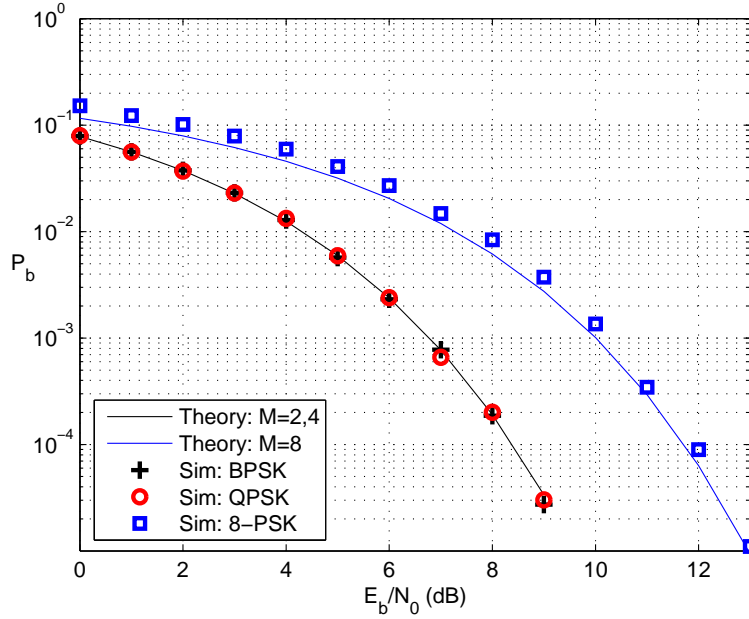


Figure 5.9: Baseline SMSE⁺ performance: P_b vs E_b/N_o in AWGN channel with *No Interference Present*. (Analytic results are taken from [165].) The SMSE⁺ signal combines attributes from OFDM, MC-CDMA, and TDCS signals.

5.2.5 Summary of Baseline Results. As shown in Fig. 5.6 through Fig. 5.9, the modeling and simulation results for the SMSE framework are consistent with the corresponding analytic expressions. Table 5.2 summarizes the mean absolute error and associated standard deviation for each signal modeled in this section.

Table 5.2: Summary of errors (simulated versus analytic) for results in Fig. 5.6 through Fig. 5.9.

Signal Type	Mean Absolute Error	Standard Deviation
OFDM	4.9×10^{-3}	4.8×10^{-3}
MC-CDMA	4.2×10^{-3}	3.8×10^{-3}
TDCS	4.6×10^{-3}	4.1×10^{-3}
SMSE ⁺	4.7×10^{-3}	4.0×10^{-3}

5.3 Fading Channel Demonstration

Performance of the four SMSE-candidate signals is now demonstrated in fading channels using the SMSE analytic framework. These results demonstrate expected communication performance over Rayleigh fading channels, which are more realistic than AWGN channels for mobile, wireless communication.

Specifically, the subsections below demonstrate performance for Rayleigh flat fading *and* frequency selective fading. The frequency selective fading results were generated using two multipath replicas ($N_{MP} = 2$) and a 2-finger ($L = 2$) Rake receiver. For each signal type, Rayleigh flat fading results are presented first to illustrate the possible performance degradation resulting from fading for narrowband communications. Next, Rayleigh frequency selective fading results are presented, which illustrate improvement that can be gained by using a Rake receiver to exploit multipath diversity for wideband communications.

These demonstrations show the applicability of the SMSE framework to single-channel receivers and multi-channel receivers in flat and frequency selective fading environments, respectively. The SMSE framework accommodates reception of data streams and/or blocks depending on the communication channel and receiver structures.

5.3.1 OFDM in a Fading Channel. The OFDM performance within the SMSE framework is characterized in a Rayleigh flat fading channel. As shown in Fig. 5.10, the simulated performance matches the theoretical expressions for BPSK, QPSK, 8-PSK, and 16-QAM over Rayleigh flat fading channels. Collectively, the data exhibits a mean absolute error of 5.6×10^{-3} and standard deviation of 10.8×10^{-3} for E_b/N_o values from 0 to 30 dB.

5.3.2 MC-CDMA in a Fading Channel. The MC-CDMA performance is characterized within the SMSE framework using m -sequence coding with $\theta_{c_m} \in \{0, \pi\}$ for both Rayleigh flat and frequency selective fading channels. As shown in Fig. 5.11,

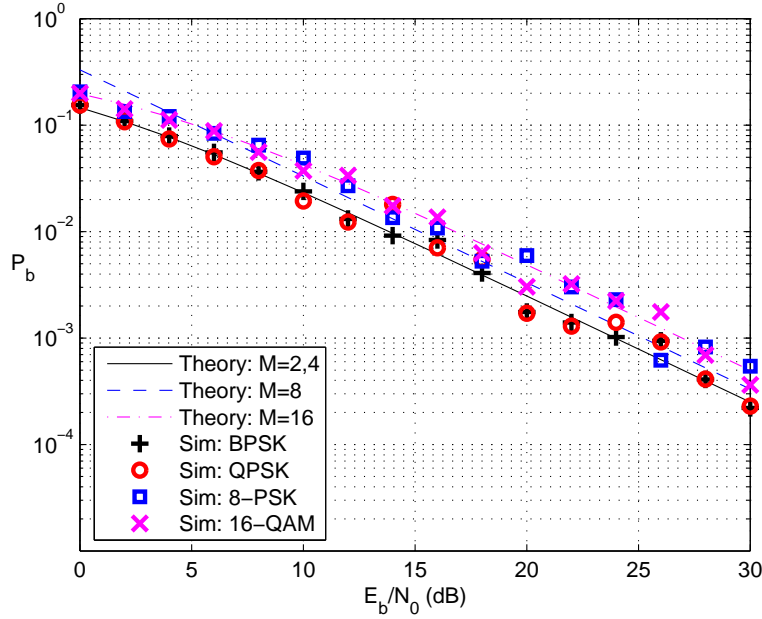


Figure 5.10: OFDM: P_b vs E_b/N_o in a Rayleigh flat fading channel with *No Interference Present*. (Analytic results are taken from [165,214].)

the simulated performance matches the theoretical expressions for BPSK, QPSK, and 8-PSK over Rayleigh flat fading channels. Collectively, the data exhibits a mean absolute error of 6.0×10^{-3} and standard deviation of 12.3×10^{-3} for E_b/N_o values from 0 to 30 dB. These results are representative of the performance obtained when using either random or Walsh coding in a single-user scenario.

When processed with a Rake receiver, multipath components are resolvable in a Rayleigh frequency selective channel. As shown in Fig. 5.12, the simulated performance closely matches the theoretical expressions for BPSK, QPSK, and 8-PSK over Rayleigh frequency selective fading channels. Collectively, the data exhibits a mean absolute error of 1.6×10^{-3} and standard deviation of 2.4×10^{-3} for E_b/N_o values from 0 to 20 dB.

5.3.3 TDCS in a Fading Channel. The TDCS performance, as modified to incorporate spectral data modulation while retaining temporal demodulation as in previous work [28], is characterized within the SMSE framework using Rayleigh

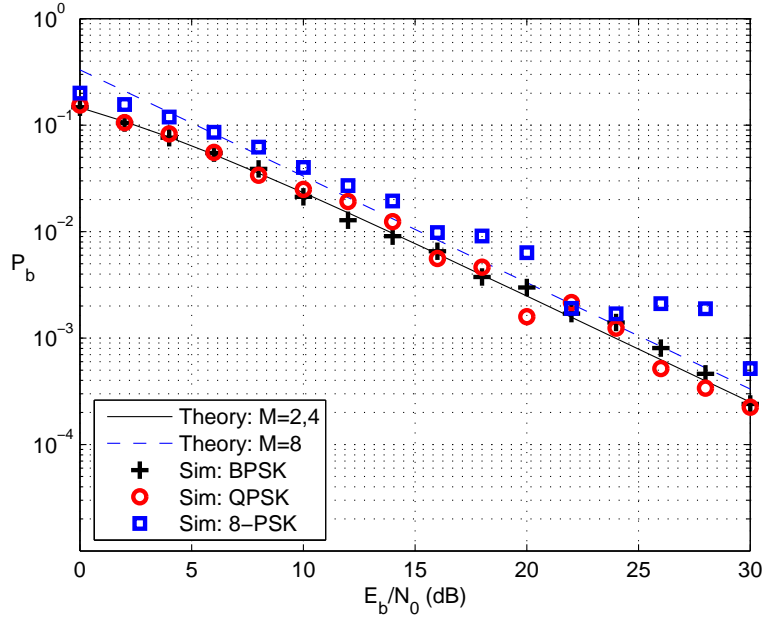


Figure 5.11: MC-CDMA: P_b vs E_b/N_o in a Rayleigh flat fading channel with *No Interference Present*. (Analytic results are taken from [165].)

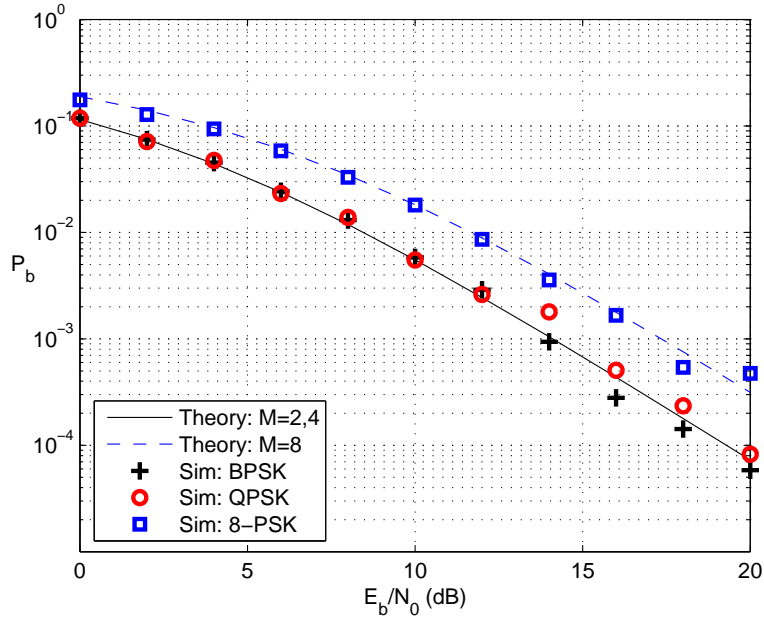


Figure 5.12: MC-CDMA: P_b vs E_b/N_o in a Rayleigh frequency selective fading channel with *No Interference Present*. (Analytic results are taken from [165].)

flat and frequency selective fading channels. As shown in Fig. 5.13, the simulated performance matches the theoretical expressions for BPSK, QPSK, and 8-PSK over Rayleigh flat fading channels. Collectively, the data exhibits a mean absolute error of 6.1×10^{-3} and standard deviation of 13.0×10^{-3} for E_b/N_o values from 0 to 30 dB.

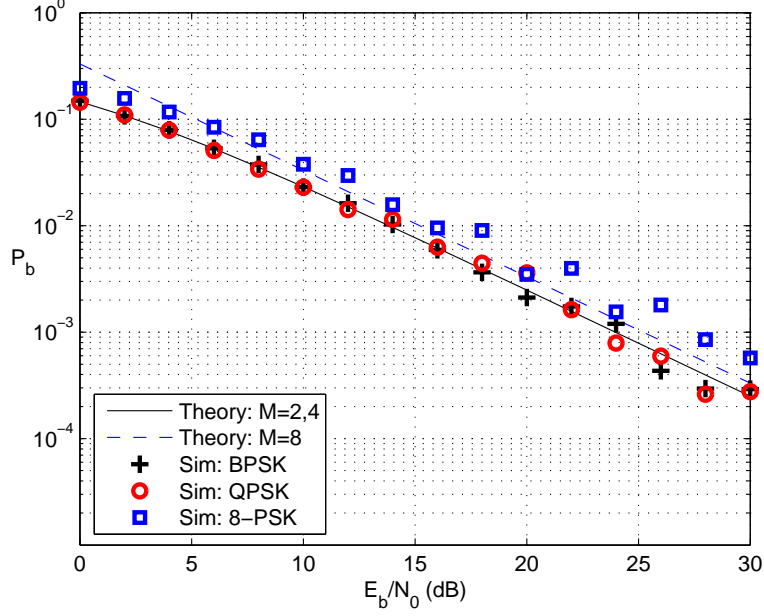


Figure 5.13: TD-CS: P_b vs E_b/N_o in a Rayleigh flat fading channel with *No Interference Present*. (Analytic results are taken from [165].)

When processed with a Rake receiver, multipath components are resolvable in a Rayleigh frequency selective channel. As shown in Fig. 5.14, the simulated performance closely matches the theoretical expressions for BPSK, QPSK, and 8-PSK over Rayleigh frequency selective fading channels. Collectively, the data exhibits a mean absolute error of 1.9×10^{-3} and standard deviation of 2.3×10^{-3} for E_b/N_o values from 0 to 20 dB.

5.3.4 SMSE⁺ in a Fading Channel. The SMSE⁺ performance within the SMSE framework is characterized in Rayleigh flat and frequency selective fading channels. The SMSE⁺ signal is a composite signal that combines attributes from OFDM, MC-CDMA, and TDCS signals (see Table 5.1). As shown in Fig. 5.15, the simulated

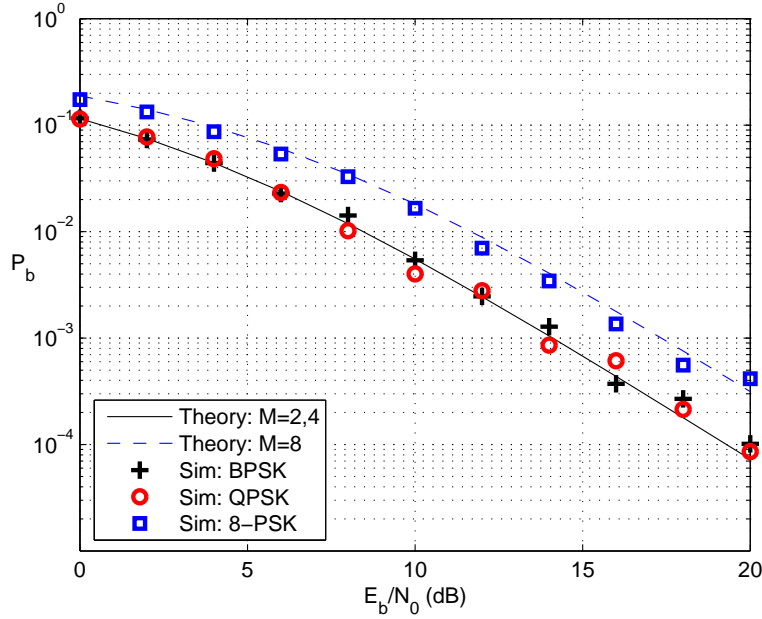


Figure 5.14: TDCS: P_b vs E_b/N_o in a Rayleigh frequency selective fading channel with *No Interference Present*. (Analytic results are taken from [165].)

performance matches the theoretical expressions for BPSK, QPSK, and 8-PSK over Rayleigh flat fading channels. Collectively, the data exhibits a mean absolute error of 5.5×10^{-3} and standard deviation of 12.0×10^{-3} for E_b/N_o values from 0 to 30 dB.

Multipath components are resolvable in a Rayleigh frequency selective channel when captured by a Rake receiver. As shown in Fig. 5.16, the simulated performance closely matches the theoretical expressions for BPSK, QPSK, and 8-PSK over Rayleigh frequency selective fading channels. Collectively, the data exhibits a mean absolute error of 2.1×10^{-3} and standard deviation of 2.9×10^{-3} for E_b/N_o values from 0 to 20 dB.

5.3.5 Summary of Fading Channel Demonstrations. As shown in Fig. 5.10 through Fig. 5.16, modeling and simulation results for the SMSE-candidate signals are consistent with the analytic expressions. Table 5.3 summarizes the mean absolute error and standard deviation of error for each signal considered in this section.

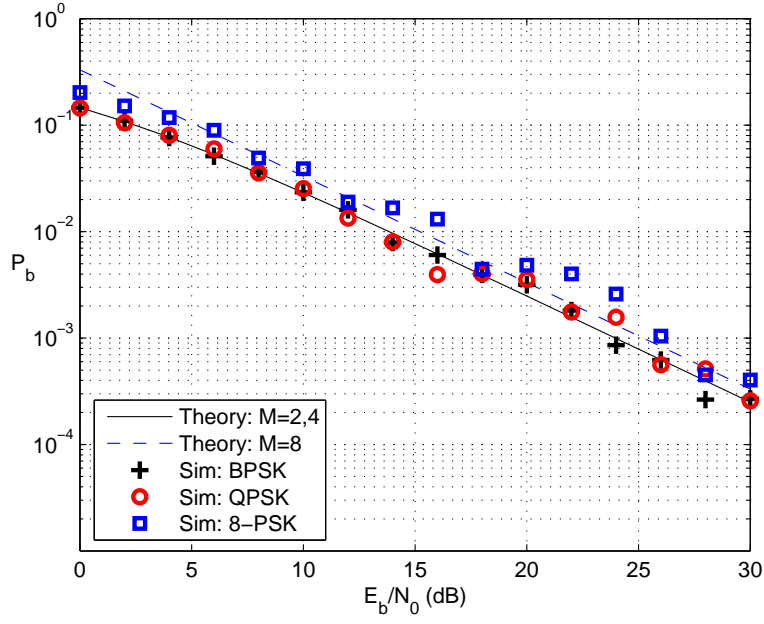


Figure 5.15: SMSE⁺: P_b vs E_b/N_o in a Rayleigh flat fading channel with *No Interference Present*. (Analytic results are taken from [165].)

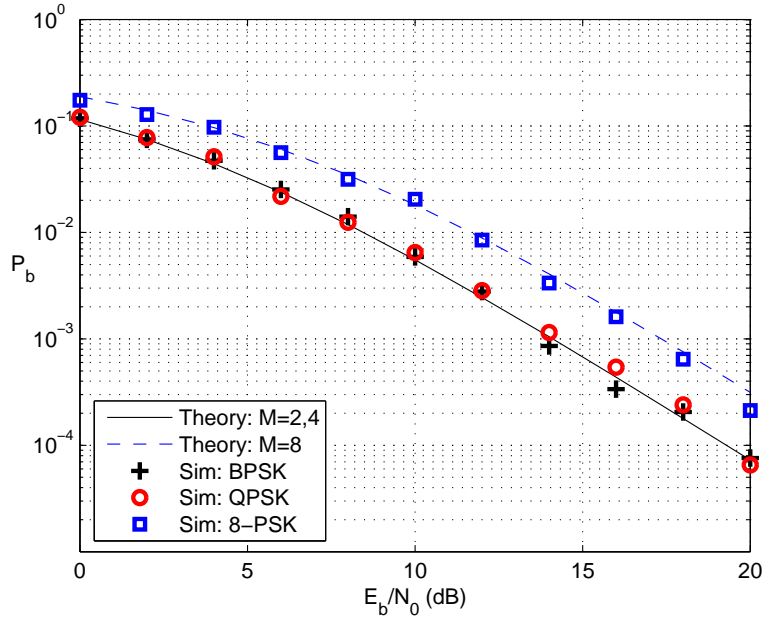


Figure 5.16: SMSE⁺: P_b vs E_b/N_o in a Rayleigh frequency selective fading channel with *No Interference Present*. (Analytic results are taken from [165].)

Table 5.3: Summary of errors (simulated versus analytic) for results in Fig. 5.10 through Fig. 5.16.

Signal Type	Fading Channel	Mean Absolute Error	Standard Deviation
OFDM	Flat	5.6×10^{-3}	10.8×10^{-3}
MC-CDMA	Flat	6.0×10^{-3}	12.3×10^{-3}
MC-CDMA	Freq Sel	1.6×10^{-3}	2.4×10^{-3}
TDCS	Flat	6.1×10^{-3}	13.0×10^{-3}
TDCS	Freq Sel	1.9×10^{-3}	2.3×10^{-3}
SMSE ⁺	Flat	5.5×10^{-3}	12.0×10^{-3}
SMSE ⁺	Freq Sel	2.1×10^{-3}	2.9×10^{-3}

5.4 Interference Suppression Demonstration

The interference suppression capability of two signals from Table 5.1, OFDM and SMSE⁺, is characterized in this section via modeling and simulation using the SMSE analytic framework. These results demonstrate expected communication performance in the presence of PBI. The subsections below show that adaptive frequency use is crucial to improving performance in the presence of PBI. The PBI in the scenarios is spectrally coexistent (coincident center frequencies) and occupies 10% of the SMSE bandwidth. The results illustrate model applicability for several data modulations (MPSK, MQAM) and channel conditions (AWGN, Rayleigh flat fading, Rayleigh frequency selective fading). Interference suppression results are based on constant E_b/N_o values to achieve fixed $P_b = 10^{-3}$. A single transmitter-single receiver system is used to compare results when adaptive spectral notching is on or off, thereby illustrating interference suppression capability.

5.4.1 OFDM with Interference. Results in Fig. 5.17 and Fig. 5.18 show OFDM interference suppression performance over AWGN and Rayleigh flat faded channels, respectively, using BPSK, QPSK, 8-PSK, and 16-QAM data modulations. The AWGN results in Fig. 5.17 are consistent with results in [101] and reflect an average *I/S improvement* (*I/S* difference between suppression on and off conditions at the desired P_b) of approximately 12 to 15 dB for each modulation type.

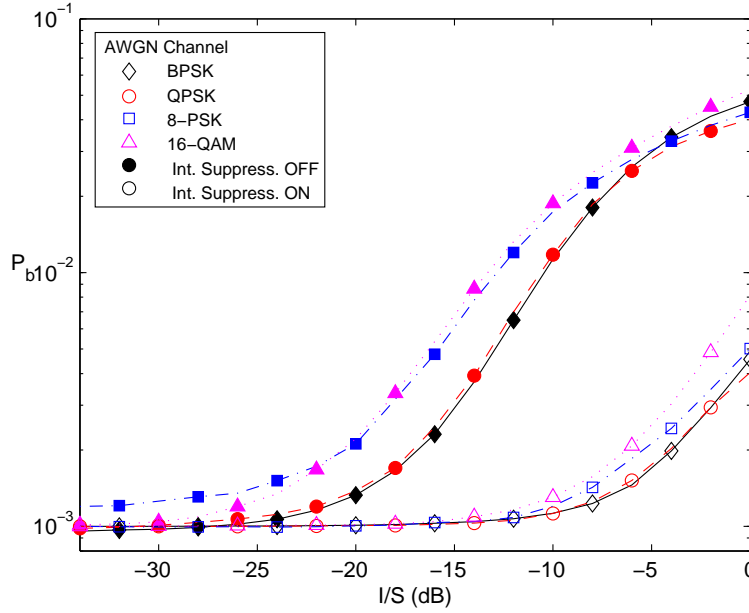


Figure 5.17: OFDM: P_b vs. I/S for AWGN channel with *Interference Present* and suppression ON or OFF as indicated.

The Rayleigh faded results in Fig. 5.18 show that interference suppression is somewhat less effective, with an average realized I/S *improvement* of approximately 9 to 15 dB for MPSK and 5 to 7 dB for 16-QAM. Overall, the interference suppression technique is less effective for 16-QAM in the more realistic Rayleigh faded channel.

Results in Fig. 5.19 and Fig. 5.20 show OFDM interference suppression performance over AWGN and Rayleigh faded channels, respectively, using BPSK, QPSK, 8-PSK, and 16-QAM data modulations with fixed $I/S = 0$ dB. The average P_b *improvement* (P_b difference between suppression on and off conditions at the desired E_b/N_o) when using interference suppression for all modulations is $5.4\times$ for $E_b/N_o \in [0, 20]_{dB}$ and $2.1\times$ for $E_b/N_o \in [0, 30]_{dB}$ for AWGN and Rayleigh faded channels, respectively. The impact of fading upon the P_b performance is obvious from the figures, i.e., mobile, wireless communication suffers fading effects even if PBI is significantly reduced.

5.4.2 $SMSE^+$ with Interference. Results in Fig. 5.21 through Fig. 5.23 show $SMSE^+$ interference suppression performance over AWGN, Rayleigh flat fading, and

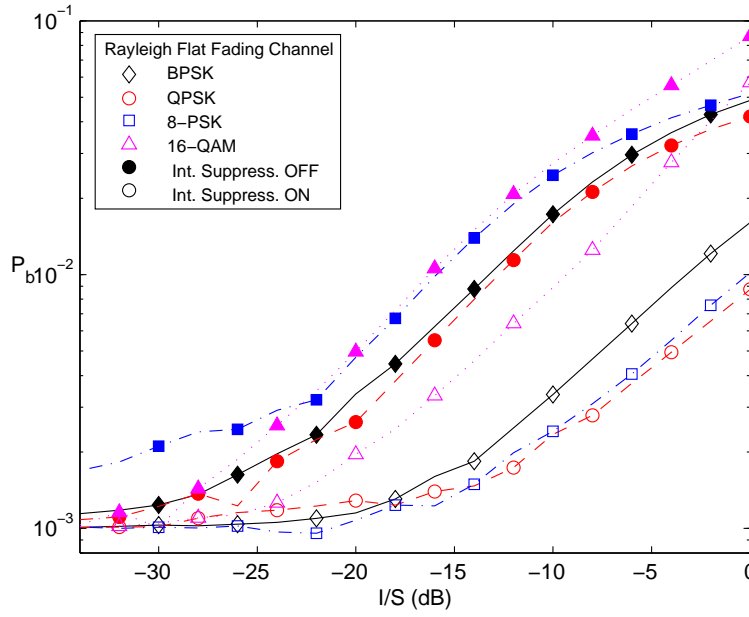


Figure 5.18: OFDM: P_b vs. I/S for Rayleigh flat fading channel with *Interference Present* and suppression ON or OFF as indicated.

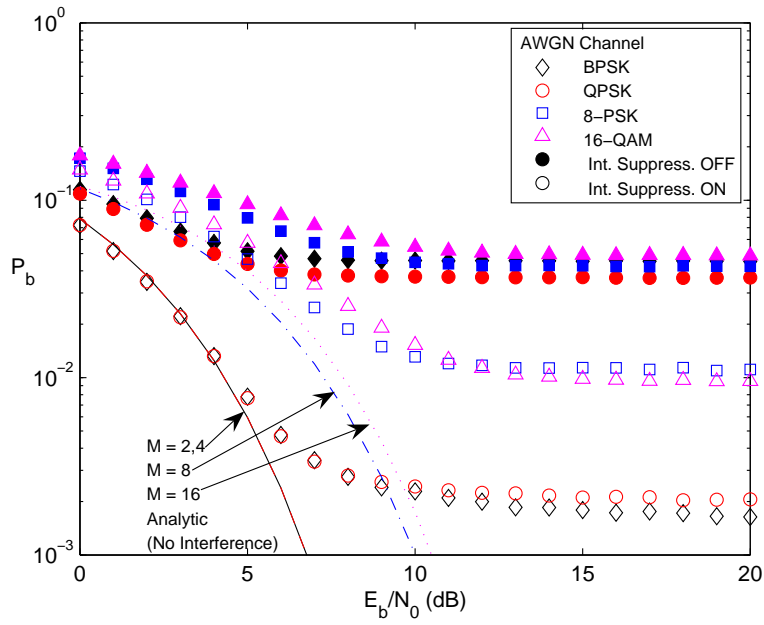


Figure 5.19: OFDM: P_b vs. E_b/N_o for AWGN channel with *Interference Present* ($I/S = 0$ dB) and suppression ON or OFF as indicated.

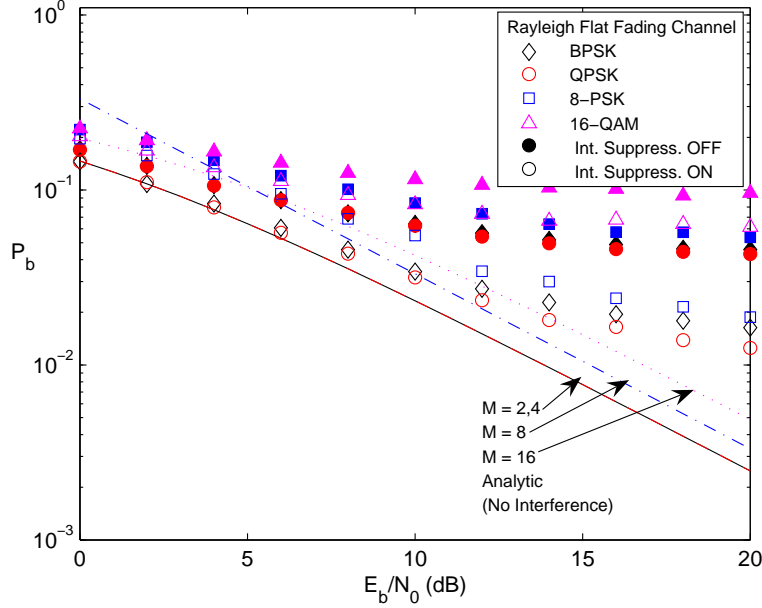


Figure 5.20: OFDM: P_b vs. E_b/N_o for Rayleigh flat fading channel with *Interference Present* ($I/S = 0$ dB) and suppression ON or OFF as indicated.

Rayleigh frequency selective fading channels, respectively, using BPSK, QPSK, and 8-PSK data modulations. The AWGN results in Fig. 5.21 reflect an average I/S *improvement* of approximately 9 to 12 dB for MPSK modulations when $M > 2$. Using BPSK modulation in AWGN with PBI appears to yield better interference suppression performance, offering an average I/S *improvement* of approximately 14 to 15 dB.

The Rayleigh flat fading results in Fig. 5.22 show that interference suppression is somewhat less effective, with an average realized I/S *improvement* of approximately 6 to 10 dB for all modulations. This improvement factor trails that of an AWGN channel due to the fading effects that remain after interference is suppressed. The Rayleigh frequency selective fading results in Fig. 5.23 reflect an average realized I/S *improvement* of 3 to 6 dB for BPSK and QPSK.

Results in Fig. 5.24 through Fig. 5.26 show $SMSE^+$ interference suppression performance over AWGN, Rayleigh flat fading, and Rayleigh frequency selective fading channels, respectively, using BPSK, QPSK, and 8-PSK data modulations with fixed

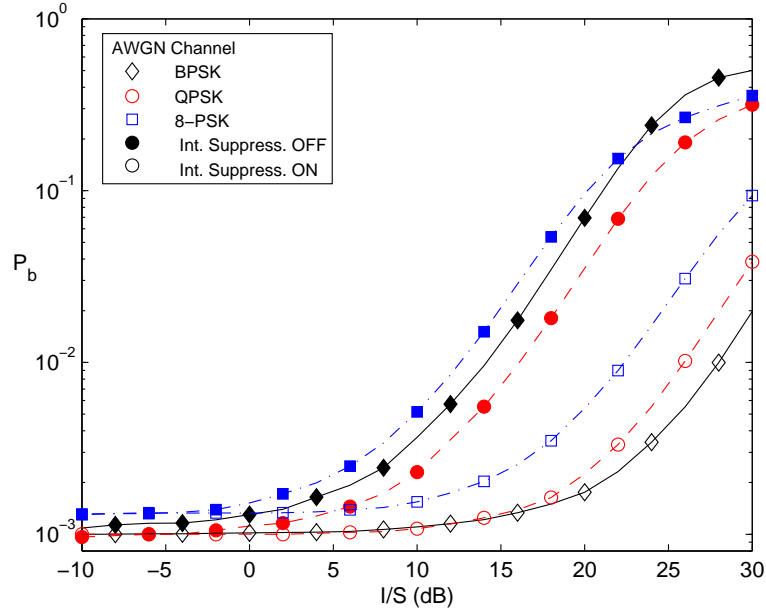


Figure 5.21: SMSE⁺: P_b vs. I/S for AWGN channel with *Interference Present* and suppression ON or OFF as indicated.

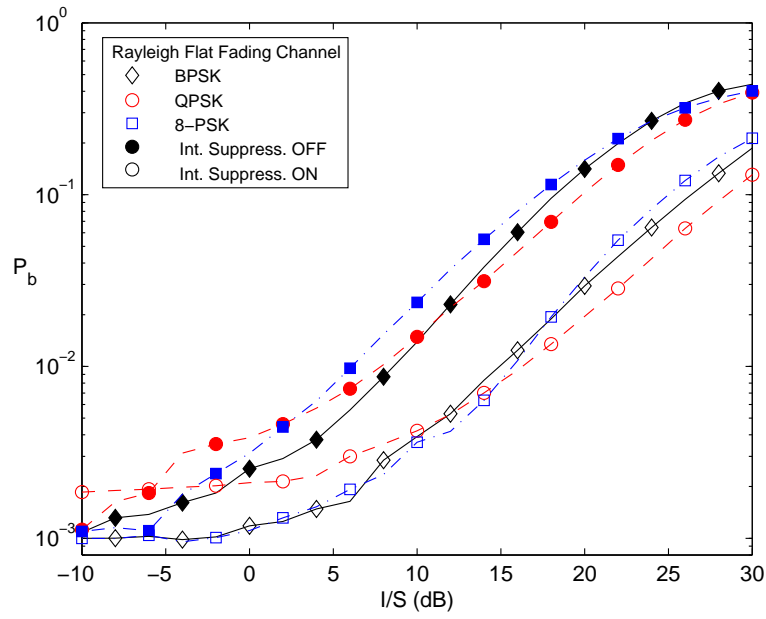


Figure 5.22: SMSE⁺: P_b vs. I/S for Rayleigh flat fading channel with *Interference Present* and suppression ON or OFF as indicated.

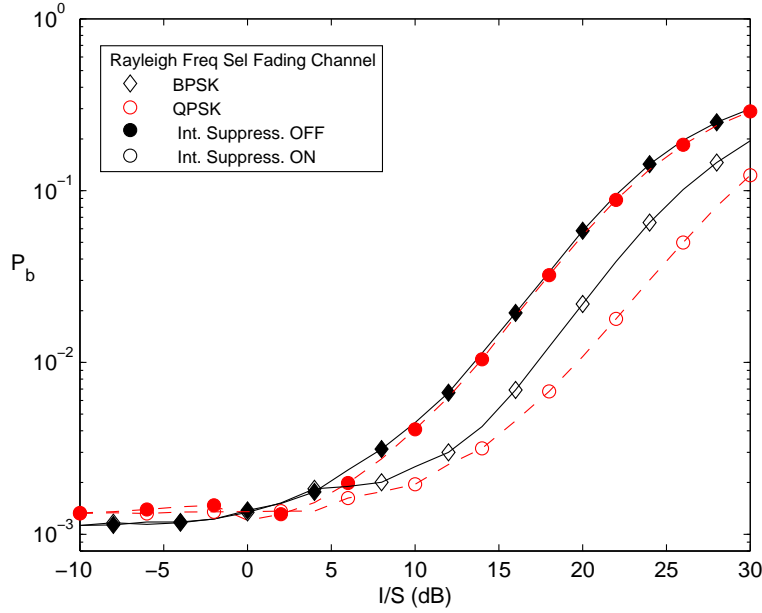


Figure 5.23: SMSE⁺: P_b vs. I/S for Rayleigh frequency selective fading channel with *Interference Present* and suppression ON or OFF as indicated.

$I/S = 15$ dB. The average P_b improvement when using interference suppression for all modulations is $2.5\times$ for $E_b/N_o \in [0, 8]_{dB}$, $3.2\times$ for $E_b/N_o \in [0, 30]_{dB}$, and $2.3\times$ for $E_b/N_o \in [0, 18]_{dB}$ for AWGN, Rayleigh flat fading, and Rayleigh frequency selective fading channels, respectively. The impact of fading upon the P_b performance is obvious from the figures, i.e., mobile, wireless communication suffers fading effects even if PBI is significantly reduced.

5.5 Multiple Access Demonstration

In this section, MC-CDMA performance is characterized under synchronous multiple access (MA) network conditions. The negative impact of having multiple users present is illustrated in two ways: 1) by varying the number of users for a fixed E_b/N_o (all signals received with equal power) and 2) by varying E_b/N_o for a fixed number of users. The results demonstrate expected communication performance in the presence of MA interference (MAI) and illustrate model applicability for syn-

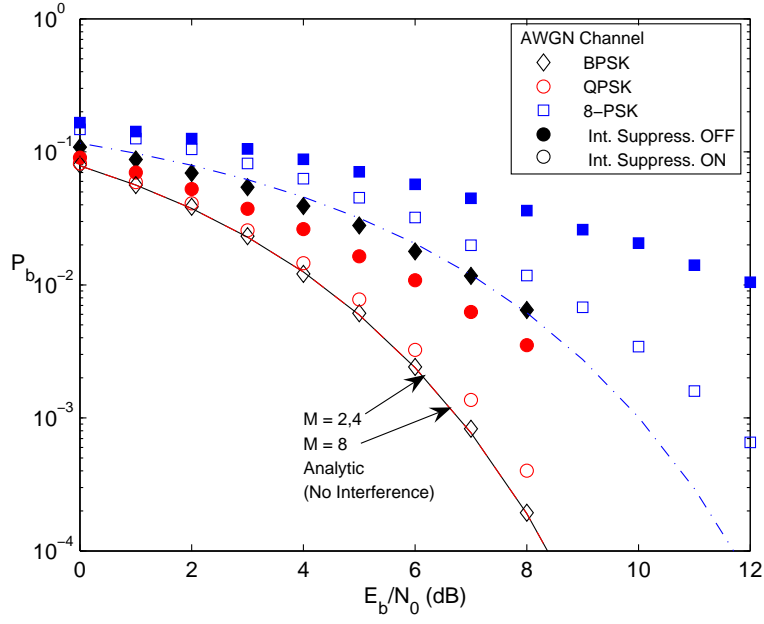


Figure 5.24: SMSE⁺: P_b vs. E_b/N_o for AWGN channel with *Interference Present* ($I/S = 15$ dB) and suppression ON or OFF as indicated.

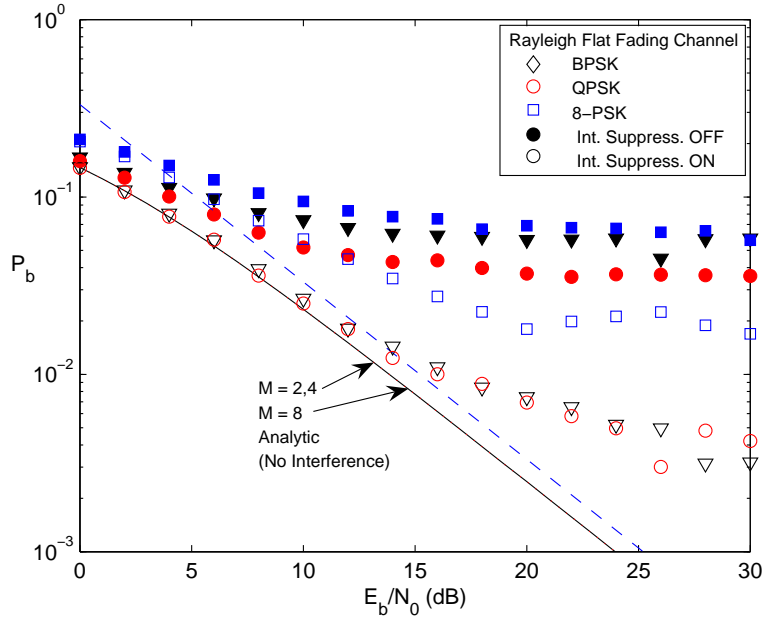


Figure 5.25: SMSE⁺: P_b vs. E_b/N_o for Rayleigh flat fading channel with *Interference Present* ($I/S = 15$ dB) and suppression ON or OFF as indicated.

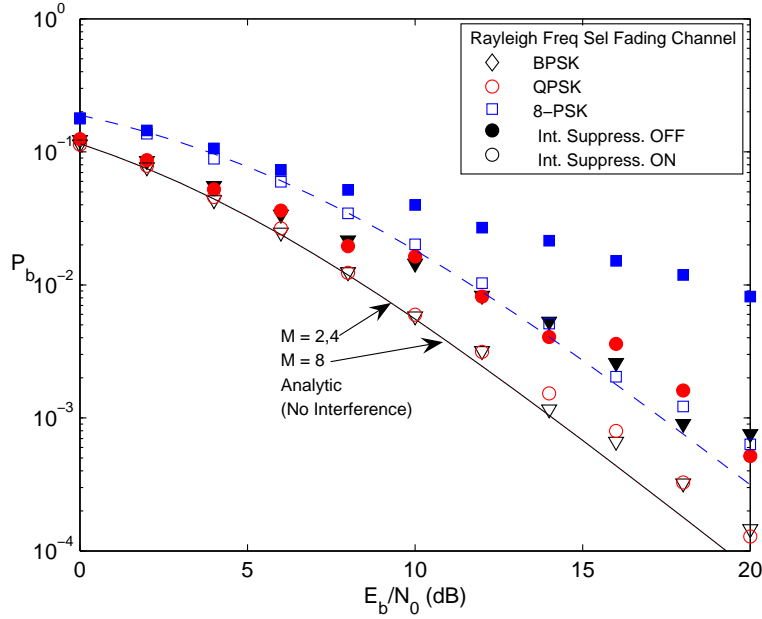


Figure 5.26: SMSE⁺: P_b vs. E_b/N_o for Rayleigh frequency selective fading channel with *Interference Present* ($I/S = 15$ dB) and suppression ON or OFF as indicated.

chronous MA networks using BPSK data modulation. Both AWGN and Rayleigh flat fading channels are addressed.

Proper instantiation of the code waveform design variable \mathbf{c} is crucial in MA scenarios, given the cross-correlation between different user codes directly impacts the amount of P_b degradation. Two binary codes are considered for demonstration purposes: random (non-orthogonal) and Walsh (orthogonal). Under synchronous MA network conditions, the code periods of the received signals are assumed to arrive coincident. The demonstrations in this section assume there are only $N_F = 32$ system frequency components available (all other scenarios assumed $N_F = 256$) and thus, code lengths of 32 are used.

In general, the P_b for a synchronous MA network using random codes to communicate over an AWGN channel is given by [63, 69]

$$P_b = Q\left(\sqrt{\frac{2E_b}{N_o + \xi N_{MAI}}}\right) \quad (5.24)$$

where ξ is a scaling factor and N_{MAI} is interfering power resulting from MA implementation. The interfering MA power is given by

$$N_{MAI} = E_b (N_U - 1) \left(\frac{1}{N_c} \right) \quad (5.25)$$

where N_c is the code length ($N_c = N_F$ here), $E[C_{k,l}^2] = 1/N_c$, and k, l are the indices for distinct codes from a given code set. Note that the code cross-correlation variance of $E[C_{k,l}^2] = 1/N_c$ is satisfied for zero-mean codes, to include the random and Walsh codes considered here.

By design, Walsh codes are orthogonal such that $E[C_{k,l}^2] = 0$, i.e., the cross-correlation between any two codes in the code set ($k \neq l$) is zero. Walsh coding is sometimes referred to as Walsh “covering” and is based on Hadamard transform matrices. Thus, it is also referred to as Walsh-Hadamard coding. Hadamard transform matrices exist for orders that are multiples of four [201]. Higher-order transform matrices are formed using the core Hadamard matrix of

$$\mathbf{H}_1 = \frac{1}{\sqrt{2}} \begin{pmatrix} 1 & 1 \\ 1 & -1 \end{pmatrix} \quad (5.26)$$

by using a Kronecker product extension [92]

$$\begin{aligned} \mathbf{H}_n &= \mathbf{H}_{n-1} \otimes \mathbf{H}_1 \\ &= \mathbf{H}_1 \otimes \mathbf{H}_{n-1} \\ &= \frac{1}{\sqrt{2}} \begin{pmatrix} \mathbf{H}_{n-1} & \mathbf{H}_{n-1} \\ \mathbf{H}_{n-1} & -\mathbf{H}_{n-1} \end{pmatrix} \end{aligned} \quad (5.27)$$

where n is the matrix order. Walsh codes (or functions) only take on values of ± 1 based on the Hadamard transform matrix and represent the basis vectors of the Hadamard transform [92]. Because the Hadamard transform matrix is real, symmet-

ric, and orthogonal (i.e., $\mathbf{H} = \mathbf{H}^* = \mathbf{H}^T = \mathbf{H}^{-1}$), either the rows *or* columns may be used as codes for MC-CDMA signaling in a MA scenario.

Results in Fig. 5.27 illustrate model adaptivity (based on BPSK data modulation and transmission over an AWGN channel) given they match the theory for $\xi = 2$ and are consistent with results in [63]. Simulation results are presented for randomly coded (filled symbols) and Walsh coded (unfilled symbols) networks operating at $P_b = 10^{-2}$ (circles) and $P_b = 10^{-3}$ (squares). Theoretical predictions for random coding are indicated by the dashed lines.

The randomly coded P_b results rise sharply as the first additional user is introduced into the MA system, indicating that random coding may only be practical for low-traffic networks. Notice that random coding performance for a desired $P_b = 10^{-3}$ degrades by an order-of-magnitude after only four users are in the system. However, the Walsh coded P_b performance only degrades slightly as N_U increases. This slight degradation in performance may seem contrary to intuition given the inherent orthogonality of Walsh codes discussed earlier. However, recall that the first (dc) component of frequency assignment vector \mathbf{a} is always nulled in the SMSE signal generation process. Thus, one element in every Walsh code is effectively set to zero (versus ± 1) which destroys orthogonality and induces a small amount of correlation between the codes (the amount of which decreases with increasing code length). While the Walsh coded P_b performance does not remain constant at 10^{-2} or 10^{-3} , it is markedly better than the corresponding randomly coded P_b performance.

Results in Fig. 5.28 demonstrate MA performance in a Rayleigh flat fading channel. The theoretical curve for AWGN is included for comparison. As expected, the multipath channel further degrades the signal. In fact, after five users enter the network, the performance curves for $P_b = 10^{-2}$ and $P_b = 10^{-3}$ are statistically equivalent for random coding, indicating that increasing power may not be enough to overcome cumulative multipath and MA interference effects when using random codes. For Walsh coding, additional degradation in Fig. 5.28 (relative to Fig. 5.27) due to

multipath effects is on the order of $1.3\times$ and $4.3\times$ for the $P_b = 10^{-2}$ (circles) and $P_b = 10^{-3}$ (boxes) data sets, respectively. These results confirm that “the orthogonality of Walsh codes breaks down in the presence of multipath” [161].

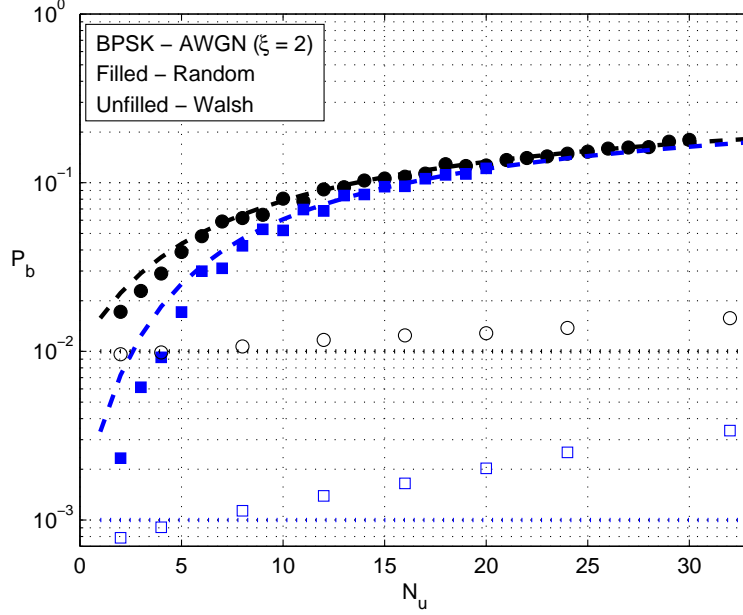


Figure 5.27: MC-CDMA: P_b vs. N_U for AWGN channel in a synchronous network with *MAI Interference*. E_b/N_o is fixed to achieve $P_b = 10^{-2}$ (circles) and $P_b = 10^{-3}$ (boxes). Theoretical P_b values for random coding are indicated by the dashed lines.

Results in Fig. 5.29 and Fig. 5.30 show MC-CDMA performance using BPSK data modulation over AWGN and Rayleigh flat fading channels, respectively. These results are for a fixed network size using random and Walsh coding with $N_U = 4$ or 16 users present. Again, the impact of fading on P_b performance is clearly evident in the figures, i.e., mobile, wireless communication suffers fading effects even if MAI is significantly reduced. The impact of MAI is readily apparent in both figures. For random coding, increasing the network load from $N_U = 4$ to $N_U = 16$ users increases P_b by a factor of $4.6\times$ for $E_b/N_o \in [0, 8]_{dB}$ and $2.8\times$ for $E_b/N_o \in [0, 20]_{dB}$ in AWGN and Rayleigh flat fading channels, respectively. For Walsh coding, increasing the network load from $N_U = 4$ to $N_U = 16$ users increases P_b by a factor of $1 - 2\times$. Once

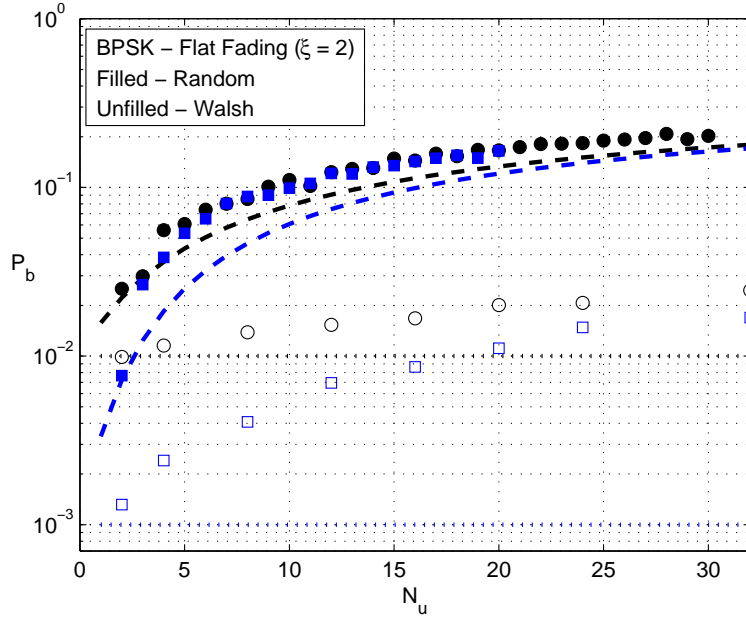


Figure 5.28: MC-CDMA: P_b vs. N_U for Rayleigh flat fading channel in a synchronous network with *MAI Interference* E_b/N_o is fixed to achieve $P_b = 10^{-2}$ (circles) and $P_b = 10^{-3}$ (boxes). Theoretical P_b values for random coding are indicated by the dashed lines.

again, this increase is mainly attributable to a loss of orthogonality versus increased traffic loading.

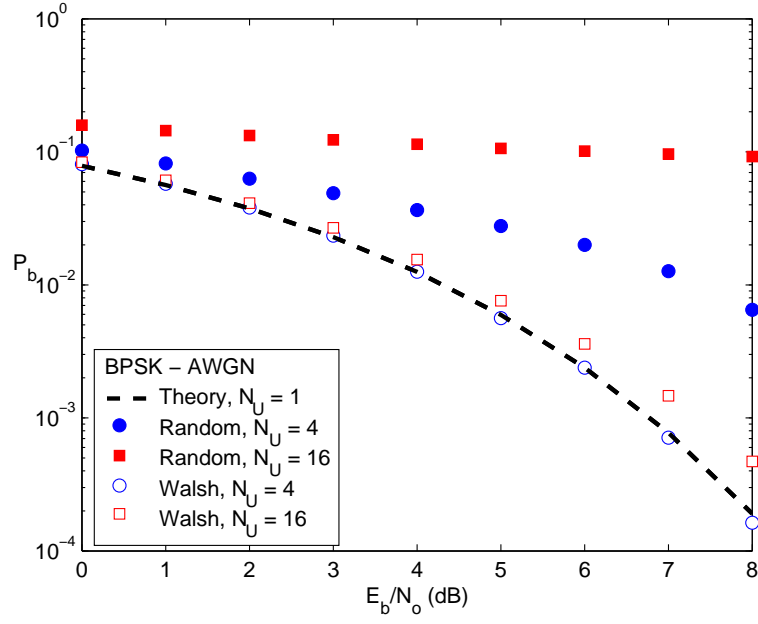


Figure 5.29: MC-CDMA: P_b vs. E_b/N_o for AWGN channel in a synchronous network with $N_U = 4, 16$.

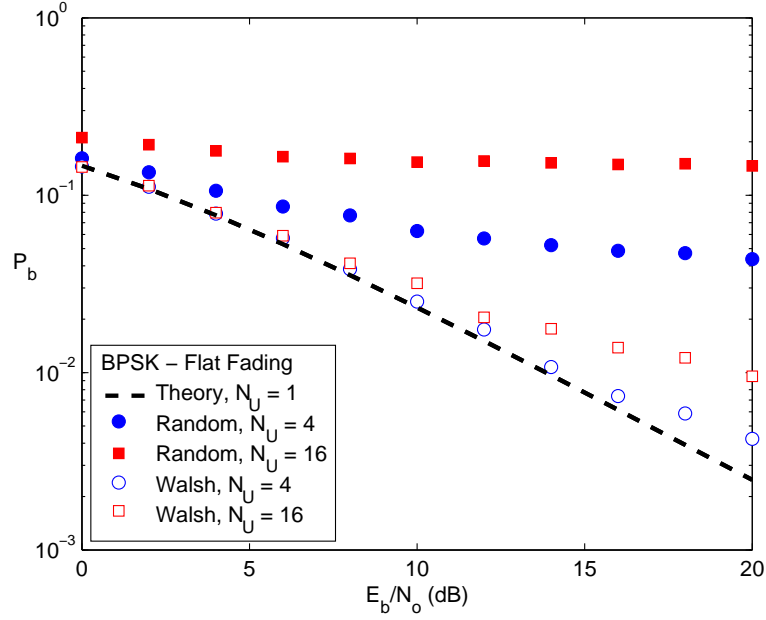


Figure 5.30: MC-CDMA: P_b vs. E_b/N_o for Rayleigh flat fading channel in a synchronous network with $N_U = 4, 16$.

VI. Conclusion

Both information-centric military forces and data-driven commercial communicators demand higher data rates, better quality, improved mobility, and unified access capabilities. Fourth generation (4G) communication systems, to include the potential for software defined radio (SDR) architectures driven by cognitive radio (CR) principles, may arrive within the coming decade. It is envisioned that near real-time, ubiquitous communication will flow between unified CR-based SDR platforms that vigilantly monitor their surroundings while adaptively transmitting-receiving to permit efficient information exchange between many types of networks and devices.

A CR-based SDR architecture represents one likely implementation vehicle for 4G communications (and beyond) because of its inherent adaptivity and proclivity for representing and implementing spectrally efficient waveforms. Industry experts forecast orthogonal frequency division multiplexing (OFDM) as a bedrock for 4G communications and CR-based SDR [82, 118, 126, 217]. OFDM-based signals possess many desirable properties, and many OFDM-based techniques have been proposed. Current SDR developments are focusing almost exclusively on software (e.g., architecture) and hardware (e.g., reconfigurable radio components) improvements. These SDR developments currently lack an analytic framework that fuses them together to permit subsequent implementation. As developed and presented herein, the spectrally modulated, spectrally encoded (SMSE) framework is an OFDM-based alternative that provides this capability.

6.1 *Research Contributions*

Paralleling a recently developed framework for temporally designed impulse signals [240], the SMSE framework presented herein provides a mathematical structure for representing and implementing OFDM-based signaling techniques, which are being envisioned for future CR-based SDR architectures. Combining emerging OFDM-based waveforms with future CR-based SDR architectures, the SMSE framework represents a synergistic union between theory and practical implementation. The primary

research contribution is a unifying, general analytic framework for representing (via analysis, characterization, and implementation) spectrally designed signals. In this framework, the myriad of OFDM-based signals which are being considered for 4G implementation are easily designed and implemented within a CR-based SDR architecture. The flexibility to implement many specific waveforms is enabled through the instantiation of six key waveform design variables.

The “alphabet soup” of wireless communication acronyms for current systems (GSM, EDGE, WCDMA, HSDPA, CDMA2000, EV-DO, EV-DV, TD-SCDMA, DECT, WLAN, WiMAX, etc.) and current signaling techniques (OFDM, COFDM, CI-OFDM, TDMA, OFDM-TDMA, CDMA, MC-CDMA, TDCS, etc.) is presented in Chapter II from a cellular generation evolutionary standpoint. By following the evolution of these systems and technologies from a coding, modulation, and multiple access viewpoint, it becomes readily apparent that many signaling techniques and related research thrusts are driving the state of current communications. Amidst the ever expanding “cloud” of acronyms, the evolutionary trail exposed a clear need for analytic commonality and operational unification of SMSE signals. The technical community substantiated this need and acknowledged its importance by publishing a survey based on details provided in Chapter II [174].

The unifying SMSE framework supports CR-based, brain-empowered instantiation of six key waveform design variables and will allow SDR systems to generate desired OFDM-based waveforms. The structure of the SMSE framework is presented in Chapter III and is compactly represented as $\mathbf{S}_{SMSE} = \mathbf{A} \odot \mathbf{\Theta} \odot \mathbf{F}$ (Hadamard products of complex magnitude, phase, and frequency factors). Discrete time and frequency domain expressions are developed for representing SMSE signals throughout various stages of the transmit-propagate-receive communication process. As developed, the general analytic framework has received recognition as being directly applicable to systems requiring waveform diversity [176].

Analytic flexibility of the SMSE framework was verified by applying the structure to several OFDM-based SMSE signals, the results of which are presented in Chapter IV. This process involved generation of variable instantiation tables which can then be used in an SDR architecture to adaptively generate desired waveforms. For all signals considered, the resultant signal expressions from applying the SMSE framework analytically agree with those in published literature as confirmed in [176, 177].

The practical utility of the SMSE framework is demonstrated via modeling and simulation, the results of which are presented in Chapter V. These results reinforce framework utility by showing that expected communication performance is achieved, i.e., the performance of signals constructed using the unifying SMSE framework correlate well with theoretical expressions. Inter-operability and coexistence is maintained through simulations that address signal perturbations from various sources, including multipath fading, partial band interference [175], and multiple access interference.

Related research contributions also include:

- Providing a better understanding of the parallel UWB framework. This was accomplished by conducting some UWB modeling and simulation work. The UWB results presented in Appendix A are original and address the performance of TH-BPPM data modulation in realistic UWB fading channels under various network loading conditions [178]. Coexistence scenarios examine the impact of a) UWB signal power on a geographically collocated WLAN receiver, and b) WLAN signal power on an UWB receiver's bit error performance. These scenarios enable better understanding of the UWB signaling and framework, as well as, establish a methodology for modeling multipath fading environments.
- Implementing and characterizing spectral demodulation in a Transform Domain Communication System (TDCS) receiver. A conventional TDCS transmitter uses spectral coding (phase modulation) followed by time domain data modulation. Thus, the conventional TDCS receiver performs time domain data demodulation. Recent work [154] shows that TDCS-like processing can be ac-

complished using spectral domain data modulation (e.g., phase shift keying) with time domain data demodulation retained in the receiver. Results presented in Chapter V (for the SMSE⁺ signal) extend this previous work by showing that spectral data demodulation can be accomplished in a TDCS-like receiver while achieving maximum likelihood detection and estimation performance.

6.2 *Future Research*

Given that an effective SMSE framework has been established for analyzing, characterizing, and implementing OFDM-based signals, and the framework has been well-received by the technical community, there are numerous additional research topics that could be investigated.

First, it seems reasonable that an all-encompassing 4G communication framework could be developed to unify the existing temporal (UWB) [240] and spectral (SMSE) [176] frameworks. As developed herein, the SMSE analytic framework parallels the analytic UWB framework of [240] and the inherent linear processing within each framework suggests that a merger may be possible. An all-encompassing framework could be very beneficial for addressing the analysis, characterization, and implementation of *joint* temporally-spectrally designed signals. However, given UWB and SMSE waveforms are fundamentally different, impulse-based versus OFDM-based, the task of developing an overall unified framework may in fact lead to the conclusion that unification is not possible, or that the resultant framework may be impractical from an SDR implementation perspective. Ideally, the resultant unifying framework would encompass both types of signals, each of which are prime candidates for 4G communications in different scenarios.

Second, the proposed framework could be used as the basis for extending CR-based SDR research into higher layers of the network open systems interconnection (OSI) model. In its current state, the SMSE framework addresses physical layer functionality which is driven by brain-empowered mechanisms. In the context of networks, brain control mechanisms such as the medium access control (MAC) reside

in higher OSI layers. Thus, it would be useful to examine and/or define the role that each of the OSI mechanisms could play in waveform parameter selection. This research would help quantify the role that the SMSE radio “brain” plays in cognitively converting incoming information (channel conditions, traffic loads, spectral crowding) to waveform parameter selection.

Third, assuming the steady pace in OFDM research and development is maintained, and OFDM-based SMSE waveforms emerge in fielded 4G communication systems, the issue of coexistence (joint temporal and spectral) with prior generation communication systems must be addressed. Unlike previous generational transitions, coexistence issues will become extremely important with the introduction of various OFDM-based 4G communication signals. The impact of widely varying amplitude and phase characteristics, both of which are inherently random on a symbol-by-symbol or frame-by-frame basis in OFDM-based signaling, must be assessed for legacy systems that will remain in operation. Furthermore, coexistence with other avionics systems (e.g., navigation, geolocation, radar, etc.) is a concern as well. The flexibility and analytic tractability of the proposed SMSE framework make it well-suited for performing these coexistence assessments.

Finally, the research assumptions stated in Chapter I could be removed and/or relaxed and the research process repeated. In some cases, this would represent a somewhat trivial exercise and produce results that might be expected. For example, the demonstration results in Chapter V could easily be expanded by considering additional OFDM-based waveforms. In other cases, relaxing the research assumptions would prove to be far more challenging and could produce results which are far more significant, a few examples of which involve the following:

- Introduce transmitter-receiver platform variation. This effort could include platform dynamic variation to address induced Doppler or platform geographic variation (separation) to address processing amidst dissimilar electromagnetic envi-

ronments. In either of these cases, the impact of dissimilar interference estimates at the transmitter and receiver would be addressed.

- Consider additional multipath faded channels. This effort could include a more complete look at Rake receiver processing in other than AWGN channels. Potential candidates for additional consideration include: frequency selective channels, non-Rayleigh faded channels, indoor propagation channels, etc.
- Conduct detailed interference suppression characterization. This effort could include a more complete characterization of SMSE performance with various interference types, including: wideband versus narrowband, swept frequency versus steady-tone, stepped-frequency, phase coded, etc.
- Conduct a detailed synchronization assessment. This effort could include a more complete characterization of SMSE performance with synchronization uncertainty. Performance assessment for common levels of synchronization (carrier, phase, symbol, frame, etc.) and errors thereof could be addressed. Also, the impact of adaptively changing CR-based SDR waveform characteristics on establishing and maintaining synchronization could be addressed.
- Consider alternate linear transforms. As driven by the OFDM signals being considered for 4G implementation, the SMSE framework is based on an inverse fast Fourier transform (IFFT) to transform between the design (spectral) and transmission (temporal) domains, with the fast Fourier transform (FFT) subsequently used to transform between the reception (temporal) and estimation (spectral) domains. Given that the SMSE framework is linear, the worked could be extended by replacing the IFFT-FFT processing with other linear transforms, e.g., the wavelet transform. Although outside the realm of what is currently being considered for 4G implementation, these alternatives could provide some additional or enhanced capabilities which have not yet been exploited.

Appendix A. Ultra Wideband Signaling Theory, Framework, and Results

The spectrally modulated, spectrally encoded (SMSE) framework proposed in this document is well-suited and specifically derived for spectrally designed signals. SMSE signals are ideal candidates for cognitive radio (CR)-based, software defined radio (SDR) implementation. A different class of signals has also been designed to combat the effects of coexistence and interference while offering higher data rates, albeit from a temporal (vice spectral) perspective. These signals are commonly called ultra wideband (UWB) and were introduced in Section 2.5.3.5.

A unifying analytic framework for UWB signals was recently proposed in [238–240]. Because the SMSE framework proposed herein uses this UWB framework as motivation for development and implementation, it is instructive to consider UWB signaling and the framework in greater detail.

This appendix begins by describing the theory behind UWB signaling in Section A.1, introducing an expression for one fundamental UWB waveform and identifying common modulation and multiple access techniques. Section A.2 describes the analytic UWB framework and provides some expressions from [240] to illustrate the parallel nature of the SMSE and UWB analytic frameworks. Finally, Sections A.3–A.5 provide some results for UWB signaling. These original results, showing performance from bit error rate (BER) and power level analyses, demonstrate some limits of UWB signals in coexistence scenarios. Note that the variables as presented in this Appendix only apply to the expressions in the Appendix and do not necessarily correlate to variables used in the SMSE expressions.

A.1 UWB Theory

A.1.1 Fundamental UWB Waveform. Traditionally, UWB signals are designed by appropriately selecting pulse shape and duration such that the transmitted pulse train consists of short-duration, low-power pulses having correspondingly wide bandwidth. These carrier-free, short-duration pulses are commonly called *monocycle*-

cles. Various derivatives of a Gaussian impulse are commonly used for UWB waveform analysis [24, 25, 160, 183, 199, 207, 218, 242, 249], with some sources indicating that higher-order derivatives are required to fully meet the FCC spectral mask criteria [199, 218]. For developmental purposes, the second derivative of a Gaussian impulse is introduced here as the fundamental UWB waveform and analytically expressed as:

$$w(t) = \left[1 - 4\pi \left(\frac{t}{\tau_m} \right)^2 \right] \exp \left[-2\pi \left(\frac{t}{\tau_m} \right)^2 \right] \quad (\text{A.1})$$

where τ_m is the impulse width parameter. For analyzing waveforms at a given frequency, a pulse width of $T_p = 1.73/f_c$ is appropriate when using the second derivative of a Gaussian impulse and $T_p = 2/f_c$ is more appropriate when using the third derivative [77], where f_c is the center frequency of interest. Fig. A.1 shows the fundamental waveform of (A.1) centered at 0.1 ns. To spectrally center this waveform at $f_c = 5.0$ GHz, near the National Unlicensed Information Infrastructure (N-UII) band, $\tau_m = 0.16 \times 10^{-9} \approx 0.4 \times T_p$ seconds, where $T_p = 0.4 \times 10^{-9}$ seconds [25, 38, 207]. Using the second-order Gaussian waveform in (A.1) effectively accounts for transmit and receive antenna effects on a Gaussian impulse [24, 25, 38, 77].

While the second derivative of a Gaussian impulse is used in analysis and showcases UWB performance, it does not meet the FCC spectral mask criteria [67, 68, 115, 160, 183]. Fig. A.2 highlights the frequency response from different Gaussian mono-cycle derivatives. Higher derivatives produce an upward frequency translation. Using the pulse width provided above, the fourth derivative of a Gaussian appears to more closely meet the FCC spectral mask.

For the modeled second derivative of a Gaussian impulse, the impact of pulse width variation is illustrated in Fig. A.3, where greater pulse widths produce a downward frequency translation and smaller bandwidth. Appropriate selection of a mono-cycle shape (i.e., Gaussian derivative) and pulse width is necessary to meet the FCC spectral mask while simultaneously providing a desired data rate.

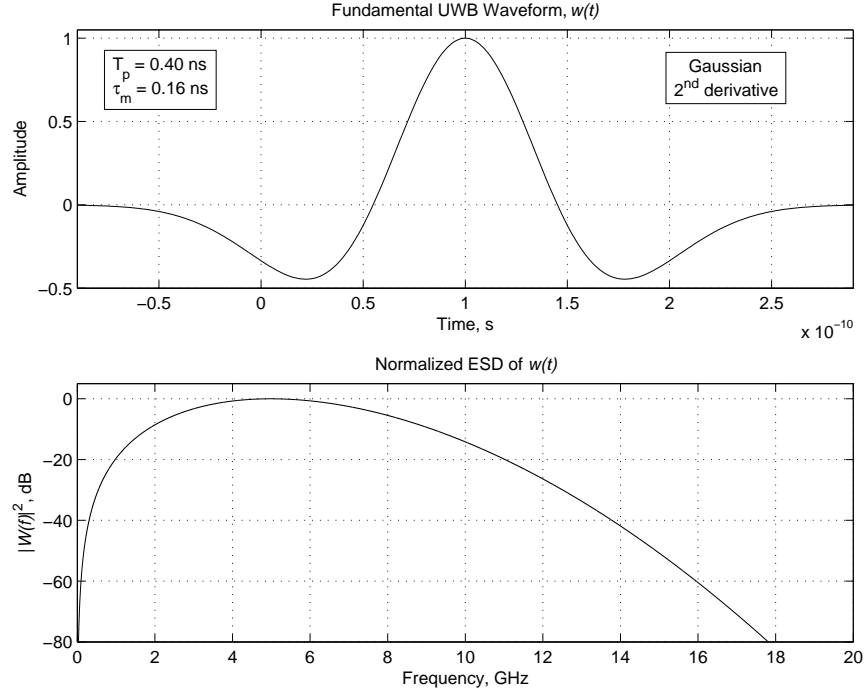


Figure A.1: Fundamental UWB waveform (top) from (A.1) and corresponding normalized energy spectral density (bottom).

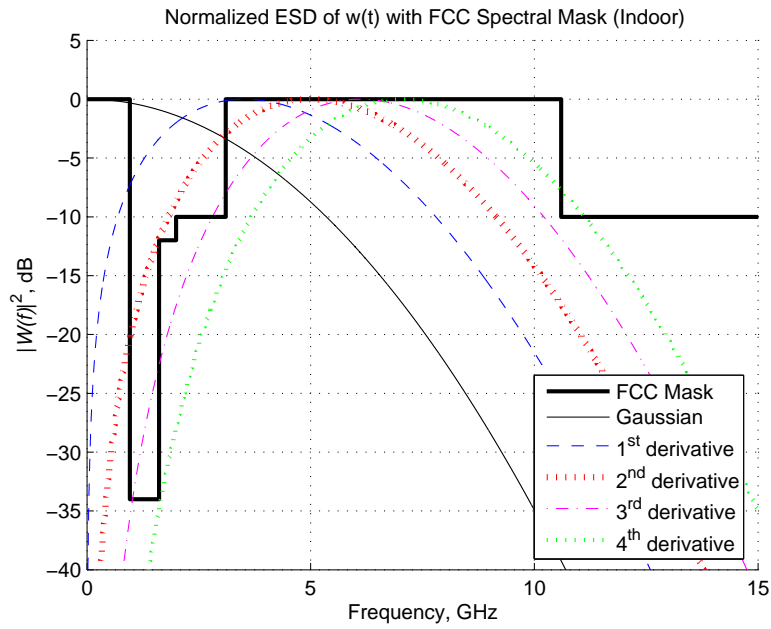


Figure A.2: Normalized energy spectral density of UWB waveform for different Gaussian impulse derivatives as the monocycle. The FCC spectral mask [52] is shown for reference.

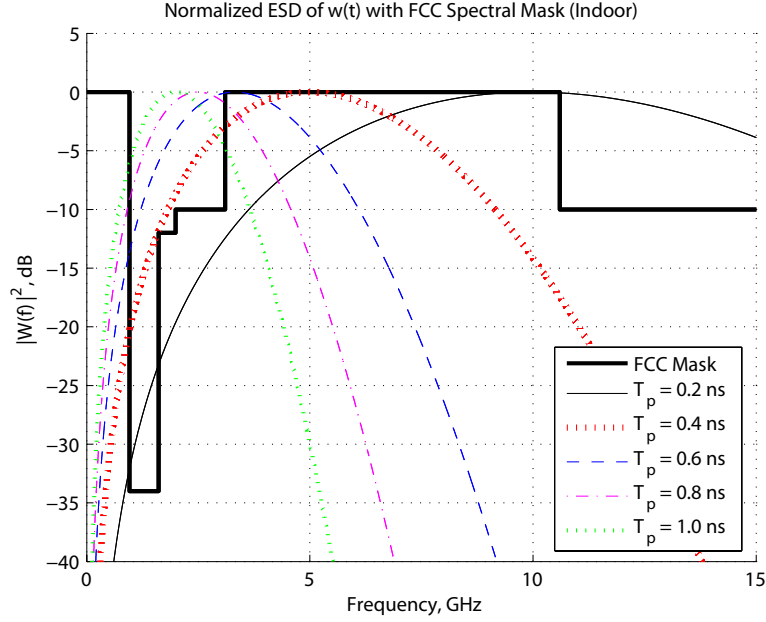


Figure A.3: Normalized energy spectral density of UWB waveform for different pulse widths using a second derivative Gaussian impulse as the monocycle.

A.1.2 UWB Modulation Techniques. Since UWB is a temporal signaling technique, it frequently uses modulations that rely upon pulse position and/or amplitude to transmit data. Perhaps the most common modulation technique is pulse position modulation (PPM) [192]. This technique relies upon pulse position within a specified pulse repetition interval (see Fig. A.4) to convey the data that is being transmitted. Another common modulation technique is pulse amplitude modulation (PAM) [77]. This technique relies upon pulse amplitude to convey the data that is being transmitted. A final technique that is very common is binary phase shift keying (BPSK) [54]. This technique relies upon the phase of the pulse (see Fig. A.6) to convey the data that is being transmitted. In this technique, the 180° phase shifts are manifested by pulse inversions.

A.1.3 UWB Multiple Access Techniques. Three UWB multiple access (MA) techniques are introduced. Time hopping PPM (TH-PPM) and direct sequence UWB (DS-UWB) have been developed within the past decade. More recently, biorthogonal PPM (BPPM) has been combined with TH (TH-BPPM) to offer M -ary signal-

ing advantages and provide equivalent MA performance as binary TH-PPM techniques [23, 38, 246].

A.1.3.1 Time Hopping PPM (TH-PPM). TH-UWB signals typically use PPM for data modulation. In PPM, the pulse position relative to the pulse repetition interval (PRI) contains the information being conveyed. The PPM data modulated waveform is subsequently time position coded in accordance with a pseudo-random sequence to allow for MA and spectral coexistence. PPM is perhaps the most common data modulation technique used with UWB signaling, and in many papers, TH-PPM is used synonymous with TH-UWB [25, 77, 139, 203]. Much of the recent TH-PPM research builds upon the foundational work by Scholtz presented in [192]. Subsequent works present performance analyses of TH-PPM using both analog and digital receiver processing, and both binary [233, 234] and M-ary [170] modulations. A more detailed examination of code selection is found in [24, 56].

Using the fundamental UWB waveform of (A.1), the TH-PPM signal for the v^{th} user can be analytically expressed as [24, 25, 38, 170, 192, 233, 234]:

$$s_{TH}^{(v)}(t) = \sqrt{P_v} \sum_{j=1}^{\infty} \sum_{n=(j-1) \cdot N_{ss}}^{j \cdot N_{ss}-1} w\left(t - nT_o - c_n^{(v)}T_c - (-1)^{d_j^{(v)}}\Delta\right) \quad (\text{A.2})$$

where P_v is the average signal power, T_o is the PRI or frame duration, T_c is the spreading code chip duration, N_{ss} is the number of communication symbol repetitions (dictates processing gain), $c_n^{(v)}$ is the n^{th} element of the chip offset sequence, $d_j^{(v)}$ is the j^{th} element of the data modulation sequence, and Δ is the relative PPM offset. The chip offset sequence is denoted by $[c_0, c_1, \dots, c_{N_c-1}]$ and is periodic with length N_c , i.e., $c_n = c_{n+mT_c} \forall m, n$, and $c_n \in \{0, 1, \dots, (N_s - 1)\}$ where N_s is the number of chip intervals within T_o . In general, $N_s \cdot T_c \leq T_o$, i.e., there are at least N_s chip intervals available per symbol repetition interval T_o . A representative TH-PPM waveform is shown in Fig. A.4 for $N_s = 5$ chip intervals per T_o and a symbol replication factor of $N_{ss} = 3$.

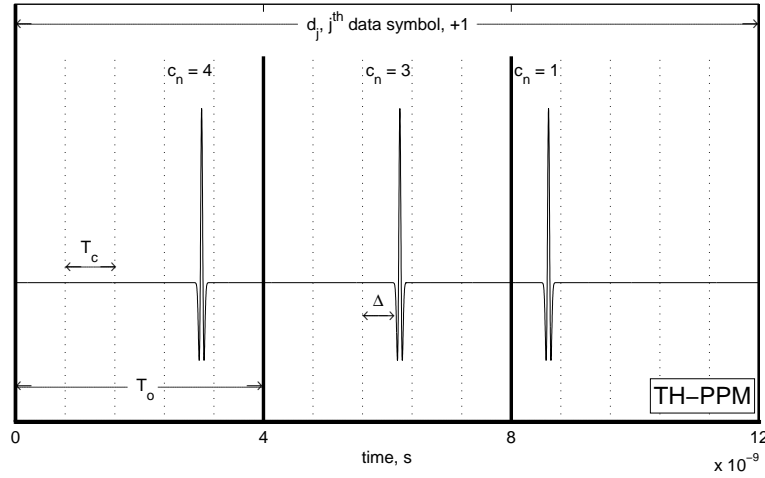


Figure A.4: TH-PPM waveform illustration, $N_s = 5$ and $N_{ss} = 3$.

In TH-PPM, each communication symbol is repeated N_{ss} times over a duration of $N_{ss} \cdot T_o$ seconds at specific times dictated by c_n , i.e., replicas of each communication symbol are transmitted within specific chip intervals in distinct T_o intervals. The chip offset sequence $\{c_n\}$ can be generated from a pseudorandom sequence in a fashion similar to CDMA [183]. The j^{th} data symbol impacts the pulse position within chip interval T_c , and the n^{th} element of the chip offset sequence impacts the pulse position within T_o . The corresponding processing gain, or pulse integration gain, equals N_{ss} which is the number of times each symbol is repeated per transmission. In general, there is no requirement for N_{ss} to equal the chip sequence length N_c or the number of available chip intervals N_s .

A.1.3.2 Biorthogonal TH-PPM. Biorthogonal UWB signaling is achieved by combining binary PPM with BPSK to produce biorthogonal PPM (BPPM). The resultant communication symbols using the fundamental UWB waveform of (A.1) can be analytically represented by [38]

$$s_m(t) = (-1)^{a_{2m}} \cdot w(t - (-1)^{[a_{2m} \oplus a_{2m-1}]} \cdot \Delta) \quad (\text{A.3})$$

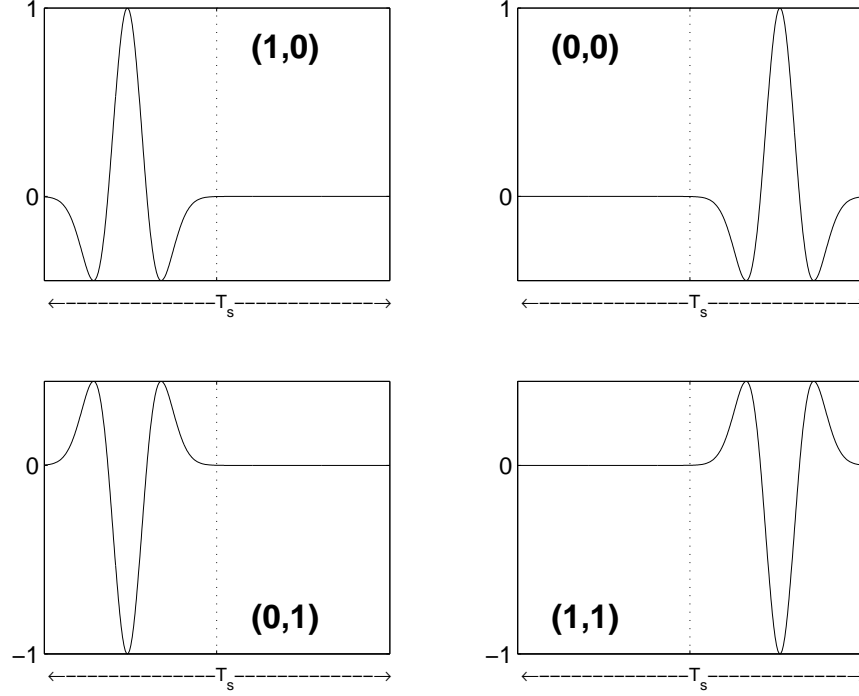


Figure A.5: Illustration of 4-ary biorthogonal UWB waveforms generated from (A.1) and (A.3) using bit patterns of (a_{2m-1}, a_{2m}) as indicated [38].

for $t_m \leq t \leq t_m + T_s$ where m is the symbol number, a_{2m} and a_{2m-1} are binary input data equaling 1 or 0, \oplus represents modulo-2 addition, T_s is the symbol duration, and Δ is the relative PPM offset. For results in Section A.3, a PPM relative offset of $\Delta = T_{sym}/4 = T_p/2 = 0.2$ ns is used. Fig. A.5 graphically illustrates the four possible communication symbols when using TH-BPPM with (A.1) and (A.3).

For the TH-BPPM technique, the signal information contained in both relative pulse position and amplitude characteristics is preserved upon implementing MA capability. This information can be reliably recovered using temporal “spreading”, i.e., repeating communication symbols across time. The 4-ary biorthogonal modulated signals described by (A.3) are used in conjunction with preassigned, uniquely coded time hopping sequences to implement MA capability. The analytic representation for the biorthogonal TH-BPPM MA technique follows directly from the orthogonal TH-PPM MA technique commonly used in research [24, 192], with the v^{th} user’s signal

given by

$$s_{TH-BPPM}^{(v)}(t) = \sqrt{P_v} \times \sum_{j=1}^{\infty} \sum_{n=(j-1) \cdot N_{ss}}^{j \cdot N_{ss}-1} s_m(t - nT_o - c_n^{(v)}T_c) \quad (\text{A.4})$$

where the variables are the same as those shown in (A.2).

A.1.3.3 Direct Sequence UWB (DS-UWB). DS-UWB signals rely on phase rather than pulse position to convey data, with BPSK typically preferred for UWB systems [54]. The data modulated waveform is subsequently phase coded by the DS-UWB system (rather than time coded as done in TH-PPM). Similar to conventional DS-SS, a pseudorandom code is applied to the data modulated waveform to “spread” the signal. However, unlike conventional DS-SS, the DS-UWB signal is spread across time versus frequency. Most recent DS-UWB research builds upon the foundational work of Foerster [54] which was based on concepts originally introduced by McCorkle [137]. Other foundational DS-UWB work is attributed to researchers associated with various organizations, including Intel Labs [54,183,207], Time Domain Corp. [203], and XtremeSpectrum, Inc. [184,229].

The DS-UWB signal was one of two candidates recently considered for the IEEE P802.15 physical layer standard (monitored by Task Group 3a) [102]. (The IEEE adopted standard 802.15.3 for the UWB medium access control (MAC) layer standard and was seeking to develop a standard for the UWB physical (PHY) layer [224].) The other candidate being considered was multi-band orthogonal frequency division multiplexing (MB-OFDM). MB-OFDM takes an OFDM scheme and multiplexes it with other bands. Another proposal, common signaling mode (CSM), would allow MB-OFDM and DS-UWB systems to coexist [223]. Within the past year, Task Group 3a was unable to resolve the deadlock between the DS-UWB and MB-OFDM camps and voted to disband in January 2006 [75]. The WiMedia Forum and the UWB Forum will continue to develop and promote MB-OFDM and DS-UWB, respectively, in a marketplace duel reminiscent of the VHS-Beta war in the 1980s. These recent developments motivated continued research in DS-UWB. Recent DS-UWB research has

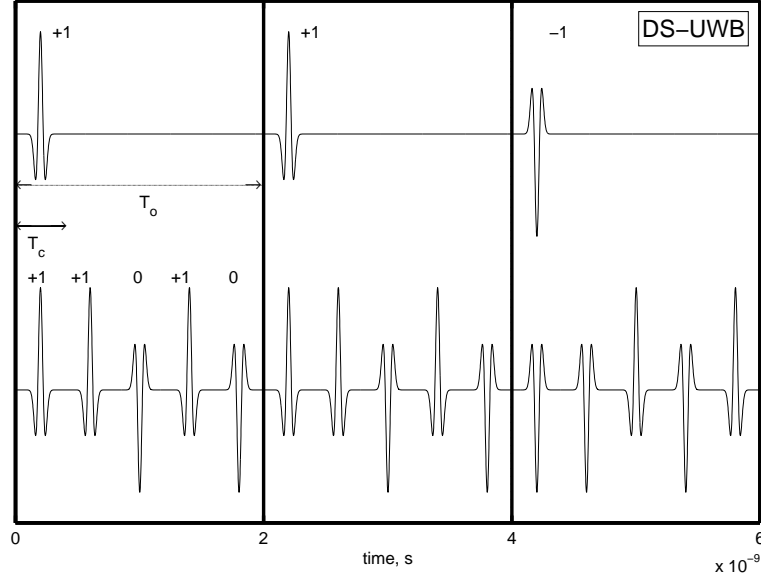


Figure A.6: DS-UWB waveform illustration for $N_{ss} = 5$.

focused on performance with imperfect power control [20], collateral interference and spectral coexistence with existing systems [77], new receiver architectures [90, 169], code assignment and selection [24, 97], and comparisons with other UWB technologies [184, 202].

Using the fundamental UWB waveform of (A.1), a DS-UWB signal for the v^{th} user signal can be analytically expressed as [20, 24, 25, 54]:

$$s_{DS}^{(v)}(t) = \sqrt{P_v} \sum_{j=1}^{\infty} \sum_{n=(j-1) \cdot N_{ss}}^{j \cdot N_{ss}-1} (-1)^{d_j^{(v)}} (-1)^{c_n^{(v)}} w(t - jT_o - nT_c) \quad (\text{A.5})$$

where $c_n \in \{0, 1\}$. A representative DS-UWB waveform is shown in Fig. A.6 for $N_{ss} = N_c = 5$ and $[c_0, c_1, c_2, c_3, c_4] = [1, 1, 0, 1, 0]$.

In DS-UWB, each communication symbol is repeated N_{ss} times per T_o with phase (sign) dictated by $c_n^{(v)}$. Hence, communication symbols within a PRI are data phase modulated (amplitude modulated with ± 1 when using BPSK) and then phase coded based upon the unique spreading code $c_n^{(v)}$ in a similar fashion to CDMA [183].

The j^{th} data symbol and the n^{th} element of the chip phase sequence directly impact the pulse phase within each T_c chip interval. The processing gain of DS-UWB (N_{ss}) is dictated by spreading a given symbol over multiple chip intervals and is given by $N_{ss} = T_o/T_c$. In general, there is no requirement for N_{ss} to equal the spreading code length N_c .

Some research suggests that DS-UWB signaling may be more desirable than MB-OFDM signaling [184]. The primary factors for fully benefiting from UWB signaling, according to military research [172], are two-fold. First, utilizing relatively large bandwidth signals is important. Second, coherent signal processing over the full bandwidth is also important. DS-UWB is the only current technique that does both to fully exploit UWB benefits [184]. Additional work also suggests that DS-UWB signaling has some advantages over TH-PPM in spectrally crowded regions [24, 202] and in the presence of multipath [24]. Other research [183, 207] suggests that with a matched filter receiver, DS-UWB is more suited for higher data rates than TH-PPM (since it can handle more users), but TH-PPM may be preferable for lower data rates (due to the adverse near-far effect inherent in DS-UWB systems). Work in [139] indicates that DS-UWB outperforms TH-PPM for high-speed indoor links which appears consistent with work in [20] that suggests DS-UWB provides higher data rates than TH-PPM systems for a given pulse width and code length.

A.2 UWB Unified Framework

In 2003, [238] presented a novel approach to UWB signaling: unifying transmission and Rake reception models for analysis and implementation. By defining key variables, the authors demonstrated that multiple UWB waveforms could be generated from a single unifying expression [238–240]. The authors’ goals were to quantify interference and compare UWB systems in terms of their coexistence with neighboring narrowband signals [239].

The UWB framework of [238] provided the impetus for developing a similar framework in this research for SMSE signals (which may encompass a portion of the

signal set of which UWB signals must coexist with). Thus, it is instructive and illuminating to examine fundamental elements of the unifying UWB framework. As identified throughout this document, the primary contribution of the SMSE framework is to support CR-based SDR systems, not only with a unifying analytic expression, but also with one that is practically implementable. In hindsight, the UWB framework model also lends itself to direct incorporation within the CR-based SDR architecture addressed throughout the research.

The subsections below present the transmitter and Rake receiver models of [240]. Effort has been taken to present the models and expressions using notation consistent with the rest of the Appendix (e.g., v represents the user index). Unless otherwise noted, all material in the following subsections is taken from [240].

A.2.1 Transmitter Model. Binary PAM is used for data modulation with only one pulse transmitted per frame T_o . Thus, the transmitted UWB signal for the v^{th} user is [240]

$$s^{(v)}(t) = \sqrt{\frac{\mathcal{E}_v}{N_{ss}}} \sum_{n=0}^{\infty} d^{(v)}\left(\left\lfloor \frac{n}{N_{ss}} \right\rfloor\right) c^{(v)}(n) p\left(t - nT_o - c_{th}^{(v)}(n)T_c\right) \quad (\text{A.6})$$

where \mathcal{E} is the energy per symbol, N_{ss} is the number of pulses $p(t)$ that represent one communication symbol, n is the pulse repetition interval or “frame,” $d^{(v)}(j) = d^{(v)}(\lfloor n/N_{ss} \rfloor)$ is the j^{th} communication symbol of user v , $c^{(v)}$ is an amplitude-related spreading code, T_o is the frame duration (thus, $T_s = T_o N_{ss}$, where T_{sym} is the symbol duration), $c_{th}^{(v)}$ is a position-related spreading code, T_c is the chip duration (where $T_c > T_p$ and $T_c = T_o/N_c$), T_p is the pulse width, and N_c is the number of chips per frame.

Four distinct UWB signals (TH-UWB, DS-UWB, baseband single-carrier UWB, and baseband multi-carrier UWB) can be generated by proper selection of parameters in (A.6). For example, to generate a TH-UWB signal, the process begins by setting $c^{(v)}(n) = 1$ and $c_{th}^{(v)}(n) \in [0, N_c - 1], \forall n$, and then defining other parameters as desired.

The resulting expression is

$$s^{(v)}(t) = \sqrt{\frac{\mathcal{E}_v}{N_{ss}}} \sum_{n=0}^{\infty} d^{(v)} \left(\left\lfloor \frac{n}{N_{ss}} \right\rfloor \right) p \left(t - nT_o - c_{th}^{(v)}(n)T_c \right) \quad (\text{A.7})$$

which resembles the form of a TH-UWB signal provided in (A.2).

A.2.2 Rake Receiver Model. Rake receiver model development begins by considering a fading multipath channel response of [240]

$$h(t) = \sum_{l=0}^L \alpha_l \delta(t - \tau_l) \quad (\text{A.8})$$

where the multipath channel has $L + 1$ paths, α_l is the Rayleigh fading coefficient on the l^{th} path, and τ_l is the delay of the l^{th} path. This expression resembles that shown in (3.39).

Continuing the process, define the received signal as [240]

$$\begin{aligned} r^{(v)}(t) &= s^{(v)}(t) * h(t) + \eta(t) \\ &= \sqrt{\frac{\mathcal{E}_v}{N_{ss}}} \sum_{n=0}^{\infty} d^{(v)} \left(\left\lfloor \frac{n}{N_{ss}} \right\rfloor \right) c^{(v)}(n) g \left(t - nT_o - c_{th}^{(v)}(n)T_c \right) + \eta(t) \end{aligned} \quad (\text{A.9})$$

where $g(t) = p(t) * h(t) = \sum_{l=0}^L \alpha_l p(t - \tau_l)$ is the composite pulse-multipath channel response with delay spread $\tau_l + T_p$ and $\eta(t)$ is the sum of AWGN and narrow band interference. A Rake receiver processes the signal using N_{rr} fingers (i.e., N_{rr} correlation channels).

Next, consider two cases: UWB reception in the absence of TH and UWB reception with TH present. For simplicity, the following only presents highlights for UWB reception in the absence of TH (the reader is referred to [240] for more information). When TH is absent, $c_{th}^{(v)}(n) = 0 \forall n$, and the template for the n_r^{th} finger's correlator is $p(t - nT_o - \tilde{\tau}_{n_r})$ for the n^{th} frame, where $\tilde{\tau}_{n_r}$ is the delay of Rake

finger n_r . Thus, the output of the n_r^{th} correlator during the n^{th} frame is

$$x^{(v)}(n; n_r) = \int_{nT_o + \tau_{n_r}}^{nT_o + \tau_{n_r} + T_p} r^{(v)}(t) p(t - nT_o - \tau_{n_r}) dt. \quad (\text{A.10})$$

Now, define the “effective channel amplitude” at the n_r^{th} finger’s correlator output as $\alpha_{n_r} = \int_{\tau_{n_r}}^{\tau_{n_r} + T_p} g(t) p(t - \tau_{n_r}) dt$. Substituting (A.9) into (A.10) and applying this definition yields [240]

$$x^{(v)}(n; n_r) = \sqrt{\frac{\mathcal{E}_v}{N_{ss}}} d^{(v)} \left(\left\lfloor \frac{n}{N_{ss}} \right\rfloor \right) c^{(v)}(n) \alpha_{n_r} + \eta(n; n_r) \quad (\text{A.11})$$

which is the output of the n_r^{th} finger’s correlator during the n^{th} frame. If output samples from N_{rr} fingers are stacked, an output vector can be formed as [240]

$$\begin{aligned} \mathbf{x}^{(v)}(n) &= [x^{(v)}(n; 0) \ x^{(v)}(n; 1) \cdots x^{(v)}(n; N_{rr} - 1)]^T \\ &= \sqrt{\frac{\mathcal{E}_v}{N_{ss}}} d^{(v)} \left(\left\lfloor \frac{n}{N_{ss}} \right\rfloor \right) c^{(v)}(n) \tilde{\boldsymbol{\alpha}} + \boldsymbol{\eta}(n) \end{aligned} \quad (\text{A.12})$$

where $\tilde{\boldsymbol{\alpha}}$ and $\boldsymbol{\eta}(n)$ are $N_{rr} \times 1$ vectors formed by stacking α_{n_r} and $\eta(n; n_r)$ (for $n_r \in [0, N_{rr} - 1]$), respectively.

Because each communication symbol is conveyed by N_{ss} monocycles, a total of $N_{ss} \cdot N_{rr}$ correlator output samples must be collected to decode one symbol (N_{rr} per frame). Hence, vectors $\{\mathbf{x}^{(v)}(n)\}_{n=j \cdot N_{ss}}^{(j+1) \cdot N_{ss} - 1}$ are concatenated into a “super vector,” with dimension $N_{ss} N_{rr} \times 1$, as [240]

$$\begin{aligned} \mathbf{y}^{(v)}(j) &= \left[(\mathbf{x}^{(v)}(jN_{ss}))^T \cdots (\mathbf{x}^{(v)}(jN_{ss} + N_{ss} - 1))^T \right]^T \\ &= \sqrt{\frac{\mathcal{E}_v}{N_{ss}}} d^{(v)}(j) (\mathbf{c}^{(v)} \otimes \tilde{\boldsymbol{\alpha}}) + \boldsymbol{\eta}(j), \end{aligned} \quad (\text{A.13})$$

where $\mathbf{c}^{(v)} = [c^{(v)}(0), \dots, c^{(v)}(N_{ss} - 1)]^T$ is the code vector and $\boldsymbol{\eta}(j) = [\boldsymbol{\eta}^T(jN_{ss}), \dots, \boldsymbol{\eta}^T(jN_{ss} + N_{ss} - 1)]^T$ is the noise and interference vector, each of dimension $N_{ss} N_{rr} \times 1$. Eqn. (A.13) is referred to as the “unifying digital model for Rake reception” in [238].

A.3 UWB TH-BPPM in a Fading Channel

In this section, TH MA coding is combined with 4-ary biorthogonal PPM to form TH-BPPM as originally introduced in [23,38] and subsequently analyzed in [246,247]. The TH-BPPM performance in [38] is simulated for synchronous and asynchronous networks using an additive white Gaussian noise (AWGN) channel. Work in [246,247] mathematically describes a multi-dimensional (NM -ary) pulse position amplitude modulation system that reduces to the original TH-BPPM of [38] when $N = M = 2$. The mathematical description and supporting simulations specify the channel capacity, error probability, and performance bounds of such systems. However, work in [246,247] does not address multipath (MP) interference effects and only synchronized network operation is considered. Related work in [123,124] does address some MP issues using a RAKE receiver implementation. In this case, an exponential decay power delay profile (PDP) is used for modeling the MP fading channel.

Extending these previous TH-BPPM efforts, the original results presented in this section characterize TH-BPPM performance using realistic UWB fading channels, i.e., using modified Saleh-Valenzuela (S-V) models as adopted by the IEEE [53,145] for personal area networks (PANs). For baseline comparison, communication performance is first characterized using a simplified AWGN channel. Single-user performance is addressed next using realistic channel models for multiple fading environments with varying MP levels. Fading channel results are then extended to include multiple access scenarios under both synchronous *and* asynchronous network conditions.

Under fixed average power and symbol length constraints, comparative analysis indicates the TH-BPPM technique provides equivalent MA performance as binary techniques while providing typical M -ary signaling advantages. Despite performance benefits afforded by TH-BPPM, MP and MA interference is shown to degrade TH-BPPM performance (with MP interference being the dominant source of error).

A.3.1 Multipath Channel Model. Researchers oftentimes apply an AWGN or Rayleigh fading channel model to explore the impact of MP signals on system performance. Although an AWGN model fails to represent realistic channel fading, it does provide a best case bound on performance. A more realistic Rayleigh fading channel model can normally be used to capture the essence of fading for narrowband systems. However, common assumptions that allow use of Rayleigh statistics to model channel fading (e.g., a large number of MP reflections exist within one received MP bin implies an amplitude response can be modeled as a complex Gaussian distribution via the central limit theorem) do not generally hold for wideband systems [145]. For example, an UWB system having a bandwidth of 7.5 GHz has a resolvable delay bin of only 4.0 cm, which means pulses within 0.133 ps of each other can be resolved. In these cases, receiver MP bins contain few MP signals (perhaps none) and the central limit theorem can no longer be invoked, negating the use of Rayleigh statistics for accurately modeling the fading channel [145].

Modified Saleh-Valenzuela (S-V) channel models, as adopted by the IEEE and presented in [53, 145], are employed in this work. These models yield statistical channel characteristics which closely match those noted in various UWB experimental measurement campaigns [27, 65]. Such characteristics include: MP signals arrive in clusters rather than continuously, the cluster inter-arrival time is exponentially distributed, the cluster amplitude components are log-normally distributed, and shadowing can exist when the line-of-sight (LOS) path is blocked. These characteristics have been captured by IEEE 802.15.3a in a “standard channel model” [145] for evaluating PAN proposals. The MP model therein contains discrete time impulse responses defined as [53, 145]

$$h_i(t) = X_i \sum_{l=0}^{N_{cluster}} \sum_{k=0}^{N_{MP}} \alpha_{k,l}^i \delta(t - T_l^i - \tau_{k,l}^i) \quad (\text{A.14})$$

where i is the realization number, X_i is a log-normal shadowing term, $N_{cluster}$ is the number of clusters, N_{MP} is the number MP components, $\alpha_{k,l}^i$ are MP gain coefficients,

T_l^i is the l^{th} cluster delay, and $\tau_{k,l}^i$ is the k^{th} MP component delay relative to the l^{th} cluster delay (T_l^i). The distributions of these MP parameters are more completely defined in [145]. The selection of parameters to fit these distributions (e.g., rms delay for the exponentially distributed cluster arrival time) vary based on the MP channel classification. As in [53, 145], four distinct UWB channel models are considered, including: 1) CM1 for LOS (0-4 m), 2) CM2 for non-LOS (NLOS) (0-4 m), 3) CM3 for NLOS (4-10 m), and 4) CM4 for extreme NLOS (i.e., 25 ns RMS delay).

The composite received waveform is a sum of multiple signals, including: 1) the direct path signal of interest (SOI), 2) direct path MA signals from other users, 3) MP signals from the SOI and other users, and 4) noise. Under perfect power control conditions, the SOI and MA signals arrive non-degraded and have equal amplitudes. The MP signals are formed by convolving each transmitted signal with a distinct channel impulse response (CIR). Thus, the composite received signal is given by

$$r(t) = \sum_{v=1}^{N_U} \left[s^{(v)}(t - \tau_v) + \sum_{l=1}^{N_{MP}} s^{(v)}(t - \tau_v) * h_l^{(v)}(t) \right] + \eta(t) \quad (\text{A.15})$$

where N_U is the number of users, N_{MP} is the number of MP reflections (assumed identical for all users), τ_v is the delay (relative to SOI $s^{(v)}(t)$ with $\tau_1 = 0$) of the v^{th} MA transmitter, and $\eta(t)$ is AWGN.

A.3.2 Communication Performance: AWGN Channel. A general “fast hopping” communication system is considered whereby each symbol is generated, replicated, time hopped, and transmitted N_{ss} times. Using the multi-channel correlation receiver of Fig. A.7 under perfect “dehopping” conditions, *coherent detection* is achieved using a collection of cumulative decision variables, or test statistics $\{z_i\}$, as generated by accumulating N_{ss} correlator outputs for each possible communication symbol $s_i(t)$ – see (A.3) [165]. Assuming the signals are equally probable, maximum likelihood (ML) estimation is achieved by estimating the symbol corresponding to

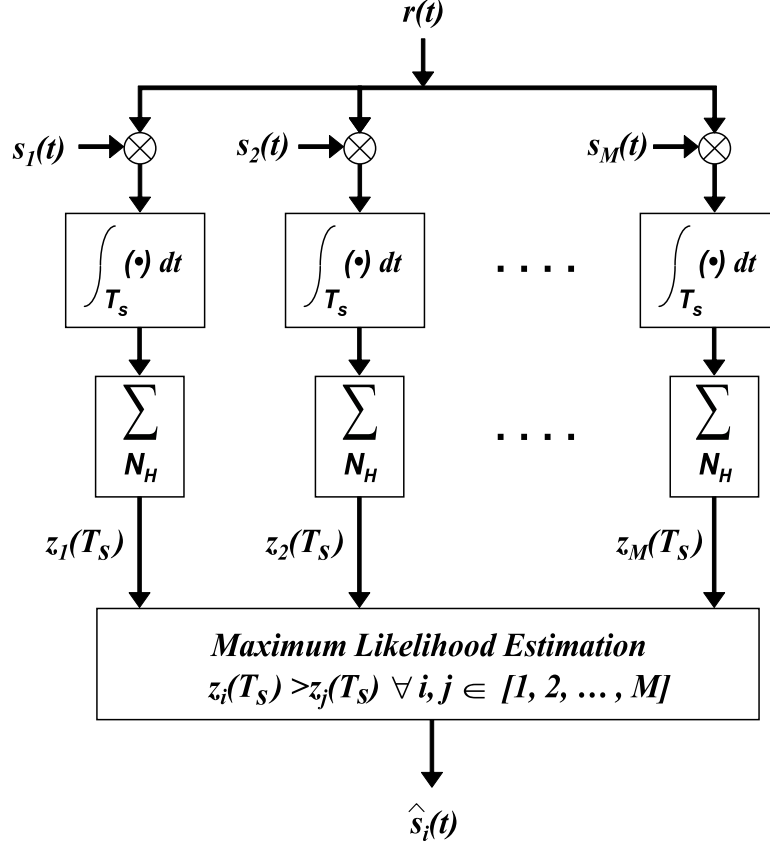


Figure A.7: Multi-channel correlation receiver for maximum likelihood estimation of time hopped UWB waveforms.

$\text{Max} \{z_i\}$. This subsection compares communication performance in AWGN for the three MA techniques previously introduced: TH-PPM, TH-BPPM, and DS-UWB.

Fundamentally, the TH-PPM technique of (A.2) approximates orthogonal signaling and the DS-UWB technique of (A.5) approximates antipodal signaling. The generation of cumulative test statistics and selection of $\text{Max} \{z_i\}$ provides the same estimation performance as a single channel receiver using N_{ss} times the received energy [165]. Therefore, the theoretical bit error probability P_b of TH-PPM, TH-BPPM, and DS-UWB signals as presented, assuming additive white Gaussian noise (AWGN) channel conditions with matched filter detection and N_{ss} pulse integration gain, is given by

$$P_b = Q \left(\sqrt{N_{ss} \cdot \frac{E_b (1 - \rho)}{N_o}} \right) \quad (\text{A.16})$$

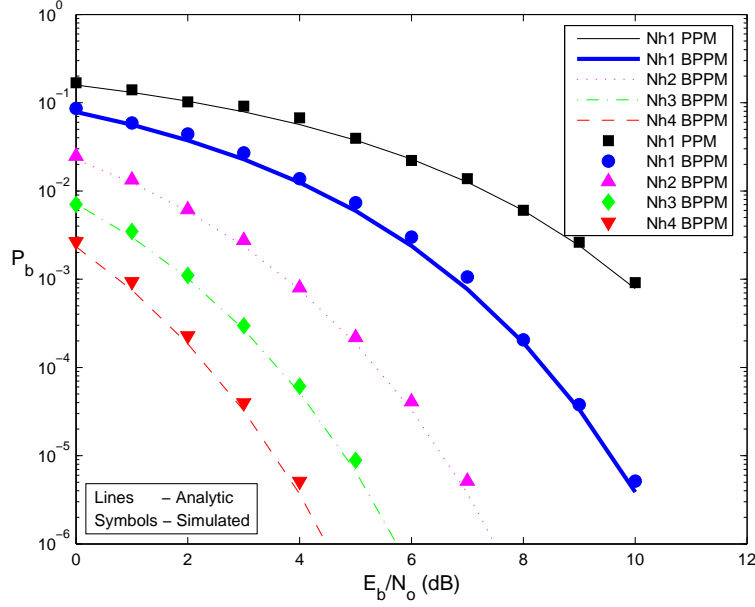


Figure A.8: Communication performance for AWGN channel: binary TH-PPM ($N_{ss} = 1$) and biorthogonal TH-BPPM ($N_{ss} = 1, 2, 3, 4$).

where correlation coefficient $\rho = -1$ for antipodal signaling (e.g., DS-UWB) and $\rho = 0$ for orthogonal signaling (e.g., TH-PPM), $Q(x) = 1/\sqrt{2\pi} \int_x^\infty \exp(-t^2/2) dt$, $x \geq 0$, E_b is the average received energy per bit, and N_o is the noise spectral density [165]. The biorthogonal constellation for (A.3), as graphically depicted in Fig. A.5, is equivalent to Gray-coded quadrature PSK (QPSK) modulation. Hence, $\rho = -1$ for TH-BPPM.

Fig. A.8 shows binary TH-PPM ($N_{ss} = 1$ only) and biorthogonal TH-BPPM ($N_{ss} = 1, 2, 3, 4$) communication performance. As indicated, simulated P_b results (symbols) are consistent with analytic results (lines) of (A.16). The median value of the mean-squared-error and standard deviation between simulated and analytic results are 6.4×10^{-7} and 7.0×10^{-4} , respectively.

UWB signals can be analyzed and compared using identical P_b values by appropriately fixing E_b/N_o values for each signal. The results in this section and Section A.5 use $E_b/N_o = 6.79$ dB for DS-UWB and TH-BPPM and $E_b/N_o = 9.80$ dB for TH-PPM to yield identical P_b values of 1×10^{-3} . By fixing P_b and symbol duration for each

UWB MA system, the signal-to-noise ratio (SNR), data rate, and average power for each communications symbol remain constant.

Multiple access capability is achieved for $N_{ss} \geq 1$ where a processing gain of N_{ss} is realized. Here, signal discrimination is obtained using chip offsets $c_n^{(v)}$ derived from pseudorandom sequences. For *consistency* with previous work [24, 38, 189], 31-length Gold codes are used to generate chip offset sequences [optimality is not claimed for this selection and the reader is encouraged to see [193] for more details]. Chip offset sequences were derived from Gold code sequences by mapping (binary-to-decimal conversion) Gold code elements to integer values using a 5-element wide sliding window and single code element shifts such that $N_c = 2^5 = 32$ and $c_j \in \{0, 1, \dots, 31\}$.

Baseline MA performance is established using $N_{ss} = 1$ in an AWGN channel (to isolate code selection and assignment effects without time hopping pulse repetition gain present) for a network containing up to $N_U = 10$ transmitters. In this case, the receiver under test receives one desired signal and $(N_U - 1)$ undesired, direct path MA interferers. For all MA results, the received power of *all* undesired interfering MA signals is assumed identical to the received desired signal power. The receiver under test is perfectly synchronized to the SOI while all other signals are received either synchronously or asynchronously. For the asynchronous network, all MA interferers are randomly offset (delayed) in time over $[0, T_c]$.

Simulation results are shown in Fig. A.9 for the TH-PPM, TH-BPPM, and DS-UWB *synchronous* (filled symbols) and *asynchronous* (unfilled symbols) networks. For this example, TH-PPM and TH-BPPM users transmit one pulse per symbol repetition interval T_o (unity processing gain for $N_{ss} = 1$), and DS-UWB users transmit multiple pulses per symbol repetition interval T_o (processing gain $N_{ss} = 10\log\{N_c = 31\}$). Thus, the DS-UWB system has an inherent processing gain, or pulse integration gain, that must be considered when comparing TH-UWB and DS-UWB results. A symbol repetition interval of $T_o = 25$ ns is used here and approximates a 40 Mb/s data rate. In all cases, the composite received waveform

consists of N_U total signals, including one direct *desired* signal, and $(N_U - 1)$ direct MA *interfering* signals.

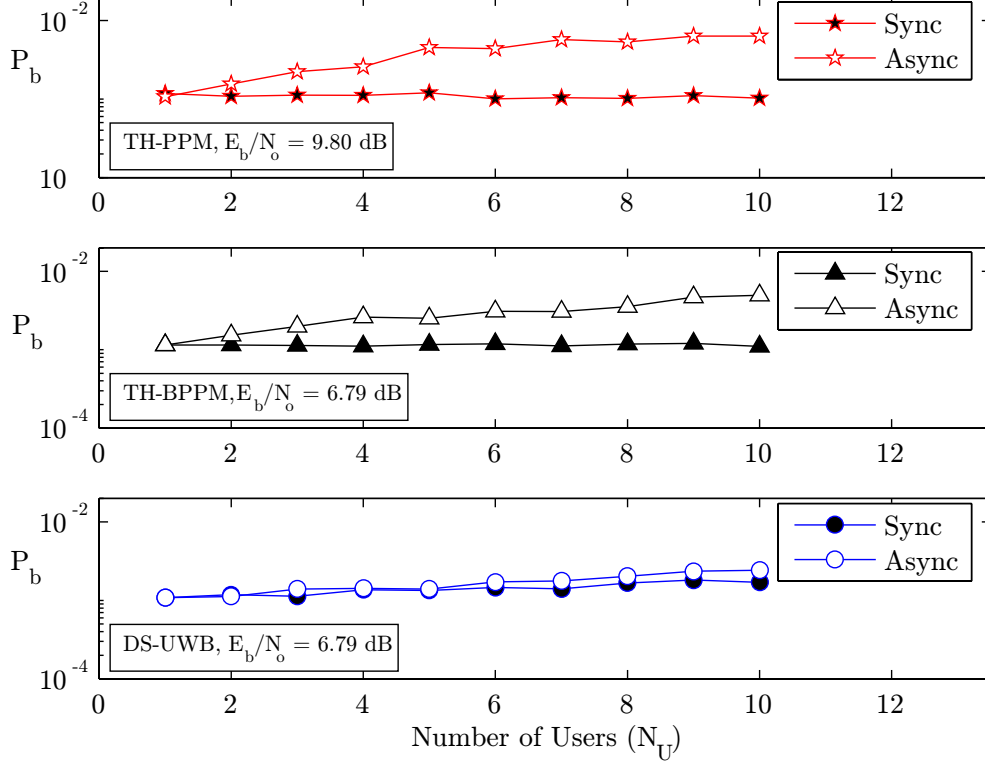


Figure A.9: Multiple access performance for TH-PPM (top), TH-BPPM (middle), and DS-UWB (bottom) networks.

As in previous binary TH-PPM work [24,38], synchronous TH-PPM, TH-BPPM, and DS-UWB networks experience minimal symbol collisions with Gold code assignment and BER performance is virtually unaffected by variation in N_U . To permit reliable comparison with the other results, the specific set of Gold codes assigned to users when generating Fig. A.9 results is maintained for related results presented later.

Conversely, asynchronous TH-PPM and DS-UWB networks experience a higher number of symbol collisions (intersymbol interference) since synchronization is not imposed. Consequently, the asynchronous BER performance in Fig. A.9 reflects greater degradation as N_U increases. This degradation is more apparent in TH networks

because they lack the inherent processing gain of the DS-UWB networks. For the TH-PPM network, the P_b increases by a factor of $5.7\times$; for the TH-BPPM network, the P_b increases by a smaller factor of $4.5\times$; for the DS-UWB network, the P_b increase is more subtle and on the order of about 50%.

A.3.3 Communication Performance: Fading Channel. Performance results in Section A.3.2 represent a best case bound given that fading effects are not incorporated. The introduction of MP signals in a fading environment serves to degrade bit error performance. This section first highlights the degradation inflicted upon a single user by varying the number of MP signals and channel type. Analysis is then extended to multi-user synchronous and asynchronous networks, with performance degradation highlighted for joint MP interference (MPI) and multiple access interference (MAI).

A.3.3.1 Multipath Interference (MPI). MPI effects for a single user are characterized using one of four fading models: CM1, CM2, CM3, and CM4, with rms time delays of 5.0, 8.0, 15.0, and 25.0 ns, respectively [145]. Fig. A.10 shows 10 representative impulse responses for CM1 and CM4 fading channel models. As indicated, the duration of MP responses for CM1 can last up to 50 ns. Thus, for symbols generated herein with $T_o = N_s \cdot T_c \approx 25$ ns, the MP responses can impact the current and/or subsequent symbols. As the MP rms delay increases (as in CM2, CM3, and CM4 models) so does the MP response duration. The duration of MP responses for CM4 can last approximately four times longer (up to 200 ns), but the amplitudes are limited due to equal energy constraints within each channel model. Hence, a MP signal can effectively impact estimation of multiple symbols at varying strengths depending upon the chosen channel model.

To simulate single-user TH-BPPM performance amidst MPI, E_b/N_o is varied between -2 and 10 dB and P_b is estimated. To permit isolation of MPI effects, analysis is limited here to the $N_{ss} = 1$ case using up to $N_{MP} = 20$ MP replicas. Each MP replica is generated by convolving the transmitted SOI with an independent realization of the channel impulse response. The resultant channel responses are summed with the

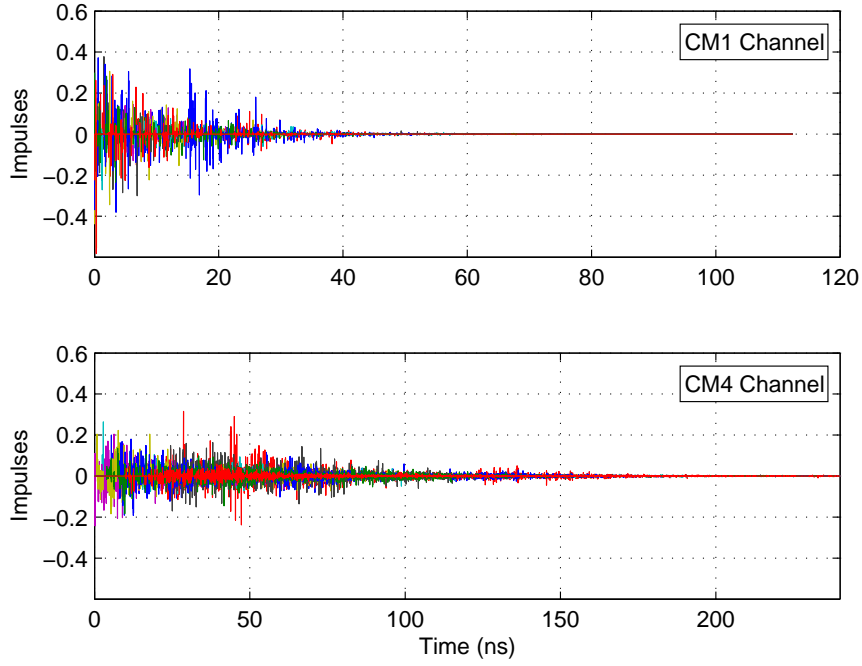


Figure A.10: Overlay of ten representative impulse responses for CM1 (top) and CM4 (bottom) fading channel models (note the different time scales).

SOI and AWGN. The receiver processes one direct, *desired* signal and N_{MP} indirect, *un-desired* MP signals.

Fig. A.11 illustrates the performance of a single TH-BBPM user under CM1 (dashed line, filled symbols), CM2 (solid line, unfilled symbols), CM3 (dotted line, filled symbols), and CM4 (dashed-dotted line, unfilled symbols) conditions. As expected, performance in AWGN (no fading) represents best case performance with inclusion of MP signals increasing P_b for a given E_b/N_o and channel model condition. The characteristics of the CM1 channel model appear to more severely degrade performance. The P_b significantly worsens as the number of multipath signals increases and as the amplitude of the multipath signals increases, emphasizing the severity of the dense UWB MP channels.

A.3.3.2 Multiple Access Interference (MAI). MAI effects upon a UWB network are characterized using one of four fading models: CM1, CM2, CM3,

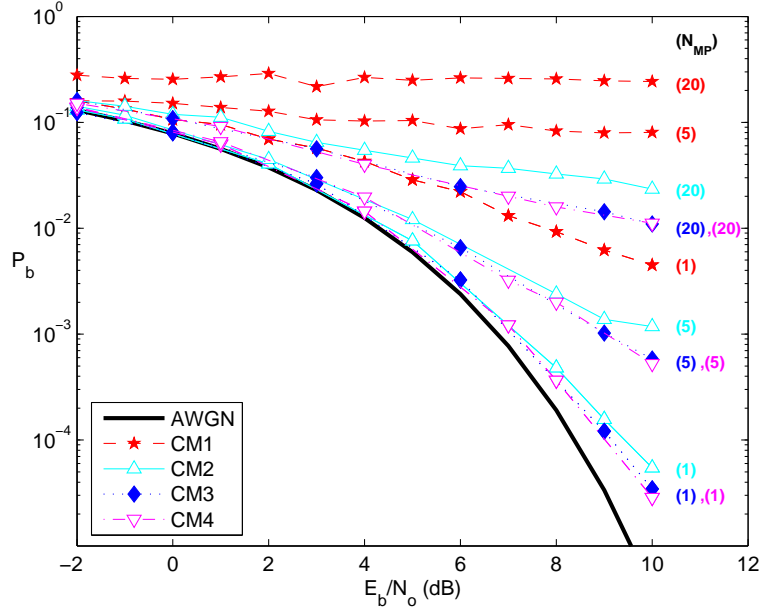


Figure A.11: Communication performance for *Single-User* TH-BPPM within AWGN, CM1, CM2, CM3, and CM4 channel models using $N_{MP} = 1, 5$, and 20 multipath replicas (in parentheses).

and CM4. MAI in an AWGN channel provides baseline network performance – see Fig. A.9. To simulate network TH-BPPM performance amidst MPI *and* MAI, conditions are fixed to yield $P_b = 10^{-3}$ (i.e., $E_b/N_o = 6.79$ dB) and the number of users is varied between 1 and 10. As before, MA P_b performance is estimated, and MAI effects are isolated using $N_{ss} = 1$ for $N_{MP} = 20$ MP replicas. The composite received waveform now consists of $N_U \times (N_{MP} + 1)$ total signals, including one direct *desired* signal, $(N_U - 1)$ direct MA *interfering* signals (using perfect power control conditions), and $N_U \times N_{MP}$ delayed MP *interfering* signals.

Figures A.12 and A.13 illustrate performance using up to $N_U = 10$ TH-BPPM transmitters under CM1, CM2, CM3, and CM4 conditions for both *asynchronous* and *synchronous* networks, respectively. As expected, increasing N_{MP} and/or N_U increases P_b . The results exhibit the expected performance degradation as N_U and N_{MP} increase; most notably, synchronization advantages, which are apparent in the $N_{MP} = 0$ case, quickly diminish with MPI present. However, perhaps a somewhat

less obvious results is that at lower MPI levels (e.g., $N_{MP} = 1$), synchronous networks exhibit better P_b performance, while at higher MPI levels (e.g., $N_{MP} = 20$), asynchronous networks exhibit better P_b performance. For $N_{MP} = 1, 5$, and 20 , the collective mean P_b improvement (κ) across all fading channels when using synchronous instead of asynchronous networks is $\kappa = 1.4, 1.1$, and 0.8 , respectively.

The results in Figures A.12 and A.13 for CM2, CM3, and CM4 channels can be theoretically approximated by adding a term to the denominator of (A.16), i.e. N_o is replaced by $N_o + \gamma N_{MAI}$, where γ is a scaling factor and N_{MAI} was defined in (5.25). Scaling factor γ can be approximated by $\kappa \cdot N_{MP}/2$ for $N_{MP} \gg 1$, where $\kappa = 1$ for synchronous networks and κ equals the improvement factors in the previous paragraph for asynchronous networks.

Ergo, in similar scenarios with Gold coding and MP fading channels, it is clearly evident that MPI (versus MAI) becomes the dominant factor in decreasing communication performance. A comparison of fading channel results (see Figures A.12 and A.13) with AWGN channel results (see Fig. A.9) emphasizes the severity of the dense UWB MP channels.

A.3.4 Summary of TH-BPPM Fading Channel Results. TH-BPPM performance is characterized amidst MPI and MAI in UWB fading channels. Modified S-V UWB channel models, as adopted by the IEEE for PANs, have been considered. As validated through simulation, 4-ary TH-BPPM provides MA performance comparable to binary TH-PPM techniques with added advantages of M -ary signaling, i.e., an effective doubling of data rate under fixed average power and fixed symbol length constraints. Performance is characterized using up to 20 MP signals from each of 10 users in both synchronous and asynchronous networks. With the introduction of MP signals, advantages provided by Gold coding in a synchronous network quickly diminish. This degradation can be minimized by increasing processing gain, i.e., coherently processing multiple replicas of transmitted communication symbols. It is

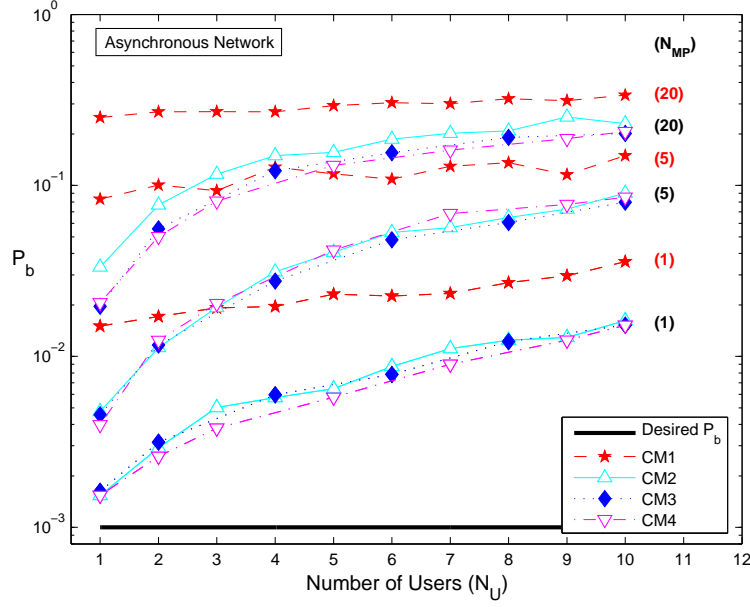


Figure A.12: Multipath (MPI) and multiple access (MAI) interference effects for an *Asynchronous Network* using $N_{MP} = 1, 5$, and 20 replications (in parentheses) with CM1, CM2, CM3, and CM4 channel models.

shown that MPI, not MAI, is the most dominant degrading factor when considering realistic channel fading.

A.4 Spectral Coexistence Scenarios: In-Band Power Analysis

Given the inherent excessive bandwidth in UWB signals, collateral interference and spectral coexistence with neighboring (spatially and/or spectrally) narrowband or wideband signals must be fully examined. This issue has been researched extensively [11, 54, 67, 77, 128, 144, 249] with considerable emphasis placed on simulation. Because they are designed to share spectral bands, UWB signals are restrictively low-power by definition, i.e., they are power limited to -41.3 dBm/MHz or less from 3.1 to 10.6 GHz and out-of-band transmissions are even further power limited [52, 195]. To analyze coexistence impacts, energy spectral density (ESD) and power spectral density (PSD) analytical expressions for the UWB signals are considered.

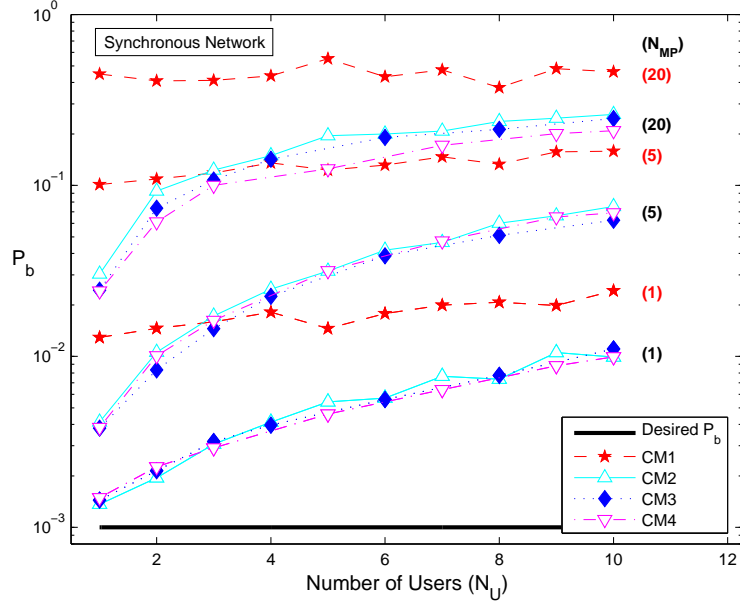


Figure A.13: Multipath (MPI) and multiple access (MAI) interference effects for a *Synchronous Network* using $N_{MP} = 1, 5$, and 20 replications (in parentheses) with CM1, CM2, CM3, and CM4 channel models.

Coexistence can be nominally characterized by comparing the received in-band UWB interfering signal power $P_{r,UWB}$ and received SOI power $P_{r,SOI}$, with each expressed as [11]:

$$\begin{aligned}
 P_{r,UWB}(d_{UWB}) &= P_{UWB} \left(f_c - \frac{B}{2}, f_c + \frac{B}{2} \right) - PL(d_{UWB}) \\
 P_{r,SOI}(d_{SOI}) &= P_{SOI} \left(f_c - \frac{B}{2}, f_c + \frac{B}{2} \right) - PL(d_{SOI})
 \end{aligned} \tag{A.17}$$

where the PL factors account for free-space path loss between the transmitters and receivers and d is the signal propagation distance. The transmitted power terms, P_{UWB} and P_{SOI} , contain only the in-band power; for coexistence analysis, spectrally “in-band” is dictated by SOI receiver filter characteristics, including center frequency f_c and bandwidth B as indicated.

A.4.1 Energy Spectral Density (ESD) of Fundamental UWB Waveform.

Given the fundamental UWB waveform in (A.1) is a single pulse, its ESD is used to

characterize energy distribution as a function of frequency. When (A.1) is used for UWB signaling, the signal's power distribution as a function of frequency is characterized by its PSD. The ESD $\Psi_w(f)$ of (A.1) is given as follows [204]:

$$\Psi_w(f) = |W(f)|^2 \quad (\text{A.18})$$

where $W(f)$ is the Fourier transform (FT) of (A.1) given by [71]:

$$W(f) = \frac{\pi \tau_m^3 f^2}{\sqrt{2}} \exp \left[-\frac{\pi \tau_m^2 f^2}{2} \right]. \quad (\text{A.19})$$

Figure A.1 shows representative time and normalized ESD responses for the fundamental UWB waveform of (A.1) using $\tau_m = 0.16$ ns which corresponds to a pulse width of $T_p = 0.40$ ns.

A.4.2 Power Spectral Density (PSD) of TH-PPM Signals. The PSD derivation for a TH-UWB signal using PPM data modulation and time coding for MA is given in [71] and follows the process found in [120,121,181]. In these works, the transmitted UWB signal $s(t)$ is described in terms of a data modulation process $m(t)$ and a fundamental pulse shape $w(t)$ and is given by $s(t) = m(t) * w(t)$ where $*$ denotes convolution and $w(t)$ is given by (A.1). The data modulation process $m(t)$ is defined as [71]

$$m(t) = \sum_{k=-\infty}^{\infty} A_k \delta(t - kT_{sym} - B_k \Delta) \quad (\text{A.20})$$

where A_k and B_k are factors which determine the modulation type, T_{sym} is the symbol duration, and Δ is the relative PPM offset. The PSD of the data modulation process, found by taking the FT of the time-average autocorrelation function (time-averaging is required because the autocorrelation is periodic in τ , the shift, with the symbol

duration), is given by [71, 121]

$$S_{mm}(f) = \frac{E[A_0^2]}{T_{sym}} + \frac{1}{T_{sym}} \sum_{l=-\infty}^{\infty} E[A_o A_l] E[e^{-j2\pi f(B_l - B_0)\Delta}] \left[\frac{1}{T_{sym}} \delta\left(f - \frac{l}{T_{sym}}\right) - 1 \right]. \quad (\text{A.21})$$

For the TH-PPM waveform given by (A.2) which uses binary data modulation, $A_k = 1$ and $B_k = \pm 1$ in accordance with the data modulation. Assuming that each B_k value is equally likely, (A.21) can be expressed as [71]

$$S_{mm}(f) = \frac{1}{2T_{sym}} [1 - \cos(4\pi f\Delta)] + \frac{1}{2T_{sym}^2} [1 + \cos(4\pi f\Delta)] \sum_{l=-\infty}^{\infty} \delta\left(f - \frac{l}{T_{sym}}\right) \quad (\text{A.22})$$

which is used in conjunction with the following to provide the TH-PPM PSD

$$S_{TH}(f) = S_{mm}(f) |W(f)|^2. \quad (\text{A.23})$$

Using (A.19), (A.22), and (A.23), the resultant TH-PPM PSD for the signal given in (A.2) is given by

$$S_{TH}(f) = \left\{ \frac{1}{2T_{sym}} [1 - \cos(4\pi f\Delta)] + \frac{1}{2T_{sym}^2} [1 + \cos(4\pi f\Delta)] \times \sum_{l=-\infty}^{\infty} \delta\left(f - \frac{l}{T_{sym}}\right) \right\} \times |W(f)|^2. \quad (\text{A.24})$$

Examination of the TH-PPM PSD expression in (A.24) reveals that it contains spectrally continuous and discrete components. Research has shown the by either time dithering the data modulated symbols [146, 167, 203] or by employing antipodal data modulation in conjunction with PPM [38, 120, 121, 146, 181, 229], the discrete spectral components of the PSD are reduced and/or eliminated. The expression in (A.24) can be rewritten for finite duration signals (useful for simulation) by introducing a

symmetric time windowing function $r(t)$ which effectively limits the data modulation process $m(t)$ to a finite number of symbols. The TH-PPM PSD for a finite length signal of N_{sym} total symbols is shown to be [71]

$$\tilde{S}_{TH}(f) = \frac{1}{N_{sym}T_{sym}}\tilde{S}_{mm}(f)|W(f)|^2 \quad (\text{A.25})$$

where $\tilde{S}_{mm}(f)$ is the modified data modulation PSD. The continuous part of (A.24) is unaffected by this change. However, the discrete part is affected and the effect is manifested in the following way [71]

$$S_{TH}(f) = \left\{ \frac{1}{2T_{sym}} [1 - \cos(4\pi f \Delta)] + \frac{N_{sym}}{2T_{sym}} [1 + \cos(4\pi f \Delta)] \times \sum_{l=-\infty}^{\infty} \text{sinc} \left(N_{sym} \left(f - \frac{l}{T_{sym}} \right) T_{sym} \right) \right\} \times |W(f)|^2. \quad (\text{A.26})$$

It is evident from (A.26) that increasing the number of symbols N_{sym} in a finite duration UWB signal causes a corresponding increase in spectral line magnitudes. Figure A.14 shows a comparison between analytic and simulated PSDs of a TH-PPM signal using parameter values of $\tau_m = 0.4T_p = 0.16$ ns, $f_c = 5$ GHz, pulse width $T_p = 2/f_c = 0.4$ ns, symbol duration $T_{sym} = 2T_p = 0.8$ ns, symbol repeat interval $T_o = T_{sym}$, PPM offset $\Delta = T_p/2 = 0.2$ ns, unity processing gain with $N_{ss} = 1$, and $N_{sym} = 1000$ symbols. The randomness in the simulated TH-PPM PSD is a result of using a random, uniformly distributed stream of zeros and ones for data modulation [71]. As shown in (A.24) and (A.26) and illustrated in Fig. A.14, the TH-PPM PSD contains uniformly spaced discrete peaks which are spectrally coincident with nulls of the continuous response.

A.4.3 Power Spectral Density (PSD) of DS-UWB Signals. Derivation of the PSD for DS-UWB signals using BPSK data modulation and pseudorandom phase coding for MA is provided in [218, 242]. For this development it is convenient to

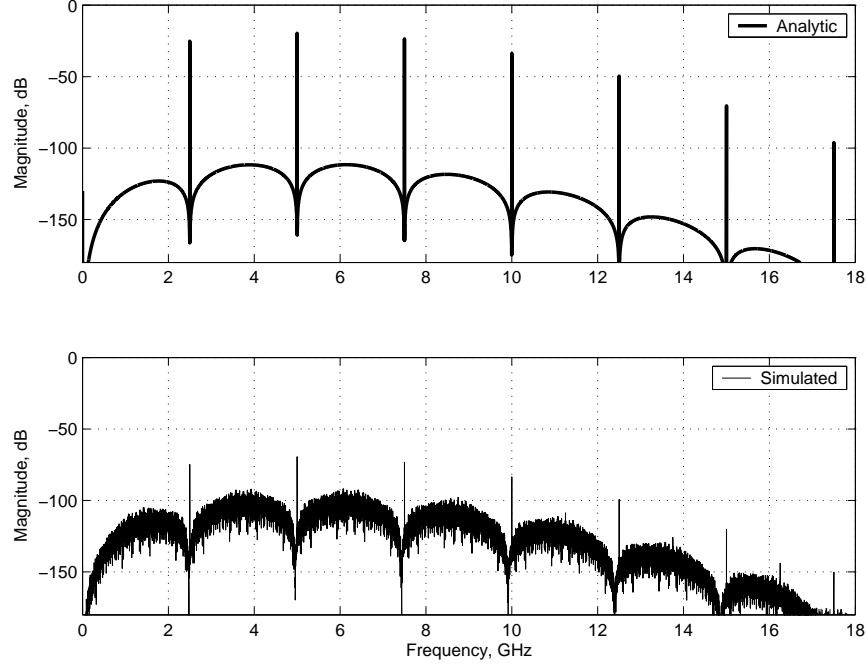


Figure A.14: TH-PPM analytic PSD (top) from (A.24) and simulated PSD (bottom) for waveform parameters provided in Section A.4.2.

redefine the DS-UWB signal given by (A.5) as follows [242]

$$s_{DS}^{(v)}(t) = \sqrt{P_v} \sum_{j=-\infty}^{\infty} \sum_{n=1}^{N_{ss}} w(t - jT_o - nT_c) c_n^{(v)} d_j^{(v)} \quad (\text{A.27})$$

where this reformulation is possible given that $c_n \in [0, 1]$ in (A.5). After exchanging variables and determining the autocorrelation function, the PSD of the DS-UWB signal given by (A.27) is [242]

$$S_{DS}(f) = \frac{1}{T_c} |W(f)|^2 S_{\alpha\alpha}(f) \quad (\text{A.28})$$

where $W(f)$ is given by (A.19). $S_{\alpha\alpha}(f)$ is the FT of the autocorrelation of α , where α is defined as $\alpha_i \equiv \alpha_{j,n} = \{c_n \times d_j\}$, a modified PR sequence containing elements from a term-by-term multiplication of the phase code and the BPSK data modulation. Given this modified PR sequence α has mean μ_α , variance σ_α^2 , is real-valued, and is

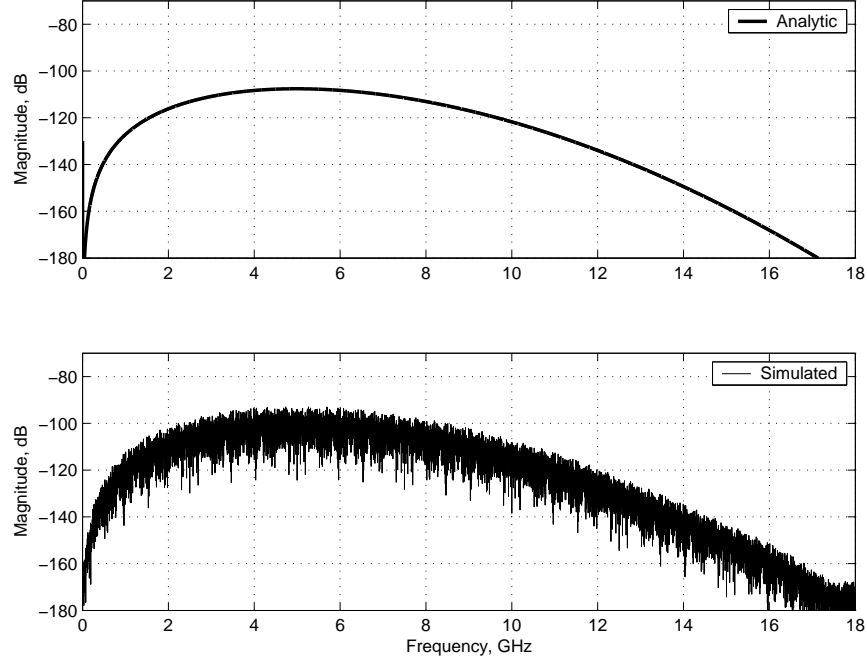


Figure A.15: DS-UWB analytic PSD (top) from (A.30) and simulated PSD (bottom) for waveform parameters provided in Section A.4.3.

mutually uncorrelated, (A.28) can be expressed as [242]

$$S_{DS}(f) = \frac{\sigma_\alpha^2}{T_c} |W(f)|^2 + \frac{\mu_\alpha^2}{T_c^2} \sum_{m=-\infty}^{\infty} \left| W\left(\frac{m}{T_c}\right) \right|^2 \delta\left(f - \frac{m}{T_c}\right). \quad (\text{A.29})$$

Further assuming the modified PR sequence is zero mean ($\mu_\alpha = 0$), the discrete part of $S_{DS}(f)$ vanishes and (A.29) reduces to [242]

$$S_{DS}(f) = \frac{\sigma_\alpha^2}{T_c} |W(f)|^2. \quad (\text{A.30})$$

Figure A.15 shows a comparison between analytic and simulated PSDs of a DS-UWB signal using parameter values of $\tau_m = 0.4T_p = 0.16$ ns, $f_c = 5$ GHz, pulse width $T_p = 2/f_c = 0.4$ ns, symbol duration $T_{sym} = 2T_p = 0.8$ ns, chip duration of $T_c = T_{sym}$, unity processing gain with $N_{ss} = 1$, and $N_{sym} = 1250$ symbols. For the analytic plot, the mean of the PR phase is assumed to be zero. In this example, there are 32 samples per symbol duration for a total of 40,000 samples in the DS-UWB pulse train.

The PSD for a DS-UWB signal can be alternately stated to account for N_U multiple users with each having N_{MP} multipath replicas. The DS-UWB PSD for this case is given by [218]

$$S_{DS}(f) = \frac{|W(f)|^2}{N_{ss}T_c} \sum_{v=1}^{N_U} \left| \sum_{l=0}^{N_{MP}} g_l^{(v)} e^{-j2\pi f \lambda_l^{(v)}} \right|^2 \quad (\text{A.31})$$

where $g_l^{(v)}$ is the amplitude and $\lambda_l^{(v)}$ is the excess delay of the l^{th} multipath replica for the v^{th} user. The apparent differences between (A.31) and (A.30) include the $1/N_{ss}$ factor and the sum of magnitude-squared terms. The expression in (A.31) implies the DS-UWB PSD is a sum of distinct PSDs corresponding to N_U different users, and the v^{th} user's multipath effect is evident by the magnitude-squared terms containing the channel frequency response [218].

A.4.4 Analytical In-Band Power Expressions. The “in-band” power for DS-UWB is shown in this subsection as an example, with a similar development possible for TH-PPM. The analytical expression for in-band interfering DS-UWB power using (A.29) can be written as [242]

$$P_{UWB} \left(f_c - \frac{B}{2}, f_c + \frac{B}{2} \right) = \frac{2\sigma_\alpha^2}{T_c} \int_{f_c - \frac{B}{2}}^{f_c + \frac{B}{2}} |W(f)|^2 df + \frac{2\mu_\alpha^2}{T_c^2} \sum_{\frac{m}{T_c} - f_c \in \left[-\frac{B}{2}, \frac{B}{2}\right]} \left| W \left(\frac{m}{T_c} \right) \right|^2 \quad (\text{A.32})$$

where the band of interest is determined by center frequency f_c and bandwidth B . Thus, DS-UWB interfering signal power incident on a coexisting receiver is determined by three primary factors, including 1) the chip rate, 2) the ESD of the fundamental UWB waveform, and 3) the PSD of the modified PR sequence. First, a higher chip rate (increase in $1/T_c$) produces a higher in-band power for a DS-UWB system. Second, the ESD $\Psi_w(f)$ of (A.18) and (A.19) indicates greater in-band power with increasing impulse width τ_m . Recall from (A.1) that the impulse width parameter τ_m controls

pulse shape and is determined by pulse width T_p ; increasing T_p increases τ_m and the magnitude-squared response of (A.19) yields greater in-band interfering power. Third, PSD characteristics of $S_{\alpha\alpha}(f)$ are determined by the mean μ_α and variance σ_α^2 which directly impact continuous and discrete factors of (A.32). Assuming a random sequence with $\mu_\alpha = 0$, the expression in (A.32) reduces to

$$P_{UWB} \left(f_c - \frac{B}{2}, f_c + \frac{B}{2} \right) = \frac{2\sigma_\alpha^2}{T_c} \int_{f_c - \frac{B}{2}}^{f_c + \frac{B}{2}} |W(f)|^2 df. \quad (\text{A.33})$$

In this case, the discrete spectral lines completely disappear. However, in realistic DS-UWB systems the discrete spectral lines do not totally disappear as the chip sequence is not truly mutually uncorrelated. The application of the phase coding causes μ_α to approach zero and helps “whiten” the PSD via scrambling of phase values [242].

A.4.5 In-Band Power Analysis Results. For illustrative purposes, consider a scenario where the SOI receiver, perhaps a member of an 802.11a WLAN or similar network [11], is operating in one of three 100 MHz U-NII bands near 5.0 GHz and a UWB transmitter is spatially located nearby. The question is posed: How much in-band UWB interfering power will impact SOI receiver performance?

In this analysis, in-band power from TH-PPM and DS-UWB signals is calculated for three SOI receiver bandwidths over a range of filter center frequencies. Figure A.17 (TH-PPM) and Fig. A.18 (DS-UWB) show the in-band UWB interfering power P_{UWB} (neglecting path loss effects) versus filter center frequency F_f which ranges from 4.9 to 5.9 GHz using filter bandwidths of 10 MHz, 20 MHz (consistent with 802.11a WLAN), and 50 MHz as indicated. As used for establishing these interfering power results, the corresponding PSDs over the range of center frequencies considered are shown in Fig. A.16. For these results, the center frequency of the UWB signal was established as 5.775 GHz and its pulse width was $1.73/f_c \approx 0.3$ ns.

Figure A.17 and Fig. A.18 show varying in-band interfering power for TH-PPM and DS-UWB waveforms, respectively, operating at maximum authorized UWB power

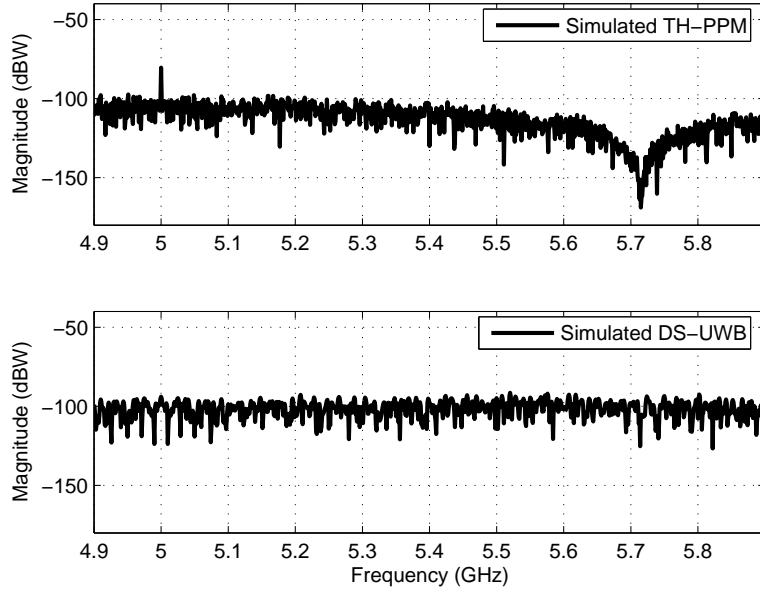


Figure A.16: TH-PPM (top) and DS-UWB (bottom) PSD responses from Fig. A.14 and Fig. A.15, respectively, over frequency range spanning the U-NII frequency bands.

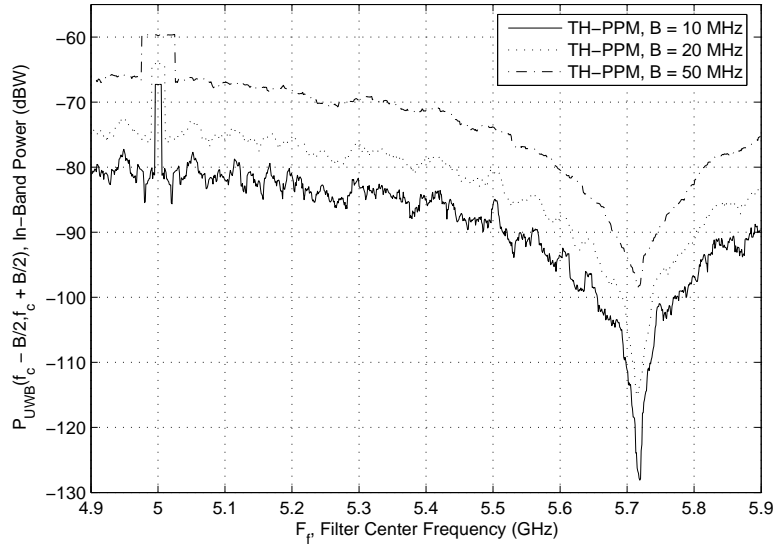


Figure A.17: In-band interfering TH-PPM signal power for PSD shown in Fig. A.16. Interfering P_{UWB} (dB) versus ideal filter center frequency F_f for three bandwidths B (neglecting path loss).

levels. In both cases, the results reflect a natural dependence on PSD shape (compare with Fig. A.16) and SOI receiver filter characteristics. As the center frequency of the

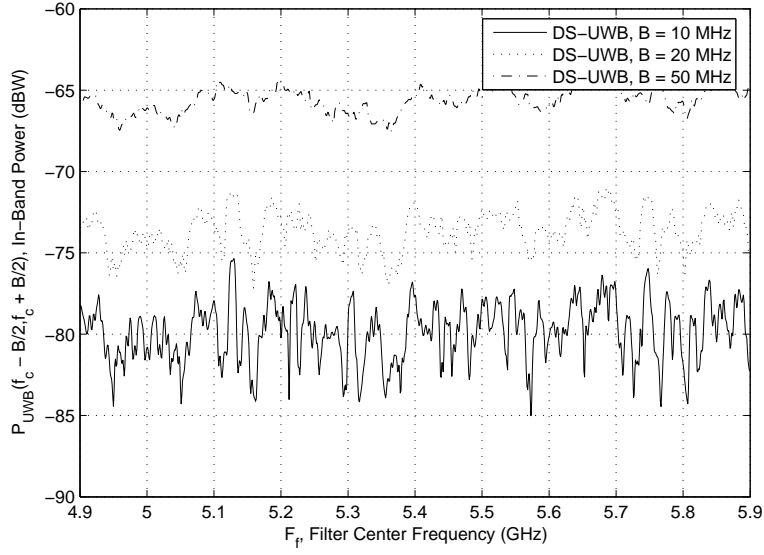


Figure A.18: In-band interfering DS-UWB signal power for PSD from Fig. A.16. Interfering P_{UWB} (dB) versus ideal filter center frequency F_f for three bandwidths B (neglecting path loss).

SOI receiver filter varies, the in-band interfering power generally follows the spectral shape of the PSDs. As the bandwidth of the SOI receiver filter increases, the filtering has the effect of smoothing the PSD responses. Assuming the SOI receiver is part of an 802.11a WLAN network operating in a U-NII band with 20 MHz bandwidth, the in-band interfering power of the TH-PPM and DS-UWB signals could be as large as -74.0 dBW (TH-PPM) and -71.0 dBW (DS-UWB). Depending on network topology and environmental conditions, such interfering power levels could exceed noise floor levels and potentially impact SOI receiver operation.

A.4.6 Summary of In-Band Power Analysis. Two temporal MA techniques are emerging as strong contenders for 4G UWB implementation, namely TH-UWB and DS-UWB. The analytic PSD for each of these UWB-MA techniques is provided based on recent research [71, 218, 242]. For the TH-PPM PSD, the weight of discrete spectral lines, uniformly spaced $1/T_{sym}$ apart, is directly impacted by the number of communication symbols in the UWB signal and time coding randomness. For the DS-UWB PSD, discrete spectral lines are weighted according to the mean of a modified

PR sequence. In both cases, the ESD of the fundamental UWB waveform $\Psi_w(f)$ plays a key role in spectral analysis, especially in defining the shape of the resultant PSDs. UWB system operation “near” (spatially and/or spectrally) coexistent narrow band systems can potentially degrade performance based on in-band power characteristics.

Ideal RF filter results are presented that indicate degradation is possible from both TH-PPM and DS-UWB waveforms, with the degree of degradation dependent upon the PSD shape, maximum allowed transmit power, transmitter-receiver separation distance, relative center frequency offset, and relative bandwidths.

A.5 Spectral Coexistence Scenarios: Bit Error Rate (BER) Analysis

The analysis in this section focuses on coexistence of TH-PPM and DS-UWB UWB-MA networks with narrowband WLAN signals, based primarily upon IEEE 802.11b specifications. Previous UWB coexistence research has 1) characterized UWB interference *upon* narrowband systems [19, 35, 68, 129, 216], 2) focused on power comparisons rather than bit error rate performance [11, 68, 77, 115, 242], 3) focused solely on MA performance without considering interference [25, 86], or 4) did not specifically consider 802.11b specifications for a WLAN narrowband interferer [11, 26, 51, 54, 77, 78, 241]. There appears to be limited work, if any, that *simultaneously* addresses the coexistence (as measured by BER) of TH-UWB and DS-UWB synchronous and asynchronous networks with an 802.11b signal in a MA environment.

A.5.1 Narrowband WLAN Signal. The coexisting narrowband WLAN signal is modeled here as an IEEE 802.11b signal constructed in accordance with [110]. As such, it uses three non-overlapping channels (1, 6, 11) at 2412, 2437, and 2462 MHz in accordance with FCC requirements. Each channel contains a direct sequence spread spectrum (DS-SS) signal modulated using differential quaternary phase shift keying (DQPSK) in conjunction with complementary code keying to achieve a channel data rate of 11 Mb/s. Two 802.11b signals are considered, including 1) an “offset” signal operating at the frequencies described above, and 2) a “centered” signal operating in

the lower U-NII band. This “centered” signal is spectrally located closer to the UWB peak PSD response (5 GHz) on channels 36, 40, and 44 (i.e., 5180, 5200, and 5220 MHz).

A.5.2 Interference-to-Signal (I/S) Ratio. In-band interference power at a UWB receiver from a nearby 802.11b signal can be calculated by integrating its PSD over the frequency band of interest – see Section A.4. This interference power is compared to the received power from the UWB SOI, the PSD of which is given by (A.26) or (A.30). Narrowband WLAN interference effects upon a UWB receiver are quantified in this section using an interference-to-signal (I/S) ratio. I/S ratios are increased from 0 to 20 dB in 2 dB increments and corresponding BER performance is estimated for asynchronous and synchronous networks using TH-UWB and DS-UWB signals. An I/S of 20 dB at UWB receiver is assumed realistic given the restrictive UWB transmit power spectral masks (low UWB transmit power) and the close proximity of WPAN devices (low interferer path loss).

Figures A.19 and A.21 show the BER performance as a function of I/S ratio for TH-PPM networks with 1 and 12 users, respectively. Corresponding information is shown in Figures A.20 and A.22 for DS-UWB signals. Asynchronous and synchronous results are identical for $N_U = 1$ given there are no additional MA users in the system. When $N_U = 12$, synchronous and asynchronous results differ at low I/S ratios because the MA interference (MAI) dominates the error. As the interference power increases, the synchronous and asynchronous results merge because the WLAN narrowband interference (NBI) (versus MAI) becomes the dominant source of error.

By comparing Fig. A.19 and Fig. A.20 results, the frequency of the coexisting 802.11b signal appears to have a greater influence on P_b for TH-PPM than for DS-UWB. As an 802.11b signal shifts in frequency from the 2.4 GHz band to the lower U-NII band, TH-PPM results in Fig. A.19 indicate the system must transmit 10 to 15 dB more power to achieve similar BER performance in the presence of the coexisting signal. However, DS-UWB results in Fig. A.20 indicate the system only requires

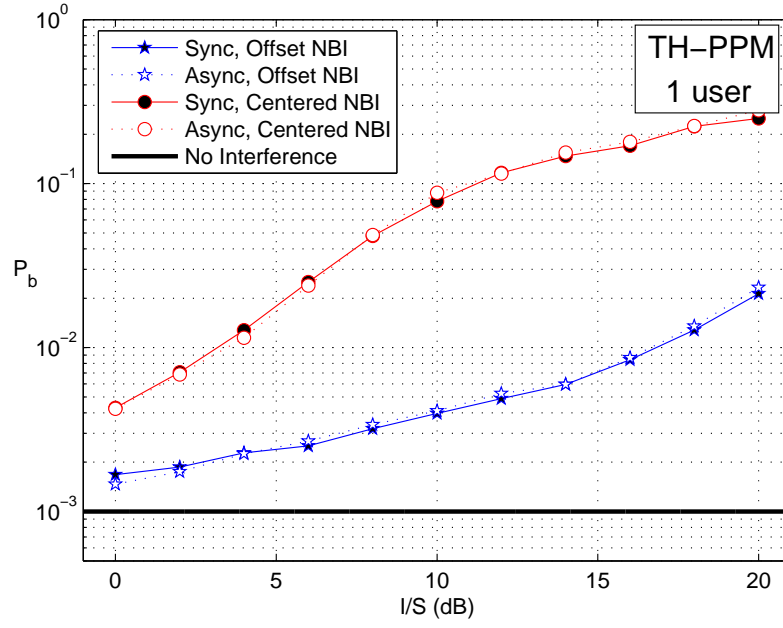


Figure A.19: Impact of WLAN interference on $N_U = 1$ user *TH-PPM*: P_b vs I/S for different interferer frequencies and networks.

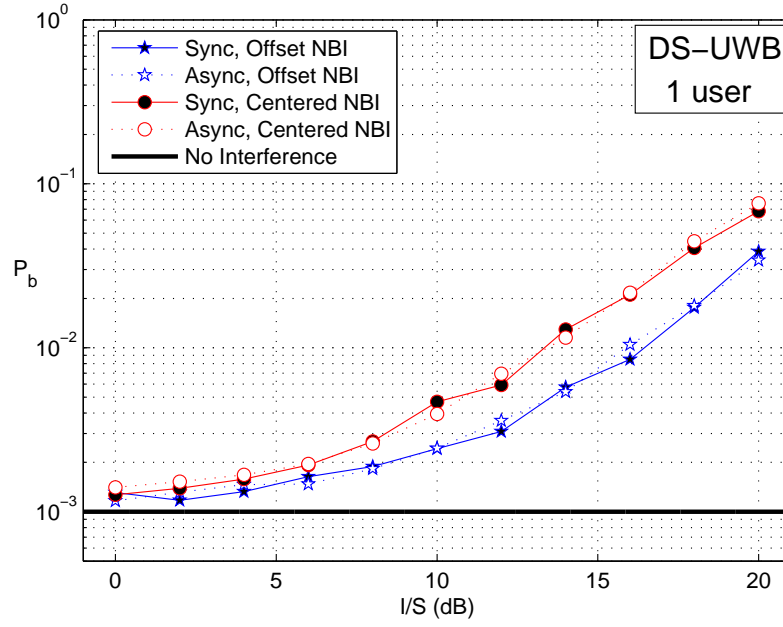


Figure A.20: Impact of WLAN interference on $N_U = 1$ user *DS-UWB*: P_b vs I/S for different interferer frequencies and networks.

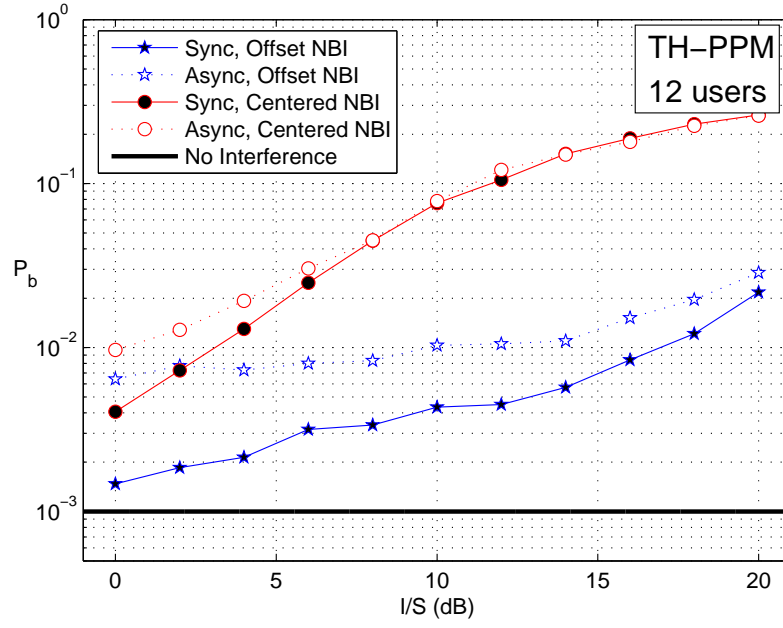


Figure A.21: Impact of WLAN interference on $N_U = 12$ users *TH-PPM*: P_b vs I/S for different interferer frequencies and networks.

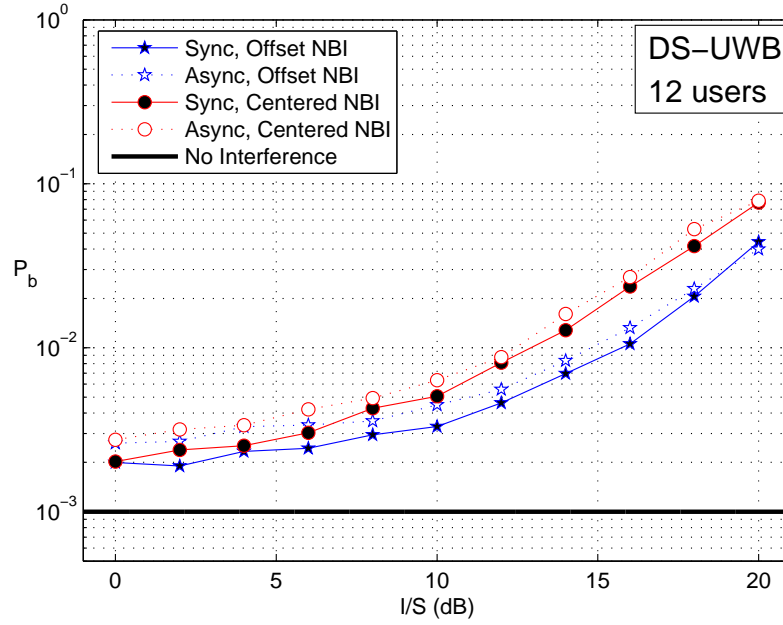


Figure A.22: Impact of WLAN interference on $N_U = 12$ users *DS-UWB*: P_b vs I/S for different interferer frequencies and networks.

2 to 4 dB more power to achieve similar BER performance in the presence of the coexisting signal under an identical frequency shift. This result could be due in part to the flatter PSD response of a DS-UWB signal. While the DS-UWB systems appear to be more robust in the presence of interference at low I/S ratios, as interference power increases in an offset 802.11b signal, TH-PPM systems become marginally more attractive, i.e., the P_b of DS-UWB at $I/S = 20$ dB with an offset NBI is about twice the P_b of TH-PPM in the same scenario. These results support the hypotheses that, 1) concentrated interference power near 2.4 GHz (spectrally located away from the UWB f_c) degrades TH-PPM P_b performance less than equivalent interference power spread over the entire UWB signal bandwidth, and 2) a DS-UWB system is more susceptible to concentrated DS-SS interference power than the equivalent interfering power distributed across the entire UWB signal bandwidth.

Given the baseline MA performance provided in Fig. A.9 and the UWB coexistence performances shown in Fig. A.19 through Fig. A.22, the next logical step is to analyze UWB-MA network performance in the presence of various interfering signals as a function of the number of users.

A.5.3 UWB Coexistence with Narrowband WLAN in Multiple Access Environment. TH-UWB and DS-UWB coexistence with a narrowband 802.11b signal is now evaluated in synchronous and asynchronous networks having up to 12 users at three I/S values, including 6 dB, 12 dB, and $-\infty$ dB (i.e., no interference present).

Figures A.23 and A.24 show multiple access performance for TH-PPM synchronous and asynchronous networks, respectively. As expected, performance degrades as interfering power increases or as the interfering signal is spectrally located closer to the maximum UWB spectral response. For synchronous networks, an offset 802.11b signal increases P_b by factors of $2.4\times$ and $4.4\times$ for I/S levels of 6.0 and 12.0 dB, respectively, and a centered 802.11b signal raises the P_b by factors of $22.5\times$ and $102.9\times$ for I/S levels of 6.0 and 12.0 dB, respectively. Similar degradation factors are noted for asynchronous networks with few users. However, as the number of users

increases, the degradation decreases because of the higher baseline P_b , a result of greater MAI caused by more collisions. Note that once WLAN NBI dominates MAI (or the interferer is more concentrated in the UWB spectrum), the P_b performance stabilizes and becomes more predictable.

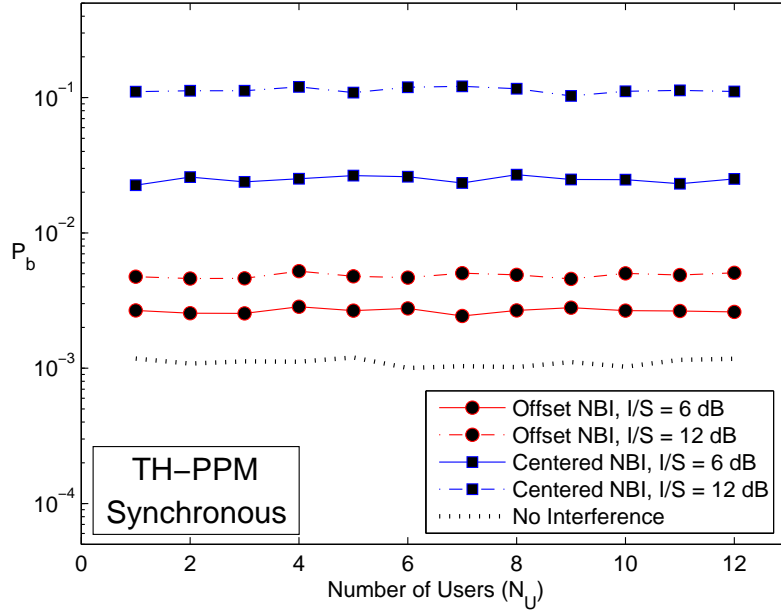


Figure A.23: Multiple access performance in a *TH-PPM Synchronous* network for different narrowband interference characteristics.

Figures A.25 and A.26 show multiple access performance for DS-UWB synchronous and asynchronous networks, respectively. As expected, performance degrades as interfering power increases or as the interfering signal is positioned more closely to the maximum UWB spectral response, although not as much as noted in the TH-PPM networks. For synchronous and asynchronous DS-UWB networks, an offset 802.11b signal degrades P_b by factors of $1.2\times$ to $1.6\times$ and $2.1\times$ to $4.8\times$ for I/S levels of 6.0 and 12.0 dB, respectively, and a centered 802.11b signal raises the P_b by factors of $1.6\times$ to $1.7\times$ and $3.4\times$ to $6.3\times$ for I/S levels of 6.0 and 12.0 dB, respectively.

Overall, the DS-UWB system appears more robust in the presence of interference in a MA environment, i.e., its inherent processing gain provides additional protection

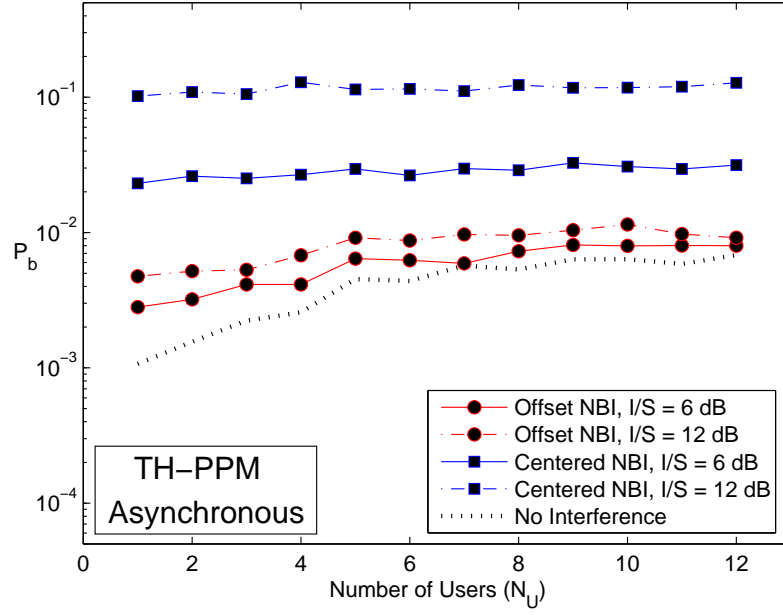


Figure A.24: Multiple access performance in a *TH-PPM Asynchronous* network for different narrowband interference characteristics.

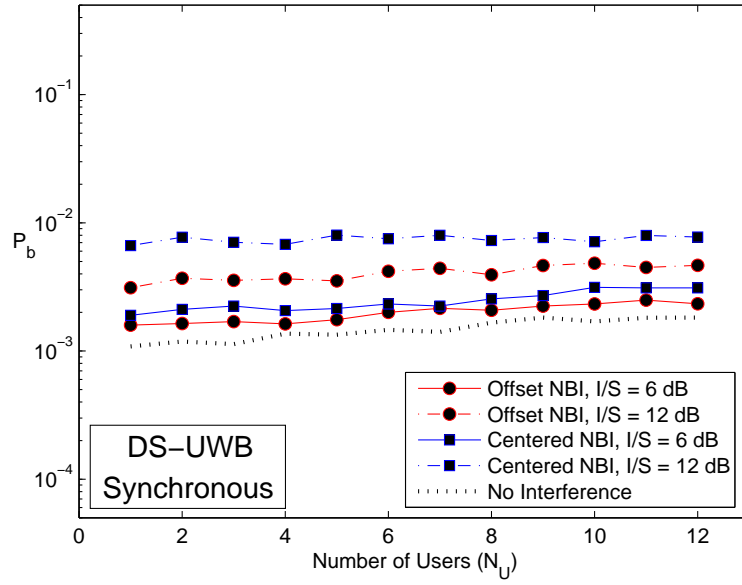


Figure A.25: Multiple access performance in a *DS-UWB Synchronous* network for different narrowband interference characteristics.

against spectrally *centered* coexisting signals which is not reflected in TH-PPM results. Additionally, although the DS-UWB system appears to be *slightly* more affected by

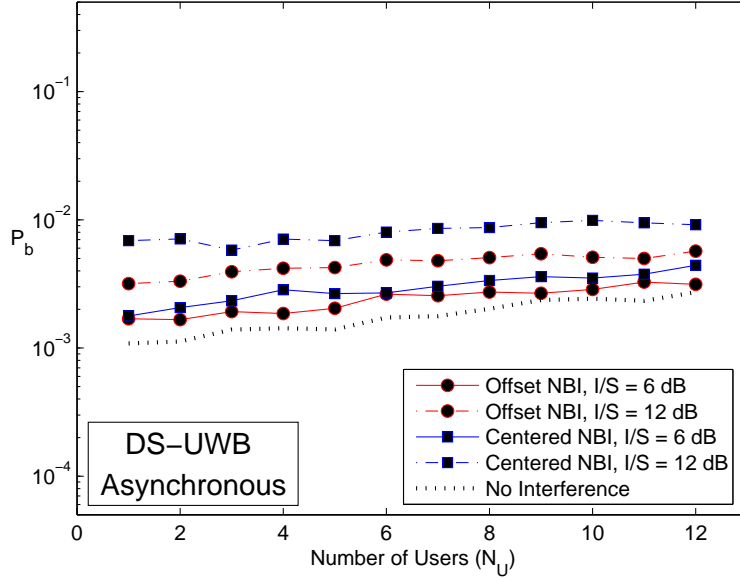


Figure A.26: Multiple access performance in a *DS-UWB Asynchronous* network for different narrowband interference characteristics.

spectrally *offset* coexisting signals (i.e., there is a maximum $6.3\times$ increase in P_b for DS-UWB versus a maximum $4.4\times$ increase in P_b for TH-PPM), its stronger performance amidst asynchronously arriving MA signals results in lower overall P_b . In other words, the TH-PPM and DS-UWB systems reflect similar BER performance in synchronous, 12-user networks when an offset coexisting signal is present; however, the DS-UWB system reflects lower BER performance in asynchronous, 12-user networks when an offset coexisting signal is present.

A.5.4 Summary of Bit Error Rate Analysis. Coexistence of TH-UWB and DS-UWB multiple access networks with narrowband WLAN signals is characterized using BER (P_b) as the criterion. The TH-UWB signal is obtained by combining PPM data modulation with pseudorandom time coding. Conversely, the DS-UWB signal is obtained by combining BPSK data modulation with PR phase coding. Multiple access performance is evaluated for synchronous and asynchronous networks containing up to 12 users. With the introduction of a narrowband 802.11b interfering signal, advantages provided by Gold coding in a synchronous network quickly diminish; the

degradation from interference results in approximately equivalent performance in both synchronous and asynchronous networks. However, in both cases this degradation can be minimized by introducing processing gain ($N_{ss} > 1$) into the system, i.e., by coherently processing multiple replicas of transmitted communication symbols, provided the processing gain is sufficient to overcome the impact of interfering signal power at the UWB receiver. Results indicate DS-UWB systems are more robust in the presence of a centered 802.11b coexisting signal, and their inherent MAI-suppression gives them better overall performance in the presence of an offset 802.11b coexisting signal.

Bibliography

1. “3G Today Home Page”. URL <http://www.3gtoday.com>.
2. 3GPP2. “CDMA2000 High Rate Packet Data Interface Specification”. C.S0024-B v2.0, August 2005.
3. Agathangelou, M. C. “Comparing Current and Emerging CDMA Forward Link PHYs”. *CommsDesign*, November 12, 2003. URL <http://www.commsdesign.com/>.
4. Ahmadi, S. and M. Jelinek. “On the Architecture, Operation, and Applications of VMR-WB: The New cdma2000 Wideband Speech Coding Standard”. *IEEE Commun. Mag.*, 44(5):74–81, May 2006.
5. Akyildiz, I. F., S. Mohanty, and J. Xie. “A Ubiquitous Mobile Communication Architecture for Next-Generation Heterogeneous Wireless Systems”. *IEEE Commun. Mag.*, 43(6):S29–S36, June 2005.
6. Al-Muhtadi, J., D. Mickunas, and R. Campbell. “A Lightweight Reconfigurable Security Mechanism for 3G/4G Mobile Devices”. *IEEE Wireless Commun. Mag.*, 9(2):60–65, April 2002.
7. Alexiou, A. and M. Haardt. “Smart Antenna Technologies for Future Wireless Systems: Trends and Challenges”. *IEEE Commun. Mag.*, 42(9):90–97, September 2004.
8. Andren, C. F., L. V. Lucas, and J. A. Schachte. “Low Probability-of-Intercept Communication System”. Harris Corp., U.S. Patent 5 029 184, July 1991.
9. Apostol, T. M. *Mathematical Analysis*. Addison Wesley Longman, Reading, MA, 2nd edition, 1974.
10. Badgett, C. D. *Performance Evaluation of Automated Digital Modulation Recognition Algorithms*. Master’s thesis, Air Force Institute of Technology, 2006.
11. Bellorado, J., S. S. Ghassemzadeh, L. J. Greenstein, T. Sveinsson, and V. Tarokh. “Coexistence of Ultra-wideband Systems with IEEE 802.11a Wireless LANs”. *IEEE Conf. on Global Commun. (GLOBECOM)*, vol. 1, 410–414. San Francisco, CA, December 2003.
12. Benedetto, S., D. Divsalar, G. Montorsi, and F. Pollara. “Serial Concatenation of Interleaved Codes: Performance analysis, Design, and Iterative Decoding”. *IEEE Trans. Inform. Theory*, 44(3):909–926, May 1998.
13. Benedetto, S. and G. Montorsi. “Design of Parallel Concatenated Convolutional Codes”. *IEEE Trans. Commun.*, 44(5):591–600, May 1996.

14. Benedetto, S. and G. Montorsi. “Unveiling Turbo Codes: Some Results on Parallel Concatenated Coding Schemes”. *IEEE Trans. Inform. Theory*, 42(2):409–428, March 1996.
15. Berrou, C. and A. Glavieux. “Near Optimum Error Correcting Coding and Decoding: Turbo-Codes”. *IEEE Trans. Commun.*, 44(10):1261–1271, October 1996.
16. Berrou, C., A. Glavieux, and P. Thitimajshima. “Near Shannon Limit Error-Correcting Coding and Decoding: Turbo-Codes”. *IEEE Int’l Conf. on Commun. (ICC)*, vol. 2, 1064–1070. Geneva, Switzerland, May 1993.
17. Bi, Q., G. I. Zysman, and H. Menkes. “Wireless Mobile Communications at the Start of the 21st Century”. *IEEE Commun. Mag.*, 39(1):110–116, January 2001.
18. Bokolamulla, D. and T. Aulin. “Reduced Complexity Iterative Decoding for Concatenated Coding Schemes”. *IEEE Int’l Conf. on Commun. (ICC)*, vol. 5, 3135–3139. Anchorage, AK, May 2003.
19. Borah, D. K., R. Jana, and A. Stamoulis. “Performance Analysis of IEEE 802.11a Wireless LANs in the Presence of Ultra-wideband Interference”. *IEEE Wireless Commun. and Networking Conf. (WCNC)*, vol. 1, 83–87. New Orleans, LA, March 2003.
20. Boubaker, N. and K. B. Letaief. “Performance Analysis of DS-UWB Multiple Access Under Imperfect Power Control”. *IEEE Trans. Commun.*, 52(9):1459–1463, September 2004.
21. Buracchini, E. “The Software Radio Concept”. *IEEE Commun. Mag.*, 38(9):138–143, September 2000.
22. “Call for Papers - 4G Wireless Systems”. *IEEE Commun. Mag.*, 42(8):S47, August 2004.
23. Canadeo, C. M. *Ultra Wide Band Multiple Access Performance Using TH-PPM and DS-BPSK Modulations*. Master’s thesis, Air Force Institute of Technology, 2003.
24. Canadeo, C. M., M. A. Temple, R. O. Baldwin, and R. A. Raines. “Code Selection for Enhancing UWB Multiple Access Communication Performance Using TH-PPM and DS-BPSK Modulations”. *IEEE Wireless Commun. and Networking Conf. (WCNC)*, vol. 1, 678–682. New Orleans, LA, March 2003.
25. Canadeo, C. M., M. A. Temple, R. O. Baldwin, and R. A. Raines. “UWB Multiple Access Performance in Synchronous and Asynchronous Networks”. *IEE Electronics Letters*, 39(11):880–882, May 2003.
26. Cano, E. and S. McGrath. “TH-UWB and DS-UWB in Lognormal Fading Channel and 802.11a Interference”. *IEEE Conf. on Personal, Indoor and Mobile Radio Commun. (PIMRC)*, vol. 4, 2978–2982. Barcelona, Spain, September 2004.

27. Cassioli, D., M. Z. Win, and A. F. Molisch. "The Ultra-Wide Bandwidth Indoor Channel: From Statistical Model to Simulations". *IEEE J. Select. Areas Commun.*, 20(6):1247–1257, August 2002.
28. Chakravarthy, V., A. K. Shaw, M. A. Temple, A. S. Nunez, and J. P. Stephens. "TDCS, OFDM and MC-CDMA: A Brief Tutorial". *IEEE Commun. Mag.*, 43(9):S11–S16, September 2005.
29. Chakravarthy, V. D., A. K. Shaw, M. A. Temple, and J. P. Stephens. "Cognitive Radio – An Adaptive Waveform with Spectral Sharing Capability". *IEEE Wireless Commun. Networking Conf. (WCNC)*. New Orleans, LA, March 2005.
30. Chandran, N. and M. C. Valenti. "Three Generations of Cellular Wireless Systems". *IEEE Potentials*, 20(1):32–35, Feb.-Mar. 2001.
31. Chang, R. W. "Synthesis of Band-Limited Orthogonal Signals for Multichannel Data Transmission". *Bell Syst. Tech. J.*, 45:1775–1796, December 1966.
32. Chang, R. W. "Orthogonal Frequency Division Multiplexing". U.S. Patent 3 488 445, January 1970.
33. Chatterjee, S., W. A. C. Fernando, and M. K. Wasantha. "Adaptive Modulation Based MC-CDMA Systems for 4G Wireless Consumer Applications". *IEEE Trans. Consumer Electron.*, 49(4):995–1003, November 2003.
34. Cherry, S. M. "The Wireless Last Mile". *IEEE Spectr.*, 40(9):18–22, September 2003.
35. Choi, S.-S. and W.-J. Oh. "Analysis the Interference of Pulse Position Modulated UWB into IEEE 802.11a WLAN". *Joint IEEE Conf. on UWB Sys. and Tech. (UWBST) and Int'l Workshop on UWB Sys. (IWUWBS)*, 328–331. Kyoto, Japan, May 2004.
36. Cimini, L. J., Jr. "Analysis and Simulation of a Digital Mobile Channel Using Orthogonal Frequency Division Multiplexing". *IEEE Trans. Commun.*, COM-33(7):665–675, July 1985.
37. Clabaugh, D. J. *Characterization of Ultra Wideband Multiple Access Performance Using Time-Hopped Biorthogonal Pulse Position Modulation*. Master's thesis, Air Force Institute of Technology, 2004.
38. Clabaugh, D. J., M. A. Temple, R. A. Raines, and C. M. Canadeo. "UWB Multiple Access Performance Using Time Hopped Pulse Position Modulation with Biorthogonal Signaling". *IEEE Conf. on UWB Sys. and Tech. (UWBST)*, 330–333. Reston, VA, November 2003.
39. Costlow, T. "Cognitive Radios will Adapt to Users". *IEEE Intell. Syst.*, 18(3):7, May-June 2003.
40. Daneshgaran, F., M. Laddomada, and M. Mondin. "Interleaver Design for Serially Concatenated Convolutional Codes: Theory and Application". *IEEE Trans. Inform. Theory*, 50(6):1177–1188, June 2004.

41. *Detailed Specification of the Radio Interfaces of International Mobile Telecommunications - 2000 (IMT-2000)*. ITU-R Rec. M.1457, May 2000.
42. Dornan, Andy. "Mobile Satellite Services: From Third World to Third Generation". *IT Architect Mag.*, July 7, 2002. URL <http://www.itarchitect.com/>.
43. *EDGE: Introduction of High-Speed Data in GSM/GPRS Networks*. White paper, Ericsson, 2003.
44. Ellis, J., K. Siwiak, and R. Roberts. *TG3a Technical Requirements*. IEEE Report P802.15-03/030r0, December 2002.
45. Emery, T. "Cell phones: Hot/cold affair". *The Cincinnati Enquirer*, January 21, 2004.
46. Engels, M. (editor). *Wireless OFDM Systems: How to Make Them Work?*, chapter 3. Kluwer Academic Publishers, Boston, MA, 2002.
47. "ENTC 455, Wireless Transmission Systems". Online Class Notes, Spring 2006. URL <http://etidweb.tamu.edu/classes/entc455/Lectures.html>. Texas A&M Univ.
48. "The Evolution to 3G Mobile – Status Report". *International Telecommunication Union (ITU) News Mag.*, July 29, 2003.
49. Falahati, S., A. Svensson, T. Ekman, and M. Sternad. "Adaptive Modulation Systems for Predicted Wireless Channels". *IEEE Trans. Commun.*, 52(2):307–316, February 2004.
50. Falconer, D. D., F. Adachi, and B. Gudmundson. "Time Division Multiple Access Methods for Wireless Personal Communications". *IEEE Commun. Mag.*, 33(1):50–57, January 1995.
51. Firoozbakhsh, B., T. G. Pratt, and N. Jayant. "Analysis of IEEE 802.11a interference on UWB systems". *IEEE Conf. on UWB Sys. and Tech. (UWBST)*, 473–477. Reston, VA, November 2003.
52. "First Report and Order: Revision of Part 15 of the Commission's Rules Regarding Ultra-wideband Transmission Systems". ET Docket 98-153. Federal Communications Commission, Government Printing Office, Washington DC, April 2002.
53. Foerster, J., ed. "Channel Modeling Sub-committee Report Final". IEEE P802.15-02/490r1-SG3a, February 2003. URL <http://ieee802.org/15/>.
54. Foerster, J. R. "The Performance of a Direct-Sequence Spread Spectrum Ultra-wideband System in the Presence of Multipath, Narrowband Interference, and Multiuser Interference". *IEEE Conf. on UWB Sys. and Tech. (UWBST)*, 87–91. Baltimore, MD, May 2002.
55. Forney, G. D., Jr. *Concatenated Codes*. MIT Press, Cambridge, MA, 1966.

56. Forouzan, A. R., M. Nasiri-kenari, and J. A. Salehi. "Performance Analysis of Ultrawideband Time-Hopping Code Division Multiple Access Systems: Uncoded and Coded Schemes". *IEEE Int'l Conf. on Commun. (ICC)*, vol. 10, 3017–3021. St. Petersburg, Russia, June 2001.
57. Fu, X., D. Hogrefe, S. Narayanan, and R. Soltwisch. "QoS and Security in 4G Networks". *Proc. 1st CIC/IEEE Global Mobile Congress (GMC)*, 117–122. Shanghai, China, October 2004.
58. Futaki, H. and T. Ohtsuki. "Low-density parity-check (LDPC) coded OFDM systems". *IEEE Vehicular Tech. Conf. (VTC)*, vol. 1, 82–86. Atlantic City, NJ, October 2001.
59. Gallager, R. G. "Low-Density Parity-Check Codes". *IRE Trans. Inform. Theory*, 21–28, January 1962.
60. Gaona, C. M. *Performance of a Spectrally Encoded Multi-Carrier Phase Shift Keying Communication System in a Frequency-Selective, Slowly-Fading Multipath Channel*. Master's thesis, Air Force Institute of Technology, 2005.
61. Gast, M. *802.11 Wireless Networks: The Definitive Guide*, 164–213. O'Reilly, Sebastopol, CA, 2002.
62. Gatherer, A. *14th VA Tech/MPRG Symposium on Wireless Personal Commun.* Blacksburg, VA, June 10, 2004. Speaker's luncheon.
63. Geraniotis, E. and B. Ghaffari. "Performance of Binary and Quaternary Direct-Sequence Spread-Spectrum Multiple-Access Systems with Random Signature Sequences". *IEEE Trans. Commun.*, 39(5):713–724, May 1991.
64. German, E. H. *Transform Domain Signal Processing Study Final Report*. Technical Report, Contract: Air Force F30602-86-C-0133, Reistertown, MD, August 1988.
65. Ghassemzadeh, S. S., R. Jana, C. W. Rice, W. Turin, and V. Tarokh. "Measurement and Modeling of an Ultra-Wide Bandwidth Indoor Channel". *IEEE Trans. Commun.*, 52(10):1786–1796, October 2004.
66. Ghosh, A., D. R. Wolter, J. G. Andrews, and R. Chen. "Broadband Wireless Access with WiMax/802.16: Current Performance Benchmarks and Future Potential". *IEEE Commun. Mag.*, 43(2):129–136, February 2005.
67. Giuliano, R., G. Guidoni, F. Mazzenga, and F. Vatalaro. "On the UWB Coexistence with UMTS Terminals". *IEEE Int'l Conf. on Commun. (ICC)*, vol. 6, 3571–3575. Paris, France, June 2004.
68. Giuliano, R. and F. Mazzenga. "On the Coexistence of Power-Controlled, Ultrawide-Band Systems with UMTS, GPS, DCS1800, and Fixed Wireless, Systems". *IEEE Trans. Veh. Technol.*, 54(1):62–81, January 2005.

69. Glen, M. G. *Multiple Access Interference Characterization for Direct-Sequence Spread-Spectrum Communications Using Chip Waveform Shaping*. Master's thesis, Air Force Institute of Technology, 2004.
70. Glossner, J., D. Iancu, J. Lu, E. Hokenek, and M. Moudgill. "A Software-Defined Communications Baseband Design". *IEEE Commun. Mag.*, 41(1):120–128, January 2003.
71. Gronholz, B. D. *Non-cooperative Detection of Ultra Wideband Signals*. Master's thesis, Air Force Institute of Technology, 2004.
72. Gudmundson, M. "UTRA". *TIA Wireless Info. Session '98*. Minneapolis, MN, October 1998.
73. Guizzo, E. "Closing in on the Perfect Code". *IEEE Spectr.*, 41(3):36–42, March 2004.
74. Hachman, M. "Freescale Pulls Out of UWB Forum to Focus on Cable Free". *ExtremeUWB*, April 06, 2006. URL <http://www.extremeuwb.com/>.
75. Hachman, M. "UWB Standards Group Calls It Quits". *ExtremeUWB*, January 19, 2006. URL <http://www.extremeuwb.com/>.
76. Haghighat, A. "A Review on Essentials and Technical Challenges of Software Defined Radio". *IEEE Conf. on Military Commun. (MILCOM)*, vol. 1, 377–382. Anaheim, CA, October 2002.
77. Hamalainen, M., V. Hovinen, R. Tesi, J. J. J. Iinatti, and M. Latva-aho. "On the UWB System Coexistence with GSM900, UMTS/WCDMA, and GPS". *IEEE J. Select. Areas Commun.*, 20(9):1712–1721, December 2002.
78. Hamalainen, M., R. Tesi, and J. Iinatti. "UWB Coexistence with IEEE 802.11a and UMTS in Modified Saleh-Valenzuela Channel". *Joint IEEE Conf. on UWB Sys. and Tech. (UWBST) and Int'l Workshop on UWB Sys. (IWUWBS)*, 45–49. Kyoto, Japan, May 2004.
79. Hanson, W. "Georgia County Pilots WiMAX Wireless Network". *Government Technology*, July 9, 2004. URL <http://www.govtech.net/>.
80. Hanzo, L., M. Münster, B. J. Choi, and T. Keller. *OFDM and MC-CDMA for Broadband Multi-User Communications, WLANs and Broadcasting*. John Wiley & Sons, Inc., 2003.
81. Haraldsvik, R. "Two Worlds Come Together Over IP". *Wireless Week*, 31, June 15, 2004.
82. Haykin, S. "Cognitive Radio: Brain-Empowered Wireless Communications". *IEEE J. Select. Areas Commun.*, 23(2):201–220, February 2005.
83. Hoor, R. and H. Tomlinson. "Delay-Hopped Transmitted-Reference RF Communications". *IEEE Conf. on UWB Sys. and Tech. (UWBST)*, 265–269. Baltimore, MD, May 2002.

84. "Home Networks – Implementation and Standards". *IEEE Consumer Commun. and Networking Conf. (CCNC)*. Las Vegas, NV, January 4, 2005. Panel Sess. 4.
85. "HSDPA and Beyond". Nortel White Paper, 2005.
86. Hu, B. and N. C. Beaulieu. "Accurate Evaluation of Multiple Access Performance in TH-PPM and TH-BPSK UWB Systems". *IEEE Trans. Commun.*, 52(10):1758–1766, October 2004.
87. Huang, X. and Y. Li. "Generating Near-White Ultra-wideband Signals with Period Extended PN Sequences". *IEEE Vehicular Tech. Conf. (VTC)*, vol. 2, 1184–1188. Rhodes, Greece, May 2001.
88. Hui, S. Y. and K. H. Yeung. "Challenges in the Migration to 4G Mobile Systems". *IEEE Commun. Mag.*, 41(12):54–59, December 2003.
89. "IEEE 802.15 WPAN High Rate Alternative PHY Task Group 3a (TG3a) Home Page". URL <http://www.ieee802.org/15/pub/TG3a.html>.
90. Im, S. and E. J. Powers. "An Iterative Decorrelating Receiver for DS-UWB Multiple Access Systems Using Biphase Modulation". *IEEE Workshop on Signal Processing Sys. (SIPS)*, 59–64, October 2004.
91. "IMT-2000 Project". URL <http://www.itu.int/osg/imt-project/>. Int'l Telecommunication Union website.
92. Jain, A. K. *Fundamentals of Digital Image Processing*, 141–157. Prentice Hall, Upper Saddle River, NJ, 1989.
93. Jain, R. K. *The Art of Computer Systems Performance Analysis*. John Wiley & Sons, Inc., New York, NY, 1991.
94. Jamalipour, A., T. Wada, and T. Yamazato. "A Tutorial on Multiple Access Technologies for Beyond 3G Mobile Networks". *IEEE Commun. Mag.*, 43(2):110–117, February 2005.
95. "Joint Tactical Radio System (JTRS) Program". URL <http://jtrs.army.mil>.
96. "Joint Vision 2020". Chairman of the Joint Chiefs of Staff, Government Printing Office, Washington DC, June 2000. URL <http://www.dtic.mil/jointvision/>.
97. Jones, R. A., D. H. Smith, and S. Perkins. "Assignment of Spreading Codes in DS-CDMA UWB Systems". *IEEE Conf. on UWB Sys. and Tech. (UWBST)*, 359–363. Reston, VA, November 2003.
98. Jung, P., P. W. Baier, and A. Steil. "Advantages of CDMA and Spread Spectrum Techniques Over FDMA and TDMA in Cellular Mobile Radio Applications". *IEEE Trans. Veh. Technol.*, 42(3):357–364, August 1993.
99. Kim, Y. H., I. Song, H. G. Kim, T. Chang, and H. M. Kim. "Performance Analysis of a Coded OFDM System in Time-Varying Multipath Rayleigh Fading Channels". *IEEE Trans. Veh. Technol.*, 48(5):1610–1615, September 1999.

100. Kim, Y.-K. and B. K. Yi. "3G Wireless and CDMA2000 1× Evolution in Korea". *IEEE Commun. Mag.*, 43(4):36–40, April 2005.
101. Klein, R. W., M. A. Temple, R. A. Raines, and R. L. Claypoole, Jr. "Interference Avoidance Communications Using Wavelet Domain Transformation Techniques". *IEE Electronics Letters*, 37(15):987–989, July 19, 2001.
102. Kohno, R., M. Welborn, M. McLaughlin, and et. al. *DS-UWB Physical Layer Submission to 802.15 Task Group 3a*, July 2004.
103. Kölbl, A. *The Evolution from GSM to UMTS*. Master's thesis, Vienna Institute of Technology, 2001.
104. Kolding, T. E., F. Frederiksen, and P. E. Mogensen. "Performance Aspects of WCDMA Systems with High Speed Downlink Packet Access (HSDPA)". *IEEE Vehicular Tech. Conf. (VTC)*, vol. 1, 477–481. Vancouver, Canada, September 2002.
105. Kolding, T. E., K. I. Pedersen, J. Wigard, F. Frederiksen, and P. E. Mogensen. "High-Speed Downlink Packet Access: WCDMA Evolution". *IEEE Veh. Tech. Society (VTS) News*, 50(1):4–10, February 2003.
106. Kuramoto, M. and M. Shinji. "Second Generation Mobile Radio Telephone System in Japan". *IEEE Commun. Mag.*, 24(2):16–21, February 1986.
107. Kwon, H., Y. Kim, J.-K. Han, D. Kim, H. W. Lee, and Y. K. Kim. "Performance Evaluation of High-Speed Packet Enhancement on cdma2000 1×EV-DV". *IEEE Commun. Mag.*, 43(4):67–73, April 2005.
108. Kwon, S., K. Kim, Y. Yun, S. G. Kim, and B. K. Yi. "Power Controlled H-ARQ in CDMA2000 1×EV-DV". *IEEE Commun. Mag.*, 43(4):77–81, April 2005.
109. LAN/MAN Standards Committee of the IEEE Computer Society. *Part 11: Wireless LAN Medium Access Control (MAC) and Physical Layer (PHY) Specifications: High-Speed Physical Layer in the 5 GHz Band*, 1999.
110. LAN/MAN Standards Committee of the IEEE Computer Society. *Part 11: Wireless LAN Medium Access Control (MAC) and Physical Layer (PHY) Specifications: Higher-Speed Physical Layer Extension in the 2.4 GHz Band*, September 1999.
111. LAN/MAN Standards Committee of the IEEE Computer Society. *Part 11: Wireless LAN Medium Access Control (MAC) and Physical Layer (PHY) Specifications: Further Higher Data Rate Extension in the 2.4 GHz Band*, June 2003.
112. LAN/MAN Standards Committee of the IEEE Computer Society and IEEE Microwave Theory and Techniques Society. *Part 16: Air Interface for Fixed Broadband Wireless Access Systems*, April 2002.
113. LAN/MAN Standards Committee of the IEEE Computer Society and IEEE Microwave Theory and Techniques Society. *Part 16: Air Interface for Fixed*

Broadband Wireless Access Systems - Amendment 2: Medium Access Control Modifications and Additional Physical Layer Specifications for 2-11 GHz, April 2003.

114. LAN/MAN Standards Committee of the IEEE Computer Society and IEEE Microwave Theory and Techniques Society. *Part 16: Air Interface for Fixed Broadband Wireless Access Systems*, October 2004.
115. Lee, J.-H. and T.-J. Lee. "Design Issues of Ultra-wideband Systems for High-Rate Wireless PANs: Modulation Schemes and Coexistence with WLANs". *IEEE Topical Conf. on Wireless Commun. Tech.*, 459–460. Honolulu, HI, October 2003.
116. Lee, W. C. Y. "Overview of Cellular CDMA". *IEEE Trans. Veh. Technol.*, 40(2):291–302, May 1991.
117. Lee, W. C. Y. "CS-OFDMA: A New Wireless CDD Physical Layer Scheme". *IEEE Commun. Mag.*, 43(2):74–79, February 2005.
118. LeFevre, M. and P. Okrah. "Making the Leap to 4G Wireless". *CommsDesign*, July 1, 2001. URL <http://www.commsdesign.com/>.
119. LeFloch, B., M. Alard, and C. Berrou. "Coded Orthogonal Frequency Division Multiplex". *Proc. IEEE*, 83(6):982–996, June 1995.
120. Lehmann, N. and A. M. Haimovich. "New Approach to Control the Power Spectral Density of a Time Hopping UWB Signal". *Conference on Information Sciences and Sys. (CISS)*, March 2003.
121. Lehmann, N. and A. M. Haimovich. "The Power Spectral Density of a Time Hopping UWB Signal: A Survey". *IEEE Conf. on UWB Sys. and Tech. (UWBST)*, 234–239. Reston, VA, November 2003.
122. Li, Bo, D. Xie, S. Cheng, J. Chen, P. Zhang, W. Zhu, and Bin Li. "Recent Advances on TD-SCDMA in China". *IEEE Commun. Mag.*, 43(1):30–37, January 2005.
123. Li, W., T. A. Gulliver, and H. Zhang. "Performance and Ultra-Wideband Transmission with Biorthogonal Pulse Position Modulation over Multipath Fading Channels". *IEEE Int'l Conf. on UWB (ICUWB)*, 225–229. Zurich, Switzerland, September 2005.
124. Li, W., T. A. Gulliver, and H. Zhang. "Performance of Ultra-Wideband Transmission with Pulse Position Amplitude Modulation and RAKE Reception". *IEEE/ACES Wireless Commun. and Applied Computational Electromagnetics Conf.*, 1–4. Honolulu, HI, April 2005.
125. Linnartz, J.-P. M. G. "Performance Analysis of Synchronous MC-CDMA in Mobile Rayleigh Channel With Both Delay and Doppler Spreads". *IEEE Trans. Veh. Technol.*, 50(6):1375–1387, November 2001.

126. Lipman, J. "Wireless Enters the 4th(G) Dimension". *TechOnLine*, April 3, 2003. URL <http://www.techonline.com/>.
127. Locke, T., S. Nguyen, and D. Moreuil. "Dealing with the EDGE Evolution". *CommsDesign*, September 24, 2002. URL <http://www.commsdesign.com/>.
128. Lopez, J. *Analysis of Electromagnetic Interference of Ultra Wideband Signals*. Master's thesis, Air Force Institute of Technology, 2004.
129. Lopez, J., R. A. Raines, M. A. Temple, and R. O. Baldwin. "An Empirical Study of Electromagnetic Interference Caused by Ultra Wideband Transmissions in an IEEE 802.11a Wireless Local Area Network". *IEEE Radio and Wireless Conf. (RAWCON)*, 517–520. Atlanta, GA, September 2004.
130. Lundby, S. "High-Rate Data Communications Using CDMA2000 1×EV-DO and 1×EV-DV". *14th VA Tech/MPRG Symposium on Wireless Personal Commun.* Blacksburg, VA, June 9, 2004. Short course.
131. MacKay, D. J. C. "Good Error-Correcting Codes Based on Very Sparse Matrices". *IEEE Trans. Inform. Theory*, 45(2):399–431, March 1999.
132. Mannion, P. "Sharing Spectrum the Smarter Way". *CommsDesign*, April 5, 2004. URL <http://www.commsdesign.com/>.
133. Marek, S. "Vendors Ready HSDPA for Reality". *Wireless Week*, 8–9, March 15, 2005.
134. Martin, J. A. "What's Next for Wireless?" *PCWorld*, July 29, 2004. URL <http://www.pcworld.com/>.
135. Matthias, C. "Getting an Early Handle on 4G". *EE Times*, November 12, 2001. URL <http://www.eetimes.com/>.
136. Mazor, S. "The History of the Microcomputer-Invention and Evolution". *Proc. IEEE*, 83(12):1601–1608, December 1995.
137. McCorkle, J. *A Tutorial on Ultrawideband Technology*. submission to IEEE 802.15 task group 3a IEEE 802.15-00/082r1, March 2000.
138. Metroka, M. P. "An Introduction to Narrowband AMPS". *IEEE Conf. on Global Commun. (GLOBECOM)*, vol. 2, 1463–1468. December 1991.
139. Mielczarek, B., M.-O. Wessman, and A. Svensson. "Performance of Coherent UWB Rake Receivers with Channel Estimators". *IEEE Vehicular Tech. Conf. (VTC 2001)*, vol. 3, 1880–1884. Orlando, FL, October 2003.
140. Miller, S. K. "Facing the Challenge of Wireless Security". *IEEE Computer*, 34(7):16–18, July 2001.
141. Milstein, L. B. "Wideband Code Division Multiple Access". *IEEE J. Select. Areas Commun.*, 18(8):1344–1354, August 2000.

142. Mitola, J. "The Software Radio Architecture". *IEEE Commun. Mag.*, 33(5):26–38, May 1995.
143. Mitola, J., III. "Cognitive Radio for Flexible Mobile Multimedia Communications". *IEEE Int'l Workshop Mobile Multimedia Commun. (MoMuC)*, 3–10. San Diego, CA, November 1999.
144. Mittelbach, M., C. Muller, D. Ferger, and A. Finger. "Study of Coexistence Between UWB and Narrowband Cellular Systems". *Joint IEEE Conf. on UWB Sys. and Tech. (UWBST) and Int'l Workshop on UWB Sys. (IWUWBS)*, 40–44. Kyoto, Japan, May 2004.
145. Molisch, A. F., J. R. Foerster, and M. Pendergrass. "Channel Models for Ultrawideband Personal Area Networks". *IEEE Wireless Commun. Mag.*, 10(6):14–21, December 2003.
146. Nakache, Y.-P. and A. F. Molisch. "Spectral Shape of UWB Signals - Influence of Modulation Format, Multiple Access Scheme and Pulse Shape". *IEEE Vehicular Tech. Conf. (VTC)*, vol. 4, 2510–2514. Jeju, South Korea, April 2003.
147. Nassar, C. R., B. Natarajan, and S. Shattil. "Introduction of Carrier Interference to Spread Spectrum Multiple Access". *IEEE Emerging Technologies Symp.*, 4.1 – 4.5. Richardson, TX, April 1999.
148. Natarajan, B., C. R. Nassar, S. Shattil, M. Michelini, and Z. Wu. "High-Performance MC-CDMA via Carrier Interferometry Codes". *IEEE Trans. Veh. Technol.*, 50(6):1344–1353, November 2001.
149. Natarajan, B., Z. Wu, C. R. Nassar, and S. Shattil. "Large Set of CI Spreading Codes for High-Capacity MC-CDMA". *IEEE Trans. Commun.*, 52(11):1862–1866, November 2004.
150. *Network Centric Warfare*. Report to congress, Department of Defense, Washington, DC, July 31, 2001. URL <http://www.dod.mil/nii/NCW/>.
151. "Networking Will Drive ISR Success". *C4ISR Journal*, August 1, 2004. URL <http://www.isrjournal.com>.
152. "NeXt-Generation Communications". DARPA Program, 2006. URL <http://www.darpa.mil/ato/programs.htm>.
153. Ngo, C. "A Service-Oriented Wireless Home Network". *IEEE Consumer Commun. and Networking Conf. (CCNC)*, 618–620. Las Vegas, NV, January 2004.
154. Nunez, A. S., M. A. Temple, R. F. Mills, and R. A. Raines. "Interference Avoidance in Spectrally Encoded Multiple Access Communications Using MPSK Modulation". *IEEE Wireless Commun. and Networking Conf. (WCNC)*. New Orleans, LA, March 2005.
155. Ojala, P., A. Lakaniemi, H. Lepänaho, and M. Johimies. "The Adaptive Multirate Wideband Speech Codec: System Characteristics, Quality Advances, and Deployment Strategies". *IEEE Commun. Mag.*, 44(5):59–65, May 2006.

156. Oliphant, M. W. "Radio Interfaces Make the Difference in 3G Cellular Systems". *IEEE Spectr.*, 37(10):53–58, October 2000.
157. O'Shea, D. "Welcome to the Wireless Home". *Wireless Review*, December 1, 2004. URL <http://www.wirelessreview.com/>.
158. Ozdemir, M. K., E. Arvas, and H. Arslan. "Dynamics of Spatial Correlation and Implications on MIMO Systems". *IEEE Commun. Mag.*, 42(6):S14–S19, June 2004.
159. Padgett, J. E., C. G. Günther, and T. Hattori. "Overview of Wireless Personal Communications". *IEEE Commun. Mag.*, 33(1):28–41, January 1995.
160. Parr, B., B. Cho, K. Wallace, and Z. Ding. "A Novel Ultra-wideband Pulse Design Algorithm". *IEEE Commun. Lett.*, 7(5):219–221, May 2003.
161. Peterson, R. L., R. E. Ziemer, and D. E. Borth. *Introduction to Spread Spectrum Communications*. Prentice-Hall, Englewood Cliffs, NJ, 1995.
162. Porcino, D. and W. Hirt. "Ultra-wideband Radio Technology: Potential and Challenges Ahead". *IEEE Commun. Mag.*, 41(7):66–74, July 2003.
163. Prasad, A. and P. Schoo. "IP Security for Beyond 3G Towards 4G". *Proc. 7th Wireless World Research Forum (WWRF)*. Eindhoven, The Netherlands, December 2002.
164. Prasad, R. and S. Hara. "An Overview of Multi-Carrier CDMA". *IEEE Int'l Symp. on Spread Spectrum Tech. and Apps. (ISSSTA)*, 107–114. Mainz, Germany, September 1996.
165. Proakis, J. G. *Digital Communications*. McGraw-Hill, New York, NY, 4th edition, 2001. ISBN 0-07-232111-3.
166. Pucker, L. and G. Holt. "Extending the SCA Core Framework Inside the Modem Architecture of a Software Defined Radio". *IEEE Commun. Mag.*, 42(3):S21–S25, March 2004.
167. Quincy, E. A. "Victim Receiver Response to Ultrawideband Signals". *IEEE Conf. on Military Commun. (MILCOM)*, vol. 1, 20–24. Washington, DC, October 2001.
168. Radcliffe, R. A. and G. C. Gerace. "Design and Simulation of a Transform Domain Communication System". *IEEE Conf. on Military Commun. (MILCOM)*. Monterey, CA, October 1997.
169. Rahman, M. A., S. Sasaki, J. Zhou, S. Muramatsu, and H. Kikuchi. "Evaluation of Selective Rake Receiver in Direct Sequence Ultra Wideband Communications in the Presence of Interference". *Joint IEEE Conf. on UWB Sys. and Tech. (UWBST) and Int'l Workshop on UWB Sys. (IWUWBS)*, 221–225. Kyoto, Japan, May 2004.

170. Ramirez-Mireles, F. "Performance of Ultrawideband SSMA Using Time Hopping and M-ary PPM". *IEEE J. Select. Areas Commun.*, 19(6):1186–1196, June 2001.
171. Rappaport, T. S. *Wireless Communications: Principles and Practice*. Prentice-Hall, Upper Saddle River, NJ, 1996.
172. Ressler, M. A. and J. W. McCorkle. "Evolution of the Army Research Laboratory Ultra-wideband Test Bed". L. Carin and L. B. Felson (editors), *Ultra-wideband Short-Pulse Electromagnetics*. Plenum Press, New York, NY, 1995.
173. Richardson, T. J., M. A. Shokrollahi, and R. L. Urbanke. "Design of Capacity-Approaching Irregular Low-Density Parity-Check Codes". *IEEE Trans. Inform. Theory*, 47(2):619–637, February 2001.
174. Roberts, M. L., M. A. Temple, R. F. Mills, and R. A. Raines. "Evolution of the Air Interface of Cellular Communication Systems Toward 4G Realization". *IEEE Commun. Surveys & Tutorials*, 8(1):2–23, 1st Quarter 2006.
175. Roberts, M. L., M. A. Temple, R. F. Mills, and R. A. Raines. "Interference Suppression Characterization for Spectrally Modulated, Spectrally Encoded Signals". *IEE Electronics Letters*, accepted for publication, to appear October 2006.
176. Roberts, M. L., M. A. Temple, M. E. Oxley, R. F. Mills, and R. A. Raines. "A General Analytic Framework for Spectrally Modulated, Spectrally Encoded Signals". *IEEE Int'l Conf. on Waveform Diversity and Design*. Lihue, HI, January 2006.
177. Roberts, M. L., M. A. Temple, M. E. Oxley, R. F. Mills, and R. A. Raines. "A Spectrally Modulated, Spectrally Encoded Analytic Framework for Carrier Interferometry Signals". *ACM Int'l Wireless Commun. and Mobile Computing Conf (IWCMC)*. Vancouver, Canada, July 2006.
178. Roberts, M. L., M. A. Temple, R. A. Raines, and D. J. Clabaugh. "Time Hopping Biorthogonal Pulse Position Modulation in Modified Saleh-Valenzuela UWB Fading Channels". *IEEE Int'l Conf. on UWB (ICUWB)*. Waltham, MA, September 2006 (to appear).
179. Roberts, M. L., M. A. Temple, R. A. Raines, and E. P. Magee. "Initial Acquisition Performance of a Transform Domain Communication System: Modelling and Simulation Results". *IEEE Conf. on Military Commun. (MILCOM)*, vol. 2, 1119–1123. Los Angeles, CA, October 2000.
180. Roberts, R. A. and C. T. Mullis. *Digital Signal Processing*, 483–558. Addison-Wesley, Reading, MA, 1987.
181. Romme, J. and L. Piazzo. "On the Power Spectral Density of Time Hopping Impulse Radio". *IEEE Conf. on UWB Sys. and Tech. (UWBST)*, 241–244. Baltimore, MD, May 2002.
182. Rose, B. "Home Networks: A Standards Perspective". *IEEE Commun. Mag.*, 39(12):78–85, December 2001.

183. Roy, S., J. R. Foerster, V. S. Somayazulu, and D. G. Leeper. "Ultrawideband Radio Design: The Promise of High-Speed, Short-Range Wireless Connectivity". *Proc. IEEE*, 92(2):295–311, February 2004.
184. Runkle, P., J. McCorkle, T. Miller, and M. Welborn. "DS-CDMA: The Modulation Technology of Choice for UWB Communications". *IEEE Conf. on UWB Sys. and Tech. (UWBST)*, 364–368. Reston, VA, November 2003.
185. Rush, S. "Cingular Goes High Speed". *Wireless Week*, December 6, 2005.
186. Sadler, B. M. and A. Swami. "On the Performance of UWB and DS-Spread Spectrum Communication Systems". *IEEE Conf. on UWB Sys. and Tech. (UWBST)*, 289–292. Baltimore, MD, May 2002.
187. Saltzberg, B. R. "Performance of an Efficient Data Transmission System". *IEEE Trans. Commun. Technol.*, COM-15:805–813, December 1967.
188. Santhi, K. R., V. K. Srivastava, G. SenthilKumaran, and A. Butare. "Goals of True Broad Band's Wireless Next Wave (4G-5G)". *IEEE Vehicular Tech. Conf. (VTC)*, vol. 4, 2317–2321. Orlando, FL, October 2003.
189. Sarwate, D. V. and M. B. Pursley. "Crosscorrelation Properties of Pseudorandom and Related Sequences". *Proc. IEEE*, 68(5):593–619, May 1980.
190. Schiller, J. *Mobile Communications*, chapter 4. Addison-Wesley, 2nd edition, 2003.
191. Schmitt, R. *Electromagnetics Explained*, 86–87. Newnew Press, Amsterdam, 2002.
192. Scholtz, R. A. "Multiple Access with Time-Hopping Impulse Modulation". *IEEE Conf. on Military Commun. (MILCOM)*, vol. 2, 447–450. Boston, MA, October 1993.
193. Scholtz, R. A., P. V. Kumar, and C. J. Corrada-Bravo. "Signal Design for Ultrawideband Radio". *Sequences and Their Applications Conf. (SETA)*, May 2001.
194. Schwartz, M. *Mobile Wireless Communications*. Cambridge Univ. Press, Cambridge, UK, 2005.
195. "Second Report and Order: Revision of Part 15 of the Commission's Rules Regarding Ultra-wideband Transmission Systems". ET Docket 98-153. Federal Communications Commission, Government Printing Office, Washington DC, December 2004.
196. Shannon, C. E. "A Mathematical Theory of Communication". *Bell System Tech. J.*, 27:379–423, 623–656, Jul, Oct 1948.
197. Shaver, D. "Broadband and 4G Communications Architectures". *TxTEC Conference*. College Station, TX, January 2002.

198. Sheikh, A. U. H. *Wireless Communications Theory and Techniques*. Kluwer, Boston, MA, 2004.
199. Sheng, H., P. Orlik, A. M. Haimovich, L. J. Cimini, and J. Zhang. "On the Spectral and Power Requirements for Ultra-wideband Transmission". *IEEE Int'l Conf. on Commun. (ICC)*, vol. 1, 738–742. Anchorage, AK, May 2003.
200. Shimizu, I., K. Kobayashi, K. Nagata, S. Urabe, and S. Yuki. "A New Mobile Subscriber Set for High-capacity Land Mobile Communication System". *IEEE Vehicular Tech. Conf. (VTC)*, vol. 1, 228–232. May 1989.
201. Shlichta, P. J. "Higher Dimensional Hadamard Matrices". *IEEE Trans. Inform. Theory*, IT-25(5):566–572, September 1979.
202. Siriwongpairat, W., M. Olfat, and K. J. R. Liu. "On the Performance Evaluation of TH and DS UWB MIMO Systems". *IEEE Wireless Commun. and Networking Conf. (WCNC)*, vol. 3, 1800–1805. Atlanta, GA, March 2004.
203. Siwiak, K., P. Withington, and S. Phelan. "Ultra-wide Band Radio: The Emergence of an Important New Technology". *IEEE Vehicular Tech. Conf. (VTC)*, vol. 2, 1169–1172. Rhodes, Greece, May 2001.
204. Sklar, B. *Digital Communications: Fundamentals and Applications*. Prentice-Hall, Englewood Cliffs, NJ, 2nd edition, 2001.
205. Smith, B. "Engineers on Path to Raising MIMO". *Wireless Week*, 16, August 15, 2004.
206. Smith, B. "Door to Digital Home Hinges on 802.11n". *Wireless Week*, 17, March 01, 2005.
207. Somayazulu, V. S. "Multiple Access Performance in UWB Systems Using Time Hopping vs. Direct Sequence Spreading". *IEEE Wireless Commun. and Networking Conf. (WCNC)*, vol. 2, 522–525. Orlando, FL, March 2002.
208. Soni, R. A. and R. M. Buehrer. "On the Performance of Open-Loop Transmit Diversity Techniques for IS-2000 Systems: A Comparative Study". *IEEE Trans. Wireless Commun.*, 3(5):1602–1615, September 2004.
209. Stroh, S. "Ultra-Wideband: Multimedia Unplugged". *IEEE Spectr.*, 40(9):23–27, September 2003.
210. Strömberg, F. "Virtual Antenna Arrays: Results and Ongoing Studies". *Affordable Wireless Services and Infrastructure (AWSI) Workshop*. Stockholm, Sweden, June 2004.
211. Su, H., E. Shlomot, and H. K. Nakamura. "Selectable Mode Vocoder Emerges for CDMA2000 Designs". *CommsDesign*, January 7, 2003. URL <http://www.commsdesign.com/>.

212. Yu Su, Huan, E. Shlomot, and H. K. Nakamura. "Selectable Mode Vocoder Emerges for cdma2000 Designs". *CommsDesign*, January 7, 2003. URL <http://www.commsdesign.com/>.
213. "Support for GSM Continues to Grow". *IEE Review*, 50(3):21, March 2004.
214. Surendra Raju, M., A. Ramesh, and A. Chockalingam. "BER Analysis of QAM with Transmit Diversity in Rayleigh Fading Channels". *IEEE Conf. on Global Commun. (GLOBECOM)*, 641–645. December 2003.
215. Swackhammer, P. J., M. A. Temple, and R. A. Raines. "Performance Simulation of a Transform Domain Communication System for Multiple Access Applications". *IEEE Conf. on Military Commun. (MILCOM)*, vol. 2, 1055–1059. Atlantic City, NJ, November 1999.
216. Swami, A., B. Sadler, and J. Turner. "On the Coexistence of Ultra-wideband and Narrowband Radio Systems". *IEEE Conf. on Military Commun. (MILCOM)*, vol. 1, 16–19. Washington, DC, October 2001.
217. Tachikawa, K. "A Perspective on the Evolution of Mobile Communications". *IEEE Commun. Mag.*, 41(10):66–73, October 2003.
218. Taha, A. and K. M. Chugg. "On the Power Spectral Density of Wireless Multiple-Access UWB Impulse Radio Under Realistic Propagation Conditions". *IEEE Vehicular Tech. Conf. (VTC)*, vol. 2, 1298–1302. Orlando, FL, October 2003.
219. Tanenbaum, A. S. *Computer Networks*. Prentice-Hall, Upper Saddle River, NJ, 3rd edition, 1996.
220. Taylor, N., M. A. Cooper, S. M. D. Armour, and J. P. McGeehan. "Performance Evaluation of Carrier Interferometry Implementations of MC-CDMA Over a Wideband Channel Suffering Phase Noise". *IEEE Vehicular Tech. Conf. (VTC)*, vol. 5, 3043–3047. Stockholm, Sweden, May 2005.
221. "Telephony's Complete Guide to WiMAX". White Paper, May 31, 2004. URL <http://www.wimaxforum.org/>.
222. Toskala, A. "HSDPA Helps W-CDMA Nets Compete with DSL, Cable Services". *CommsDesign*, January 13, 2004. URL <http://www.commsdesign.com/>.
223. "UWB Forum Home Page". URL <http://www.uwbforum.org/>.
224. "UWB Forum Reaches 30 Member Mark; Demonstrates Growing Support for Common Signaling Mode". *PRNewswire*, May 5, 2004.
225. vanNee, R. D. J. and R. Prasad. *OFDM for Wireless Multimedia Communications*. Artech, Boston, MA, 2000.
226. VanRooyen, P. "Advances in Space-Time Processing Techniques Open up Mobile Apps". *CommsDesign*, November 8, 2002. URL <http://www.commsdesign.com/>.

227. Varshney, U. and R. Jain. "Issues in Emergin 4G Wireless Networks". *IEEE Computer*, 34(6):94–96, June 2004.
228. Weinstein, S. B. and P. M. Ebert. "Data Transmission by Frequency-Division Multiplexing Using the Discrete Fourier Transform". COM-19(5):628–634, October 1971.
229. Welborn, M. L. "System Considerations for Ultra-wideband Wireless Networks". *IEEE Radio and Wireless Conf. (RAWCON)*, vol. 2, 5–8. Boston, MA, August 2001.
230. Wiegandt, D. A. and C. R. Nassar. "High Performance OFDM via Carrier Interferometry". *IEEE Intl. Conf. 3rd-Generation Wireless and Beyond (3G Wireless '01)*, 404–409. San Francisco, CA, 2001.
231. Wiegandt, D. A., C. R. Nassar, and Z. Wu. "Overcoming Peak-to-Average Power Ratio Issues in OFDM via Carrier Interferometry Codes". *IEEE Veh. Tech. Conf. (VTC)*, 660–663. Atlantic City, NJ, 2001.
232. Wiegandt, D. A., Z. Wu, and C. R. Nassar. "High-Throughput, High-Performance OFDM via Pseudo-Orthogonal Carrier Interferometry Spreading Codes". *IEEE Trans. Commun.*, 51(7):1123–1134, July 2003.
233. Win, M. Z. and R. A. Scholtz. "Impulse Radio: How it Works". *IEEE Commun. Lett.*, 2(2):36–38, February 1998.
234. Win, M. Z. and R. A. Scholtz. "Ultra-wide Bandwidth Time-Hopping Spread-Spectrum Impulse Radio for Wireless Multiple-Access Communications". *IEEE Trans. Commun.*, 48(4):679–689, April 2000.
235. Wu, Z. and C. R. Nassar. "Narrowband Interference Rejection in OFDM via Carrier Interferometry Spreading Codes". *IEEE Trans. Wireless Commun.*, 4(4):1491–1505, July 2005.
236. Xu, Hao, Dimitry Chizhik, Howard Huang, and Reinaldo Valenzuela. "A Generalized Space-Time Multiple-Input Multiple-Output (MIMO) Channel Model." *IEEE Trans. Wireless Commun.*, 3(3):966–975, May 2004.
237. Yallapragada, R. "Latest Trends and New Enhancements in 3G Wireless Communications". Joint IEEE COMSOC, Sig. Proc. Society, and Comp. Society distinguished lecture series, April 12, 2004.
238. Yang, L. and G. B. Giannakis. "Ultra-Wideband Multiple Access: Unification and Narrowband Interference Analysis". *IEEE Conf. on UWB Sys. and Tech. (UWBST)*, 320–324. Reston, VA, November 2003.
239. Yang, L. and G. B. Giannakis. "Unification of Ultra-Wideband Multiple Access Schemes and Comparison in the Presence of Interference". *37th Asilomar Conf. on Signals, Sys. and Comp.*, vol. 2, 1239–1243. Pacific Grove, CA, November 2003.

240. Yang, L. and G. B. Giannakis. "A General Model and SINR Analysis of Low Duty-Cycle UWB Access through Multipath and NBI with Rake Reception". *IEEE Trans. Wireless Commun.*, 4(4):1818–1833, July 2005.
241. Ye, Z., A. S. Madhukumar, , X. Peng, and F. Chin. "Performance Analysis of a DS-UWB System in the Presence of Narrowband Interference". *IEEE Vehicular Tech. Conf. (VTC)*, vol. 5, 2590–2594. Genoa, Italy, May 2004.
242. Ye, Z., A. S. Madhukumar, and F. Chin. "Power Spectral Density and In-band Interference Power of UWB Signals at Narrowband Systems". *IEEE Int'l Conf. on Commun. (ICC)*, vol. 6, 3561–3565. Paris, France, June 2004.
243. Yee, N. and J.-P. Linnartz. *Multi-Carrier CDMA in an Indoor Wireless Radio Channel*. Memorandum UCB/ERL M94/6, Univ. of Cal., Berkeley, CA, 1994.
244. Yee, N., J.-P. Linnartz, and G. Fettweis. "Multi-Carrier CDMA in Indoor Wireless Radio Networks". *IEEE Conf. on Personal, Indoor and Mobile Radio Commun. (PIMRC)*, 109–113. Yokohama, Japan, September 1993.
245. Zahariadis, T. "Trends in the Path to 4G". *IEE Commun. Engr.*, 1(1):12–15, February 2003.
246. Zhang, H. and T. A. Gulliver. "Biorthogonal Pulse Position Modulation for Time-Hopping Multiple Access UWB Communications". *IEEE Trans. Wireless Commun.*, 4(3):1154–1162, May 2005.
247. Zhang, H., W. Li, and T. A. Gulliver. "Pulse Position Amplitude Modulation for Time-Hopping Multiple-Access UWB Communications". *IEEE Trans. Commun.*, 53(8):1269–1273, August 2005.
248. Zhang, P., X. Tao, J. Zhang, Y. Wang, and Y. Wang. "A Vision from the Future: Beyond 3G TDD". *IEEE Commun. Mag.*, 43(1):38–44, January 2005.
249. Zhao, L. and A. M. Haimovich. "Performance of Ultra-wideband Communications in the Presence of Interference". *IEEE J. Select. Areas Commun.*, 20(9):1684–1691, December 2002.
250. Zheng, K., L. Huang, W. Wang, and G. Yang. "TD-CDM-OFDM: Evolution of TD-SCDMA Toward 4G". *IEEE Commun. Mag.*, 43(1):45–52, January 2005.
251. Ziemer, R. E. "Diversity in 3G Wireless – Wideband and Multicarrier CDMA Compared". IEEE COMSOC distinguished lecture series, May 30, 2001.
252. Zou, W. Y. and Y. Wu. "COFDM: An Overview". *IEEE Trans. Broadcast.*, 41(1):1–8, March 1995.

Vita

Major Marcus L. Roberts graduated from Broken Arrow High School in Broken Arrow, OK in 1991. He entered the United States Air Force Academy (USAFA) and graduated with a Bachelor of Science in Electrical Engineering in May 1995. While at USAFA, he earned academic distinction by graduating in the top 7% of his academic class.

Major Roberts' first assignment was to Eglin AFB, FL. As an engineer in the Air Force Research Laboratory Munitions Directorate (AFRL/MN), he worked on several precision guided weapon programs to "make smart bombs smarter." In August 1998, Major Roberts entered the Graduate School of Engineering, Air Force Institute of Technology (AFIT), Wright-Patterson AFB, OH. He completed his Master of Science in Electrical Engineering in March 2000, earning the AFCEA Research Excellence Award "in recognition of outstanding research accomplishments in the area of Command, Control, Communications, and Intelligence."

Upon graduation, Major Roberts was assigned to the 453d Electronic Warfare Squadron, Air Force Information Warfare Center (AFIWC), Lackland AFB, TX. While at AFIWC, he led the production of hundreds of independent engineering-based analyses of the performance, vulnerability, and survivability of Air Force radar, navigation, and communication systems. In August 2003, Major Roberts returned to AFIT and Wright-Patterson AFB, OH to obtain a Doctor of Philosophy in Electrical Engineering.

Major Roberts is a member of Tau Beta Pi, Eta Kappa Nu, the Institute of Electrical and Computer Engineers (IEEE), and the Armed Forces Communications and Electronics Association (AFCEA). After graduation, he will be assigned to Fort Meade, MD.

REPORT DOCUMENTATION PAGE					Form Approved OMB No. 0704-0188	
<p>The public reporting burden for this collection of information is estimated to average 1 hour per response, including the time for reviewing instructions, searching existing data sources, gathering and maintaining the data needed, and completing and reviewing the collection of information. Send comments regarding this burden estimate or any other aspect of this collection of information, including suggestions for reducing this burden to Department of Defense, Washington Headquarters Services, Directorate for Information Operations and Reports (0704-0188), 1215 Jefferson Davis Highway, Suite 1204, Arlington, VA 22202-4302. Respondents should be aware that notwithstanding any other provision of law, no person shall be subject to any penalty for failing to comply with a collection of information if it does not display a currently valid OMB control number. PLEASE DO NOT RETURN YOUR FORM TO THE ABOVE ADDRESS.</p>						
1. REPORT DATE (DD-MM-YYYY)		2. REPORT TYPE		3. DATES COVERED (From — To)		
14-09-2006		Doctoral Dissertation		Sept 2003 — Sept 2006		
4. TITLE AND SUBTITLE A General Framework for Analyzing, Characterizing, and Implementing Spectrally Modulated, Spectrally Encoded Signals				5a. CONTRACT NUMBER		
				5b. GRANT NUMBER		
				5c. PROGRAM ELEMENT NUMBER		
6. AUTHOR(S) Marcus L. Roberts, Maj, USAF				5d. PROJECT NUMBER		
				5e. TASK NUMBER		
				5f. WORK UNIT NUMBER		
7. PERFORMING ORGANIZATION NAME(S) AND ADDRESS(ES) Air Force Institute of Technology Graduate School of Engineering and Management 2950 Hobson Way WPAFB OH 45433-7765				8. PERFORMING ORGANIZATION REPORT NUMBER AFIT/DS/ENG/06-06		
9. SPONSORING / MONITORING AGENCY NAME(S) AND ADDRESS(ES) Mr. James P. Stephens, AFRL/SNRW, james.stephens@wpafb.af.mil 2241 Avionics Circle, Wright-Patterson AFB, OH 45433, (937) 255-5579 x3547 Mr. Mark E. Minges, AFRL/IFGD, mark.minges@wpafb.af.mil 2241 Avionics Circle, Wright-Patterson AFB, OH 45433, (937) 255-4947 x3401				10. SPONSOR/MONITOR'S ACRONYM(S)		
				11. SPONSOR/MONITOR'S REPORT NUMBER(S)		
12. DISTRIBUTION / AVAILABILITY STATEMENT Approved for Public Release; Distribution Is Unlimited.						
13. SUPPLEMENTARY NOTES						
14. ABSTRACT Fourth generation (4G) communications will support many capabilities while providing universal, high speed access. One potential enabler for these capabilities is software defined radio (SDR). When controlled by cognitive radio (CR) principles, the required waveform diversity is achieved via a synergistic union called CR-based SDR. Research is rapidly progressing in SDR hardware and software venues, but current CR-based SDR research lacks the theoretical foundation and analytic framework to permit efficient implementation. This limitation is addressed here by introducing a general framework for analyzing, characterizing, and implementing spectrally modulated, spectrally encoded (SMSE) signals within CR-based SDR architectures. Given orthogonal frequency division multiplexing (OFDM) is a 4G candidate signal, OFDM-based signals are collectively classified as SMSE since modulation and encoding are spectrally applied. The proposed framework provides analytic commonality and unification of SMSE signals. Applicability is first shown for candidate 4G signals, and resultant analytic expressions agree with published results. Implementability is then demonstrated in multiple coexistence scenarios via modeling and simulation to reinforce practical utility.						
15. SUBJECT TERMS Adaptive communications, wireless communications, cellular communications, 4G, software defined radio (SDR), cognitive radio (CR), orthogonal frequency division multiplexing (OFDM)						
16. SECURITY CLASSIFICATION OF:			17. LIMITATION OF ABSTRACT	18. NUMBER OF PAGES	19a. NAME OF RESPONSIBLE PERSON	
a. REPORT	b. ABSTRACT	c. THIS PAGE			Dr. Michael A. Temple, AFIT/ENG	
U	U	U	UU	250	19b. TELEPHONE NUMBER (include area code) (937) 255-3636, ext 4279	